# BERICHTE

## aus dem Fachbereich Geowissenschaften der Universität Bremen

**No. 228**

**Kopf, A., Bannert, B., Brückmann, W., Dorschel, B., Foubert, A.T.G., Grevemeyer, I., Gutscher, M.-A., Hebbeln, D., Heesemann, B., Hensen, C., Kaul, N.E., Lutz, M., Magalhaes, V.H., Marquardt, M.J., Marti, A.V., Nass, K.S., Neubert, N., Niemann, H., Nuzzo, M., Poort, J.P.D., Rosiak, U.D., Sahling, H., Schneider von Deimling, J., Somoza Losada, L., Thiebot, E., Wilkop, T.P.**

**REPORT AND PRELIMINARY RESULTS OF SONNE CRUISE SO175, MIAMI - BREMERHAVEN, 12.11 - 30.12.2003**

Berichte, Fachbereich Geowissenschaften, Universität Bremen, No. 228, 218 pages, Bremen 2004

ISSN 0931-0800

The "Berichte aus dem Fachbereich Geowissenschaften" are produced at irregular intervals by the Department of Geosciences, Bremen University.

They serve for the publication of experimental works, Ph.D.-theses and scientific contributions made by members of the department.

Reports can be ordered from:


Monika Bachur

Forschungszentrum Ozeanränder, RCOM

Universität Bremen

Postfach 330 440

**D 28334 BREMEN**

Phone: (49) 421 218-8960

Fax: (49) 421 218-3116

e-mail: MBachur@uni-bremen.de



Citation:

Kopf, A. and cruise participants

Report and preliminary results of SONNE Cruise SO175, Miami - Bremerhaven, 12.11 - 30.12.2003.

Berichte, Fachbereich Geowissenschaften, Universität Bremen, No. 228, 218 pages, Bremen, 2004.

ISSN 0931-0800

**Table of Contents**

**Preface**

The expedition SO175, a.k.a. *GAP* (=Gibraltar Arc Processes) cruise, revisits the Gulf of Cadiz area more than a decade, and exactly 100 legs after the region has been seismically investigated by BGR (Roeser et al., 1992) using German research vessel *FS Sonne*. *GAP* is part of a larger initiative that combines national and international funding programmes such as TTR (half a dozen cruises up to now, e.g. TTR-9, TTR-10, TTR-11, TTR-12), EU projects like Mediflux, Moundforce and MVseis, Euromargins projects SWIM, WestMed and Voltaire, earlier TASYO (1998-2002) MATESPRO projects, and future GADES (2003-2006), IMPULS (2005) and DELILA (2005) cruises, to name just a few. As a consequence of the wealth of previous and ongoing projects, *GAP* aimed for a multi-disciplinary, complementary research programme.

The main interest in the area arises from the fact that the Gulf of Cadiz region is an ideal natural laboratory to study a variety of (often linked) processes, which include

- (micro)seismicity and active faulting,
- mud volcanism and diapirism,
- formation of carbonate mounds with cold water corals,
- microbial AOM and related processes
- episodic (and sometimes tsunamigenic) mega-earthquakes,
- landslides and turbidites due to slope failure,
- tectonic interaction between olistostrome bodies, evaporites, a sediment wedge and basement highs,
- gas hydrate processes,
- oceanographic peculiarities due to the saline, warm Mediterranean outflow water (MOW).

All those phenomena can be studied in a regionally confined area close to shore and readily accessible from major ports in Portugal and Spain. The GAP cruise tries and add to the existing knowledge in each of the above fields by performing a series of interdisciplinary measurements and sampling for roughly one month. Expertise from earlier cruises is guaranteed by the international group of scientists from the UK, Spain, France, Portugal and Germany.

In addition to the extension of our knowledge in each of the above fields, the main objective of GAP has been to provide a more profound data base for (i) a long term monitoring station in the area (possibly within the EU *ESONET* project), and for (ii) an IODP (Integrated Ocean Drilling Program) proposal to have deep drillholes in the region eventually. A first step into this direction have been continuous maps and heat flow profiles along crucial parts of the Gibraltar wedge. A second step has been the deployment of a temperature-pore pressure probe which will monitor an active mud volcano for 4 weeks. Data will arrive at home via satellite long after the *GAP* cruise has terminated. We believe that only long-term observation of crucial physical parameters will help to broaden the understanding of complex dynamic, often interacting processes along ocean margins.

**Personnel aboard RV SONNE**

**SO175-Leg 1 (12.11.-25.11.2003, Miami - Lisbon)**

| | |
|---|---|
| Erwin Suess | GEOMAR Kiel |
| Heiko Sahling | RCOM Bremen |
| Falk von Seck | RF Bremen |

**SO175-Leg 2 (25.11.-03.12.2003, Lisbon - Cadiz)**

| | |
|---|---|
| Achim Kopf | RCOM Bremen |
| Ingo Grevemeyer | GEOMAR Kiel |
| Bernd Heesemann | Univ. Bremen |
| Norbert Emanuel Kaul | Univ. Bremen |
| Jeffrey Pepijn Dylan Poort | Univ. Ghent |
| Marco Lutz | Univ. Bremen |
| Marc-Andre Gutscher | Univ. Brest |
| Luis Somoza Losada | IGME Madrid |
| Alexis V. Marti | CMIMA Bracelona |
| Marianne Nuzzo | Univ. Bristol |
| Thomas Peter Wilkop | MPI Bremen |
| Helge Niemann | MPI Bremen |
| Matthias Jonathan Marquardt | GEOMAR Kiel |
| Kristin Sabrina Nass | GEOMAR Kiel |
| Nadja Neubert | Univ. Bremen |
| Christian Hensen | GEOMAR Kiel |
| Uwe Dieter Rosiak | Univ. Bremen |
| Dierk Hebbeln | Univ. Bremen |
| Boris Dorschel | Univ. Bremen |
| Bernhard Bannert | Oktopus, Nordenweststedt |
| Warner Brückmann | GEOMAR Kiel |
| Heiko Sahling | RCOM Bremen |
| Kathrin Sänger | Spiegel-TV |
| Bernd Zühlke | Spiegel-TV |
| Philip Fleischer | Spiegel-TV |

**SO175-Leg 3 (03.12.-23.12.2003, Cadiz - Lisbon)**

| | |
|---|---|
| Achim Kopf | RCOM Bremen |
| Ingo Grevemeyer | GEOMAR Kiel |
| Bernd Heesemann | Univ. Bremen |
| Norbert Emanuel Kaul | Univ. Bremen |
| Jeffrey Pepijn Dylan Poort | Univ. Ghent |
| Marco Lutz | Univ. Bremen |
| Marc-Andre Gutscher | Univ. Brest |
| Emanuelle Thiebot | Univ. Brest |
| Luis Somoza Losada | IGME Madrid |
| Jens Schneider von Deimling | GEOMAR Kiel |
| Alexis V. Marti | CMIMA Barcelona |
| Marianne Nuzzo | Univ. Bristol |
| Thomas Peter Wilkop | MPI Bremen |
| Helge Niemann | MPI Bremen |
| Matthias Jonathan Marquardt | GEOMAR Kiel |
| Kristin Sabrina Nass | GEOMAR Kiel |
| Nadja Neubert | Univ. Bremen |
| Christian Hensen | GEOMAR Kiel |
| Uwe Dieter Rosiak | Univ. Bremen |
| Dierk Hebbeln | Univ. Bremen |
| Boris Dorschel | Univ. Bremen |
| Bernhard Bannert | Oktopus, Nordenweststedt |
| Warner Brückmann | GEOMAR Kiel |
| Anneleen T. G. Foubert | Univ. Ghent |
| Vitor Hugo da Silva Magalhaes | Univ. Bremen |

**SO175-Leg 4 (23.12.-31.12.2003, Lisbon - Bremerhaven)**

| | |
|---|---|
| Achim Kopf | RCOM Bremen |
| Chantal Cowan | RCOM Bremen |
| Carmen Murken | RCOM Bremen |
| Gisela Boelen | RCOM Bremen |

**Participating institutions**

DFG-Research Centre Ocean Margins (RCOM) and FB 5
University Bremen
Klagenfurter Strasse
28359 Bremen
Germany

GEOMAR Research Centre
University Kiel
Wischhofstrasse 1-3
24148 Kiel
Germany

Max Planck Institute for Marine Microbiology
Celsiusstrasse 1

28359 Bremen
Germany

Instituto Geológico e Mineiro (Geological Survey)
Departamento de Geologia Marinha
Bairro do Zambujal
Apartado 7586
2721-866 Alfragide
Portugal

Marine Geology
IGME Instituto Geológico y Minero de España / Geological Survey of Spain
Rios Rosas 23
28003 Madrid
Spain

Universite de Bretagne Occidentale / Institut Universitaire Europeen de la Mer
UMR 6538 Domaines Oceaniques
Place Nicolas Copernic
29280 Plouzane
France

Unitat de Tecnologia Marina - CSIC
Centre Mediterrani d'Investigacions Marines i Ambientals (CMIMA)
Passeig Marítim de la Barceloneta, 37-49
08003 Barcelona
Spain

Renard Centre of Marine Geology (RCMG)
Department of Geology and Soil Science
University of Ghent
Krijgslaan 281 S8
9000 Gent
Belgium

Marine Geology Department
Geological and Mining Institute
Estrada da Portela, Apartado 7586
2721-866 Alfragide
Portugal

Department of Earth Sciences
Wills Memorial Building
University of Bristol
Queens Road
Bristol BS8 1RJ
U.K.

Oktopus GmbH
Kieler Strasse 51
24594 Hohenweststedt
Germany

Spiegel-TV
Brandswiete 19
20457 Hamburg
Germany

Reederei Forschungsschifffahrt (RF)
Blumenthalstrasse 15
28209 Bremen
Germany

## 1. Abstract

Expedition SO175 using *FS Sonne* aimed for a multidisciplinerary geoscientific approach with an international group of researchers. Methods covered the entire span from geophysical data acquisition (seafloor mapping, echography, seismic reflection), sediment coring at sites of active fluid venting, *in situ* heat flow measurements across the entire length of the Gibraltar thrust wedge, the deformation front, landslide bodies, and mud volcanoes, and finally the deployment of a long-term pore pressure probe. Video-supported operations helped to identify fluid vent sites, regions with tectonic activity, and other attractive high priority targets. Qualitative and quantitative examinations took place on board and are continued on land with respect to pore pressure variation, geomicrobiology, sediment- and fluid mobilization, geochemical processes, faunal assemblages (e.g. cold water corals), and gas hydrates (flammable methane-ice-crystals). Main focus of the expedition has been a better understanding of interaction between dynamic processes in a seismically active region region with slow plate convergence.

In the context of earthquake nucleation and subduction zone processes, the SO175 research programme had a variety of goals, such as:

- To test the frictional behaviour of the abyssal plain sediments.
- To explore the temperature field of the 1755 thrust earthquake event via heat flow measurements.
- To assess the role of fluid venting and gas hydrate processes control slope stability and mud volcanic activity along the Iberian continental margin.
- To measure isotope geochemistry of pore waters and carbonates of deep fluids.
- To quantify microbial activity in Gibraltar wedge sediments.
- To test whether microseismicity in the area corresponds to in situ pore pressure changes.
- To find out if enhanced heat flow max be indicative of active subduction.

Initial tentative results during the cruise suggest that there is a component of active thrusting at the base of the wedge, as attested by heat flow data. Based on mostly geochemical evidence, mud volcanism was found less active than previously assumed. Highlights from post-cruise research include the successful deployment of the long-term station and high frictional resistance of all incoming sediment on the three abyssal plains.

## 2. Introduction

The main thrust of the *GAP* cruise has been the study of earthquake-related processes in the Gibraltar region. They include elevated heat flow due to friction of coarse-grained, well drained sediments, faulting and landsliding, and mud volcanic activity. The cruise is part of a joint effort of several European groups working in the area. In the long run, these efforts will provide a full coverage bathymetry of the Gibraltar Arc sediment wedge, seismic lines across it, and monitoring sites for seismicity, temperature and pore pressure (ESONET project). One key aspect is clearly the earthquake risk in the region, with the most prominent 1755 Great Lisbon earthquake, but also strong, more recent events in the 1960's (up to M 7.9).

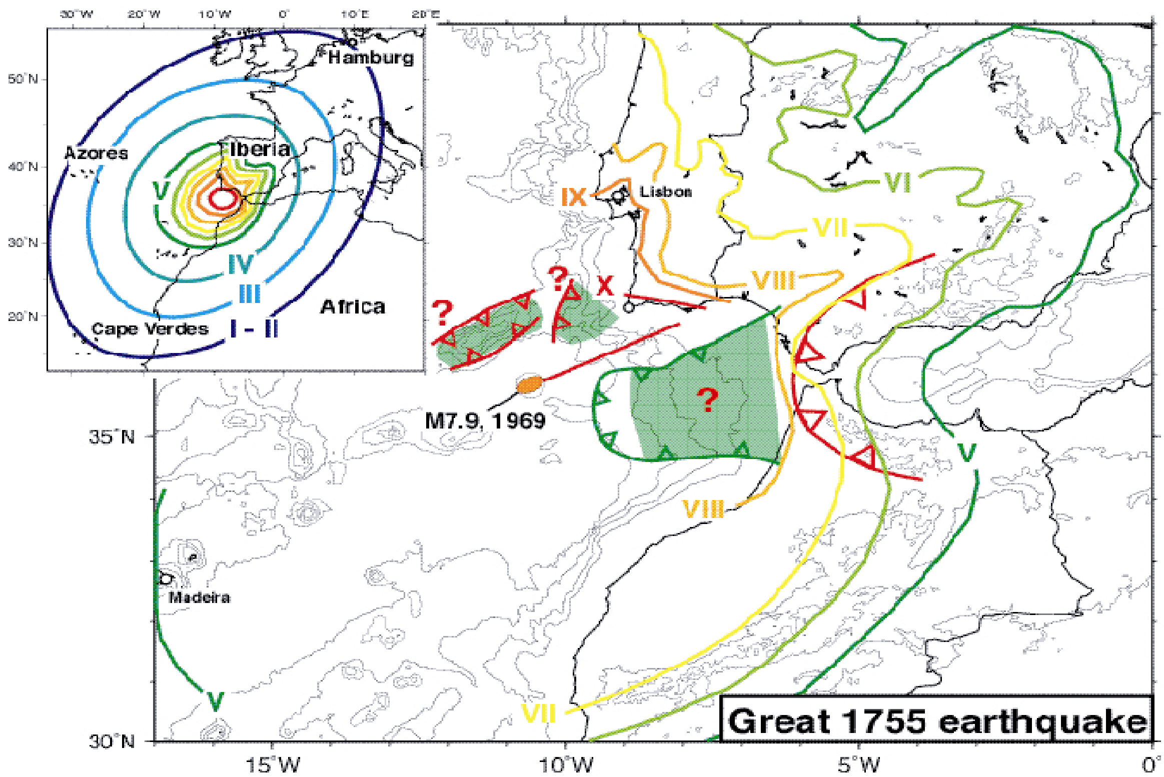


**Fig. 2.1**: *GAP* study area including potential source areas of the 1755 Lisbon earthquake, the latter marked by question marks. Numbers refer to earthquake magnitude as felt in the indicated areas. Modified from Gutscher et al., 2004.

On November 1st 1755, the most destructive earthquake in European history occurred with an estimated magnitude of 8.5 - 9.0 (Martinez-Solares et al., 1979; Johnston, 1996) (**Fig. 2.1**). It caused tens of thousands of deaths (approximately 1/4 of Lisbon's population at the time), triggered a devastating tsunami along the coasts of Southwest Iberia and Northwest Morocco, could be felt all the way to Hamburg and changed water levels of lakes in e.g., Switzerland. Political powers changed as a result of the earthquake, and initiated a philosophical debate between Rousseau, Kant and others. The exact source of the earthquake remains unknown to geoscientists to this day (Baptista et al., 1998). Its likely source region off SW Iberia is located at the eastern end of the portion of the Africa – Eurasia plate boundary commonly referred to as the Azores – Gibraltar transform (Sartori et al., 1994; Tortella et al., 1997; Jimenez-Munt et al., 2001). In Southern Iberia, the plate boundary is not clearly defined and encompasses a broad region of deformation at least 200 km wide (in a N-S direction) marked by moderately high seismicity (Negredo et al., 2002; Stich et al., 2003) (**Fig. 2.1**). Recent marine geophysical data, combined with tomographic images, provide compelling evidence for current activity of eastward dipping subduction beneath the Gibraltar Arc. Seismic reflection profiles and wide-angle profiles in the Gulf of Cadiz document an accretionary wedge, with active thrust faults soling out to an east-dipping decollement and overlying an eastward dipping basement (Gutscher et al., 2002).

**3. Objectives**

Expedition SO175 using *RV Sonne* aims to carry out a multidisciplinary investigation with a group of European geoscientists including geophysical data acquisition (seafloor mapping, seismic reflection), sediment coring at sites of active fluid venting as well as heat flow measurements across the entire length of the wedge, the deformation front, landslide bodies, and mud volcanoes. Video-supported operations will help to identify fluid vent sites and regions with tectonic activity on the basis of the appearance of typical biological communities. Qualitative and quantitative examinations will take place on board and later on land with respect to pore pressure variation, geomicrobiology, sediment- and fluid mobilization, geochemical processes, faunal assemblages (e.g., cold water corals), and gas hydrates (methane clathrates). The main focus of the expedition will be a better understanding of interaction between dynamic processes in a seismically active region region with slow plate convergence.

In the context of earthquake nucleation and subduction zone processes, the SO175 research programme will test a variety of hypotheses, such as:

- Mapping and seismic reflection profiling image the nature of the Gibraltar Arc thrust wedge, a proposed subduction zone.
- Frictional behaviour of the abyssal plain sediments (Tagus, Horseshoe, Seine) controls the position and seismic character of the subduction thrust.
- The temperature field of the 1755 thrust earthquake event can be imaged via heat flow measurements across the wedge and at the Gorringe Bank.
- Fluid venting, seismicity and gas hydrate processes control slope stability and mud volcanic activity along the Iberian continental margin.
- Characteristic sedimentological features relate to seismic tremor.
- Isotope geochemistry of pore waters and carbonates indicate deep fluid mobilization.
- Microbiological studies as well as *in situ* pore pressure and heat flow measurements attest efficient drainage of the Gibraltar imbricate wedge, because plate convergence is low.
- There is a temporal relationship between the backflux of Mediterranean outflow water (MOW) and gas hydrate decomposition.
- Deglaciation some 12 ka BP is responsible for some islands in the Straits of Gibraltar having been submerged, now representing prominent topographic highs.

In order to test these hypotheses, a total of 100 stations have been visited during *GAP*. They cover the full range of geological settings from the abyssal plains (*Tagus, Horseshoe, Seine*), the deformation fronts (NW, W, and SW ends of the Gibraltar wedge (**Fig. 3.1**), the wedge itself, mud domes and coral mounds on the wedge, the Iberian and Moroccan shallow (>500 m water depth) margins, and the Straits of Gibraltar.

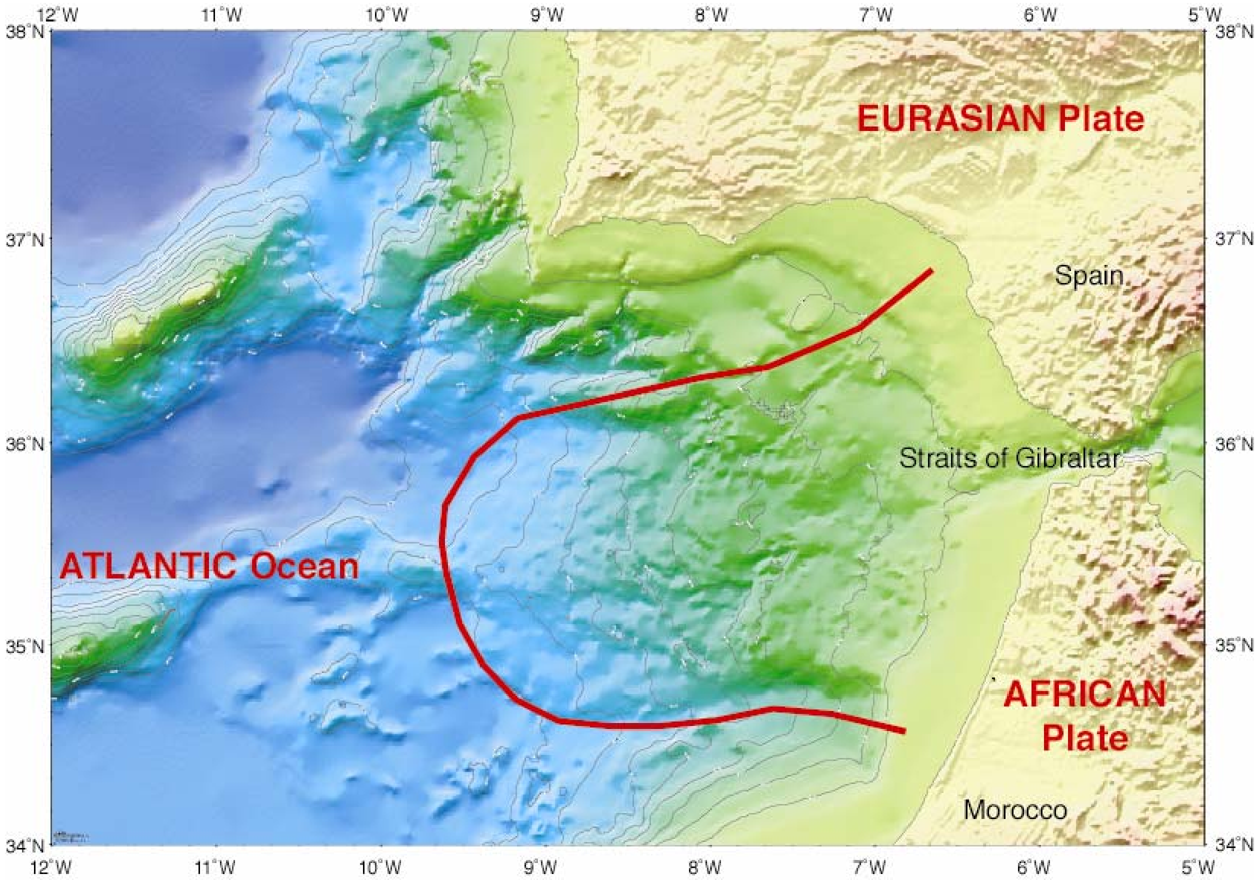


**Fig. 3.1**: Bathymetric map of the study area using the global GEBCO data base. Red line marks the outline of the Gibraltar thrust wedge based on earlier cruises.

# 4. Geological setting

## *4.1 The Gulf of Cadiz/Gibraltar Arc region*

The Gibraltar region features the arcuate Betic - Rif mountain belt with outward directed thrusting (Maldonado et al., 1999), surrounding a zone of strong Neogene subsidence and crustal thinning in the Western Alboran Sea (Docherty and Banda, 1995). Until now its geodynamic interpretation has remained controversial (Lonergan and White, 1997; Calvert et al., 2000). The Gibraltar Arc is located at the eastern end of the Azores-Gibraltar transform, a diffuse transpressional plate boundary between the Iberian and African Plates (Sartori et al., 1994) (**Fig. 4.1A, inset**). Relative convergence between the two plates here is slow, only 4 mm/yr in a NW-SE direction (Argus et al., 1989). However, attention has recently been focussed on this plate boundary, while seeking the likely source of the destructive Lisbon great earthquake (M>8.5) and tsunami of 1755 (Zitellini et al., 2001).

Northward vergent thrusting in the Internal Betics and southward vergent thrusting in the Rif is coeval with subsidence in the Alboran domain. Further west in the Gulf of Cadiz, a chaotic sedimentary melange, interpreted as an olistostrome, shows signs of intense deformation and westward transport, attributed primarily to gravity sliding (Maldonado et al., 1999; Torelli et al., 1997). Intermediate depth seismicity (60 - 120 km depth) is observed beneath the Gibraltar Arc and westernmost Alboran Sea (Casado et al., 2001) and deep focus earthquakes (600 - 660 km) occur beneath southern Spain, near Granada (**Fig. 4.1A, B**) (Buforn et al., 1991). Early tomographic studies indicated a low-velocity P-wave anomaly beneath the Alboran Sea underlain by a high-velocity body below roughly in 150 km depth (Blanco and Spakman, 1993; Seber et al., 1996) (**Fig. 4.1B**).

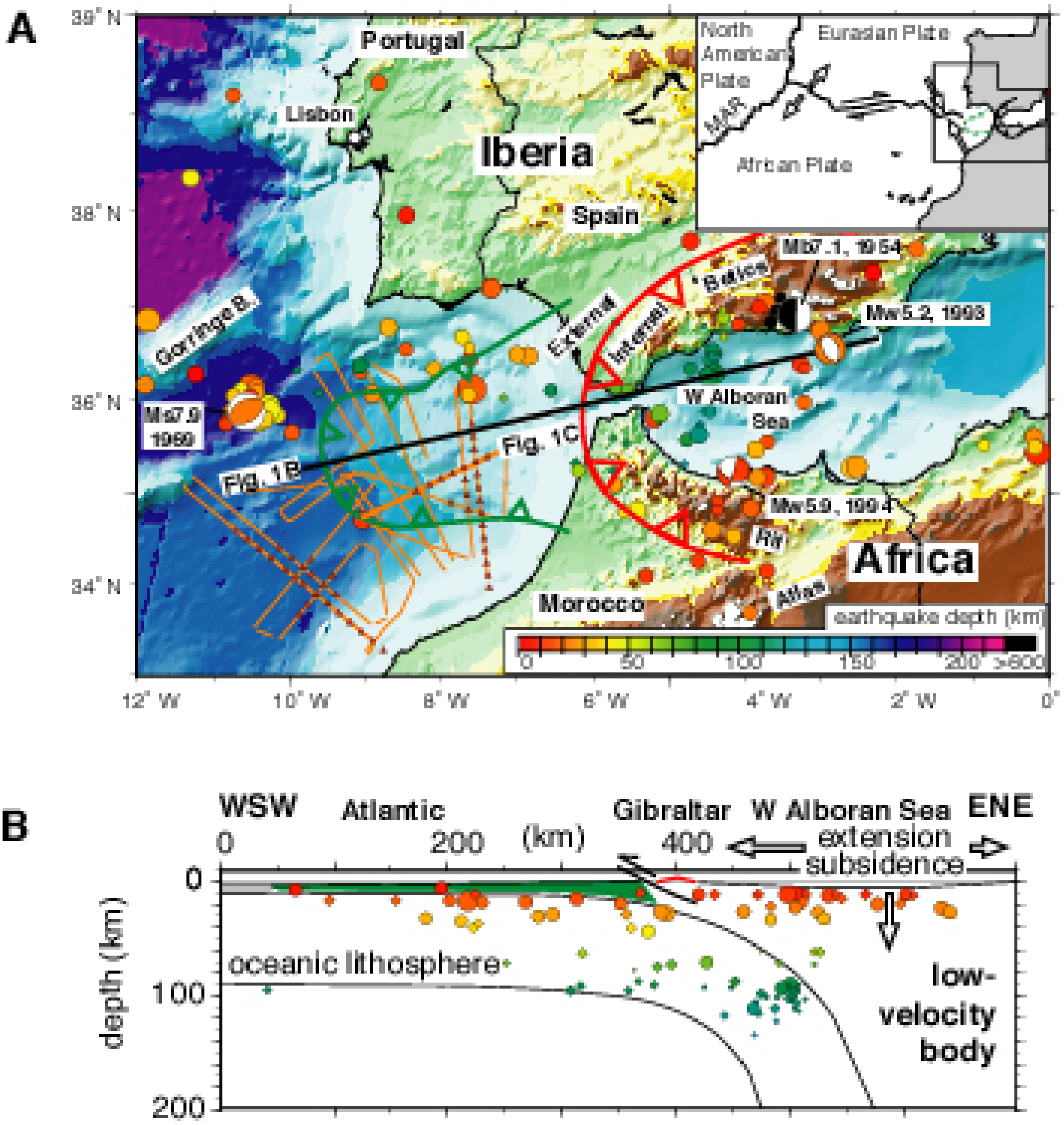


**Fig. 4.1: A)** Location map of the GAP study area with shaded hill relief (Smith and Sandwell, 1997) and seismicity (Engdahl et al., 1998; Preliminary Determination of Earthquakes [PDE] Catalog, 1973–present; Centroid Moment Tensor [CMT] Catalog, 1976– present) (M >3). Red thrust teeth symbols indicate Gibraltar Arc; green thrust teeth symbols indicate active Gibraltar thrust wedge. Seismicity sampling box (for B) is given. French SISMAR seismic profiles are shown as orange lines and positions of ocean bottom seismometer are as shown as black triangles, with red fill. MAR is Mid-Atlantic Ridge. Inset shows plate kinematic scenario. **B)** Lithospheric cross section showing earthquake hypocenters and principal tectonic domains. Modified from Gutscher et al., 2002.

A variety of tectonic models have been proposed to explain these different observations, including past or present subduction or alternatively, delamination of overthickened continental lithosphere (Platt and Vissers, 1989; Seber et al., 1996; Calvert et al., 2000). Subduction models have been proposed with southward (Sanz de Galdeano, 1990; Morales et al., 1999), northward (Torres-Roldan et al., 1986), eastward (Royden, 1993; Lonergan and White, 1997) and westward dips (Docherty and Banda, 1995; Zeck, 1997).

In the Alpine-Mediterranean compressional system, which has formed in response to the convergence between the African and Eurasian plates, the emplacement of allochthonous units took place in the Gulf of Cadiz during the Tortonian (ca 7.1-11.2 Ma) (Maldonado et al., 1999). Four main tectonic allochthonous provinces surround the internal zones of the Gibraltar arc orogenic belt, which overlies both the Iberian and African passive margins. These include: (1) the flysch units of the Campo de Gibraltar complex; (2) the external zones, a tectonically detached Mesozoic sedimentary succession ranging from Lower Jurassic to Upper Cretaceous-Paleocene pre-tectonic units; (3) the Triassic Diapir Zone, composed mainly of salts, gypsum and shallow carbonate deposits emplaced as diapiric expulsion structures by thrusting of thick nappes of Mesozoic sediments (Berastegui et al., 1998); and (4) the front of a deformed wedge, mainly formed by plastic clays and marls of Early-Middle Miocene age (Maldonado et al., 1999).

The most frontal parts of the Gibraltar arc are composed of Triassic evaporites and Miocene plastic marls and have been referred to traditionally as the 'Olistostrome Zone' (Perconig, **1960-62**) or 'Gualdalquivir Allochthonous Unit' (Blankenship, 1992) (**Fig. 4.1**). Major gravitational gliding nappes, which have been identified in the Gulf on the Spanish-Portuguese (Cadiz Salt Nappe) and Moroccan margins, were detached from the front of the Gibraltar arc (Lowrie et al., 1999). Since the early Pliocene, the former plastic olistostrome mass, with a thickness exceeding 2.4 km, has extended from the shelf towards the Horseshoe and Seine abyssal plains, west of the Gibraltar arc (Torelli et al., 1997).

Deformation structures observed on migrated multifold seismic lines along the shelf and slopes of the Gulf of Cadiz provide geometric evidence for shale/salt tectonics and related hydrocarbon seepage on the sea floor (Baraza and Ercilla, 1996; Battista et al., 2000; Somoza et al., 2001). Overpressure compartments generated beneath salt/shale wedges provide avenues for hydrocarbon gases, fluids (brine waters) and fluidised sediments to flow or seep upwards through contractional toe-thrust structures to form seepage-related structures on the sea floor (Lowrie et al., 1999).

### *4.2. The great 1755 Lisbon earthquake*

The Great Lisbon earthquake of 1755 is the most destructive earthquake in European history, with an estimated magnitude of 8.5 - 9.0 (Martinez-Solares et al., 1979; Johnston, 1996) (**Fig. 2.1**). Yet, the tectonic source of this earthquake, which caused tens of thousands of deaths and triggered a devastating tsunami along the coasts of Southwest Iberia and Northwest Morocco remains unknown to this day (Baptista et al., 1998). Several authors have recently proposed one or more basement highs at the SW extremity of the SW Iberian Margin to be the source of the 1755 earthquake (Zitellini et al., 2001; Terrinha et al., 2003; Gracia et al., 2003a). However, the structures proposed appear to be too small to generate an event of magnitude >8.5. The source region off SW Iberia is located at the eastern end of the portion of the Africa – Eurasia plate boundary commonly referred to as the Azores – Gibraltar transform (Sartori et al., 1994; Tortella et al., 1997; Jimenez-Munt et al., 2001). In Southern Iberia, the plate boundary is not clearly defined and encompasses a broad region of deformation at least 200 km wide (in a N-S direction) marked by moderately high seismicity (Negredo et al., 2002; Stich et al., 2003) (**Fig. 4.1B**). Present day plate convergence between Africa and Eurasia here is slow, only 4 mm/a along a NW-SE vector (Argus et al., 1989). However, plate kinematic reconstructions of the evolution of the adjacent Western Mediterranean region indicate periods of rapid micro-plate movement and subduction from the Oligocene to present (Rehault et al., 1985; Lonergan and White, 1997; Facenna et al., 2001). Subduction of Tethyan oceanic lithosphere beneath the SW margin of Europe, led to back-arc rifting and locally to seafloor spreading and provoked large scale rotation and migration of Alpine crystalline massifs to present day positions in Calabria, the Kabylies and the Betic-Rif belt.

The arcuate Betic-Rif orogen is comprised of internal Alpine crystalline units and Eocene and younger allocthonous units with NW and SW vergent thrust nappes. This so called Gibraltar Arc is non-volcanic and surrounds the West Alboran Sea, a region where strong Neogene subsidence occurred co-evally during westward nappe transport (Lonergan and White, 1997). Miocene and older calc-alkaline volcanism is scattered across the West Alboran Sea. The geodynamics of this region has been interpreted in terms of east dipping subduction (Royden, 1993; Lonergan and White, 1997), though many alternate models exist. Geochemical studies of Alboran Sea magmatic rocks indicate subduction volcanism occured here until at least Miocene times (Duggen et al., 2003; 2004). Recent marine geophysical data, combined with tomographic images, provide compelling evidence for current activity of eastward dipping subduction beneath the Gibraltar Arc. Seismic reflection profiles and wide-angle profiles in the Gulf of Cadiz document an accretionary wedge, with active thrust faults soling out to an east dipping decollement and overlying an eastward dipping basement (Gutscher et al., 2002). The discovery of active mud volcanoes throughout the accretionary wedge lends further support to the interpretation of currently active subduction (Pinheiro et al., 2003).

Thiebot and Gutscher (2004) propose that the active subduction zone represents a possible source region for the 1755 earthquake. Their investigation is based on the 3-D geometry of the shallow, east dipping fault plane associated with the Gibraltar subduction system from seismic reflection data (**Fig. 4.2**), gravity modeling, the distribution of hypocenters, tomographic cross sections to determine the deeper geometry (>20 km), and thermal modelling of the potentially seismogenic zone from the Gibraltar Arc to the Alboran Sea. Seismic profiles image the deformation front at numerous locations arrayed along a horseshoe pattern in the deep Gulf of Cadiz at 2000 – 4300 m water depth. The same pattern is observed repeatedly; undeformed horizontal basal reflectors, beneath a detachment horizon, seaward vergent (W, SW or NW) ramps intersecting the seafloor at a slope break between the horizontal abyssal plain surface, and the gentle 1° undulating surface slope at the toe of the accretionary wedge (Thiebot and Gutscher, 2004; **Figs. 4.2 and 4.3**). The east dipping decollement and top basement interfaces demonstrate that deformation is tectonic and not gravitational in origin.

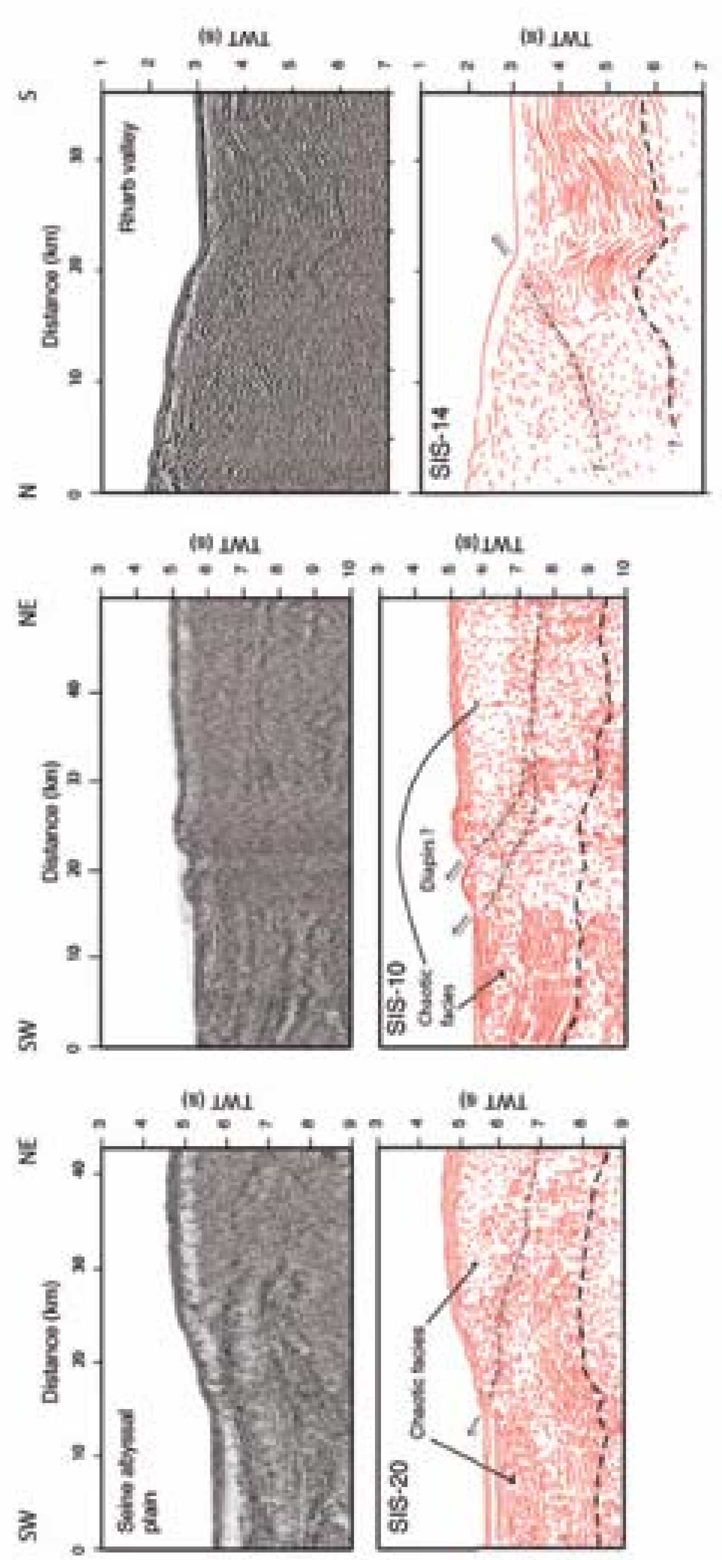


**Fig. 4.2.** Multichannel seismic profile SIS-16, pre-stack depth migrated section. Central panel shows the entire 185 km long profile at a vertical exaggeration of 3:1. The lower panel is an interpreted line drawing (a depth cross-section). Upper panels show zooms of ramp thrusts emerging at the seafloor and the basal undeformed strata beneath the decollement. Thin dashed line is the decollement. Thick dashed line is top basement, inferred to be oceanic. Top continental basement has shorter dashing. Modified from Thiebot and Gutscher et al., 2004.

The heat flow models presented by the same authors offer further proof of active subduction since only an actively sinking slab can generate the vigorous back-arc convection and rapid transfer of cold lithosphere to the 660 km discontinuity. These characteristics (offered by models with subduction velocities of 10 – 20 mm/a) are necessary to explain the high back-arc heat flow (120 $mW/m^2$ in the West Alboran Sea) as well as deep focus seismicity at 660 km depth. Very slow to inactive subduction cannot generate the wedge shaped zone of hot material seen in tomographic sections. Thermal modeling indicates a 200 km down-dip width of the seismogenic zone. Together with the seismic data, a potentially locked subduction fault plane with dimensions of about 180 km (N-S) x 200 km (E-W) is indicated. Such a fault is capable of generating an M 8.6 - 8.8 earthquake for 10 – 20 m of co-seismic slip.

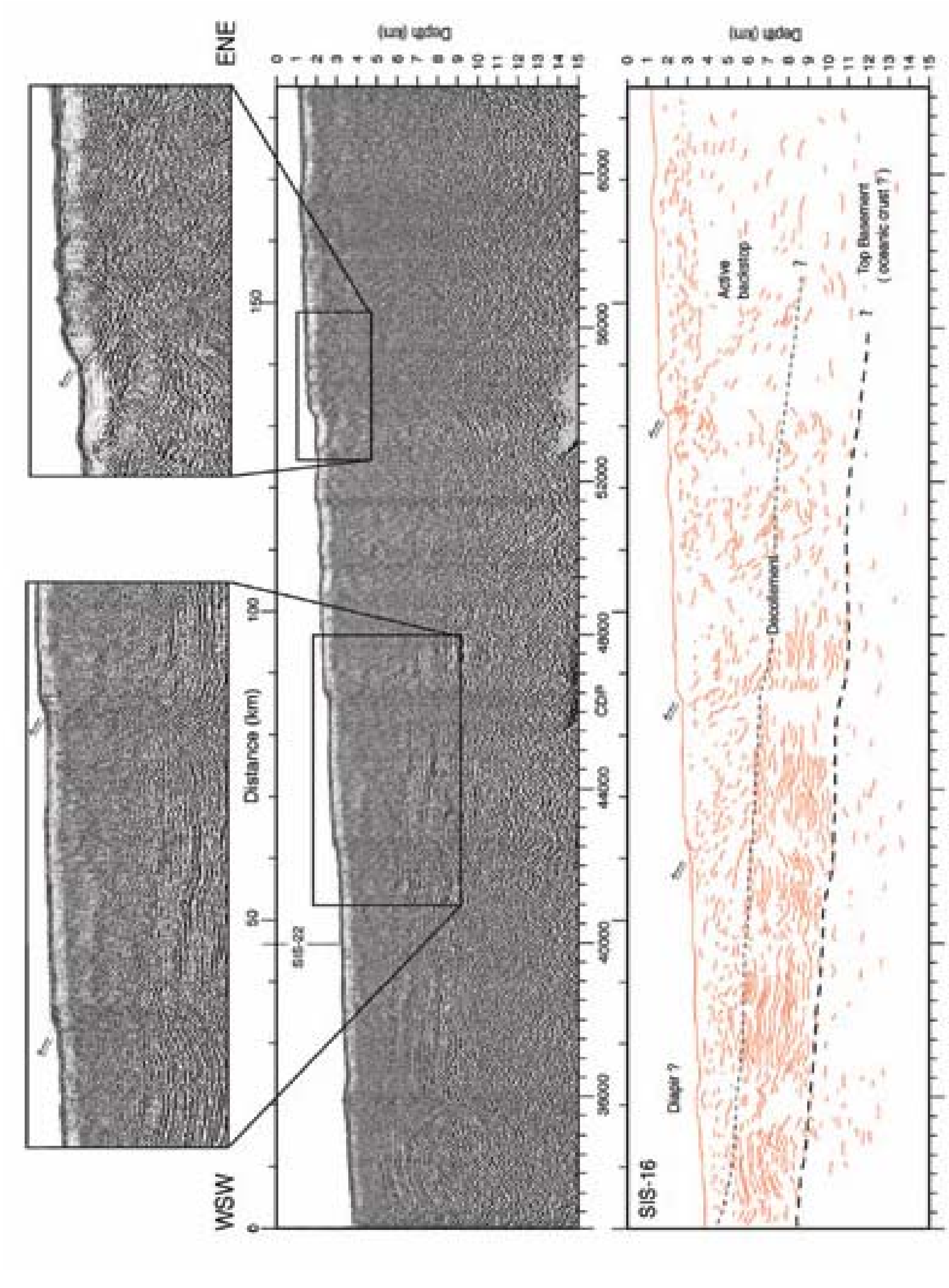


**Fig. 4.3.** Close-up views of the deformation front along several SISMAR multichannel seismic profiles accompanied by interpreted line drawings (time sections in TWT). A: SIS-10, B: SIS-14, C: SIS-20. For positions see **Fig. 4.1.A**. In each case ramp thrusts can be seen at the deformation front rising to the seafloor from the detachment horizon. A basal series of undeformed horizontal sediments is imaged beneath the decollement. The two dome shaped features observed on profile SIS-10 may be anticlinal ridges related to ramp thrusts, mud volcanoes or salt diapirs.Modified from Thiebot and Gutscher, 2004.

# 5. Methods

## 5.1. Sea Floor Mapping, Multibeam swathmapping, Water Sound Velocity (CTD)

(I. Grevemeyer, A. Kopf)

*Echosounder*

During the SO175 cruise, the Simrad EM120 multibeam echosounder was used for a continuous mapping of the seafloor. The echosounder consists of several units: (i) a transmit and a receive transducer array is fixed in a Mills cross below the keel of the vessel; (ii) a preamplifier unit contains the preamplifiers for the received signals; (iii) the transducer unit contains the transmit and receive electronics and processors for beam-forming and control of all parameters with respect to gain, ping-rate and transmit angles. Furthermore, the system monitors via serial interfaces the ship's motion, such as roll, pitch and heave, external (GPS) time and vessel position. A high performance SUN workstation is used as an Operator station. The Operator station processes the collected data, applies standard corrections, displays the results, and logs the raw data to internal or external disks.

Simrad EM120 uses a frequency of about 12 KHz with a whole angular coverage sector of up to 150° (75° per port-/starboard-side). One ping is sent and the receiving signal is formed into 191 beams by the transducer unit through the hydrophones in the receiver unit. The beam spacing can be defined as equidistant or equiangular, or a mix of both. Running the system in full 150°-configuration the EM120 maps a swath of roughly 4-5 times the water depth. The ping-rate depends on the water depth and the runtime of the signal through the water column. Depending on the state of the sea, an opening angle of 60-70° was used, restricting the coverage to a max. 14 km wide swath to gain an more continuous spacing of beams on the ocean floor. The spacing within this limits was controlled automatically by the echosounder system.

To convert the recorded travel times into depth several water velocity profiles were obtained with the shipboard CTD and entered into the operator SUN workstation. During the cruise data handling of the bathymetric data was done by the ship's system administrators. Each beam was corrected for ray bending using the appropriate sound velocity profile and the ship's motion and were finally stored with GPS position. To generate maps the data were averaged using the nearest neighbour gridding algorithm of GMT (Smith and Wessel, 1991) and displayed with the

GMT mapping software. However, data were not edited for bad beams. Final data editing of the data has to be done in a post-cruise phase.

*CTD*

To obtain information about the distribution of the water masses along the Iberian coast a CTDOS (Conductivity, Temperature, Depth, Oxygen, Salinity) profiler combined with a rosette water sampler (24 Niskin bottles, 1 l volume, HydroBios) was used at two different sites during SO175 (**Fig. 5.1**). One crucial aspect was to determine where the areas with a strong influence of saline, warm Mediterranean outflow water (MOW) may be. The CTD data were also needed for the conversion of the recorded SIMRAD EM120 travel times into depth values.

**Figure 5.1.** CTD on main deck of RV *Sonne* prior to deployment.

### 5.2. Parasound profiling

(M.-A. Gutscher, L. Somoza)

The PARASOUND system works both as a low-frequency sediment echosounder and as a high-frequency narrow beam sounder to determine the water depth. It makes use of the parametric effect, which produces additional frequencies through non-linear acoustic interaction of finite amplitude waves. If two sound waves of similar frequencies (here 18 kHz and e.g. 22 kHz) are emitted simultaneously, a signal of the difference-frequency (e.g., 4 kHz) is generated for sufficiently high primary amplitudes. The new component is travelling within the emission cone of the original high frequency waves, which are limited to an angle of only 4° for the equipment used. Therefore, the footprint size of 7% of the water depth is much smaller than for conventional systems and both vertical and lateral resolution are significantly improved.

The PARASOUND system is permanently installed on the ship. The hull-mounted transducer array has 128 elements on an area of ~1 $m^2$. It requires up to 70 kW of electric power due to the low degree of efficiency of the parametric effect. In 2 electronic cabinets, beam forming, signal generation and the separation of primary (18, 22 kHz) and secondary frequencies (4 kHz) is carried out. With the third electronic cabinet in the echosounder control room the system is operated on a 24-hour watch schedule.

Since the two-way travel time in the deep sea is long compared to the length of the reception window of up to 266 ms, the PARASOUND System sends out a burst of pulses at 400 ms intervals, until the first echo returns. The coverage of this discontinuous mode depends on the water depth and produces non-equidistant shot distances between bursts. On average, one seismogram is recorded about every second providing a spatial resolution on the order of a few meters on seismic profiles at 4.9 knots.

The main tasks of the operators are system and quality control and the adjustment of the upper limit of the reception window. Because of the limited penetration of the echosounder signal into the sediment, only a small depth window close to the sea floor is recorded.

In addition to the analogue recording features with the b/w DESO 25 device, the PARASOUND System was equipped with the digital data acquisition system PARADIGMA, which was developed at the University of Bremen (Spiess, 1993). The data were stored using the standard, industry-compatible SEGY-format. The 486-processor based PC allows the buffering, transfer, and storage of the digital seismograms at very high repetition rates. From the emitted series of pulses, usually every second pulse could be digitised and stored, resulting in recording intervals of 800 ms within a pulse sequence. The seismograms were sampled at a frequency of 40 kHz, with a typical registration length of 266 ms for a depth window of ~200 m. The source signal was a band limited, 2-6 kHz sinusoidal wavelet of 4 kHz dominant frequency with a duration of 2 periods (~500 μs total length).

Already during the acquisition of the data an online processing was carried out. For all profiles PARASOUND sections were plotted with a vertical scale of several hundred meters. Most of the changes in window depth could thereby be eliminated. From these plots a first impression of variations in sea floor morphology, sediment coverage and sedimentation patterns along the ships track could be gained. To improve the signal-to-noise ratio, the echogram sections were filtered with a wide band pass filter. In addition the data were normalised to a constant value much smaller than the maximum average amplitude, to amplify in particular deeper and weaker reflections. The main aim of using the PARASOUND system was the selection of suited sites for sediment sampling and deployment of the pore pressure lance, and to characterize the toe of teh Gibraltar wedge.

### 5.3. Seismic reflection

(I. Grevemeyer, N. Kaul, B. Heesemann, E. Thiebot)

#### *Instrumentation*

*Seismic Source*

The seismic signal was generated by one GI gun. The total volume of the GI gun is 150 $in^3$ (1,7 l). GI Guns are pneumatic seismic sources which are constituted of 2 independent air guns within the same body casing. The first gun generates the primary pulse (generator). The second air gun (injector) is used to control oscillation of bubble produced by the generator. Each gun has its own reservoir, its own shuttle, its own set of exhaust ports, and its own solenoid valve. Volumes of both generator and injector can be adjusted by inserting plastic volume reducers inside respective chambers. For both chambers standard volumes are 45, 75, and 105 $in^3$. Port hole reducers are available as well.

During this cruise we used the "True GI Mode". No volume reducers were used on this cruise. In this case the total air consumption is 150 $in^3$. No port hole reducers are used. In GI mode, injection is tuned to optimally suppress the oscillation of the bubble (**Fig. 5.2**). The hydrophone signal was passed to an oscilloscope for source signal control (**Fig. 5.2**).

Compressed air is provided by build in LMF compressors at maximum nominal pressure of 160 bar.

The trigger signal was supplied from a dedicated PC system with a programmable SORCUS timing card . This system provided trigger pulses for generator and injector valve and for the recording system. Time base is the SORCUS card.

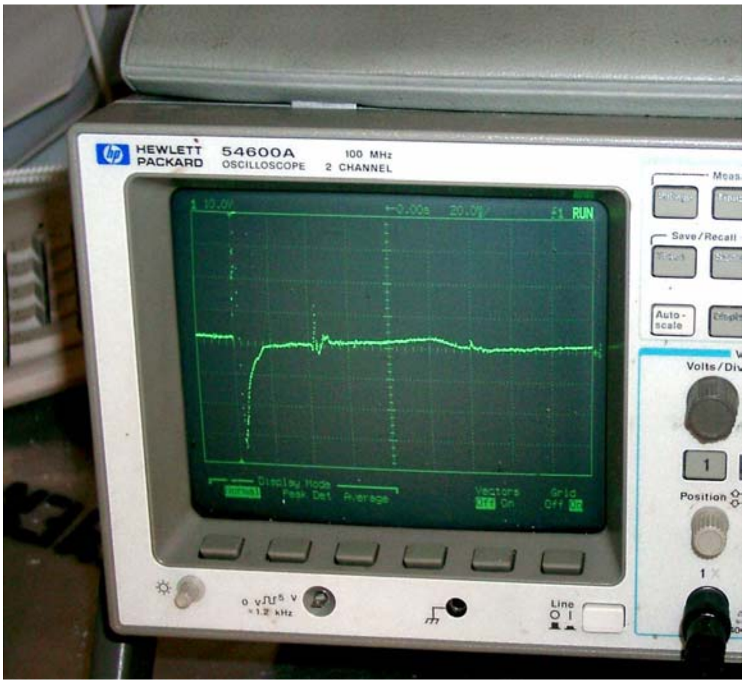


**Figure 5.2.** Near field signal of GI GUN in "True GI Mode". The oscillation of the bubble is optimally suppressed.

During SO175, the seismic source is operated from the port side of the aft deck. The mechanical set up has been as follows: one buoy is fixed to the rear eye of the gun hanger with app. 3 m of rope. The seismic source is mounted horizontally 1 m below the gun hanger. The 18 mm steel wire from the air gun rail on port side is employed as tow wire. It was fixed to the center of the gun hanger. The strength wire of the umbilical is fixed to the front eye of the hanger. In this configuration, towing force is provided through the central steel wire. Position of air gun is 15-20 m behind the vessel.

The components and setting of the systems in use are:

- GI gun, 1.7 l, true GI mode, 20 - 50 ms delay @ 140 bar as source
- Teledyne streamer, 16 channels, 6.25 m each, 25 m stretch section, 125 m lead in as receiver
- Bison 48 Jupiter system, 48 channels, 0.250 ms sampling interval
- DLT drive @ 20 GB uncompressed
- Time trigger system with SORCUS card, allowing water delay and GI delay modification.
- Shot distance 10 sec. @ 5 kn survey speed

The system is trimmed for high resolution therefore the source depth is at 1.5-4 m and the streamer depth at 5 m. A subbottom penetration of app. 300 ms can be achieved.

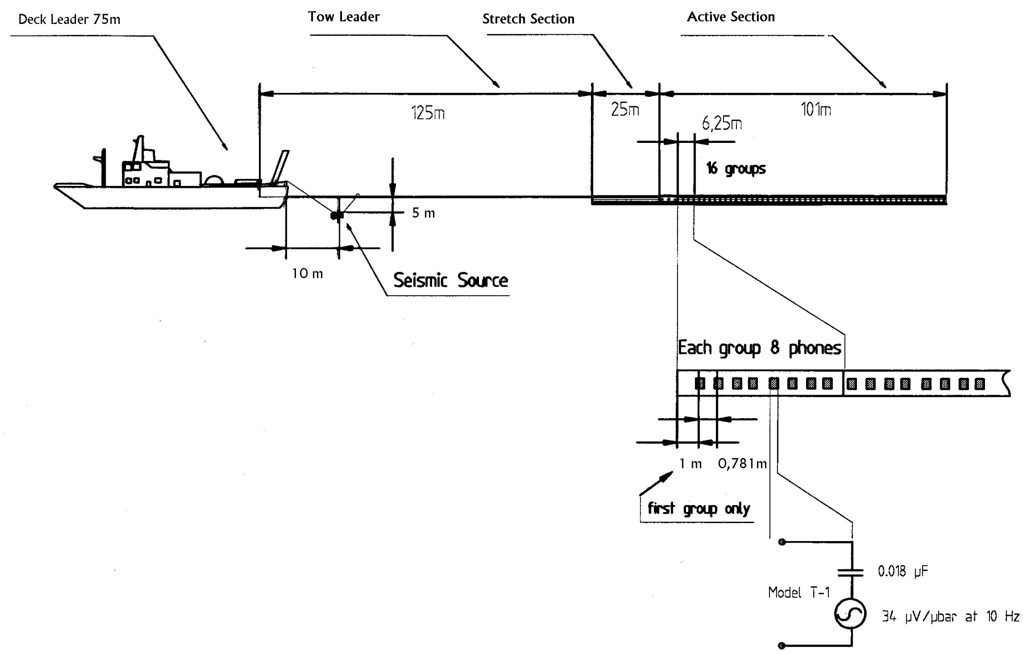


**Figure 5.3.** Schematic sketch of the seismic acquisition configuration

*Data Acquisition*

The reflection seismic data are obtained using a 100 m active length streamer. It is a 16 channel unit built by Teledyne Exploration Co. in 1993. The system comprises four parts, a 101 m active length, a 25 m stretched section, a 120 m tow leader, and a 75 m deck leader (**Fig. 5.3**). The active length is separated into 16 groups of 8 hydrophones. Within one group the hydrophones are 0.78 m apart building a 6.25 m long unit. The whole unit is stored and operated from a manual winch amidship of RV SONNE. Tailrope is 20 m. The streamer is towed from the starbord side of the aft deck.

For recording, a BISON 48 Jupiter system from the University of Bremen has been used. Data are recorded with a record length of 3 s, a sample interval of 0,25 ms, and a water delay of 1-4 s. Data are filtered by a programmable analog input filter of the acquisition system which in this case is active from 8-4000 Hz.

Quality control of each channel showed a good signal to noise ratio in channels 1, 2, 3, 4, 5, 9, 10, 12, 14, and 16. Channels 6, 7, 8, 11, 13, 15 are dead. All data are stored on tape and are edited afterwards for poor traces. Data are stored on a 20 GB DLT tape in uncompressed mode.

### 5.4. Heat flow measurements

(N. Kaul, B. Heesemann, I. Grevemeyer, J. Poort)

#### 5.4.1. Heat Probe and Shipboard Operation

On cruise SO175 the heat flow probe, a Lister type violin bow design (**Fig. 5.4**), from the University of Bremen, *Meerestechnik und Sensorik* was used to obtain temperature gradients and *in-situ* thermal conductivities by a pulsed heat source method. The active length of sensor string is 3 m, with 11 thermistors spaced every 0.3 m. Two 8-channel 16 bit A/D converters are used to record the digital data into solid state memory. The instrument is used in conjunction with an online data transmission (**Fig. 5.5**). Additionally, miniaturised autonomous temperature data loggers (MTL, **Fig. 5.6**; Pfender and Villinger, 2002) were used to obtain thermal gradients at selected coring stations. Four MTLs were attached at 1.1 m interval to the gravity corer to gain sediment temperatures. At stations in waters deeper than 4500 m, MTLs were used to make temperature determinations instead of the Lister probe, which is rated to water depth of 4500 m. Four temperature loggers were mounted onto the strength member of the heat probe. The spacing of the loggers was 0.8 m.


**Figure 5.4.** Photograph of heat flow probe during SO175.

On this cruise, following instruments were in service:

Parameters of Lister-type heat probe:

| | |
|---|---|
| Probe #: | #6845 |
| Pressure sensor: | #60779 |
| Stings: | 96-5;20-11-02;96-1 |
| Heating current: | 8 Amp |
| Heat pulse: | 600 J/m |
| Pulse duration: | 20 sec |
| Sample rate: | 10 sec |
| Online data transmission: | 2400 Baud net via coax wire |
| Wire: | 7760 m 18 mm deep sea cable (W1) with LWL and coax |

Parameters of autonomous temperature data loggers:

| | |
|---|---|
| Instruments: | 1854116A, 050A, 051A, 052A |
| Sample rate: | 1 sec |
| Recording length: | 18:03 h potential maximum |
| Spacing: | 1.10 to 0.8 m |

The University of Bremen Lister type heat probe (**Fig. 5.4**) has the capability of autonomous operation for at least 48 hours due to memory and power capacity. During a single deployment a minimum of 20 heat pulses, equating to 20 sets of thermal conductivity measurements, can be made. Data security is guaranteed by two-fold recording into solid state memory and on deck data logging.

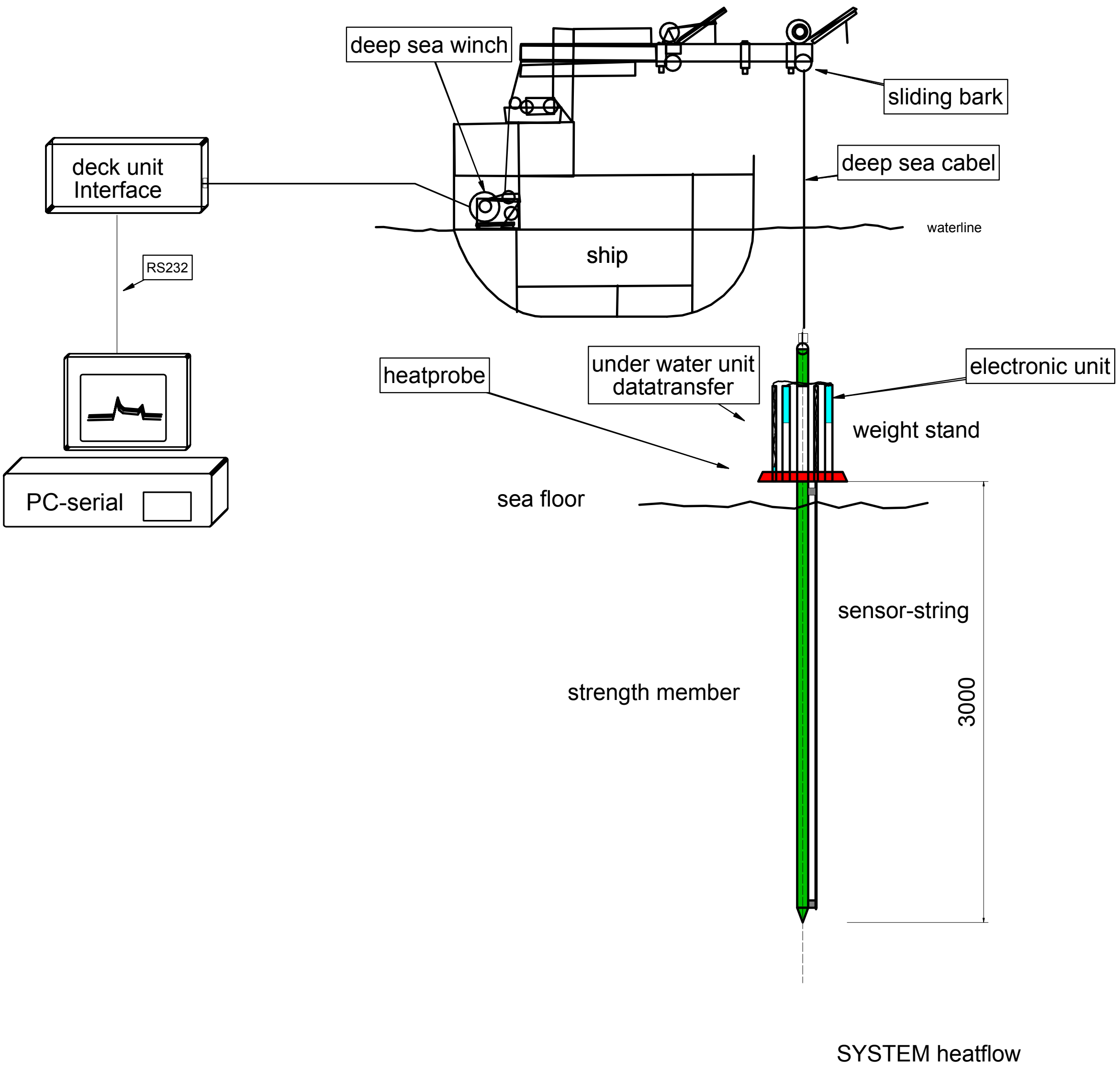


**Figure 5.5** Schematic sketch of the heat flow probe.

Measurements are made in so called ‘pogo-style’, performing many penetrations in a row at small distances. Each penetration consists of raising the probe some hundred meters above the sea floor from the previous penetration, slowly moving the ship to the next penetration site and letting the wire angle become nearly vertical before dropping the probe into the sediment for the next penetration. Once the probe is in the bottom, it is left undisturbed for 7 minutes for the equilibrium temperature measurements and another 7 minutes, if a thermal conductivity measurement is made. For the penetration spacing used in this survey, transit between penetration points lasts about 30 – 75 minutes, a recording cycle in the sea floor is either 7 or 14 minutes, yielding a rate of about one hour per penetration. Transit speed is governed by the trade-off between keeping the wire angle small and minimising the time between penetration points.

Winch speed during payout and retrieval of wire is 1-1.2 m/s. The initial penetration velocity is generally 1.2 m/s. Deployment of the instrument is amid ship on the starboard side (**Fig. 5.4**), employing a beam crane and one assistance crane. This procedure ensures safe operation even during medium sea state and minimum interference due to the ships vertical movement during station work. Two deckhands are necessary during deployment because the assistance crane can not be run simultaneously with the beam crane. A bottom finding pinger is mounted 50 m above the instrument and can be monitored via a Atlas DESO pinger recorder, switched to passive mode. This set-up is useful as a backup in case of other failures.

**Figure 5.6** Photograph of mini-temperature logger installed on gravity core.

To achieve spatially high resolution of heat flow determinations, penetrations were usually positioned between 300 (on top of mud volcanoes) and 1000 to 2000 m apart for regional studies.

### 5.4.2. Heat flow data reduction

Processing temperature data includes calibration of thermistor sensors, calculation of sediment temperatures and temperature gradients, correction for probe tilt during penetration, and calculation of thermal conductivites. While the 7 minute wait is not long enough for the sediment temperatures to return to equilibrium after the frictional disturbance of penetration, it is long enough to extrapolate to an equilibrium temperature with a high degree of precision. Each temperature-time series, from each thermistor, is extrapolated to an equilibrium temperature by the program T2C (Hartmann and Villinger, 2002). Because the calibration of each thermistor by the manufacturer is only good to 0.1°C, a secondary calibration is applied. This is usually done in deep marine environment (> 3000 m water depth) where negligible thermal gradients exist within the limits of observation. In other marine environments temperature gradients in the water column are surveyed with a CTD. For the secondary calibration purposes the heat flow probe is allowed to equilibrate at a certain depth (usually 200 m above seafloor).

Fourier's law of heat conduction in one-dimension shows that heat flow (Q) is the product of the thermal gradient (dT/dz) and thermal conductivity (k). If these terms are constant over the depth of the measurements then the calculation of heat flow is trivial. However if these values are changing proportionately to each other, as is the case for a constant basal heat flux, then heat flow can be derived from Bullard's (1939) relation given by,

$$\Delta T = Q \; S \; \Delta \tilde{z}_i k_i,$$

Where $\Delta z_i$ is the thickness and $k_i$ is the thermal conductivity over the i-th interval. In this case heat flow can easily be calculated as the slope of the line given by the summation. To properly calculate the temperature gradient a correction for the penetration tilt angle is applied. In most cases the tilt angle is less than 10° and the tilt correction is modest. Determination of thermal conductivity requires the knowledge of the amount of heat, dissipated into the sediment. Therefore a pulsed heat source is used (approximated by a 20 second pulse of 600 J/m), producing a set of 11 thermal conductivities. Because thermal conductivities are sensitive to the sediment porosity over the depth range of the measurements, these measurements can reflect the reduction of porosity within the upper three meters of sediment. Thermal conductivities are summarized as harmonic means.

### 5.5. Ocean Floor Pore Pressure System

(N. Kaul, B. Heesemann)

On R/V *Sonne* Cruise 175 to the Gulf of Cadiz one pore pressure probe is deployed. It was developed within the gas hydrate related and BMBF funded project INGGAS. The aim of the instrument is to measure *in situ* differential pore pressure within the uppermost 3 m of sediment column. Differential pore pressure is a prerequisite for fluid flow which is the final goal of the investigation.

**Scientific Rationale**

Gas hydrates, which are abundant in the Gulf of Cadiz below a water depth of approximately 800 m are a result of accumulated methane. State of discussion is that accumulation of either biogenic or thermogenic methane is accelerated by upward moving pore fluid. Vertical movement through the gas hydrate stability zone (GHSZ) and accumulation of high concentration then leads to generation of gas hydrates.

As enhanced concentration of methane and free gas occur in the water column above the GHSZ at certain location (i.e. Håkon Mosby mud volcano, off Norway; Mount Culebra, off Costa Rica), it is still an open question, if the GHSZ represents a dynamic equilibrium for clathrates and if fluid flow through the GHSZ occurs at reasonable rates. Fluid flow may or may not be associated with increased heat transport.

**Instrument**

The differential pore pressure tool (**Fig. 5.7**) is a new development *Universität Bremen, Fachgebiet Meerestechnik und Sensorik*, together with industrial partners for electronic components. It consists of three major components:

- lance of 4.5 m length with attached pressure ports and temperature sensors.

- data collection compartment with 8 channel AD converter, a high precession differential pressure gauge and a hydraulic multiplexer.
- a communication buoy for data transmission, employing a satellite connection.

Three pressure ports are mounted to the bottom penetrating lance with port holes in 4, 3, 2 m below seafloor. A fourth one is open to seawater as a reference. All are connected to one hydraulic multiplexer and one differential pressure gauge. The pressure gauge, supplied by Keller Druckmesstechnik, has a resolution of 0.1 mPa.

Additionally, temperature sensors are mounted at 4, 3, 2 m below seafloor.

The deployment time is 4 weeks. The long observation duration is due to the decay time of the pressure disturbance during penetration.

Data recovery will be by file transfer via IRIDIUM satellite link. Therefore the communication buoy has to pop up to the surface after a pre-selected time span. The actual capacity is set to a maximum amount of 1 Mb of data.

**Fig. 5.7.** Deployment of INGGAS differential pore pressure probe in the Gulf of Cadiz. Major components can be identified: lance with pressure ports, data sampling compartment and satellite communication buoy.

## 5.6. Video-guided systems (Multicorer, gravity corer, TV-grab, OFOS)

(W. Brückmann, D. Hebbeln)

### 5.6.1. Video-guided Multicorer and gravity corer

The main tool for the sampling of undisturbed surface sediments and the overlying bottom water was the multicorer (MUC) equipped with six plastic tubes (diameter of 10 cm) of 60 cm length (**Fig. 5.8**). The multicorer was equipped with two video cameras allowing a deployment of the instrument at the spot. In case special targets were selected for sampling, the MUC was towed by the SONNE just above the sediment surface. When small-scale targets came into view, the MUC has been lowered to the sea floor and the target has been sampled.

**Fig. 5.8.** Photograph of TV-guided Multicorer.

In order to recover longer sediment cores, a gravity corer with tube lengths of alternatively 6 m (SL 6) or 12 m (SL 12) and a weight of 1.6 tons was used . Before using the coring tools, the plastic liners inside the steel tubes have been marked lengthwise with a straight line in order to retain the orientation of the core for subsequent paleomagnetic analyses. Once on board, the sediment core was cut into 1 m sections, closed with caps on both ends and labelled according to a standard scheme (**Fig. 5.9**).

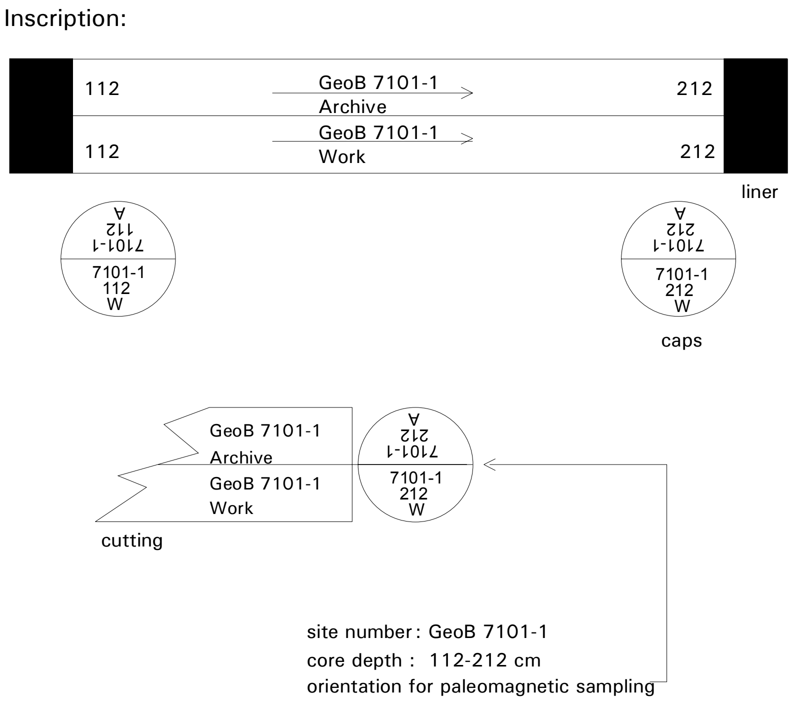


**Fig. 5.9.** Scheme of the inscription of gravity core segments

### 5.6.2. TV-guided grab sampler (TVG)

The TVG provides a means of collecting large volumes of surface sediments from the seafloor, which has proved useful especially for collecting large rock samples or gas hydrates embedded in sediment (**Fig. 5.10**). The TVG is equipped with black and white and a color video cameras looking downwards through the open lids of the grab. Positioning is provided by an SSBL responder, connected to a fibre-optic cable 50 m above the tool.

Once a sampling target has been identified, the tool is set down on the sediment surface and hydraulically closed. The energy for closing the grab is provided by deep-sea batteries which allow for about 3-5 closings, depending on the length of the operation, as the lights are also powered by the same batteries.

**Figure 5.10.** TV-guided sediment grab.

### 5.6.3. Ocean Floor Observation System (OFOS)

The OFOS system (**Fig. 5.11**) on board RV *SONNE* is a sophisticated deep-towed camera sled that has been adapted to satisfy a wide range of scientific requirements. OFOS is equipped with the following instruments: two videocameras (color camera: Deep Sea Power and Light, black and white camera: Photosea), a stereo still camera (Photosea), various xenon and halogene lights (Deep Sea power and Light), CTD (Seabird), a compass, pitch and roll sensor, and a SIMRAD SSBL (super short baseline) responder.

The sled is towed behind the ship at a speed of 0.5 - 0.8 knots (kn). The distance of about 1.5 m to the seafloor is manually adjusted by the winch operator. To aid the winch operator in assessing the distance to the seafloor, a weight on a 2 m rope is attached to the bottom of the sled. Two laser pointers can be used to scale the video image and the still camera images. The two laser pointers are parallel and 20cm apart, while a third one points downward at an oblique angle providing an estimate of the absolute distance o the seafloor.

The still camera is loaded with a slide film (Kodak Ektachrome 100) with a maximum of 800 shots. Images were taken manually by the OFOS observers – optionally images can be taken at regular time intervals. Date and time (UTC) information is superimposed on the black and white and color video signals from the two OFOS cameras. The video streams were recorded on two analog VHS video recorders, in addition the black and white stream was digitized online and recorded to DVD. Ships position data, SSBL position data, OFOS CTD data and an online protocol written by the OFOS observers are recorded in the DVS database system of the ship. After a complete OFOS deployment all relevant data were downloaded and stored in a database referenced in UTC time.

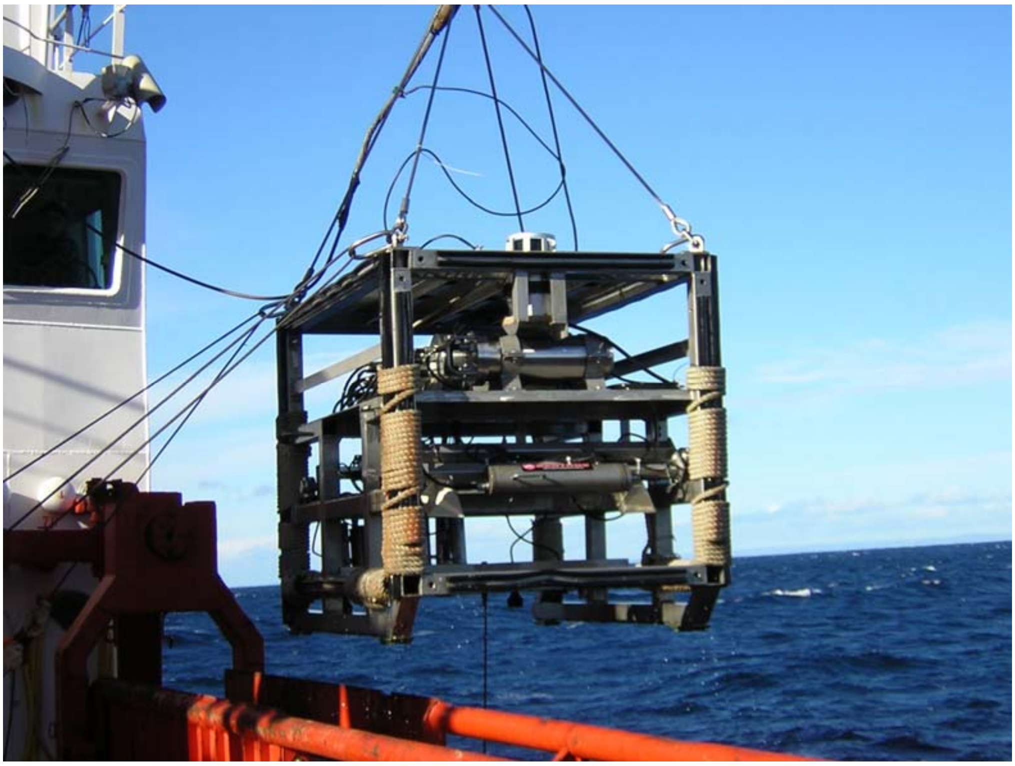

**Figure 5.11.** OFOS video sledge on deck of RV *Sonne*.

## 5.7. Core logging with MST

(W. Brückmann, A. Kopf)

The MST was used for non-destructive measurements of wet bulk density, P-wave velocity, magnetic susceptibility, and natural gamma radiation on unsplit cores. It is located in an air-conditioned, custom 20' oversea container which is placed on deck (**Fig. 5.12**). The techniques of the MST unit work as follows:

***Multisensor Track Measurements***

The first measurement station was the MST, which combines four sensors on an automated track to measure magnetic susceptibility, bulk density, P-wave velocity, and natural gamma-ray emission on whole-core sections. The four MST sensors are the magnetic susceptibility meter, the gamma-ray attenuation (GRA) bulk densiometer, the P-wave logger (PWL), and the natural gamma-ray (NGR) detector. Magnetic susceptibility, bulk density, and natural gamma-ray emission were generally measured on all cores.

***Magnetic Susceptibility***

Magnetic susceptibility was measured with a Bartington meter MS2 using an 80-mm internal diameter sensor loop (88-mm coil diameter) operating at a frequency of 565 Hz and an alternating field of 80 A/m (0.1 mT). The sensitivity range was set to the low sensitivity setting (1.0 Hz). The sample period and interval were set to 2 s and 4 cm, respectively, unless noted otherwise. The mean raw value of the measurements was calculated and stored automatically. The quality of these results degrades in XCB and RCB cores, where the core may be undersized and/or disturbed. Nevertheless, general downhole trends are useful for stratigraphic correlations. The MS2 meter measures relative susceptibilities, which have not been corrected for the differences between core and coil diameters.

***Gamma-Ray Attenuation***

Bulk density was estimated for unsplit core sections as they passed through the GRA bulk densiometer using sampling periods and intervals of 2 s and 4 cm, respectively, unless noted otherwise. The gamma-ray source was 137 Cs. For each site, the GRA bulk densities and the bulk densities measured on discrete samples were compared.

***P-Wave Velocity***

P-wave velocity was measured at 4-cm intervals and 2-s periods with the high-resolution PWL. The PWL measured P-wave velocity across the unsplit core sections. In order to determine the P-wave velocity, the PWL transmits 500-kHz P-wave pulses through the core at a frequency of 1 kHz. The transmitting and receiving transducers are aligned perpendicular to the core axis while a pair of displacement transducers monitors the separation between the P-wave transducers. Variations in the outer diameter of the liner do not degrade the accuracy of the velocities, but the unconsolidated sediment or rock core must completely fill the liner for the PWL to provide accurate results.

***Natural Gamma-Ray Emissions***

Natural gamma-ray (NGR) emission analysis is a function of the random and discrete decay of radioactive atoms and is measured through scintillating detectors as outlined by Hoppie et al. (1994). During SO175, NGR was measured for 20 s for each 20-cm length of core unless noted otherwise. NGR calibration was performed at the beginning of the leg, and sample standards were measured several times during the cruise.

**Figure 5.12.** Logging container with MST track.

## 5.8. Sediment description and physical properties

(D. Hebbeln, B. Dorschel, W. Brückmann, A. Marti, M. Lutz, A. Kopf)

### *Sediment description and colour scanning*

Split gravity cores were described from a largely sedimentological standpoint. If necessary, smear slides helped to characterize grain size and mineralogical composition. The colour of the material was determined both visually (using Munsell colour charts) and by spectrophotometry (using a Minolta CM2002 system. Video-Multicores were described through the clear plexiglass liner, and -where necessary- using discrete samples when slicing the core for other purposes like dating, etc. All core descriptions are provided within the respective thematic sections in Ch. 6.

***Physical properties***

Physical properties were measured on unsplit cores (see Ch. 5.7 above) and on the undisturbed parts of split cores. After having passed the MST, the core was then split into a working and an archive half. While the latter was used for description purposes Portions of split, but otherwise undisturbed cores that were undisturbed by drilling, sampling, gas expansion, bioturbation, cracking, and large voids were used to obtain specimens for moisture and density measurements and calculations (wet bulk density, grain density, dry bulk density, water content, void ratio, and porosity). Physical properties measurements were conducted after the cores had equilibrated to near ambient room temperature (ca. 20°C) after ~2–4 hr. A summary of each of the physical properties measurement is outlined below.

***Moisture and Density Measurements***

Moisture and density (MAD) measurements were determined by measuring wet mass, dry mass, and dry volume of specimens from split cores. Samples were collected at a frequency of two per section. Where a whole-round sample was taken from a section, one of the two MAD samples was taken adjacent to it. Care was taken to sample undisturbed parts of the core. Immediately after the samples were collected, wet sediment mass ($M_{wet}$) was measured. Dry sediment mass ($M_{dry}$) and dry sediment volume ($V_{dry}$) were determined after the samples had dried in a convection oven for 24 hr at a temperature of 105° ± 5°C. Wet and dry masses were determined using electronic balances, which compensated for the ship's motion, and dry volume was measured using a gas pycnometer.

Moisture content, grain density, bulk density, and porosity were calculated from the measured wet mass, dry mass, and dry volume as described by Blum (1997). Corrections were made for the mass and volume of evaporated seawater using a seawater density of 1.024 g/cm$^3$ and a salt density of 2.20 g/cm$^3$.

***Cone penetrometer***

A Wykeham-Farrance cone penetrometer WF 21600 (**Fig. 5.13**) was used for a first-order estimate of the sediment's stiffness. For the measurement, the metal cone was brought to a point exactly on the split core face. A manual displacement transducer was then used to measure the distance prior to and after release of the cone (i.e. penetration after free fall of the cone). Precision is 0.1 mm of displacement. The distances measured can then be translated into sediment strength post-cruise. The method is closely related to the British standard for testing soils (BS 1377, 1991).

**Figure 5.13.** WF cone penetrometer unit used on split core surface.

## 5.9. Pore water geochemistry

(C. Hensen, M. Marquardt, K. Nass, and N. Neubert)

Investigations of the geochemical composition of pore-waters provide information to investigate the forces and impacts driving redox-reactions and mineralization processes within the upper sediment column. During cruise SO 175, the pore water composition of surface sediments was investigated at XY locations to characterize and quantify sediment diagenetic processes and fluid geochemistry. Concentration vs. depth profiles of pore-waters were determined for major nutrients, total alkalinity, chloride, hydrogen sulfide, and methane to identify locations influenced by seepage and to assess the effect of methane formation and decomposition processes. Below we first give a short overview on the procedures of sediment retrieval, pore water processing, and geochemical laboratory methods followed by a selection of major results obtained during both cruises.

***Sampling, processing, and analyses***

Sediments were generally retrieved by use of a TV-directed multicorer and a gravity corer. To prevent a warming of the sediments after retrieval all cores were immediately placed in a cooling room and maintained at a temperature of about 5°C. Supernatant bottom water of the multicorer-cores was sampled and filtered for subsequent analyses. The multicorer-core was processed immediately after recovery, mostly, in a glove box under argon atmosphere. For cores with high amounts of methane and/or gas-hydrates a faster sampling procedure outside the glove box was preferred and sub-samples for methane analyses were taken. Each core was cut into slices for pressure filtration with a minimum depth resolution of 0.5 cm. Gravity cores were cut lengthwise after recovery. On the working halves pH and Eh were determined and sample intervals between 10-50 cm were taken for pressure filtration. At sampling locations where methane was expected to be present, syringe samples were taken on deck from every cut segment surface. Occasionally, higher resolution sampling for methane analysis was carried out in the cooling laboratory immediately after storing by sawing 4 x 4 cm rectangles into the PVC liner and taking syringe samples of 3 ml sediment every 30-40 cm and injected into 24 ml septum vials containing 9 ml of a concentrated NaCl-solution. After closing and subsequent shaking methane becomes enriched in the headspace of the vial. One replicate was taken and poisoned with a saturated NaOH solution for subsequent isotopic analyses.

Each sample depth for pore water squeezing was additionally sampled for (1) the calculation of sediment density and (2) for determination of redox-sensitive elements. Porosity sub-samples were filled into pre-weighed plastic vials and redox-samples were kept in specific gas-tight containers under argon atmosphere for subsequent analyses in the home laboratory.

For pressure filtration Teflon- and PE-squeezers were used. The squeezers were operated with argon at a pressure gradually increasing up to 5 bar. Depending on the porosity and compressibility of the sediments, up to 30 ml of pore water were received from each sample. The pore water was retrieved through 0.2 µm cellulose acetate membrane filters.

Pore water analyses of the following parameters were carried out during both cruises: nitrate, ammonia, phosphate, alkalinity, ferrous iron, hydrogen sulfide, chloride, methane, fluoride, silicate, calcium, Eh, and pH. The analytical techniques used on board to determine the various dissolved constituents are listed in **Table 5.1**. Modifications of some methods were necessary for samples with high sulfide concentrations. Detailed descriptions of the methods are available on http://www.geomar.de/zd/labs/labore_umwelt/Analytik.html.

| Constituent | Method | Reference |
|---|---|---|
| Nitrate | Autoanalyer/ Spectrophotometry | Grasshoff et al. (1997) |
| Alkalinity | Titration | Ivanenkov and Lyakhin (1978) |
| Silicate | Spectrophotometry | Grasshoff et al. (1997) |
| Phosphate | Spectrophotometry | Grasshoff et al. (1997) |
| Ammonium | Spectrophotometry | Grasshoff et al. (1997) |
| Chloride | Titration | Gieskes et al. (1991) |
| Hydrogen sulphide | Spectrophotometry | Grasshoff et al. (1997) |
| Methane | Gas chromatography | Niewöhner et al. (1998) |

**Table 5.1** Techniques used for pore water analyses.

Nitrate, ammonium and phosphate were measured photometrically (with help of an autoanalyser in case of nitrate) using standard methods described by Grasshoff et al. (1997). Samples of the sediment pore water for total alkalinity measurements were analyzed by titration of 0.5-1 ml pore water according to Ivanenkov and Lyakhin (1978). Titration was finished until a stable pink color occurred. During titration the sample was degassed by continuously bubbling nitrogen to remove the generated $CO_2$ or $H_2S$. The acid was standardized using a IAPSO seawater solution. The method for sulfide determination according to Grasshoff et al. (1997) has been adapted for pore water concentrations of $S^{2-}$ in the range of millimolar amounts. For reliable and reproducible results, an aliquot of pore water was diluted with appropriate amounts of oxygen-free artificial seawater; the sulfide was fixed by immediate addition of zinc acetate gelatin solution immediately after pore-water recovery. After dilution, the sulfide concentration in the sample should be less than 50 µmol/l. Chloride was determined by titration with $AgNO_3$ standardized against IAPSO seawater. High concentrations of $H_2S$ (> 1mM) in the sample affect the measurements. Therefore, these samples were pre-treated with a 1:1 dilution of 0.01 N suprapure $HNO_3$ and stored for 1-2 days, without lid, in a cool room. For the analysis of iron concentrations sub-samples of 1 ml were taken within the glove box and immediately complexed with 20 µl of Ferrozin and afterwards determined photometrically. Fluoride was determined in 1.5 ml sub-samples by an ion-sensitive electrode.

Acidified sub-samples (35µl suprapure HCl + 3 ml sample) were prepared for ICP analyses of major ions (K, Li, B, Mg, Ca, Sr, Mn, Br, and I) and trace elements. Sulfate, DIC, $\delta^{18}O$ and $\delta^{13}C$ of $CO_2$ will be determined on selected sub-samples in the shore-based laboratories.

### 5.10. Gas and microbiology program

(H. Niemann, M. Nuzzo, T. Wilkop)

#### *5.10.1. Anaerobic methane oxidation*

Sediment samples from various gravity cores (GC), multiple corers (MUC), TV grabs were incubated for microbially mediated methane oxidation and sulphate reduction rates and sampled for cultivation experiments and FISH, DNA, and biomarker analysis

*1. Methane oxidation and sulphate reduction rates*- Sediments where separately incubated with $^{14}CH_4$ and $^{35}SO_4^{2-}$ for 24 – 48 h at *in situ* temperature and finally fixed in NaOH and Zn-Ac, respectively, for further measurements of remaining substrate ($^{14}CH_4$, $^{35}SO_4^{2-}$) and product ($^{14}CO_2$, $H_2{}^{35}S$) activity. The ratio of product to substrate activity multiplied with substrate concentrations yields then actual rates.

MUC: 4 sub cores (Ø 2.5 cm), three biological and one abiological control, where sampled from neighbouring cores immediately after recovery. Radiotracer labelled substrate was injected in 1cm intervals through small, silicon sealed holes.

GC / TV- grab: five replicates and on abiological control of 5ml of sediment slurry was incubated with radio labelled substrate in glass tubes.

*2. Bacterial counts*- 2 ml of sediment volume were fixed in 9ml of 4% formaline in sea water for 2 – 4 h.

*3. FISH*- 2 ml aliquot of sediment-formaline suspension was centrifuged and supernatant was discarded. The pellet was washed two times in 1.5 ml PBS-buffer (resuspension, centrifugation, discarding of supernatant). Finally, the pellet was fixed in a 1:1 (v:v) solution of Et-OH: PBS (50% final concentrations) and kept at –20 °C until hybridisation with oligo-nucleotide probes (taxonomically very specific fluorescence staining) in Bremen.

*4. DN-*: ca. 4g of fresh sediment was frozen at –20°C until DNA analysis in Bremen.

*5. Cultivation*- 100ml of fresh sediment was collected in glass bottles and kept at *in situ* temperature until further experiments in Bremen.

6. *Biomarker*- carbonate crusts and 80 ml of sediment were filled in glass bottles and stored at 20 °C for further analysis in Bremen

### *5.10.2. Methane biogeochemistry*

Past geochemical analysis of gas from Gulf of Cadiz mud volcanoes have revealed significantly high concentrations of $C^{2+}$ hydrocarbons, but also that differences exist between individual mud volcanoes, some of them exhibiting a much higher proportion of methane (Mazurenko et al., 2002). Methane stable isotopes measurements might help understand better the origin of the gas-bearing fluids. Microbial methane production rates and the concentration of the two main methanogenic substrates ($H_2$ and acetate), are also estimated for the purpose of constraining the proportion of gas derived from deep-sourced hydrocarbon reservoirs *versus* that due to shallower bacterial activity. Note that $H_2$ data can not be considered as representative of in situ conditions, but might show over all some trends. The specific objectives for the methane biogeochemistry study are:

- To measure the stable carbon and hydrogen isotope compositions of methane, light hydrocarbon gases and $CO_2$;
- To measure the pore water abundance of volatile fatty acids and search for trends in that of $H_2$;
- To determine rates of biogenic methanogenesis using $^{14}C$-labelled tracers to investigate whether microbial activity contributes significantly to methane accumulation in the sediments;
- To create laboratory microcosms to investigate the magnitude of stable isotope fractionation during methanogenesis under different conditions of temperature and substrate availability.

All samples are collected from gravity cores (max. 6 m). Depending on sediment availability, sub-sampling is realized at a minimum of every ±30 cm or a maximum of every ±10 cm along the core depth.

### *5.10.3.Gas composition*

*5.10.3.1. Concentration in methane and higher hydrocarbons (ethane, propane, butane)*

*Stripping of the pore water gas:*

Sediment pore water methane stripping is realized according to the method of McAullife (1971). A sediment plug is collected with a stainless steel tube of a 2 cm i.d., measured and injected in a 30 ml glass vial filled with 10 ml of 10 % potassium chloride solution. It is shaken in order to dissociate the sediment plug and stop all bacterial activity. The sample is stored upside down to avoid exchanges with room air, and allowed to equilibrate with the vial headspace for 48 hours. The gas is then extracted in a syringe by injecting an equivalent amount of 10% KCl solution. A blank sample (air equilibrated with 10% KCl solution) is also taken for background corrections. No duplicates taken.

*Sample preservation:*

The gas is immediately injected in a serum vial filled (bubble-free) with a pH1 10% KCl solution by displacement of an equivalent amount of solution. The vials are stored upside down in order to avoid exchanges with air through the septum.

*Sample analysis:*

The gas is extracted in a gas-tight syringe by displacement. Its composition is analyzed in the laboratory (University of Bristol) by flame ionization gas chromatography on a Carlo Erba 5400 HRGC equipped with a Porapack QS column (1.8" x 12m). Laboratory standards for calibration consist of a range of BOC alpha-gravimetric mixtures (multi-point calibration).

#### *5.10.3.2. Methane stable carbon ($\delta^{13}C$) and stable hydrogen ($\delta D$) isotopic composition*

The sampling and sample preservation for methane stable isotope composition is as described above. No duplicates sampled. The gas samples are then analyzed in the University of Bristol by continuous flow gas chromatography combustion isotope ratio mass spectrometry (GC-IRMS) on a Thermo-Finnigan Delta XP mass spectrometer. Microliter quantities of gas samples are injected onto a Plot Q column (0.32 µl x 25m) for separation of $CH_4$ and $CO_2$.

*$\delta^{13}C$*: Methane is combusted to $CO_2$ at 1050°C in a reactor containing copper and platinum wires. The carrier gas is helium (2 ml/min) into which a trickle flow of 1% oxygen in helium (0.1 ml/min) is added just before the combustion reactor. The stable carbon-isotope values are reported relative to VPDB.

*$\delta D$*: Stable hydrogen isotope measurements on methane will be conducted on the same instrument for high concentration samples. Separation of gaseous components is achieved using the same PLOT Q column. However, the 1050°C combustion reactor is replaced by an empty reactor in which $H_2$ is formed by pyrolysis of $CH_4$ at 1400°C (Tobias and Brenna, 1997). For low concentration samples, gases are processed in an off-line vacuum extraction line (Hornibrook et al., 1997). Water and $CO_2$ are separated from samples by freezing in liquid nitrogen. Methane is combusted to $CO_2$ and $H_2O$ at 900°C in a quartz furnace packed with CuO

wire and Pt foil. $CO_2$ is separated from $H_2O$ by cryogenic distillation using an ethanol/LN slush at -110°C. The quantity of $CO_2$ from $CH_4$ combustion is measured manometrically to determine combustion yield, after which it is transferred to a breakseal for analysis by dual inlet mass spectrometry. The $H_2O$ formed from methane combustion is trapped on zinc shavings ('Indiana Zn') and sealed in a glass breakseal. It is then reacted for 25 minutes at 450°C to form $H_2$ which is then analyzed by dual inlet mass spectrometry.

*Standards:* Stable hydrogen-isotope data are reported relative to VSMOW. An inhouse laboratory $CH_4$ standard with known $\delta^{13}C$ and $\delta D$ values is analyzed along with samples for both online (GC-C-IRMS) and offline methods. Using the same extraction line, microlitre quantities of the IAEA water standards VSMOW and SLAP are injected and frozen into breakseals containing Indiana Zn. The standards are also reacted at 450°C to form $H_2$ gas which is used to normalise the D/H ratio data measured for the $CH_4$-derived water analyses.

*5.10.3.3. Carbon dioxide concentration and stable carbon ($\delta^{13}C$) isotopic composition*

*Sampling:*

A sediment plug of 2 cm i.d. is sampled from the core, measured and placed in a 40 ml glass vial. No replicates, samples taken every 30 cm. It is flushed with OFN for 4 minutes, sealed and frozen for preservation. Dissolved inorganic carbon will be analysed by an offline procedure because sediment samples cannot be acidified this might produce $CO_2$ from carbonate minerals. $CO_2$ is extracted by vacuum from the sealed samples, and collected by freezing at liquid nitrogen temperatures. Water is removed by cryogenic distillation. The amount of $CO_2$ collected is measured manometrically before it is stored in a glass breakseal for subsequent analysis by conventional dual inlet mass spectrometry.

*5.10.3.4. H, VFA, methanogenic rates and cell numbers*

*i) Hydrogen*

The sediment $H_2$ partial pressure is estimated by the means of viable sediment plugs incubations. The method is modified from Lovley and Goodwin (1988) and Hoeler et al. (1998).

*Sampling:*

A sediment plug is collected with a stainless steel tube of a 2 cm i.d., measured and injected in a 30 ml glass vial, flushed with oxygen free nitrogen (OFN) for 4 minutes and sealed. The sample is incubated at 4°C (i.e. close to in situ temperature) in the dark for 5 days to allow equilibration between the sediment steady-state concentration and the vial headspace. Duplicate samples. Duplicate blanks are also incubated for background corrections. Also, room air samples are analyzed regularly to check on air contamination of the samples.

*Analysis:*

The analysis is realized on board on a reduction gas analyzer (Peak Performer 1, Peak Laboratories, LLC). The principles for the HgO-vapour gas detector can be found, e.g. in Scranton et al. (1984). The carrier gas is Ultra Pure Nitrogen (i.e. $H_2$-free; $N_2$ Alpha Gas n° 1, Air Liquid). All syringes used are flushed thoroughly with nitrogen to minimize air contamination. 1 ml of gas is collected from the sample vial in a syringe connected to a nitrogen-full syringe. Nitrogen is allowed to flow in the vial after sampling to compensate for any pressure drop. The gas sample is immediately injected in the reduction gas analyzer. 10 ml of nitrogen are injected just before the sample, to avoid contamination by any $H_2$ traces remaining in the sampling loop. The sample is incubated for 5 days and analyzed again twice (total 15 days of incubation and 3 analysis) to check that the observed values do correspond to steady-state $H_2$ concentration in the sediment.

*ii) Pore water volatile fatty acids (VFA)*

*Sampling and preservation:*

A sediment plug is collected with a stainless steel tube of a 2 cm i.d., measured and injected in a centrifuge vial. The sample is frozen for preservation until analysis in the laboratory (University of Bristol).

*Analysis:*

The sample is thawed and centrifuged at 4°C (4500 rotations/min) for pore water extraction. The VFA's (acetate, propionate and butyrate) are analyzed by High Performance Liquid Chromatography (HPLC).

*iii) Microbial methanogenic rates*

The rates of microbial methane production are estimated in sediment incubations under in situ conditions using $^{14}C$-labelled bicarbonate and acetate substrates.

*Sampling:*

No replicates sampled: one sample is for $CO_2/H_2$ (hydrogenotrophic) methanogenic rates, the other for acetotrophic methanogenic rates.

A sediment plug is collected with a stainless steel tube of 1.2 cm i.d., and injected in a 5 ml Luer-Lock syringe. The air headspace is gently pushed out and the syringe capped (air-tight).

The syringes are placed in a bag, flushed with OFN and allowed to re-equilibrate for 18 to 24 hours in the dark at in situ temperature (± 4°C).

*$^{14}C$ substrate injection:*

The gas-tight cap is briefly removed while the substrate is injected in centre of the sediment plug from bottom to top at a steady pace. The sample is incubated again under the same conditions for 18 to 24 hours. The amount of $^{14}C$-labelled substrates injected are:

- Bicarbonate: 50 µl = 50 Kbeq as sodium $^{14}C$-bicarbonate;
- Acetate: 50 µl = 15 Kbeq as sodium 2-$^{14}C$-acetate.

Both substrates have previously been diluted with de-gassed, filter-sterilized milli water:

- Sterile bicarbonate, initially 37Mbeq (Amersham Portugal): dilution 1:70;
- Sterile acetate, initially 37Mbeq (Amersham Portugal): dilution 1:24.

*Incubation end and sample preservation:*

The incubation is terminated by slicing the syringe tip off and injecting the sediment plug in a 40 ml vial containing 20 ml of 4M NaOH. The vial is quickly tapped with a butyl-rubber stopper, shaken to stop all bacterial activity and stored upside down to avoid gas losses through the stopper.

*Analysis:*

The samples are processed through a "methane-furnace rig" by sparging of the NaOH solution with a 1% oxygen + nitrogen balance carrier gas. The sparging effluent passes through a series of chemical moisture and $CO_2$ traps leaving only $^{14}CH_4$ to be combusted in the $O_2$-rich gas stream on CuO at 900°C in a reactor furnace. The $^{14}CO_2$ formed is trapped in a liquid scintillation cocktail (scintillant: Opti-Phase 3, Perkin Elmer (UK) mixed with β-phenylethylamine) which is then quantified on Perkin Elmer Liquid Scintillation counter. Corrections are applied to account for differences in $^{14}C$ discrimination between the acetate fermentation and bicarbonate reduction pathways in the determination of the methanogenic rates from both substrates.

*iv) Total cell numbers*

The total cell numbers are estimated by epifluorescent microscopy (Acridine Orange Direct Counting) according to the method used by Cragg et al. (1995). No replicates taken, sampling done every 30 cm in the deeper core segments (methanogenic zone).

*Sampling:*

A 1 ml sample is taken from the core using sterile (autoclaved) 5 ml Luer-Lock syringe which end has been removed. It is ejected directly in a serum vial (previously furnaced at 450°C) containing 9 ml of filter-sterilized 2% formaldehyde solution in artificial sea water.

*Analysis:*

Between 5µl and 25µl of sample are stained with acridine orange (50 µl of 1 g/l solution) in 10 ml of filter-sterilized (0.1 µm pore size) 2% formaldehyde for 3 minutes and then vacuum-filtered through a polycarbonate (0.2 µm pore size) membrane. The membrane is then rinsed with 10 ml of 2% sterilized formaldehyde solution and mounted on a slide. 3 replicate filters are prepared from each sample to minimize count variance. A minimum of 200 fields of view are counted. The total number of bacteria and the numbers of dividing and divided cells are counted separately. The number of cells counted on opaque particles is doubled. Blank membranes are regularly counted.

*v) Slurry experiments*

Sediments from the deepest parts of the cores are collected for slurrying in the laboratory (University of Bristol). All samples mentioned above are taken from the sediment before it is placed in a series of bags flushed with OFN. It is stored at 4°C in the dark before slurrying.

Slurrying is realized under anaerobic and sterile conditions in an anaerobic glove-box ($N_2$-$CO_2$). The slurries are done in 2 L conical pyrex flasks, in a proportion of 50% sediment-50% media, under a range of temperatures. Experiments aiming at the enrichment of hydrogenotrophic and acetotrophic methanogens will be conducted according to the methods established by Wellsbury et al. (1996). The microcosm gas headspace and water are regularly analyzed for all the parameters mentioned before.

## 6. Cruise narratives

(A. Kopf)

### 6.1.1. Leg SO175-1

The transit between Miami and Lisbon from 12.-25. November aimed mainly at introducing the vessel and scientific equipment on R/V *Sonne* to a delegation from China, especially since there will be a research cruise into the South China Sea in 2004. For that purpose, the transit was also split into two portions, the first of which started in at 13.00 on 12. November, and ended at 19.00 on the 22nd of November in the bay of Punta Degada on the Azores. Here, the 3 scientists on board were joined by 7 Chinese and 2 German colleagues.

The main issue of the first portion was the test and maintenance of systems on board, like the SIMRAD multibeam system, the TV-guided grab, push core, and video sledge (OFOS) and the CTD. During the second part of the transit, an hydrothermally active segment had been chosen to test all seagoing equipment in one location. Due to rather bad weather conditions, none of the seagoing equipment could be lowered to the seafloor. Also, as a result of high waves, the multibeam system acquired data of poor quality and was switched off. Only parasound profiles showed good penetration and imaged the upper 80-100 meters of the sedimentary basin fill between ridges of the East Azores fracture zone beautifully. However, the weather caused severe seasickness for many of the scientists so that operations were stopped and *Sonne* went straight towards Lisbon. The vessel arrived on the river *Tejo* when the sun set.

### 6.1.2. Leg SO175-2

Leg SO175-2 started in Lisbon, Portugal on Nov. 26th, 2003, at 21:00 UTC after about 28 hrs. in port. We immediately headed south to investigate the first of a total of 5 study areas during this part of the *GAP* cruise, the Marques de Pombal fault (**Fig. 6.1**). After two days and nights of video and heat flow surveys plus some coring in the landslide-prone southern part, we moved westward to the northern portion of the deformation front (**Fig. 6.1**). Here, we conducted a heat flow survey and cored the input material into the system. Afterwards, we moved east to study *Lolita* mud diapir (**Fig. 6.1**). Given the apparent inactivity of the dome based on video observation, we focused on supposedly more active features, a set of deep-seated, "leaky faults" further north (**Fig. 6.1**). After some video surveying we took several samples, and then followed a southeastern course to *Hesperides* mud volcano (**Fig. 6.1**). After some surveying, heat flow and coring, a total of 26 stations were visited. Afterwards, we moved east to have a short port call in Cadiz, Spain. Here, we exchanged one scientist and the crew from Spiegel-TV for four scientists from France, Belgium and Germany to complement the scientific party for Leg SO175-3.

### 6.1.3. Leg SO175-3

After less than 2 hrs., RV *Sonne* left Cadiz again towards heavier weather in the west. Our first target on that long leg was *Faro* mud volcano (**Fig. 6.1**), which is located on a sigmoidal fault scarp with two similar features, *Cibeles* and *Almazan* mud domes. Footage of the video survey during the following night suggested active fluid venting in places. However, irrespective of bacterial mats and *pogonophora* colonies, it turned out to be hard to recover sediment. The silty to clayey deposits were obviously heavily cemented during earlier episodes of fluid venting. gravity cores turned out to be a more powerful weapon than the TV-grab since we recovered two long cores in cold water coral-rich areas. On the following day, we investigated *Capt. Arutyunov* mud volcano (**Fig. 6.1**), which has already been famous for an earlier gas hydrate recovery a few years back. A TV-grab recovered about a ton of gaseous, hydrate-bearing mud with claystone clasts from the central crest of the mud dome. Gravity cores further revealed sheared claystone clasts with healed veins. In the process of the survey, two smaller mud volcanoes were located east and west of *Capt. Arutyunov* mud volcano. While one of them showed nice interlayering between mud breccia flows and hemipelagic background sediments, the other one had only hemipelagics (possibly an indication of longer-term quiescence). A heat flow survey completed the study of this mud dome.

On December 6th, we started to acquire a long seismic reflection profile in E-W-direction, which we had to stop due to mechanical failure of the airgun. Instead we mapped and sampled the westernmost deformation front (**Fig. 6.1**). Surprisingly, the core was not characterized by turbidites, but relatively stiff clays. Heat flow along a more than 100 km long W-E-profile across the frontal deformation front (**Fig. 6.1**) were then followed by more mapping in the mud volcano (MV) area further east. On December 9th, we sampled two of the western mud volcanoes, *Bonjardim* MV and a smaller, so far unknown feature. Both domes revealed extruded mud with variable clast contents overlain by hemipelagic sediments. Due to the heavy weather, we decided to do largely mapping in the following. After a hump day party, which was interrupted occasionally by water entering the laboratories and lower deck, we characterized the southwestern portion of the deformation front and took two cores on the underthrust plate. We then started a seismic reflection cross section and headed northeast.

On December 11th, we reached the shallower mud volcano province and surveyed *Ginsburg* mud dome with OFOS (**Fig. 6.1**). On the following two days, we dedicated much time sampling both *Ginsburg*, *Gemini*, and a so far unknown mud dome. On our journey upslope (i.e. east towards the Moroccan margin we also mapped uncovered territory (**Fig. 6.1**). We completed mapping at this part of the Gibraltar wedge on the 14th, deployed a pore pressure probe into *Capt. Arutyunov* mud volcano, and also did some more sampling at this active feature.

After a relatively long transect northwards, we explored a topographic high west of the Straits of Gibraltar by OFOS and TV grab. Its core is apparently made up of tectonically fragmented magmatic rock of some sort. To either side of the centre, there is a plain of a few square kilometers, which has sedimentary deposits on top of a decimeter-thick cemented beach rock. During the last glacial maximum, the entire feature may have been an island. On the way back to the southwestern deformation front of the Gibraltar wedge, we spent some 30 hours measuring heat flow over thrust faults in the wedge. These data as well as a video survey across a prominent escarpment did not reveal any evidence for active fluid venting. Domes in the toe area of the wedge also seem to be salt diapirs rather than mud volcanoes. We cored one feature, *Poseidon* dome, on Dec. 17th, and gained pore water chlorinities larger than seawater. After some multibeam mapping, push cores were taken on the *Horseshoe* (Dec. 18th) and *Tagus* (Dec. 20th) abyssal plains **(Fig. 6.1**).

During the day in between, Dec. 19th, we revisited the landslide area near the southern tip of the Marques de Pombal fault and made a seismic reflection survey and took 3 gravity cores. On the last night and day of scientific operations, we carried out a heat flow survey from tagus abyssal plain via the foot of Gorringe Bank to Horseshoe abyssal plain (**Fig. 6.1**). There, we took a final video-MUC to have the most recent turbidites for dating. A total of 73 stations were visited during Leg SO175-3.

After a highly successful scientific cruise, we left the study area at 17.00 on Dec. 21st and headed north. As anticipated, we arrived in Lisbon at 9.00 on Dec. 22nd to get two containers to pack equipment and samples for the transit of the vessel to Germany. The scientific crew left R/V *Sonne* about an hour before the ship departed again at 13.20 on Dec. 23rd.

### 6.1.4. Leg SO175-4

The last leg of SO175 brought R/V *Sonne* back to Germany for the first time since 1992. As a result, the crew is frantically preparing everything for a PR-trip from Bremerhaven to Bremen up the river *Weser* on Dec. 29th, followed by an open ship day for the North German public on the 30th. The transit through the Biscaya was unexpectedly smooth, so that the entire crew had a peaceful Christmas Eve celebration.

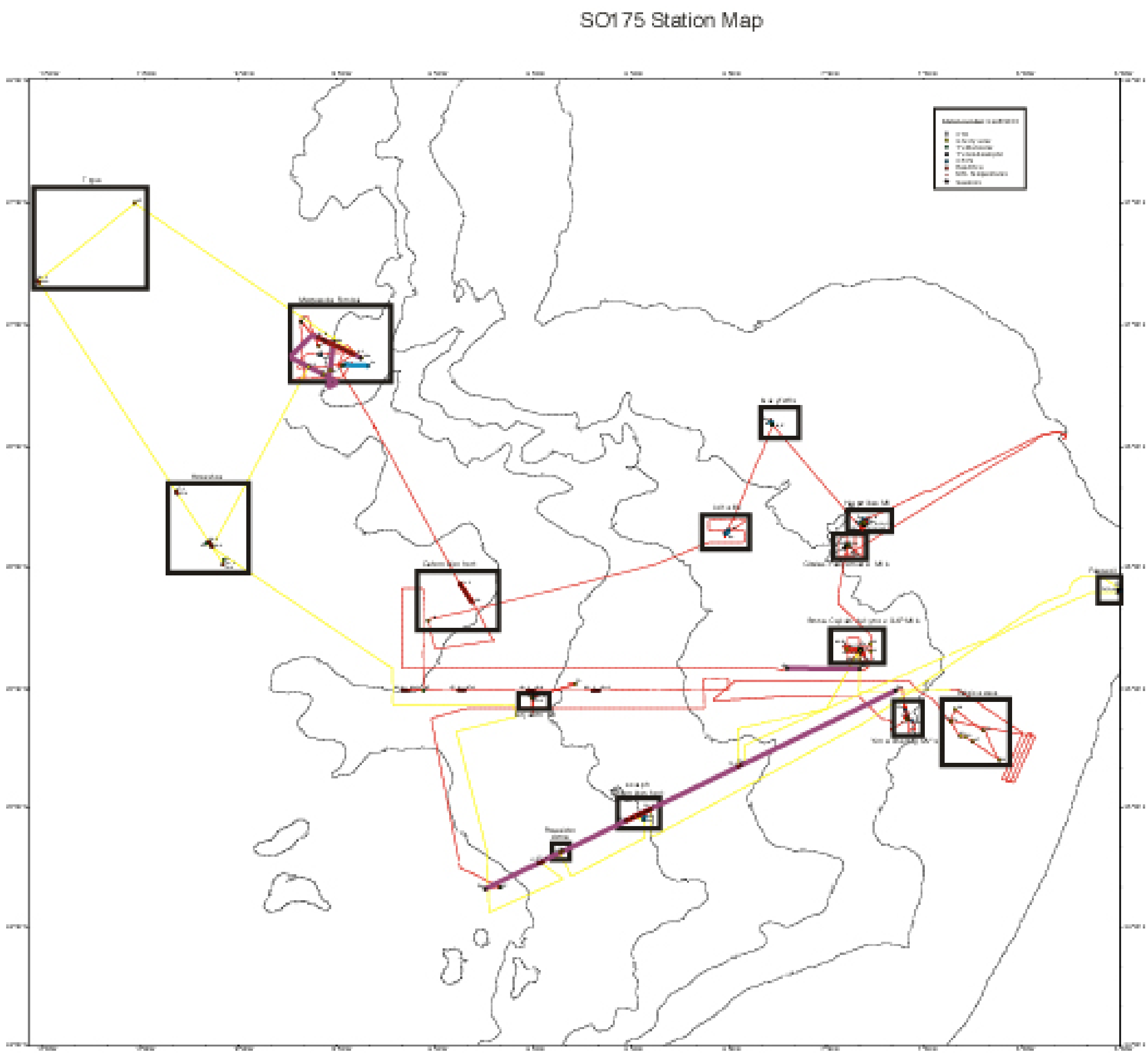


**Figure 6.1.** Map of the study area with all stations of cruise SO175.

## 6.2. Landslide studies

### *6.2.1. Introduction*

(A. Marti, A. Kopf, N. Kaul, W. Brückmann)

*General introduction and echosounder calibration*

For the landslide studies (this chapter), but also for the work on mounds (Ch. 6.3.) and tectonics (Ch. 6.4.), it became necessary to complement seafloor bathymetric charts in the area prior to sampling, measurements, etc. For that purpose, Simrad EM120 multibeam swathmapping was carried out in conjunction with Parasound profiling (see Ch. 5.1. and 5.2.). Both systems are routinely used on RV *Sonne*, but require calibration depending on salinity and temperature in the *GAP* study region.

We hence placed one CTD in the Marques de Pombal fault area in the north (station GeoB9001), where we have great water depths and no influence of Med. outflow water (MOW), and a second CTD on the Gibraltar wedge (station GeoB9026) where we anticipated saline MOW. The two water profiles were then used in the respective regimes combined with the echosounder system. For locations, see **Figure 6.1**. By using one or the other calibration profile, we obtained near-perfect match between echosounder depths and rope lengths when deploying instruments or using TV-grab, OFOS, or during coring.

*State-of-the-art: Submarine landslides*

Landsliding is an important geomorphic process at any kind of slope, be it onshore or offshore. Mass movements in marine settings are of great interest for both fundamental science and industrial companies. Enhanced knowledge of slope processes and depositional features is a priority goal for the energy industry, because of oil exploration and production in deep water and for protection of offshore infrastructure (platforms and pipelines, communication cables) against natural hazards. In addition, submarine landslides are being given increasing attention as a major cause of tsunamis, which can ravage coastal areas.

Landslides have been defined as the downward and outward movements, generally driven by gravity, of slope-forming materials, in which shear failure occurs. Most submarine landsliding originates in unlithified sediments (e.g., Hampton et al., 1996), but also at volcanic islands within volcaniclastic deposits and volcanic rocks (Urgeles et al., 1999). However, landslides occur particularly in environments where weak geological materials such as rapidly deposited fine-grained sediments or fractured rock are subject to strong environmental stresses such as earthquakes, large storm waves, and high internal pore pressures. They occur at locations where the downslope component of stress exceeds the resisting stress, causing movement along one or several concave to planar rupture surfaces. Slope failure can involve huge amounts of material and can move great distances: slide volumes as large as 20000 km$^3$ and runout distances in excess of 100 km have been reported (for reviews see Hampton et al., 1996; Mulder and Cochonat, 1996). Only a few submarine landslides in historical times, namely those that disrupted populated shoreline or offshore engineered structures, have been documented directly. In most cases an earthquake or large storm waves triggered the event. Unfortunately, even from those events little is known about the state of the slope before failure. Many questions are still unanswered; e.g., had the slope already been creeping and has been accelerated because of earthquake excitation or wave loading or was it quasi-stationary before external forces acted on the slope? Most of what we know about submarine landsliding is known from remote sensing of features associated with slides, like rupture surfaces and displaced masses of sediment or rock (e.g. Hampton et al., 1996; Mulder and Cochonat, 1996).

*Previous regional studies*

The SW Iberian Margin hosts the present-day boundary between the European and African Plates (Grimison and Chen, 1986; Buforn et al., 1995, Gracia et al., 2003a). Convergence is accommodated along a wide and diffuse deformation zone characterized by an elevated seismic activity (Gracia et al., 2003b), source of the largest and most destructive earthquakes and tsunamis in Western Europe (e.g., 1969 Horseshoe Earthquake Mw=7.9, 1755 Lisbon Earthquake and Tsunami M=8.5, Zitellini et al., 2001). A NNE-trending lineament was identified that corresponds to the rupture trace and escarpment of the 50 km long Marques de Pombal thrust fault, possible source of the 1755 Lisbon earthquake and tsunami (Zitellini et al., 2001; Gràcia et al., 2003a). Associated to this structure, a large area (~260 km2) of high acoustic backscatter in the southern half of the Marques de Pombal thrust front has been interpreted as the result of a recent complex (i.e., multiple) submarine landslide. High-resolution sub-bottom profiler sections across the toe of the landslide, allowed the identification of alternating seismic transparent units (interpreted as a landslides) and seismically well-stratified units (interpreted as pelagic sediments) suggesting cyclic activity of the Marques de Pombal fault (Gracia et al., 2003b).

One of the hypotheses to test during SO175 was that this landslide has been generated during the most recent seismic event in 1755, and could have contributed to the devastating tsunami thereafter (Baptista et al., 1998). Ways to achieve this included:

- to date the most moderns earthquake events in Marques de Pombal foult throughout turbidites in multicore and gravity core record in Tagus Abyssal Plain and in Horseshoe Abyssal Plains,
- to collect images of the water-sediment interface along the Marques de Pombal Fault, Marques de Pombal head slide, and within the slide using the OFOS system, and
- to acquire profiles across the Marques de Pombal area, *Horseshoe* and *Tagus* Abyssal Plains using Parasound echography and seismic reflection systems.

### *6.2.2. Operations*

(A. Kopf)

During SO175, the Marques de Pombal-Fault (MPF) landslide area has been visited twice. A total of 12 stations were visited, which included operations such as echographic (Parasound) and multibeam surveys (GeoB9002-1, 9003-1, 9007), two OFOS tracks (GeoB9002-2 and 9003-2), a heat flow survey (GeoB9004), a seismic reflection survey (GeoB9094; see Ch. 6.2.3. below), and 5 gravity and 2 push cores. For detailed information on exact location, see station list (Appendix Ch. 8.1).

### *6.2.3. Mapping/geophysics and OFOS*

#### *Mapping of landslides near Marques de Pombal*

(A. Kopf)

Based on some backscatter data in the area, we focused on a multiple submarine landslide at the southern end of the MPF area as well as on the tectonic footwall plain. All stations are plotted on top of the backscatter map (courtesy of Eulalia Gràcia) (**Fig. 6.2**).

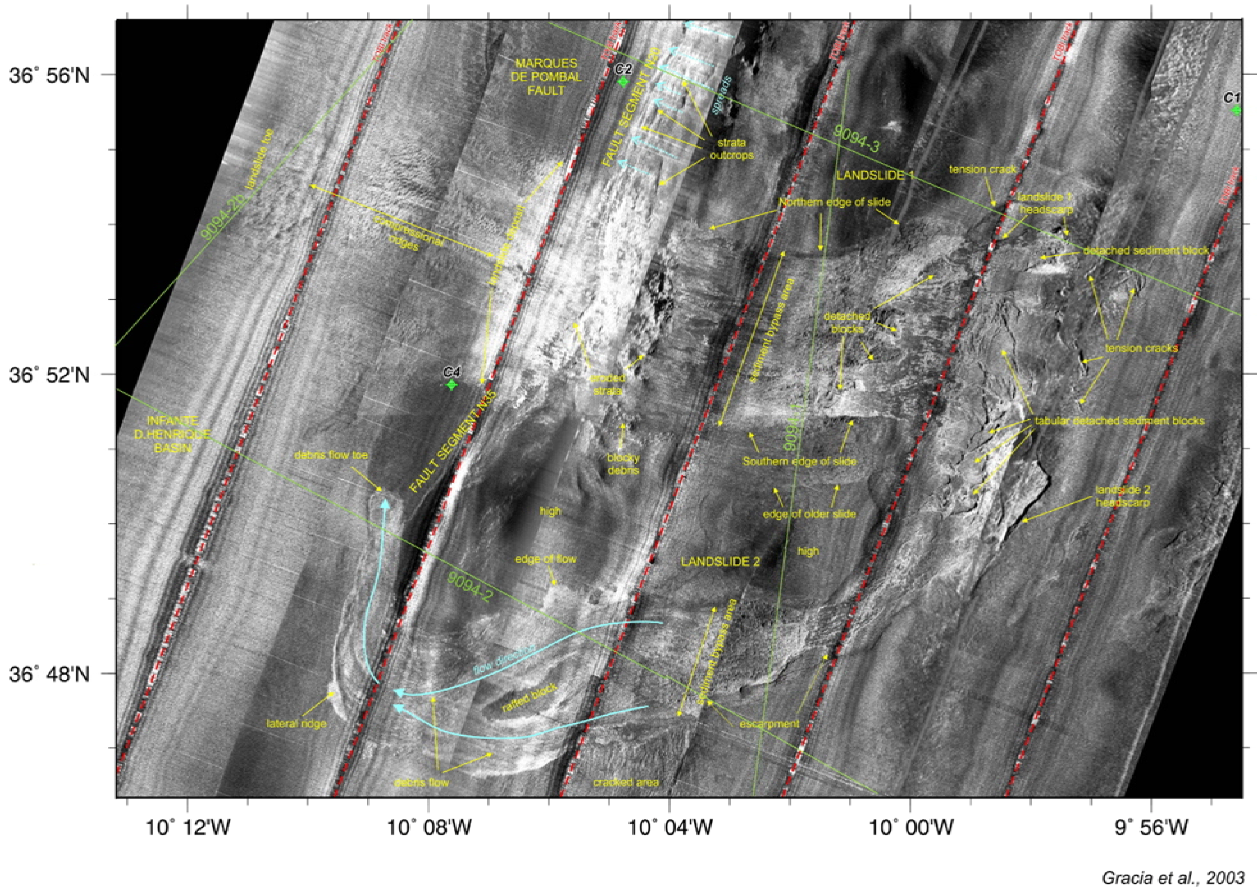


**Figure 6.2.** TOBI backscatter map of the MPF area with SO175 stations and tracks of RV *Sonne*.

In addition to the maps provided, we acquired a net of Parasound profiles and a bathymetric chart of the southern portion with the landslides. Both the backscatter (**Fig. 6.2**) and Simrad images (**Fig. 6.3**) image the (at least) two landslide events nicely. Especially the eastern and northern head walls of the eastern landslide body can clearly be seen. Given that no prominent headwall is imaged for the western landslide, it can be postulated that the western event predates the eastern event. Possibly, a third event (or, alternatively, the fine-grained fraction of the second event) moved southward initially before flowing westward around the western landslide mass, and then terminated in northward direction right along the strike of the Marques de Pombal fault scarp. In order to test this interpretation, we acquired seismic profiles across that southwestern tongueof the slides and also got gravity cores in that area (see below).

***Reflection seismic across land slide areas***

(N. Kaul, B. Heesemann)

At station GeoB9094, three seismic lines were planned across landslide features near Marques de Pombal fault zone, as identified on TOBI backscatter images.

Recording parameters were set to:

- 16 channels, 6.25 m per channel
- 1 ms sampling rate,
- 20 – 4000 ms band pass filter
- preamplifiers @ 60 dB
- 3 s recording time
- 3.5 sec. external water delay
- GI gun in true GI mode (50 ms delay)
- Source depth 4-5 m
- Shot interval 10 s @ 5 kn, 25 m resp.
- Moderate sea state (2 – 4 m wave heights )

This results in high-resolution data with a penetration depth up to 1.3 s TWT.

The first line (Pt. I) trends NNE-SSW across the northern edge of the second landslide and the location of gravity core GeoB9093 (**Fig. 6.2**).

- Start point: 36° 56' N, 10° 01'W
- End point: 36° 45.7' N 10° 2.7' W
- Shot points 15 – 780, total length: 19,1 km

The second line (Pt. II) runs SE-NW, crossing seismic line BP5 of a former survey, gravity corer stations GeoB 9092 near the escarpment and GeoB 9091 near Fault Segment N35 (**Fig. 6.2**).

- Start point: 36° 46.54' N, 10° 0.587' W
- End point: 36° 52.395' N 10° 14.483' W
- Shot points 1014 – 1851, total length: 21 km

The third line (Pt. III) closes the loop WNW-ESE back to the upper part of the landslide area, going along heat flow station GeoB9004 (**Fig. 6.2**).

- Start point: 36° 57,44' N, 10° 08'W
- End point: 36° 52.41' N 9° 53,18' W
- Shot points 2385 – 3333, total length: 23,5 km

Part I: Several sets of sub-parallel reflectors can be identified down to 1.3 s TWT below seafloor. They are all folded in long wavelength (8 km). The lowermost reflector at 5 – 5.5 s TWT has a low frequency appearance. This seismostratigraphic unit tends to thicken northward. A band of high frequency reflectors can be traced at 0.5 – 1 s TWT below seafloor. No northward thickening occurs anymore. Decrease of folding indicates lesser tectonic influence since this event. Above this band of reflectors a zone of low reflectivity occurs, 0.2 – 0.4 s TWT thick. This sequence is overlain discordantly by a low reflectivity unit from north to shot point 240. From SP 300 southward there is a band of fine laminated reflectors, thickening southward. Near SP 290 and 600, diffractions next to the seafloor indicate scarps or rough surface features.

Part II: Those three seismostratigraphic units of part I can be traced until at an abrupt end near SP 1360. (see **Fig. 6.3**) All seismic reflectors bend downward by the same amount of 0.3 s TWT and end at a near vertical fault, generating diffractions. This fault is attributed to the Marques de Pombal fault, fault segment N35. This scenario does not apply for the uppermost unit of high frequency appearance. This section terminates near SP 1270 at a structure with the appearance of a slid down sediment package. The resedimentation of this material generates reflectors across the fault. Even these reflectors up to the seafloor are disrupted by a small amount, indicating tectonic activity of this fault until recent. West of the pronounced fault is a 4 km wide wedge of seismically transparent material, most probable disrupted material which allows no coherent reflection. Further west from SP 1480 onward, a complete set of sub-parallel reflectors occurs down to 6.5 s TWT . The surface and upper 0.2 s TWT show indications of denudation and sediment drift erosion at the footwall of the scarp (SP 1490 – 1550). Beyond SP 1600 seismic stratigraphy shows low energy sedimentation.

Part III is a parallel profile to Part II approximately 7 nm to the north. A depression at the foot of the escarpment is not visible, neither in the bathymetric, nor in the seismic horizons. The major fault is not as clear visible as on profile II, at least a diffraction signature is missing. On the escarpment, two stratigraphic sections can clearly be divided: 1 s TWT below seafloor a band of strong reflections forms the upper limit of a sediment package. This underlying sediment package is slightly folded and faulted. On top, from the seafloor down to app. 1 s TWT fine-laminated reflections occur with no indication of faulting. The uppermost 0.1 s TWT have signs of differential sedimentation, probably due to flow channels.

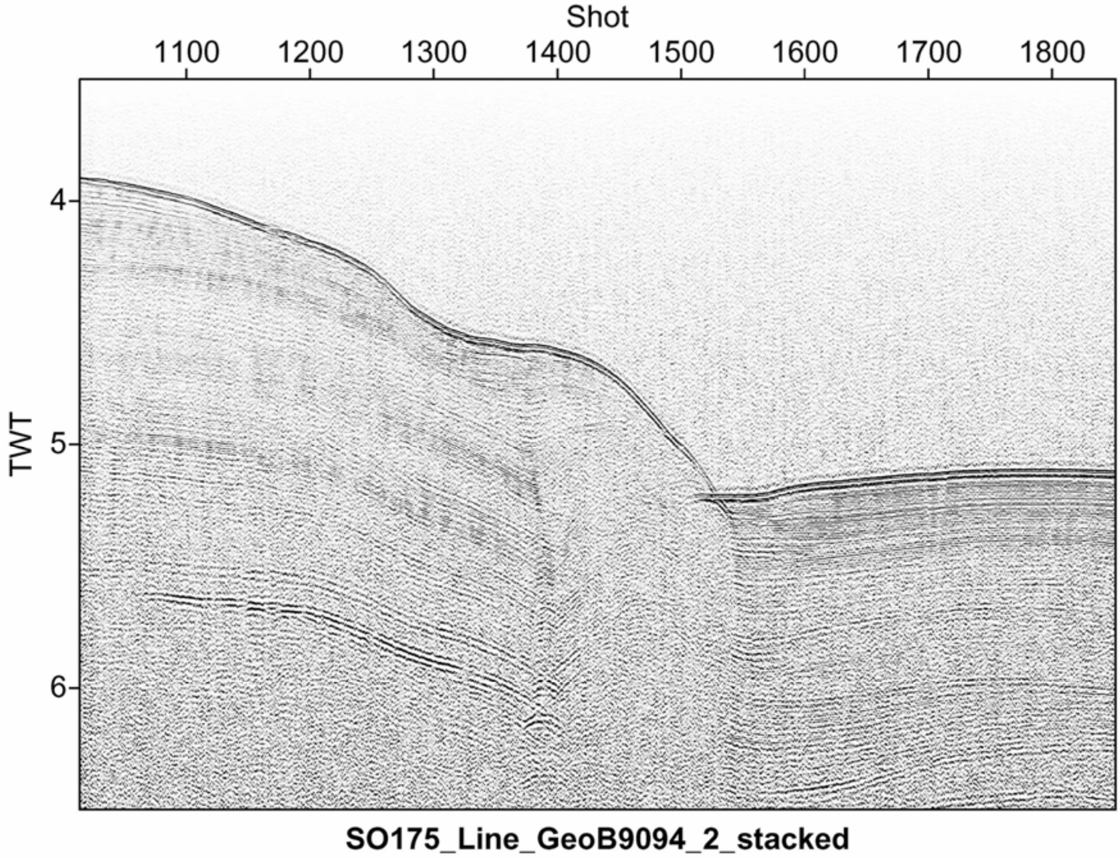


**Figure 6.3.** E-W profile across the southern part of the land slide area and Marques de Pombal fault. East is on the left side, West is right, profile length is approximately 21 km, vertical exaggeration is approximately 8. Gravity cores GeoB9091 and GeoB9092 are located on this profile.

***OFOS tracks across the landslides***

(W. Brückmann, H. Sahling, A. Kopf)

The first OFOS track (station GeoB9002-1) was located on the upper slope of the Marques de Pombal landslide area, crossing the headwall of the main slope failure as imaged in TOBI sidescan imagery (**Fig. 6.2**). During the entire period of video observation no apparent indicators of the headwall scarp could be detected. Main reason for this finding was the fact that the vessel had to deal with the regional current so that the scarp was cut in a relatively small angle by the ship's track. However, TOBI evidence suggest a vertical displacement of several meters (E. Gracia, pers. comm., 2003).

The second OFOS observation in the Marques de Pombal landslide area crossed a less pronounced scarp and rough terrain below it (station GeoB9003-1; **Fig. 6.4**). Again video observations did not show any clear evidence for tectonic features or fluid venting. Biological indicators included a few sponges, but no faunal assemblages characteristic for active fluid venting and seepage.

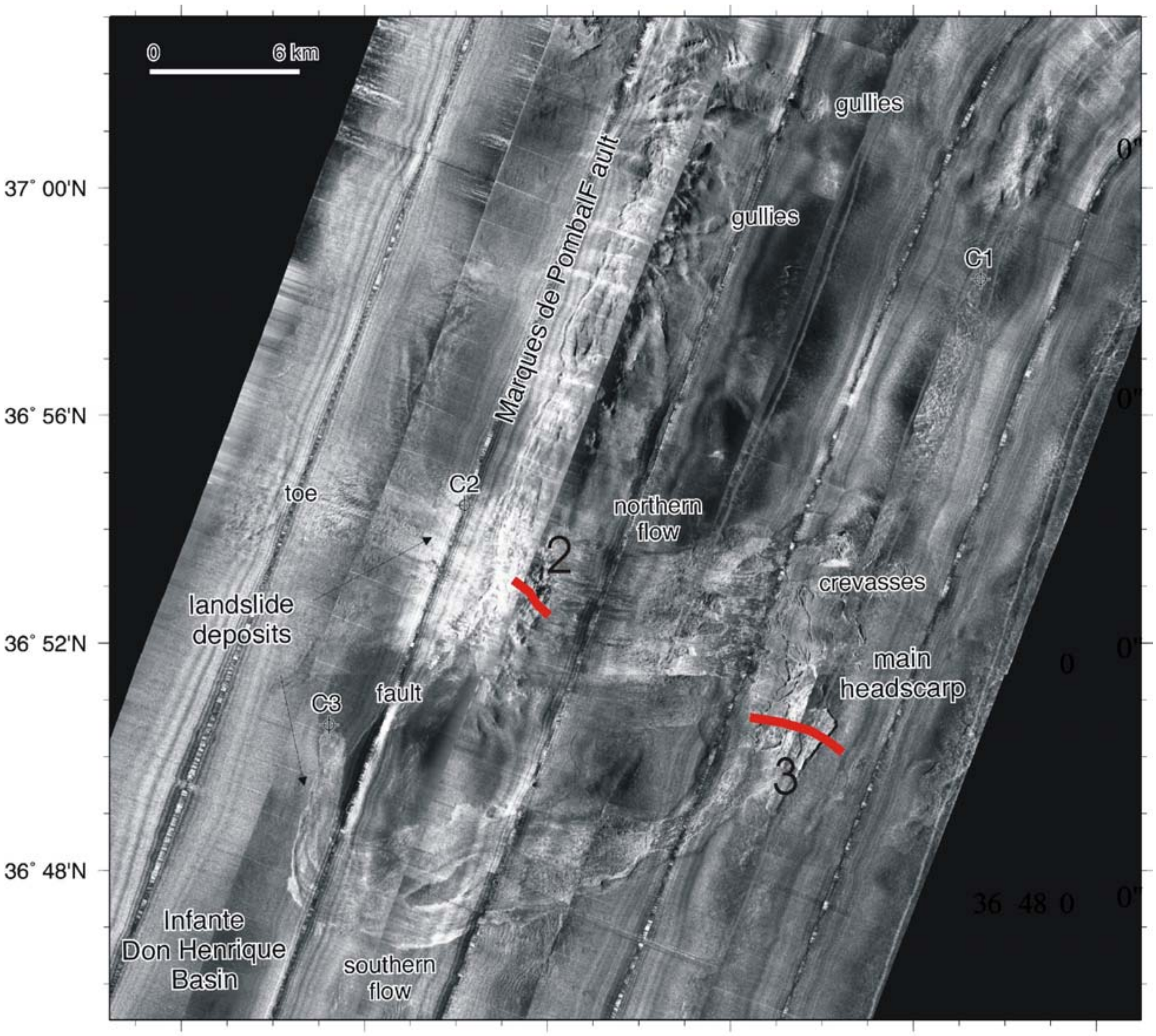


**Figure 6.4.** OFOS tracks on top of TOBI side scan chart of the landslides. TOBI data courtesy of E. Gracia.

### 6.2.4. Lithology

(D. Hebbeln, B. Dorschel, A. Marti)

The Marques de Pombal landslide area was investigated in order to analyse the sedimentary record of the slide and to see if it is related to the Great Lisbon Earthquake of 1755. Core GeoB9008-2 (see **Table 6.1**; for location, see Ch. 8.1) was taken from the headscarp area. It consists of hemipelagic muddy clays and it shows no clear indication for any slide related activity. The same holds true for three other cores (GeoB9091-1, GeoB9092-1, GeoB9093-1) taken from the slide area as it appears on the available backscatter maps. All these cores consist of hemipelagic, grey muddy clays. They do not contain any turbidites or obvious indications for hiatuses. Only in core GeoB9091 some light colour changes are observed between 180 and 250 cm bsf. These observations do not shed any light on the age of the Marques de Pombal landslides. Gravity cores reaching up to 4 m into the sediment appear to have penetrated the base of the mobilized material only at station GeoB9091 (see also Ch. 6.2.6 below). Solely core GeoB9006-1, taken in the plain adjacent to the MPF scarp (i.e. in the tectonic footwall), slightly downslope and westward of the main slide area, contains three turbidites with thicknesses of 9 to 17 cm (**Fig. 6.5**). Post-cruise work will include dating of these events.

| station no. | latitude °N | longitude °W | water depth (m) | recovery (m) | area | sediments |
|---|---|---|---|---|---|---|
| GeoB 9006-1 | 36:55.00 | 10:05.56 | 3949 | 4.30 | Marques de Pombal | hemipelagic & turbidites |
| GeoB 9008-2 | 36:50.29 | 09:58.57 | 2734 | 2.68 | Marques de Pombal | hemipelagic sediments |
| GeoB 9091-1 | 36:50.02 | 10:08.68 | 3957 | 3.47 | Marques de Pombal | hemipelagic sediments |
| GeoB 9092-1 | 36:48.01 | 10:04.00 | 3229 | 4.05 | Marques de Pombal | hemipelagic sediments |
| GeoB 9093-1 | 36:49.03 | 10:02.01 | 3006 | 3.32 | Marques de Pombal | hemipelagic sediments |

**Table 6.1.** Sediment cores taken during SO-175 in the Marques de Pombal land slide area.

**Figure 6.5.** Gravity core GeoB9006-1 with turbidite layers.

### 6.2.5. MST and Physical properties

(W. Brückmann, A. Foubert)

Good examples of some turbiditic sequences well imaged in the MST data are found in gravity core GeoB 9006-1. Here the fining-upward sequence from coarser to finer material is clearly seen in a decrease in gamma density (e.g., from 83-66 cm bsf). Less clear is the correlation of turbidite occurrences with magnetic susceptibility variations. It appears that the base of turbiditic sections is more frequently associated with higher magnetic susceptibility values.

All other cores taken in the MPF region (see **Table 6.1**) are more or less homogeneous as far as the logged parameters are concerned.

### 6.2.6. Pore water geochemistry

(C. Hensen, K. Nass, M. Marquardt)

Three gravity cores from different slides in the Marques de Pombal fault area were sampled for pore water analyses(GeoB9006-1, GeoB9008-2, and GeoB9091-1). The principal idea was that the slided sediments may carry a chemical signature which is different from that of the underlying, undisturbed sediments. Pore water geochemistry thus allows to differentiate between sediments of different origin and even might be useful to date back the occurrence of a slide event (Hensen et al., 2003).

The results of GeoB 9008-2 do not indicate that the core fully penetrated a slide mass. Pore water profiles of GeoB 9006-1 and 9091-1 (**Fig. 6.6A and B**) reflect a moderate intensity of mineralization shown by the gentle increase of alkalinity and ammonia over depth. The abrupt change within the last meter of the cores, which is most obvious for the alkalinity and silicate profiles of GeoB 9091-1, however, is indicative for the existence of a sedimentary slide, covering the upper 3 meters of the cores. The preservation of the sharp kink at about 3 mbsf at both sites allows the conclusion that the sedimentary vent has occurred sub-recently, probably in the order of some decades ago. However, this assumption still has to be verified by numerical modeling of the data.

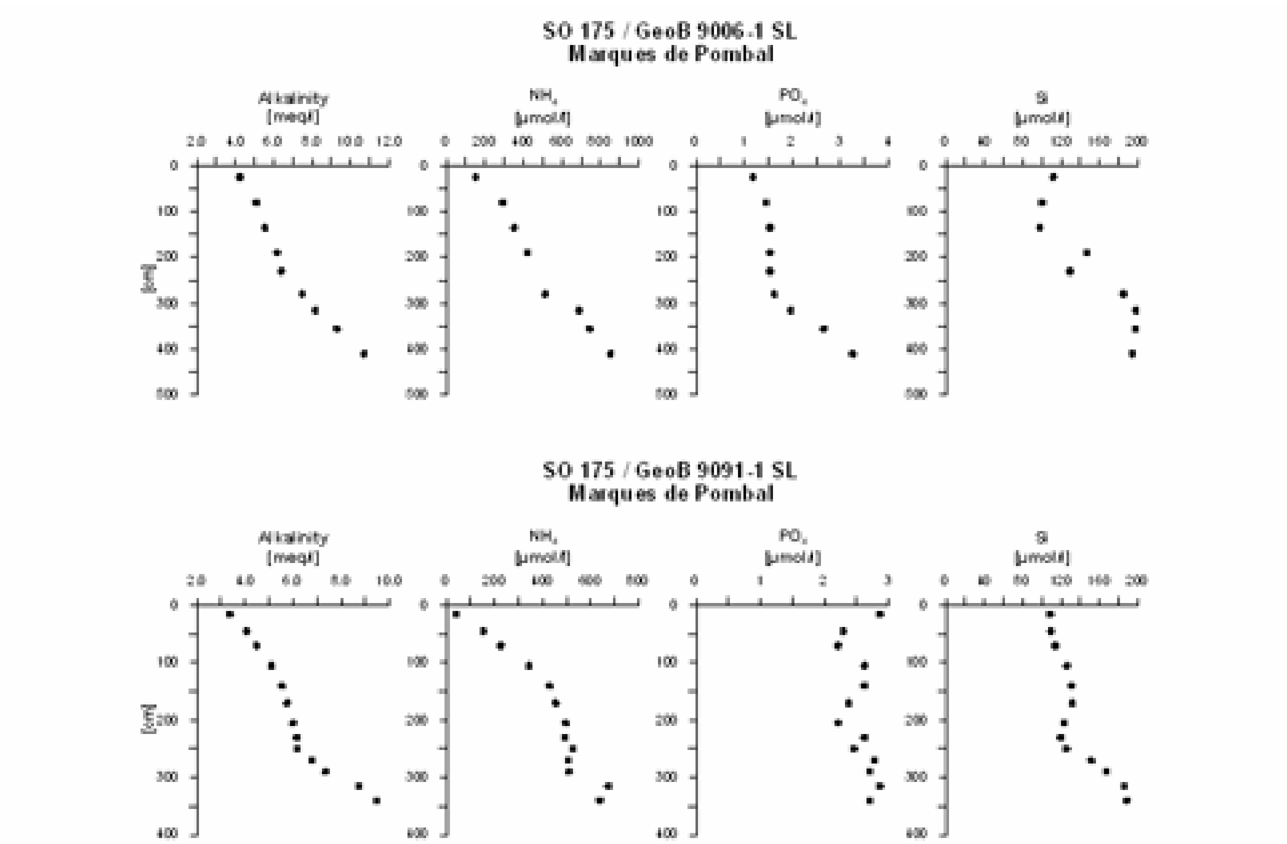


**Figure 6.6.** Pore water geochemical data from gravity cores GeoB9006-1 (**A**) and GeoB9091-1 (**B**).

### 6.2.7. Heat flow and pore pressure

(I. Grevemeyer, N. Kaul)

The source area for the great Lisbon earthquake from 1755 is still not well defined and a wealth of potential nucleation areas has been suggested. However, back-tracking of tsunami run-up heights, polarity and travel times located the source offshore SW Portugal (Baptista et al., 1998; **Fig. 6.7**) and subsequent seismic reflection surveying imaged a fault zone cutting into the continental basement off SW Portugal (Zitellini et al., 1999; 2001). Therefore, the fault zone – called the Marques de Pombal fault - was suspected to be „*The source of the 1755 Lisbon earthquake and tsunami*“ (Zitellini et al., 1999). In recent years, high resolution seismic reflection and swath mapping data revealed strong evidence for landsliding at the fault zone, which may indicate that the fault was active in historical times (Gracia et al., 2003a,b).

However, landsliding is a common feature along passive continental margins. Active thrust faulting, however, causes advection of heat into the deep fault zone and hence inherently affects the local temperature field over the fault (e.g., Molnar and England, 1990). Consequently, heat flow data may serve to reveal if the thrust fault was active in historical times.

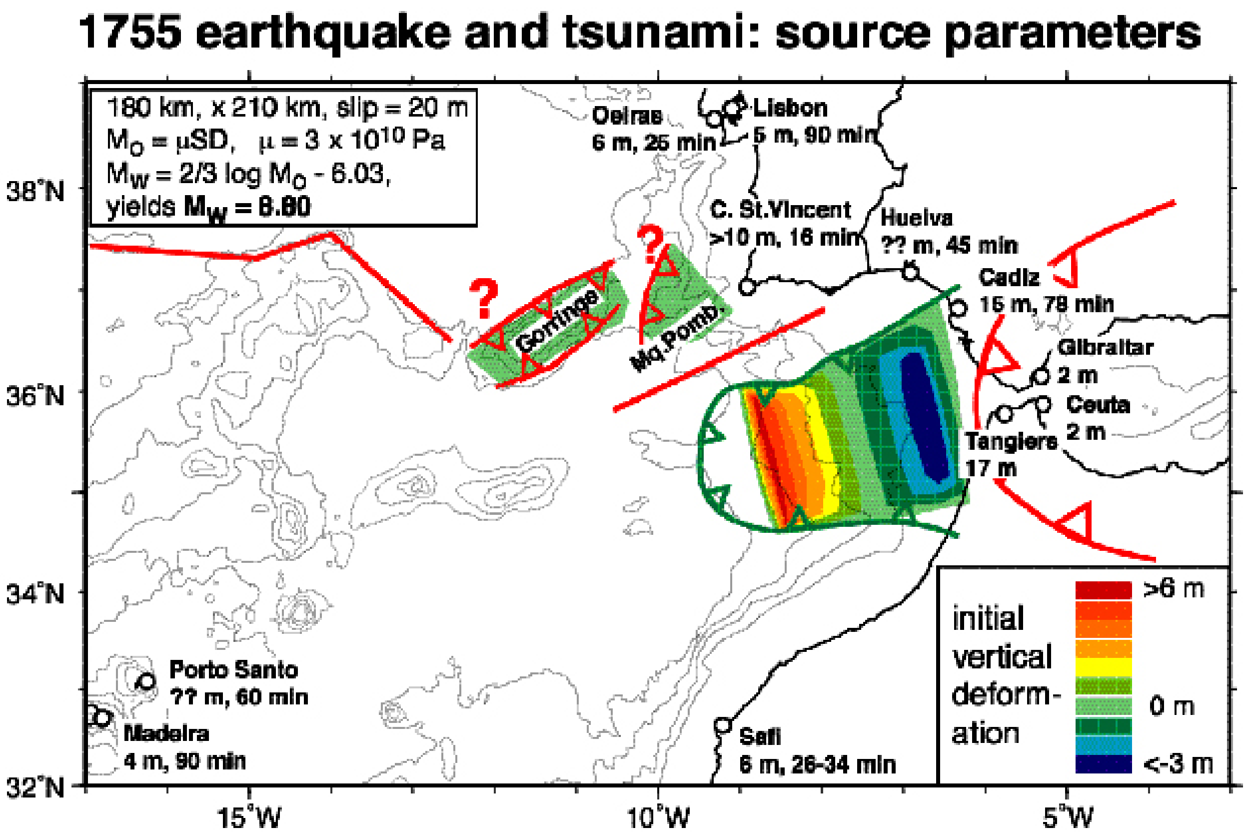


**Figure 6.7.** Tsunami run-up heights and travel times of the great Lisbon earthquake. Courtesy of Marc-Andre Gutscher.

Along a SE-NE trending line (station GeoB9004-1), we placed eleven heat flow penetrations (**Figs. 6.8 and 6.9**). Most profound, the data on the footwall provide values of ~64 mW/m$^2$, while the hanging wall is characterised by a heat flow anomaly of ~54 mW/m$^2$. This trend measured with the violin-bow design heat probe is supported by measurements with MTLs attached to two gravity cores (**Fig. 6.8**). Higher values near the area where the fault breaches the surface may either indicate the effect of thermal refraction forced by the topography or seepage. Overall, the heat flow data support the idea that the Marques de Pombal fault represents a region of active under-thrusting.

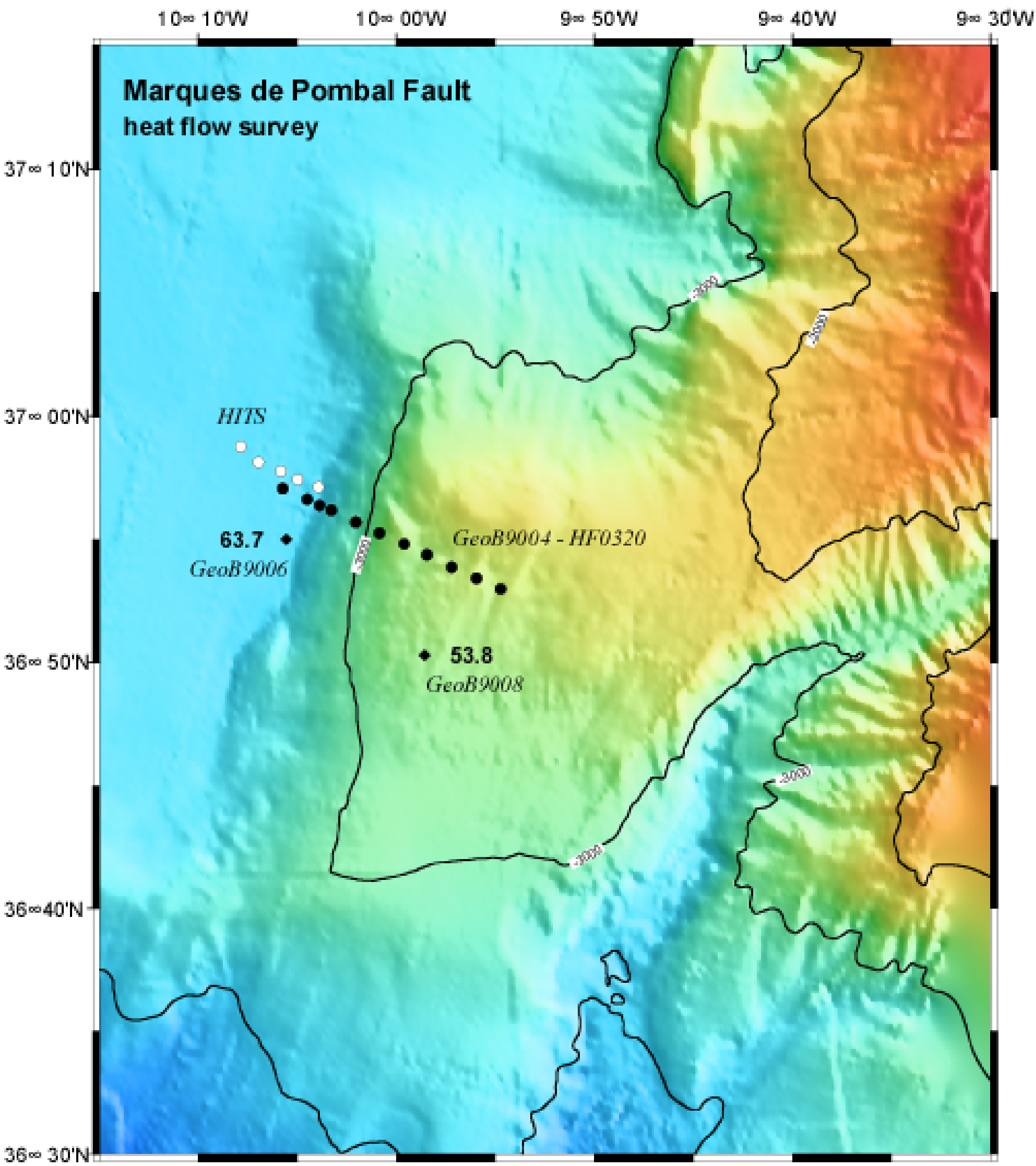


**Figure 6.8.** Heat flow data points from the previous HITS survey (white dots) and SO175 (black dots) across the MPF. The two data points south of the profiles indicate results from MTL measurements on gravity cores (in $mW/m^2$).

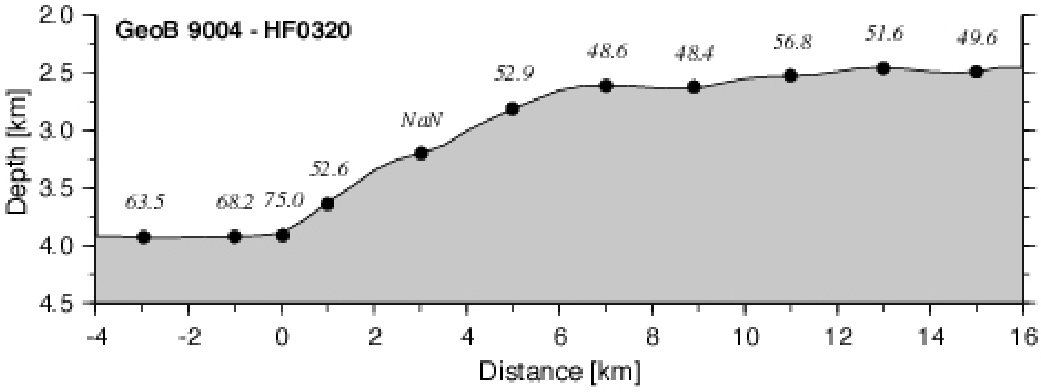


**Figure 6.9.** Results from heat flow survey (GeoB9004-1); for location see **Fig. 6.8** above.

### 6.2.8. Microbiology

(H. Niemann, T. Wilkop)

Methane concentrations were measured on board from samples taken at the cut section of gravity cores or at the lower part from MUC-cores. In the Marques de Pombal landslide area, low methane concentrations (<0.2 mM) were found (**Fig. 6.10** and **Table 6.2**). This suggests that the landslide was probably deposited long ago, and that faulting and landsliding is presently inactive.

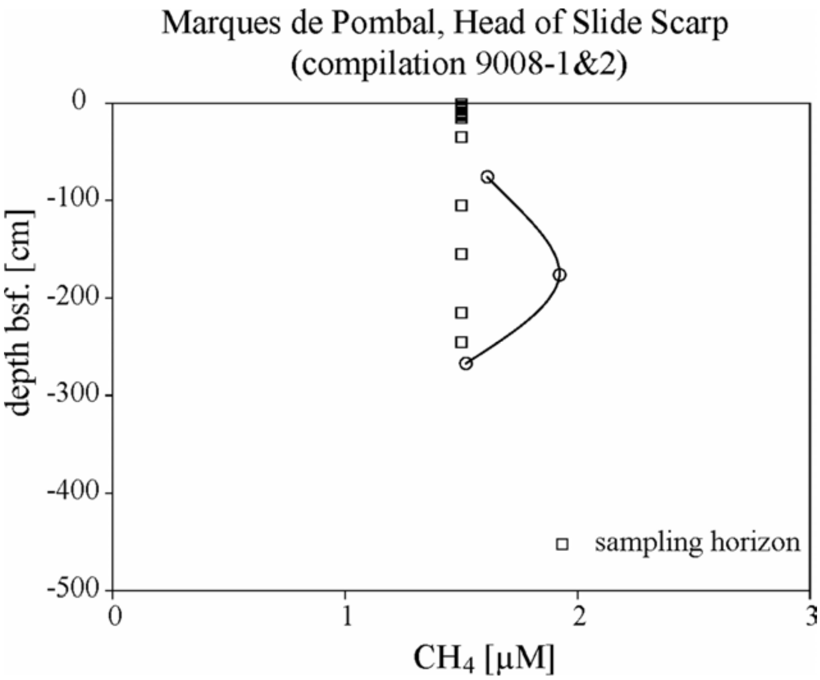


**Figure 6.10.** Methane consentration at station GeoB 9008-2.

| **Device**<br>**Name of Struct.** | **Station** | **AOM, SRR**<br>**SO4, CH4** | **FISH**<br>**DNA** | **Life**<br>**sediment** | **Bio-**<br>**marker** | **carb.**<br>**S. Noe´** |
|---|---|---|---|---|---|---|
| | - | | | | | |
| MUC | 9008-1 | 0-2 | 0-5 | | 0-5 | |
| Head of scarp | | 2-4 | 5-10 | | 5-10 | |
| at M de Pombal | | 4-6 | 15-20 | | 10-15 | |
| | | 6-8 | | | 15-20 | |
| | | 8-10 | | | | |
| | | 10-12 | | | | |
| | | 12-14 | | | | |
| | | 14-16 | | | | |
| GC | 9008-2 | 30-40 | 30-40 | | 30-40 | |
| Head of scarp | | 100-110 | 100-110 | | 100-110 | |
| at M de Pombal | | 150-160 | 150-160 | | 150-160 | |
| | | 210-220 | 210-220 | | 210-220 | |
| | | 240-250 | 240-250 | | 240-250 | |

**Table 6.2.** Microbiology results at the Marques de Pombal landslide. See text.

## 6.3. Mud volcano, diapir, carbonate mound studies

### 6.3.1. Introduction and *state-of-the-art*

(A. Kopf)

Mud volcanism has been demonstrated to be a global phenomenon (Higgins and Saunders, 1974), which is commonly associated with compressional tectonics and sediment accretion at convergent margins (e.g. Brown and Westbrook, 1988; Kopf, 2002). Quiescent as well as catastrophic emission of greenhouse gases (mostly methane) accompanies extrusion (Higgins and Saunders, 1974; Kopf, 2003). Mud domes and diapirs frequently occur in marine subduction zones at the plate boundary near the toe of accretionary prisms (Henry et al., 1996), further landward in the forearc (Mascle et al., 1999), but also on land where collisional processes and deformation are more accentuated (Lavrushin et al., 1996). Irrespective of the tectonic compression, the main driving force of mud extrusion is the negative buoyancy of the clay-rich material at depth (**Fig. 6.11**.). Fluids may either be trapped as a result of high sedimentation rates or lateral influx into clay-bearing sediments, or may be generated *in situ* owing to processes like mineral dehydration reactions and hydrocarbon generation at greater depth (e.g. Hedberg, 1974) (see fluid sources in **Fig. 6.11**.). Fluids and mud either extrude together (i.e., as diatremes), or the fluid may be expelled more rapidly than the upward-moving mud mass (i.e., mud volcanoes juxtaposing diapirs) (e.g. Brown, 1990). Quantitative fluid flux estimates show expulsion at very high rates through mud volcanoes, suggesting a profound influence on geochemical cycling and fluid budgets in subduction zones (Kopf et al., 2001).

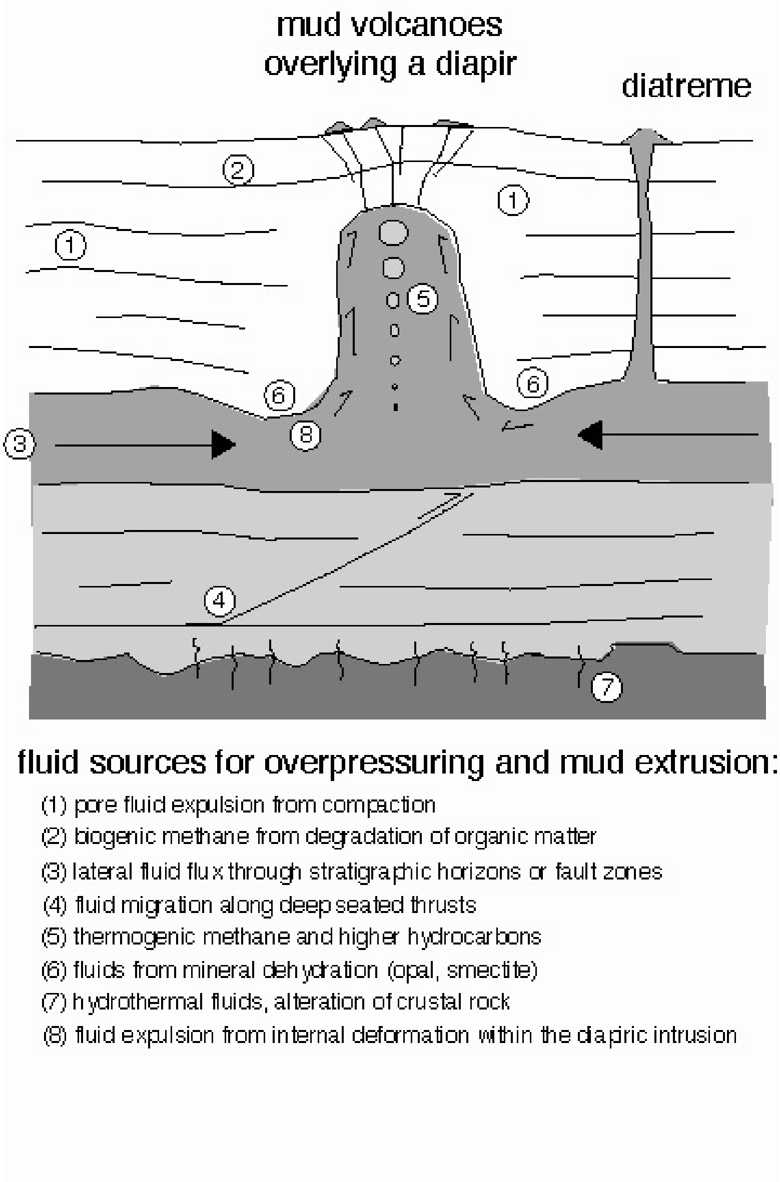


**Figure 6.11.** Fluid sources at various depth which contribute to mud mobilisation, ascent and extrusion/eruption. After Kopf, 2002.

In the Gibraltar region, many mud volcanoes have been described during earlier cruises (e.g. TTR-9, -10, -11; Kenyon et al., 2000, 2001, 2002). There has been reports that some of the domes bear gas hydrates (e.g., *Ginsburg, Bonjardim* and *Captain Arutuynov* mud volcanoes) and faunal assemblages, while others appear to be inactive (e.g., the *Lolita* feature). Some of them have been proposed to be actively venting, and one of the goals of the cruise was to cover much of the wedge with video surveys, sampling and mapping in order to see variations in fluid flow and mud flow activity. Main aims on site were to:

- observe indicators for active venting (e.g. bubbling, bacterial mats, *Pogonophora*, etc.) on seafloor video tracks,
- collect authigenic carbonate crusts and chimneys,
- recover massive gas hydrate,
- characterise the various types of deposits, such as mud breccia, gaseous clayey ooze, etc.
- detect various mud flow events at the same feature to demonstrate and date episodic activity, and
- determine from which depth interval the mud and fluid phase were mobilised.

One of the most spectacular events in the investigation of the European continental margin during the last decade has been the discovery of the giant carbonate mounds along the Celtic margin. In water depths of 700 to 1000 m, these up to 250 m high mounds are covered by extensive coral reefs (mainly cold-water corals *Lophelia pertusa* and *Madrepora oculata*). Through the last years much effort has been put in the investigation of these structures and it appears that the corals living on top of them and contributing significantly to their composition are closely related to the Mediterranean Outflow Water (MOW). However, due to a lowered sea level during glacial times (~130 m) the water mass exchange between the Mediterranean and the Atlantic was significantly reduced and no MOW reached the Celtic margin. Indeed, up to now no corals dated to a glacial age have been recovered from the well-known carbonate mound provinces of Ireland. Recently, cold water corals also have also been reported from the Gulf of Cadiz, close to the source of the MOW. There the corals have been found as a kind of by-catch during the investigation of mud volcanoes. These mud volcanoes in the Gulf of Cadiz form similar topographic features as the carbonate mounds off Ireland, although their formation related to active venting of fluids and/or gases seems to be entirely different. However, also for the formation of the carbonate mounds the role of hydrocarbons is strongly debated. Nevertheless, these mud volcanoes are host for the corals and they might form a glacial refuge area for them, as it is expected that at least some MOW reached the Gulf of Cadiz also during glacial times. Alternatively, during the glacial the corals retracted entirely into the Mediterranean, from where glacial *Lophelia* reefs have been reported.

During the GAP-cruise the investigation of living and fossil corals from the Gulf of Cadiz aimed to provide significant new information about the still poorly known cold water corals with respect to:

- species integrity in a new area,

- their spatial distribution,
- the relation of the corals to the MOW,
- the presence or absence of these corals outside the Mediterranean during the glacial,
- effects of hydrocarbon venting on the coral community.

### 6.3.2. Operations

During SO175, a total of 9 mud volcanoes have been investigated, some of them at different stations. A total of 39 stations were dedicated to mud volcano research. For detailed information on exact location, see station list (Appendix Ch. 8.1). Among the 9 mud volcanoes studied, 8 were already discovered during earlier cruises (see map in **Fig. 6.12**). The only new discovery, a small mud dome at lat 35 39.30 N, long 07 16.52 W, was named after the Greek Titan *Atlas*, son of Iapetus and Clymene. Among the operations, we carried out bathymetric mapping and echography as a standard procedure. Video sledge (OFOS) surveys were done at 6 mud volcanoes (see below), whereas seismic reflection profiling was carried out only across two mud domes (*Ginsburg* and *Yuma* mud domes; station 9056). In addition, coring (both MUC and gravity cores), TV grabs and heat flow measurements were carried out (see Appendix Ch. 8.1.).

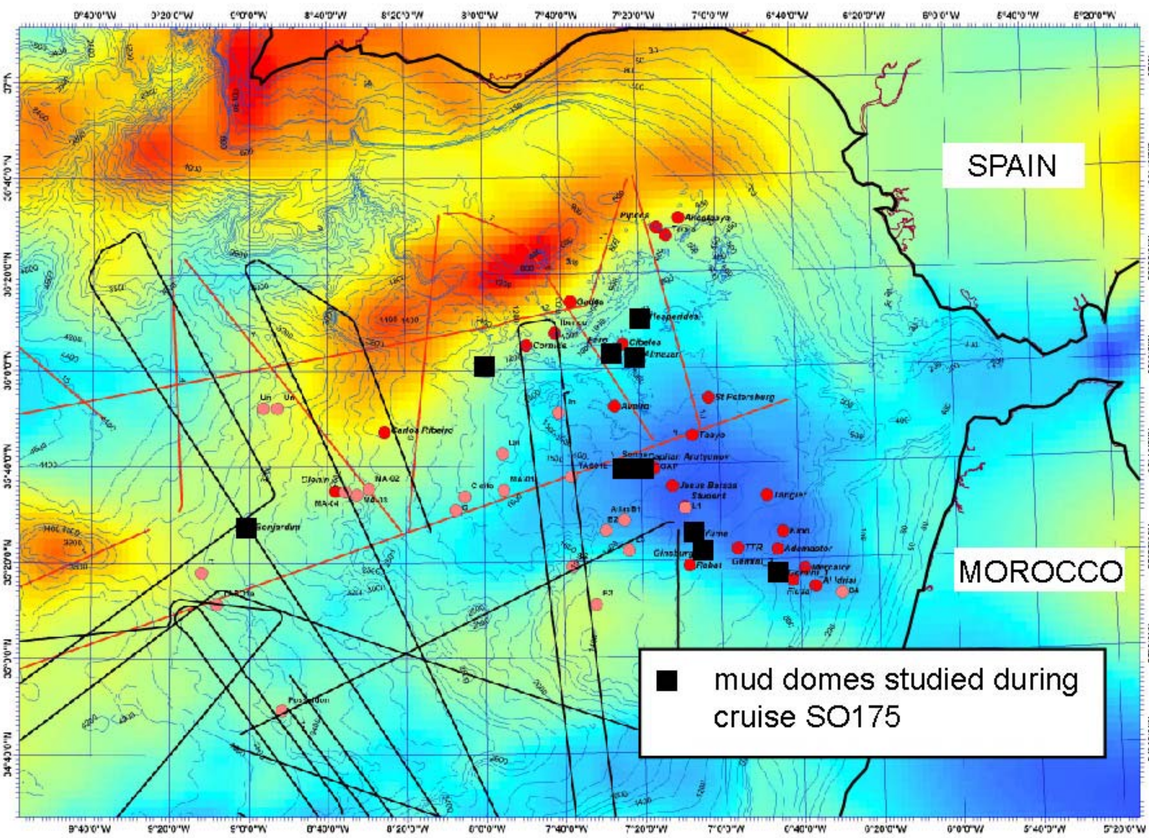


**Figure 6.12.** Bathymetric map of the study area with mud domes; features investigated are marked by black squares.

### *6.3.3. Mapping/geophysics, OFOS and TV grabs*

**a) *Lolita* Mud volcano**

The *Lolita* mud feature is probably the most prominent topographic high on the Gibraltar wedge, and can even be seen on the GEBCO bathymetric data charts (**Fig. 3.1**). However, earlier cruises have failed to fully understand the nature and origin of the feature. Main reasons include the recovery of hemipelagic sediments which hint towards inactivity of the dome for quite a while. *Lolita* rises about 500 meters relative to the surrounding seafloor, with its crest reaching a depth of about 1500 m below sea level (bsl). During SO175, was *Lolita* targeted early on with the video sledge to clarify whether there is venting, biota, or other evidence for active fluid expulsion and mud extrusion.

OFOS surveys GeoB 9012 and -9013 were carried out during the early part of the cruise; tracks are plotted as overlay to the bathymetry in Figure **6.13**. Unfortunately, the video observations have not provided the slightest hint towards gas bubbling, organisms indicative of active fluid venting, or massive authigenic precipitates. In fact, the surface was covered with slightly consolidated oozes (i.e., background sediments) and not with mud breccia. Since we aimed to sample extrusive products of active mud volcanism or diapirism, no sampling efforts were undertaken at this site.

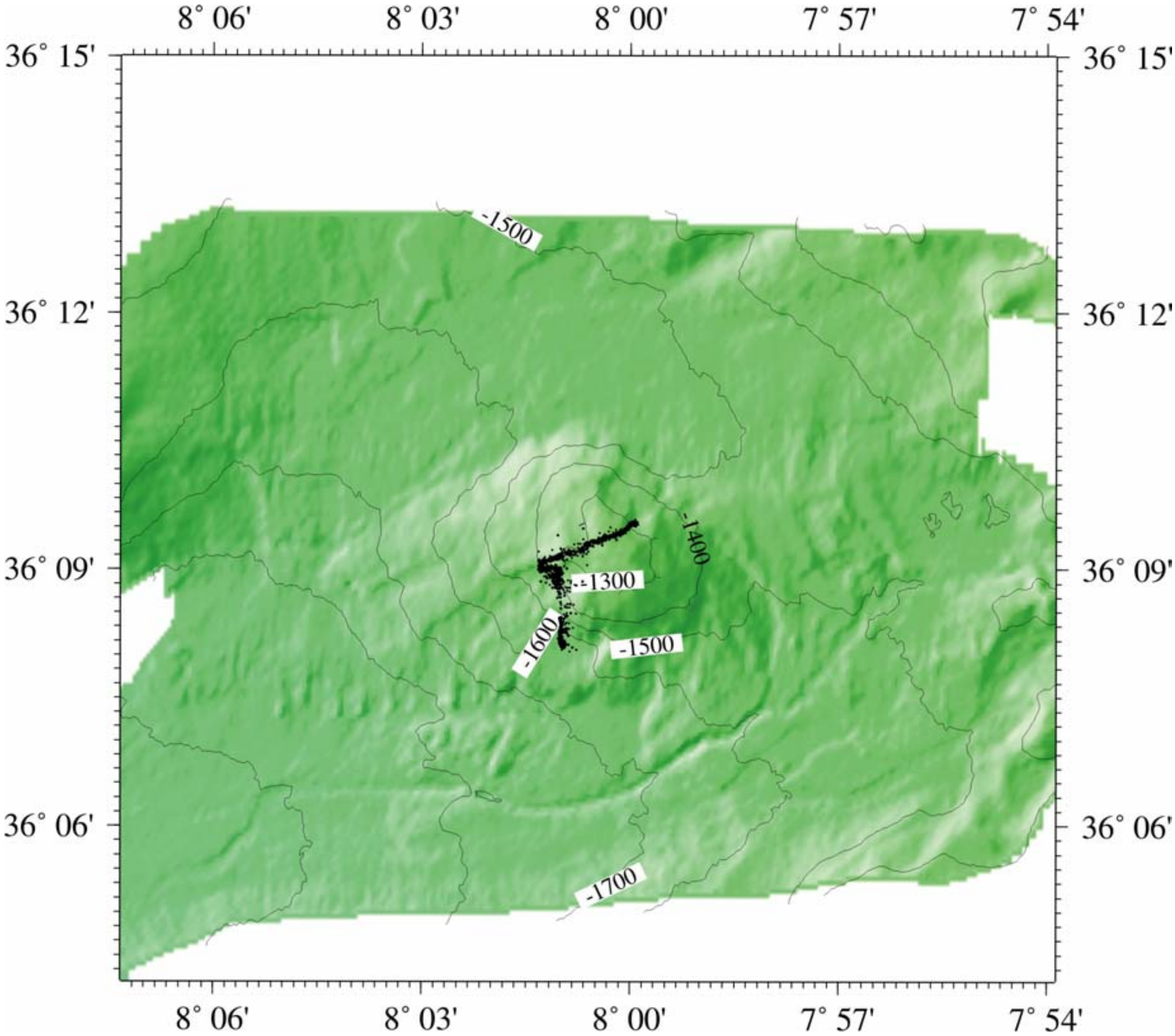


**Figure 6.13.** Bathymetric chart overlain by OFOS tracks of stations GeoB 9012 and 9013.

**b) *Hespérides* mud volcano**

The *Hespérides* is the largest structure identified in the northermost area of the Gulf of Cádiz (**Fig. 6.14.**). Previous detailed multibeam bathymetry show its composed by six single cones with a seafloor diameter of about 3 km (**Fig. 6.14**, see also Somoza et al., 2003). Previous cores from these domes yielded mud breccia that consist mainly of heterometric clasts (up 5cm) of "blue" marls, characteristic of the Early-Middle Miocene pre-olistostromic unit M1 (Maldonado et al., 1999).

Two OFOS tracks (GeoB 9016 and GeoB 9017) crossing from NE to SW and from S-N respectively, were made in order to observe fluid-venting related features and carbonate mound structures along this mud volcano complex. Another target for OFOS was to detect deep water corals, reported on previous gravity cores.

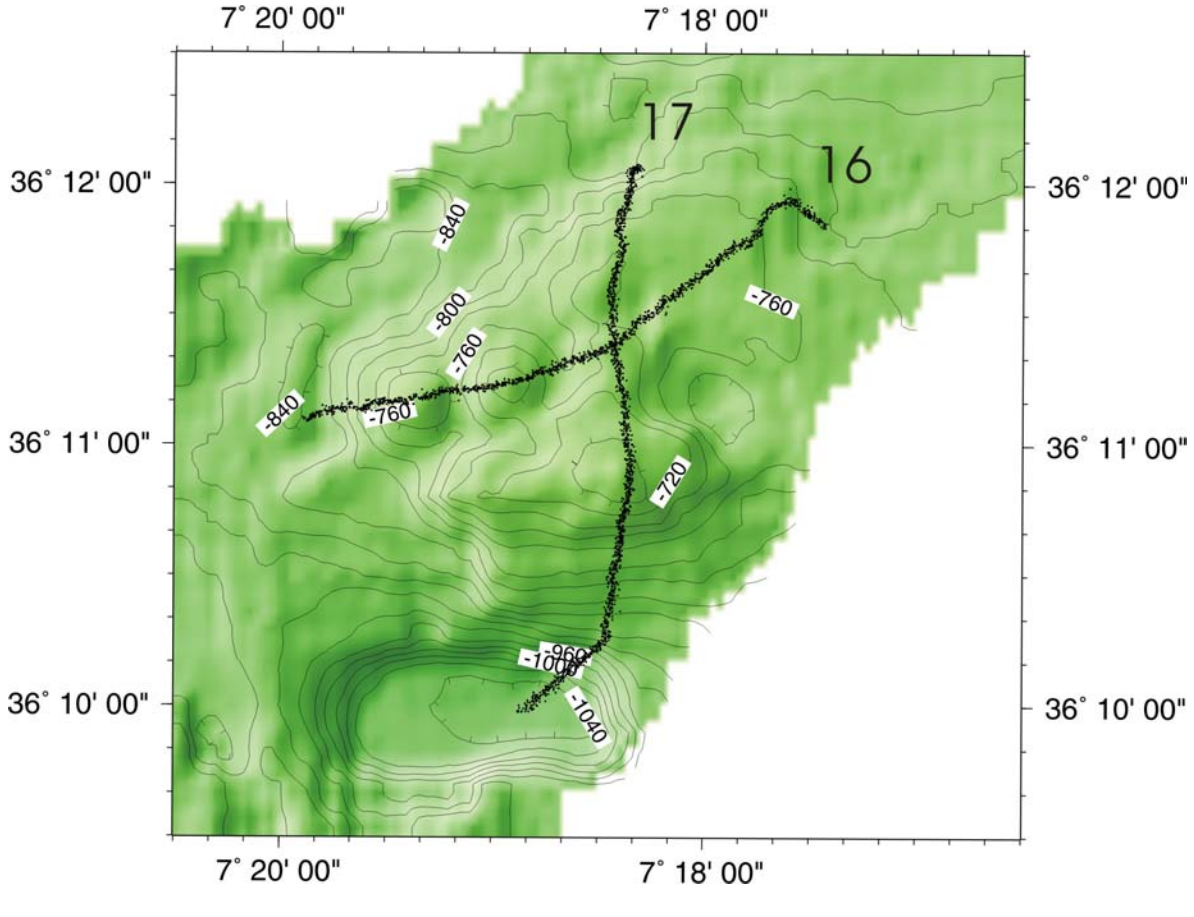


**Figure 6.14.** Bathymetric chart overlain by OFOS tracks of stations GeoB 9016 and 9017.

The first track (GeoB9016) began near the foot of the flank of the northernmost cone, and consisted of thick gravelled horizons interbedded with mud, interpreted as outcrops of older mud-breccia flows. The track continued to the southwest, rising through a broad plateau at the easternmost portion of the complex. Only some scattered carbonate clasts interbedded with rippled sandy and muddy patches were observed across this gently slope plateau. The tracks continues until the central cone of the complex, a small steep cone. The summit region of this cone was observed to be formed by vast carbonate slabs with some scattered carbonate chimneys. Abundant tubes of *Pogonophora* sp. were observed overlying the carbonate slabs. Small bubbles coming up from some fissures were observed in this area, but to date there is no confirmation of such venting. This area was the target for TV grab (Station GeoB9024), collecting considerable amounts of carbonate crusts and slabs with numerous bivalves interbedded.

Numerous sessile organisms as small corals, brachiopods, small sponges, were attached to carbonate crusts

The track continued to the northwest, descending to the westward flank of the cone. Only scattered carbonate crust and muddy patches were observed. Two more cones (named as H1 and H2) were crossed at the end of the track. Apparently, these two cones show on the multibeam bathymetry a best cone-shaped morphology, probably as a consequence of its more recent activity. However, along these two single cones, only mud breccia-type sediments were observed, sometimes interbedded with sandy patches and scattered fragments of carbonate crust. There was no evidence for recent activity of these two mud volcano cones.

Track 2 (GeoB9017) began at the northernmost flank of the Hespérides mud volcano complex. The first sight of the OFOS camera was a seafloor covered of carbonate chimneys. Small fragments of carbonate chimneys were formerly reported in the *Hespérides* area (Diaz del Rio et al., 2003), but there were no observed such amounts of chimneys like in this area, as others of the Gulf of Cádiz. The track continued upslope of the flank, composed mainly of muddy areas with patches of rippled sands and scattered carbonate crusts and chimneys. This track crosses the GeoB9016 track at the summit of the central small cone, which consists of huge amounts of carbonate slabs and crusts with abundant tubes of *Pogonophora* sp. The track continued along the flank of this cone reaching the largest and southernmost cone of the complex. The summit of this cone also exhibited, as the former, huge masses of carbonate crusts. At its southernmost flank, the seafloor was covered extensively by deep water coral forming reef-like patches. Different type of corals was sampled with the TV grab (GeoB9022) in this area. The dead coral rubble consists of a lot of small broken coral pieces and coral branches up to 30 cm high and probably originating from species such as *Lophelia pertusa*, *Madrepora oculata*, and *Desmophyllum*. Several gastropods, brachiopods and small hydrozoa were found attached on the dead coral pieces. Some small living coral species settled on the dead coral branches occasionally. Numerous carbonate slabs, crusts and fragments of chimneys were also collected. Most of the chimney pieces are oxidized as indicated by the brown to light brown colours, and are varying in shape and size from a few centimetres up to 40 cm across. Small corals and encrusting organisms are attached on the chimneys. The track continue down slope along the southernmost flank of the cone, showing steep slopes ranging between 8-12º. A high density of carbonate chimneys, some about 2 meters long, were observed descending along this flank (**Fig. 6.15**).

**Figure 6.15.** Still photograph taken with the video sledge OFOS during station GeoB 9012. A large number of chimneys and other carbonate rubble can be identified.

The area was the target for a TV grab (station GeoB9023) with more than 300 kg of carbonate chimneys collected, both cylindrical, mounded, branched, and mushroom types (Diaz del Rio et al., 2003). Small corals, sponges, brachiopods and other little organisms were attached to the chimney pieces. Examples of both chimneys (**Fig. 6.16**) and corals (**Fig. 6.17**) recovered and placed on deck RV *Sonne* are shown below. The track finished at a pool-like structure at the southernmost part of the Hespérides mud volcano complex. This oval depression shows current structures, as rippled sands, probably as consequence of the Mediterranean Outflow Water (MOW). Sea floor temperature data from heat flow probes in this area show anomalous warmer water veins flowing just 1-2 meters above seabed. At the same locality, heat flow measurements showed anomalous values due to MOW waters that give rise to reverse geothermal gradients (see station GeoB9025 and Ch. 6.3.7. below).

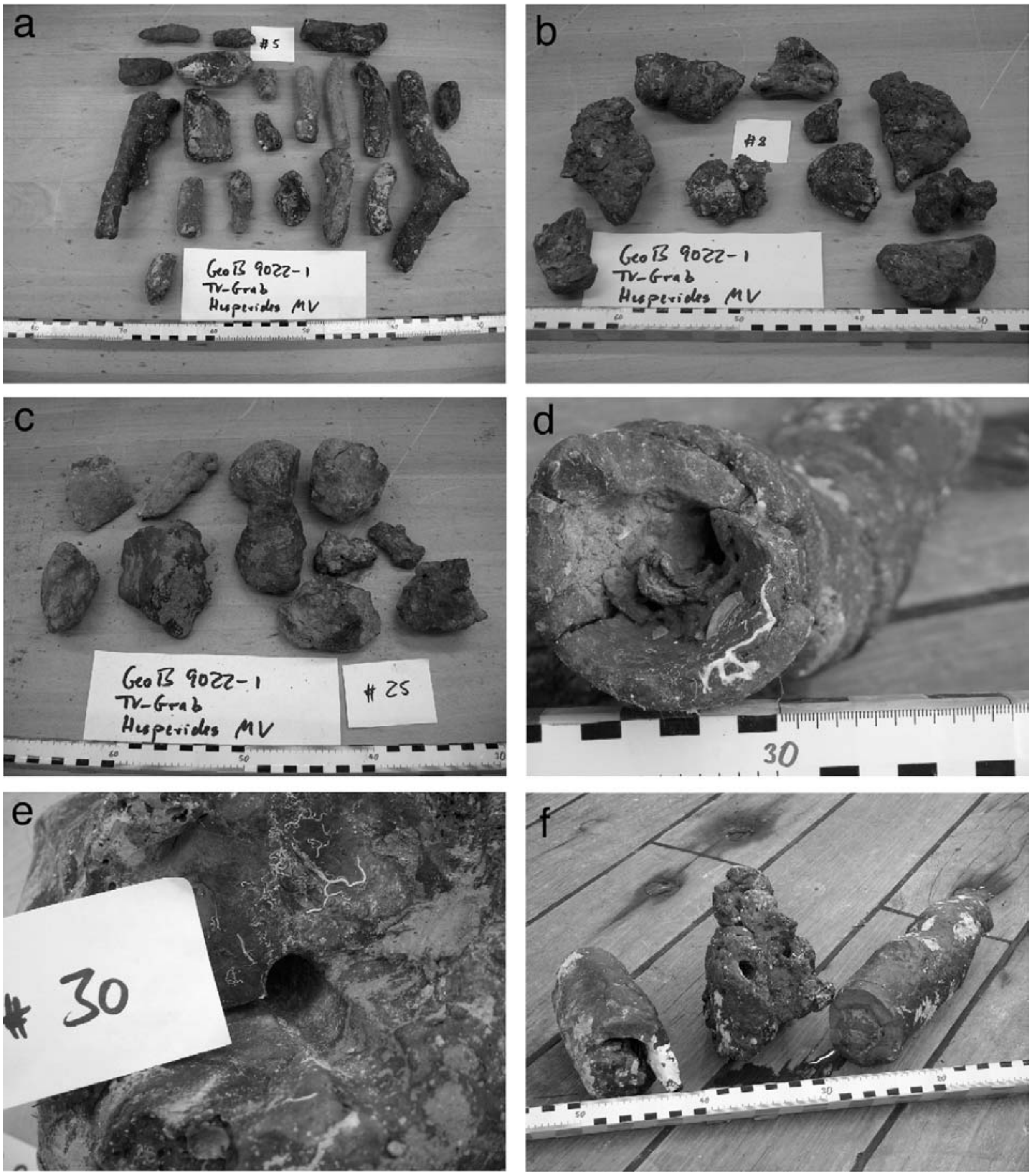


**Figure 6.16.** Photographs of carbonate chimneys on deck. Please note variable size and shape (a-f).

**Figure 6.17.** Cold water corals recovered on *Hesperides* mud dome, including corals on a carbonate chimney (left), and broken off fragments found in the mud (right). See text.

Methane concentrations made from the three cores taken on the *Hesperides* MV cones (GeoB9019, GeoB9020, GeoB9021) show low values (<0.2 mM), probably reflecting inactivity or slow rates of fluid venting forming large amounts of carbonate crust after mud volcano formation (see Ch. 6.3.8.).

**c) *Faro* mud volcano**

The *Faro* MV appeared on previous multibeam data as an oval-shaped feature with a maximum seafloor diameter of 2.6 km and exhibits 190 m of bathymetric relief (Somoza et al., 2003). Seismic lines revealed that it has a cone-shaped profile with high acoustic backscatter from its surface. *Faro* is situated along a major arcuate structure, some 8 km in diameter, that is linked to two more mud volcanoes, the *Cibeles* MV to the west and *Almazan* MV to the to east. First, the three domes were mapped using the multibeam system (**Fig. 6.18**).

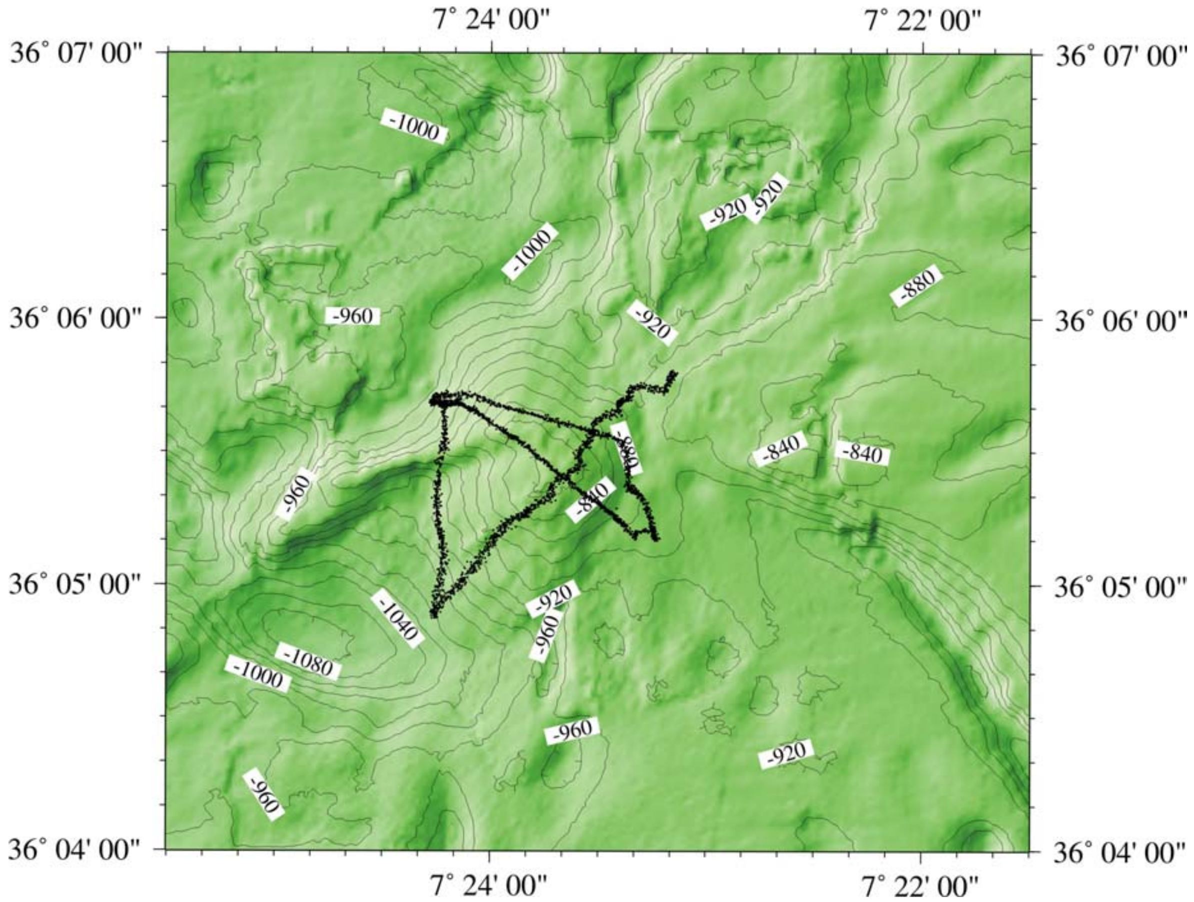


**Figure 6.18.** Bathymetric chart overlain by OFOS tracks of station GeoB 9028.

OFOS track GeoB9028 was carried out to identify active fluid venting structures, carbonate related mound features and coral patches. The first transect, NW-SE in direction, began at the northernmost flank of the *Faro* mud volcano. Scattered corals appeared on the lowest flank of the cone, whereas at the uppermost, only rippled sand with muddy patches were covering the seabed. The summit of the cone is covered by carbonate slabs and crusts, which appear less abundant and less massive than on the summit of *Hespérides*. The southernmost flank showed more abundant carbonate slabs, specially at the upper slope, forming steps well distinguished on multibeam bathymetry. The lowermost part of the flank is formed by muddy sediments showing patches of coarser grained sand. At the foot of the southern flank, the track continue to the north, in order to cross the arcuate structure observed on previous multibeam bathymetry. This second transect showed that the southernmost portion of this arcuate ridge consists of a gently sloping mud with scattered but abundant individual corals and hydrozoa. Some of the summit region is covered with hemipelagic sediment, which is strongly bioturbated in some areas. It seems that isolated corals are aligned along an E-W direction. The summit of this arcuate-shape crest again is formed by a "dyke-like", steeply dipping bed of carbonate slabs, with scattered chimneys between large slabs. *Pogonophora* sp. was also visible on some carbonate slabs. This second transect continue to descend in a S-N direction through the northern flank of the "dyke-like" structure covered only by rippled sand and muddy patches. At the bottom of this flank, the OFOS crosses a small channel-like feature probably related to MOW current. Along this channel, numerous bivalves forming low mounds were observed . At the end of this transects, and just surrounding the channel, carbonate slabs were apparently covered by bacterial mats. This was the main target for next video MUC stations (GeoB9029-1 and -2; see below). Because of hard carbonate slabs, two sampling attempts with the MUC were unsuccessful. Therefore, a TV grab was deployed in order to try to collect the bacterial mats seen in this area. The TV grab (GeoB9029-3) then surveyed the bacterial mats area. More carbonate crusts, bacterial mats and bivalves were observed. The TV grab aimed to extract bacterial mats from the carbonate slabs. Samples from this grab show mythilid bivalves likely to be related *Calyptogena sp.* (contain sulphide oxidizing bacteria in their gills) and other non-classified bivalves, but was unable to collect bacterial mats. The next target for TV grab was to try to collect some *Pogonophora* sp. associated with the "dyke-like" feature formed by extensive carbonate slabs (as recovered during TV grabs GeoB9030; see text and pictures in Ch. 6.3.4.). Large carbonate slabs, exceeding 2 m in height, were observed in a E-W transect. *Pogonophora* sp. and some scattered chimneys were also observed between carbonate slabs. The TV grab collected only greyish mud and some branches of live coral attached to grab-sampler.

**d) *Almazan* mud volcano**

*Almazan* MV was mapped during the multibeam survey in the vicinity (see pt. c above), however, did not get studied by OFOS. Sampling included video MUC, TV grab, and gravity cores (see below).

**e) *Captain Arutyunov* mud volcano**

This OFOS track (GeoB 9035) was designed to observe the N and S flank of the *Captain Arutyunov* mud volcano to identify possible targets for gas hydrate sampling (**Fig. 6.19**). Video observations along a N-S transect and a short SW-NW transect across the summit area showed very homogeneously distributed fine-grained to sandy sediments with strong bioturbation. Frequently the track areas with evenly distributed mud clasts were observed. However, no evidence for active and focussed fluid flow or biological assemblages that would indicate near-surface methane flux were discovered. Still, the feature was sampled (TV MUC, TV grab, gravity cores; see list of stations, Ch. 8.1) due to its gas hydrate abundance and proposed fluid venting when investigated during earlier cruises.

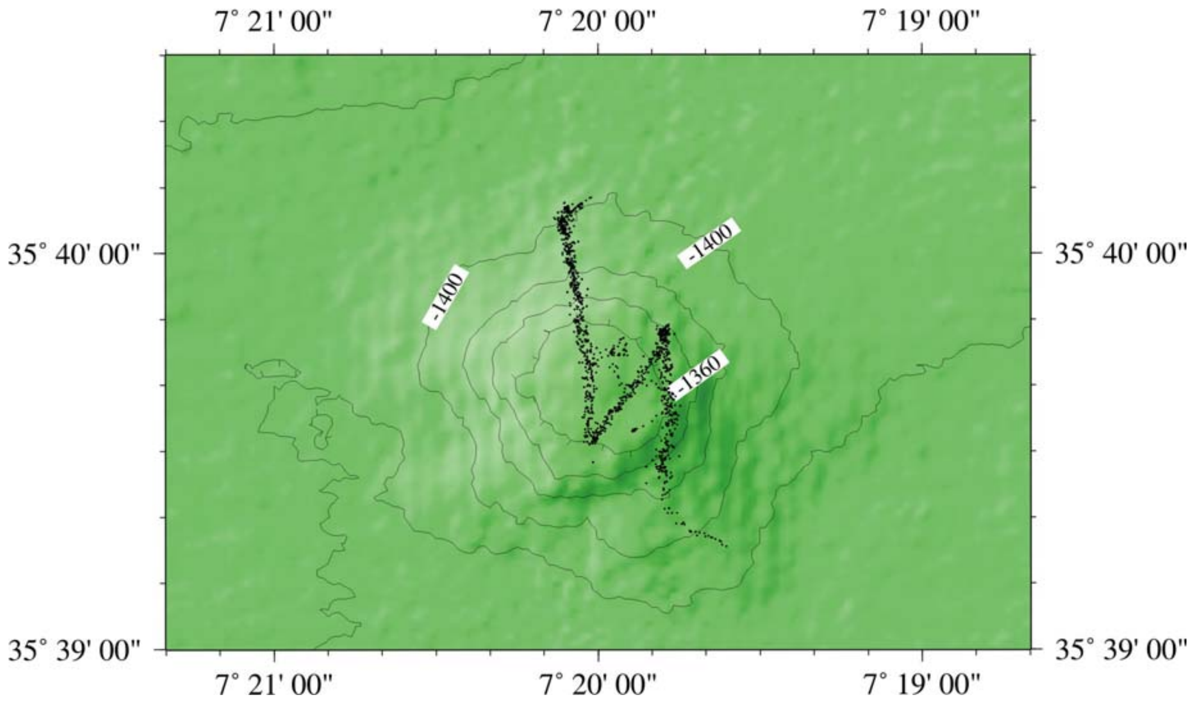


**Figure 6.19.** Bathymetric chart overlain by OFOS tracks of station GeoB 9035.

**f) *Bonjardim* mud volcano**

*Bonjardim* mud volcano is one of the few deep-water mud domes in the Gibraltar wedge area. It has previously been geophysically characterised and sampled and is known for its gas hydrate occurrence (see Kenyon et al., 2001; their Fig. 18). Since our interest was mostly the recovery of gas hydrates as well as the associated heat flow patterns, no seismic profiling or OFOS surveying was carried out here. For location, refer to **Figure 6.12**.

**g) *Ginsburg* mud volcano**

*Ginsburg* mud volcano is located in the southern Gulf of Cadiz area just south of *Yuma* mud volcano (see **Fig. 6.12**). The OFOS track (GeoB 9057) was designed to identify areas suitable for recovery of cold water corals, gas hydrates, and other sampling targets. A NE-SW course across the summit region was followed by a W-E and N-S transect on the flanks of Ginsburg mud volcano (**Fig. 6.20**). The dominant lithology was hemipelagic sediments with rare occurrence of carbonates or isolated patches with coral fragments, throughout the whole track sediments were strongly bioturbated, but little epibenthic fauna was observed. The base of the mud volcano and most showed current-induced features like ripple fields.

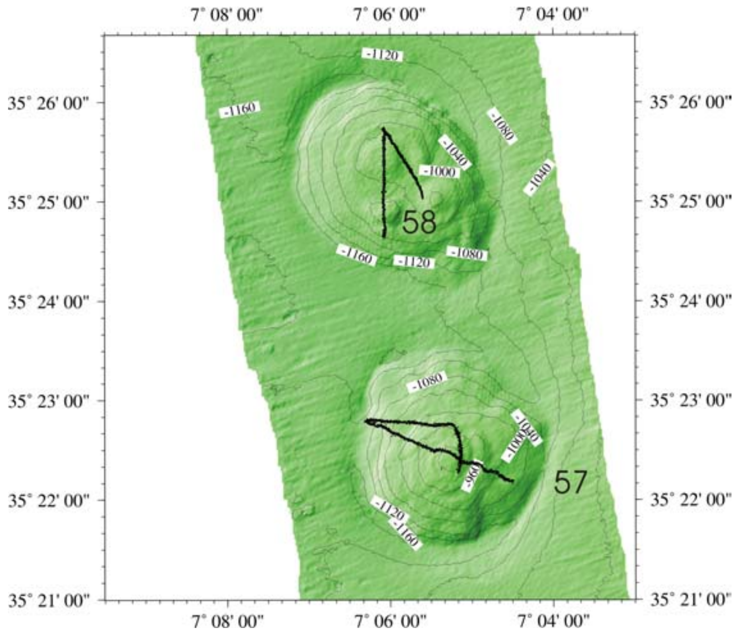


**Figure 6.20.** Bathymetric chart of *Ginsburg* (labeled "57") and *Yuma* (labeled "58"; see next pt. below) mud volcanoes overlain by OFOS tracks (stations GeoB 9057 and 9058).

**h) *Yuma* mud volcano**

Immediately in the vicinity of *Ginsburg* mud volcano we surveyed *Yuma* mud volcano with two N-S and NW-SE trending transects across the summit area and W flank (station GeoB 9058; see **Fig. 6.20**). Similar in appearance to *Ginsburg* mud volcano, *Yuma* showed mainly hemipelagic sediments with strong bioturbation features. In addition, a few areas with mud breccia and small fields with bivalves shells and were observed, but no systematic trend could be found.

A seismic reflection line was shot in roughly N-S-direction across *Yuma* and *Ginsburg* MVs (**Fig. 6.21**). The data illustrate very nicely how the ascending mud has pierced the layered hemipelagic sediments in this area off Morocco. The region immediately beneath the domes shows a seismically opaque, chaotic pattern with no patterns like bedding or structure (e.g., faults). The width of the extruded body roughly equals that of the dome at its base on the seabed. Sampling was carried out on either feature (see Ch. 6.3.4. below).

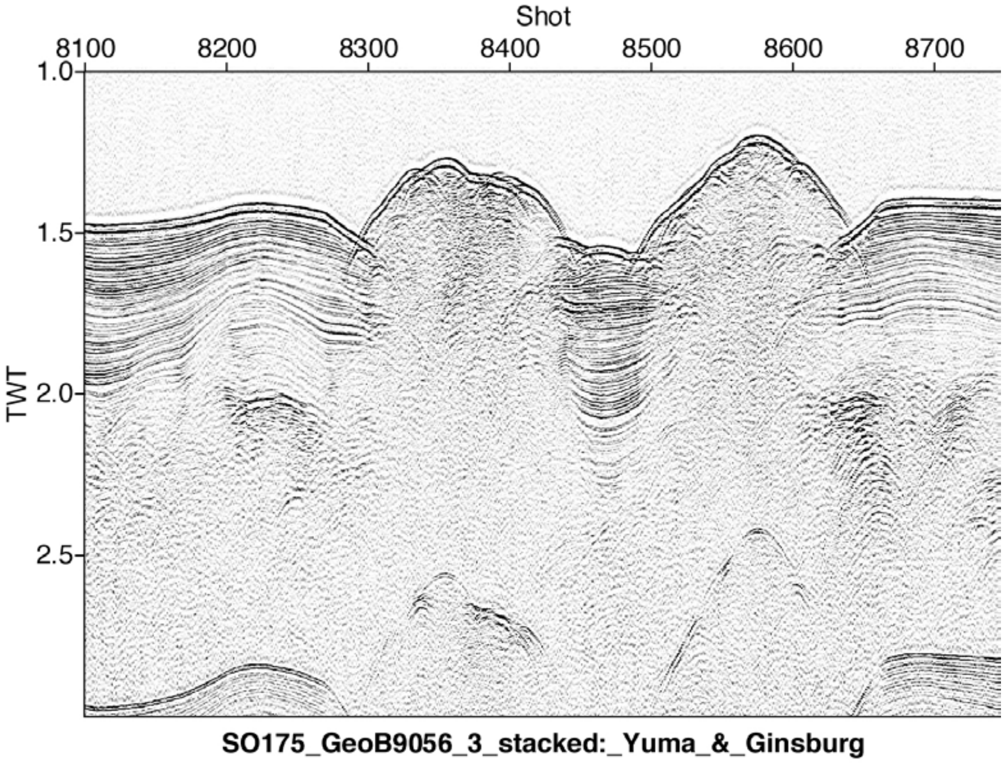


**Figure 6.21.** Seismic reflection profile across *Ginsburg* and *Yuma* mud volcanoes, roughly located N-S (station GeoB 9056).

**i) *Atlas* mud volcano**

A number of supposed mud volcanoes were sampled mid-cruise, of which only one can be positively identified as mud dome. All others had hemipelagics in the upper meters of subseafloor sediment and were conservatively termed mounds (see **Table 6.3.**). At station GeoB 9038, however, the recovery of mud breccia in a gravity core provides evidence for recent extrusive activity. The clayey matrix of yellowish grey colour contains clasts of mm- to cm- size (see Ch. 6.3.4. below).

### 6.3.4. Lithology

(D. Hebbeln, B. Dorschel, M. Lutz)

**Sediment sampling on mud volcanoes and other structural heights**

The mud volcanoes in the Gulf of Cadiz have been cored in order to sample mud breccia, as this is supposed to provide clues about the root of the mud volcanoes in the deep. Other structural heights in the area have been sampled to investigate their nature, e.g. if these are also mud volcanoes or if these are of another origin.

On the already proven mud volcanoes *Hesperides, Capt. Arutyunov, Bonjardim*, *Ginsburg* and *Gemini* mud breccia has also been found during this cruise. On *Hesperides* MV two sediment cores containing mud breccia have been taken (**Tab. 6.3**). GeoB 9019-1 only has a two centimetre thick cover of brownish hemipelagic sediments above the mud breccia. Attempting to core site GeoB 9020-1 ended with a bent core tube, which obviously got stuck in stiff mud breccia close to the sediment surface. Thus, with only a very thin veneer of hemipelagic sediments above the mud breccia it seems that the breccia must have been produced quite recently on *Hesperides* MV. Here, as on the most other sites characterised by the occurrence of mud breccia, this material appeared as a greenish-gray mixture of a fine-grained, very stiff matrix with mud clasts of various sizes. These mud clasts are of quite different lithologies including claystones, siltstones and sandstones, partly with carbonate veneers pointing to tectonic stress and can reach up to fist-size (just fitting in the core liner) or even boulder size (collected by the TV grabs).

Sampling *Hesperides* MV with the TV grab (**Tab. 6.4**) resulted in a huge amount of authigenic carbonate samples. These were either plate- and boulder-like crusts or chimneys, with the latter often being characterised by a central conduit with zonated carbonate around it. Some pieces were actually in a stage in which the soft mud breccia matrix was gradually changing into the hard carbonate crust pointing to a formation of these crusts within the sediment and not necessarily directly at the seafloor. In addition, Hesperides mud volcano has also been sampled successfully for cold-water corals, by TV grab as well as by gravity corer.

On Faro MV mud breccia has only been sampled by the TV grab (**Tab. 6.4**). Also here, a few carbonate crusts have been retrieved. On this MV the gravity corer was only used to sample cold-water coral bearing sediments.

The next mud volcano visited was *Capt. Arutyunov*. Sampling at its top by gravity corer, multi corer and TV grab supplied huge amounts of mud breccia with a considerable amount of gas hydrates. Upon leaving the gas hydrate stability field at ~500 m water depth the video-controlled instruments (MUC and grab) showed extensive degassing indicated by rising gas bubbles. On deck, especially from the voluminous grab samples, a strong $CH_4$ and $H_2S$ smell spread around. As it took some time to open the gravity cores, at the first visual inspection all the gas hydrates were gone although their former positions could be spotted by holes/cracks in the sediment associated with a high water content. Consequently, the mud breccia collected from the top of *Capt. Arutyunov* MV was partly almost soopy and by far not as stiff as observed at the other mud volcanoes. The mud breccia collected by the TV grabs also contained a few mud clasts.

A very interesting core has been collected from the slope of *Capt. Arutyunov* MV. Core GeoB 9037-1 shows an intercalation of hemipelagic sediments with mud breccia (**Fig. 6.22**). Within this 3.76 m long record three individual layers of mud breccia have been found, divided by typical hemipelagic, yellowish grey muddy clays. Thus, detailed stratigraphic analyses of the hemipelagic sediments in this core might allow to date the mud flows and to assess their frequence aiming to describe the activity pattern of *Capt. Arutyunov* MV.

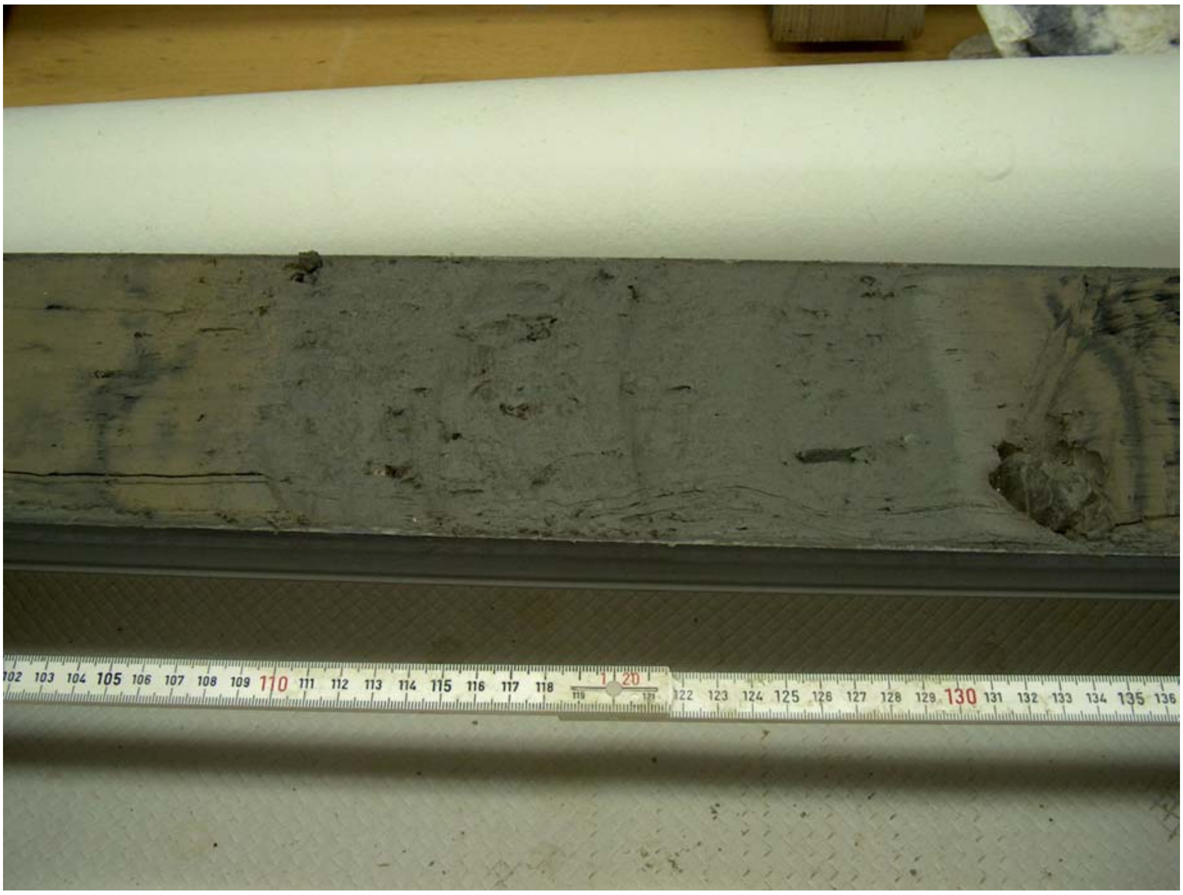

**Figure 6.22.** Interlayering of hemipelagic sediment (left and right portion of core) and gray mud breccia with mm-sized clasts from station GeoB 9037-1.

While approaching *Capt. Arutyunov* MV close to it two other structural heights have been discovered during a bathymetric survey, one to the east and one to the west. Core GeoB 9038-1 from the eastern structure revealed mud breccia overlain by ~1.5 m of hemipelagic sediments. This record proves this structure to be a mud volcano, which was subsequently termed *Atlas* MV.

Its upper part is overlain by yellow mud (**Fig. 6.23A**), while clast-bearing muds occur in the deeper section (**Fig. 6.23B**). The structure slightly west of *Capt. Arutyunov* MV was also sampled by a gravity core (GeoB 9041-1), however, the retrieved ~3.5 m sediment record consists only of hemipelagic sediments. Thus, at this stage there is no evidence that also this structure is a mud volcano.

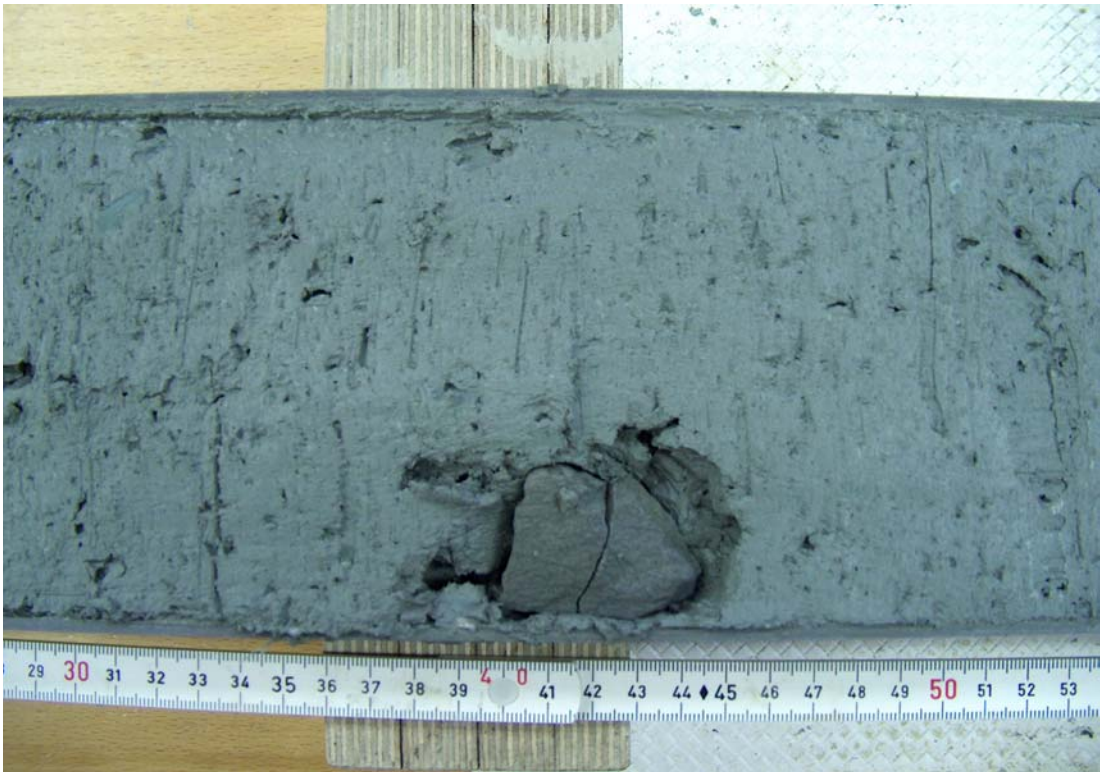


**Figure 6.23. A)** Top of gravity core GeoB 9038 with yellow mud underlain by gray mud breccia (see previous page); **B)** gray mud breccia with cm-sized clast. See text.

The mud volcano sampled in deeper waters in the Gulf of Cadiz is *Bonjardim* MV. One gravity core collected there revealed a 2.6 m sequence of mud breccia overlain only by a few centimeters of hemipelagic sediments. To assess the nature of a near-by structural height, which is formed like a mud volcano with a central depression, it was sampled by two gravity cores. None of these cores collected any mud breccia, thus, an origin as a mud volcano could not be confirmed.

*Ginsburg* MV was again sampled by gravity corer and TV grab. Both sampling gears provided mud breccia, again with only a very thin veneer of hemipelagic sediments. Thus, *Ginsburg* MV has probably produced new mud flows within the recent past. The same holds true for *Gemini* MV, which has only been sampled by one gravity core. Between these two MVs there is another proven mud volcano previously named *TTR*. Slightly to the east of *TTR* MV there is another structural height of unknown nature. Sampling by gravity corer at this spot revealed a sequence of hemipelagic sediments with high amounts of cold-water coral debris but no mud breccia.

The last unspecified structure investigated during this cruise was the tentatively named *Poseidon* dome. Two gravity cores, one from its top (GeoB 9085-1) and one from its flank (GeoB 9086-1), contained no mud breccia but only hemipelagic sediments. However, although these two cores were taken quite close to each other they showed a remarkable difference. As the top core has an undisturbed sequence of hemipelagic sediments, the flank core contained several turbidites. Probably, these turbidites came down the continental slope but had not enough energy to climb up to the top of the structure.

| station no. | latitude °N | longitude °W | water depth (m) | reco-very (m) | Area | sediments |
|---|---|---|---|---|---|---|
| GeoB 9019-1 | 36:11.18 | 07:19.15 | 767 | 1.62 | Hesperides MV | mud breccia |
| GeoB 9020-1 | 36:11.16 | 07:19.29 | 730 | 0.19 | Hesperides MV | mud breccia (core bent) |
| GeoB 9021-1 | 36:10.99 | 07:18.38 | 701 | 3.78 | Hesperides MV | hemipleagic & corals |
| GeoB 9037-1 | 35:39.93 | 07:20.08 | 1381 | 3.76 | Capt. Arutyunov MV | hemipleagic & mud breccia |
| GeoB 9038-1 | 35:39.30 | 07:16.52 | 1313 | 2.63 | Atlas MV | mud breccia |
| GeoB 9040-1 | 35:39.56 | 07:23.38 | 1380 | 3.43 | supposed MV #2 | hemipelagic sediments |
| GeoB 9041-1 | 35:39.70 | 07:19.97 | 1316 | 2.35 | Capt. Arutyunov MV | mud breccia & gas hydrates |
| GeoB 9051-2 | 35:27.61 | 09:00.03 | 3087 | 2.63 | Bonjardim MV | mud breccia |
| GeoB 9052-1 | 35:31.08 | 08:47.00 | 2747 | 4.86 | supposed MV #3 | hemipelagic sediments |
| GeoB 9052-2 | 35:31.12 | 08:47.01 | 2744 | 4.20 | supposed MV #4 | hemipelagic sediments |
| GeoB 9061-1 | 35:22.42 | 07:05.29 | 912 | 1.54 | Ginsburg MV | mud breccia |
| GeoB 9063-1 | 35:21.99 | 06:51.92 | 598 | 5.00 | supposed MV E of TTR MV | hemipelagic & corals |
| GeoB 9067-1 | 35:16.92 | 06:45.47 | 435 | 3.70 | Gemini MV | mud breccia |
| GeoB 9072-1 | 35:39.71 | 07:19.95 | 1321 | 3.25 | Capt. Arutyunov MV | mud breccia & gas hydrates |
| GeoB 9085-1 | 34:49.11 | 08:51.70 | 3457 | 5.70 | Poseidon dome | hemipelagic sediments |
| GeoB 9086-1 | 34:49.21 | 08:51.00 | 3463 | 4.69 | Poseidon dome | hemipel. sedim. w/ turbidites |

**Table 6.3.** Gravity cores taken during SO-175 on mud volcanoes and other structural heights.

| Station No. | Latitude | Longitude | Water | Area |
|---|---|---|---|---|
| | N° | W° | depth (m) | |
| GeoB 9022-1 | 36:10.98 | 07:18.36 | 676 | Hesperides MV |
| GeoB 9023-1 | 36:10.73 | 07:18.39 | 761 | Hesperides MV |
| GeoB 9024-1 | 36:11.32 | 07:18.45 | 727 | Hesperides MV |
| GeoB 9029-3 | 36:05.68 | 07:24.12 | 907 | Faro MV |
| GeoB 9030-1 | 36:05.36 | 07:24.39 | 908 | Faro MV |
| GeoB 9030-2 | 36:05.30 | 07:24.46 | 949 | Faro MV |
| GeoB 9030-3 | 36:05.10 | 07:24.52 | 980 | Faro MV |
| GeoB 9036-1 | 35:39.69 | 07:19.99 | 1320 | Capt. Arutyunov MV |
| GeoB 9059-2 | 35:22.42 | 07:05.30 | 910 | Ginsburg MV |
| GeoB 9059-3 | 35:22.40 | 07:05.33 | 909 | Ginsburg MV |
| GeoB 9060-1 | 35:22.82 | 07:05.25 | 991 | Ginsburg MV |
| GeoB 9072-3 | 35:39.71 | 07:19.99 | 1324 | Capt. Arutyunov MV |

**Table 6.4.** TV-grabs taken during SO-175 on mud volcanoes.

## Cold-water corals in the Gulf of Cadiz

The distribution of cold-water corals in the Gulf of Cadiz has been studied by using the OFOS on a number of mud volcanoes in order to see, if these topographic heights form a host for cold-water corals. At the beginning of the cruise five mud volcanoes (*Pipoca, Almazan, Tasyo, Student*, and *Rabat*) were known to be covered by corals (**Fig. 6.24**). However, most of the available records are based on samples collected with sediment cores, thus, there are hardly any indication about the presence of living cold-water corals in the Gulf of Cadiz. For this investigation, six other mud volcanoes have been surveyed by OFOS.

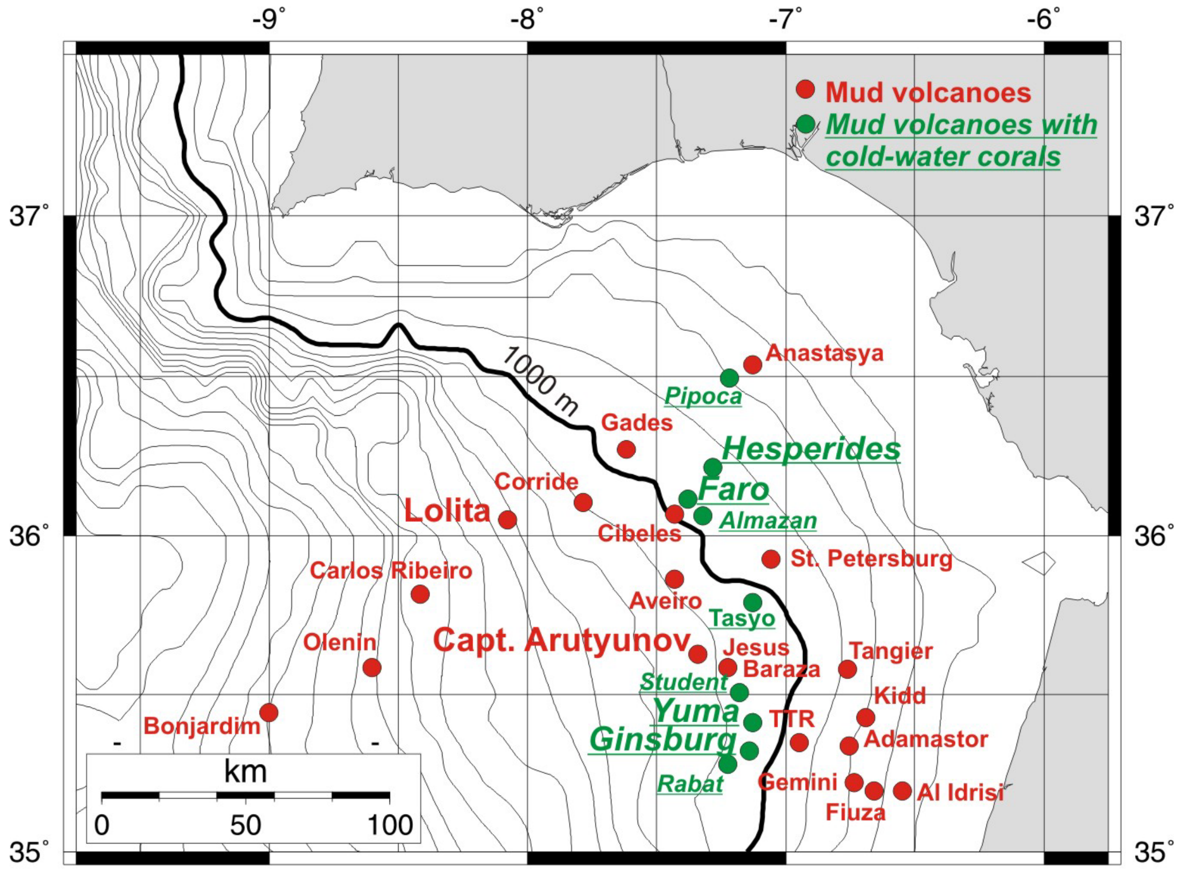


**Figure 6.24.** Distribution of cold-water corals on mud volcanoes in the Gulf of Cadiz. Those mud volcanoes indicated by the larger letters have been investigated during SO-175.

*Lolita* and *Captain Arutyunov* MVs, both in depths of >1200 m were barren of any corals. In contrast, abundant corals have been found on *Hesperides* MV, where at station GeoB 9022-1 a TV grab provided abundant sample material (**Fig. 6.25**) collected from coral thickets at the southern summit of this MV. Unfortunately, no living corals could have been collected. On the other surveyed MVs - *Faro*, *Ginsburg* and *Yuma* – cold-water corals appeared regularly but in rather low numbers. On all the coral-bearing MVs living colonies have been observed on the OFOS tracks.

**Fig. 6.25.** Samples collected by TV grab from station GeoB 9022-1 located at the southern summit of *Hesperides* MV: **A)** Overview about the variety of coral fragments; **B)** Selection of different coral species.

Putting these observations together with the earlier reports about cold-water corals in the Gulf of Cadiz a coherent pattern emerges (**Fig. 6.24**). The corals seem to be limited to water depths of <1200 m, a feature quite similar to the cold-water coral distribution on the carbonate mounds along the Celtic margin. Thus, it appears that also in the Gulf of Cadiz the corals are linked with the Mediterranean Outflow Water.

In order to study the long-term development of the corals under changing environmental conditions (e.g., glacial/interglacial changes) four sediment cores have been collected from sites, where abundant corals have been seen with the OFOS (**Tab. 6.5**). These cores have not been opened as the standard opening procedure onboard would have destroyed the original sequence of these coral-bearing sediments. Thus, these cores have been kept in full 1 m sections. In the home laboratory these will be frozen and cut with a big stone saw.

| station no. | latitude °N | longitude °W | water depth (m) | recovery (m) | area |
|---|---|---|---|---|---|
| GeoB 9018-1 | 36:10.98 | 07:18.37 | 702 | 3.47 | Hesperides MV |
| GeoB 9031-1 | 36:05.75 | 07:23.28 | 897 | 4.84 | Faro MV |
| GeoB 9032-1 | 36:05.55 | 07:23.57 | 843 | 2.20 | Faro MV |
| GeoB 9070-1 | 35:22.00 | 06:51.90 | 594 | 6.00 | unnamed MV E of TTR |

**Table 6.5.** Sediment cores containing abundant coral fragments. These cores will be opened at the home laboratory.

### 6.3.5. MST and Physical properties

(W. Brückmann, A. Foubert)

Other characteristic patterns related to specific sedimentological features are cores recovering mud breccia or mud flows. Good examples are seen in GeoB 9037-1 and GeoB 9038-1, were intervals with mud breccia are indicated sudden jumps to higher densities (86 cmbsf in GeoB 9037-1) and lower magnetic susceptibilities, as well as high frequency variations in P-wave velocities. A similar P-wave signature is seen in GeoB 9038-1 (96-135 cmbsf). However, magnetic susceptibility in this core shows an opposite trend of higher values in the breccia-rich interval.

In several gravity cores a large number of corals and coral fragments were found, which show a very characteristic pattern in all MST parameters determined. Typical examples are seen in cores GeoB 9021-1, GeoB 9063-1, and GeoB 9065-1. Here, a high frequency variability is evident in all parameters down section, especially in the gamma density and P-wave velocity. Obviously the lower density and different acoustic impedance of small coral fragments is responsible for this pattern.

Full data are shown in Appendix 8.4.

### 6.3.6. Pore water geochemistry

(C. Hensen, K. Nass, M. Marquardt)

The major goal of sampling and analyzing various mud volcanoes and mounds was to characterize the geochemical composition of methane-rich fluids hat were expected to be present at these sites. Unfortunately, OFOS observations revealed no biogenic indication at the sea floor for active seeping of methane or sulphide-rich pore fluids (i.e. typical faunal assemblages with *Calyptogena*, *Pogonophora* or specific bacterial mats), which means that the rates of upward fluid flow were not sufficient to reach the sediment surface at any of the studied sites. As a major consequence of this, most of TV-MUC deployments were not successful in order to penetrate deep enough to reach below the zone of anaerobic methane oxidation (AOM). Thus, major results are from GC deployments. Below a number of pore water profiles together with onboard methane measurements are shown and described along with some preliminary interpretation concerning the origin.

Hesperides *mud volcano*

Two gravity cores (GeoB 9019-1, 9021-1) were sampled at *Hesperides* MV. **Figure 6.26** shows that significant amounts of methane are not present within the upper 4 mbsf. Relatively high amounts of $H_2S$ of up to 2 mmol/l are due to diffusion or slow upward flow from deeper sediment layers. Interestingly, there is a small but significant (5%) increase of chloride concentrations over depth, which may indicate a highly saline brine as a possible fluid source. However, it will be difficult to further constrain this result, because the cores did not reach far enough into the fluid-bearing sediments. Otherwise suitable isotope-tracers that could be applied would probably fail to produce meaningful results , because dilution by seawater is too high.

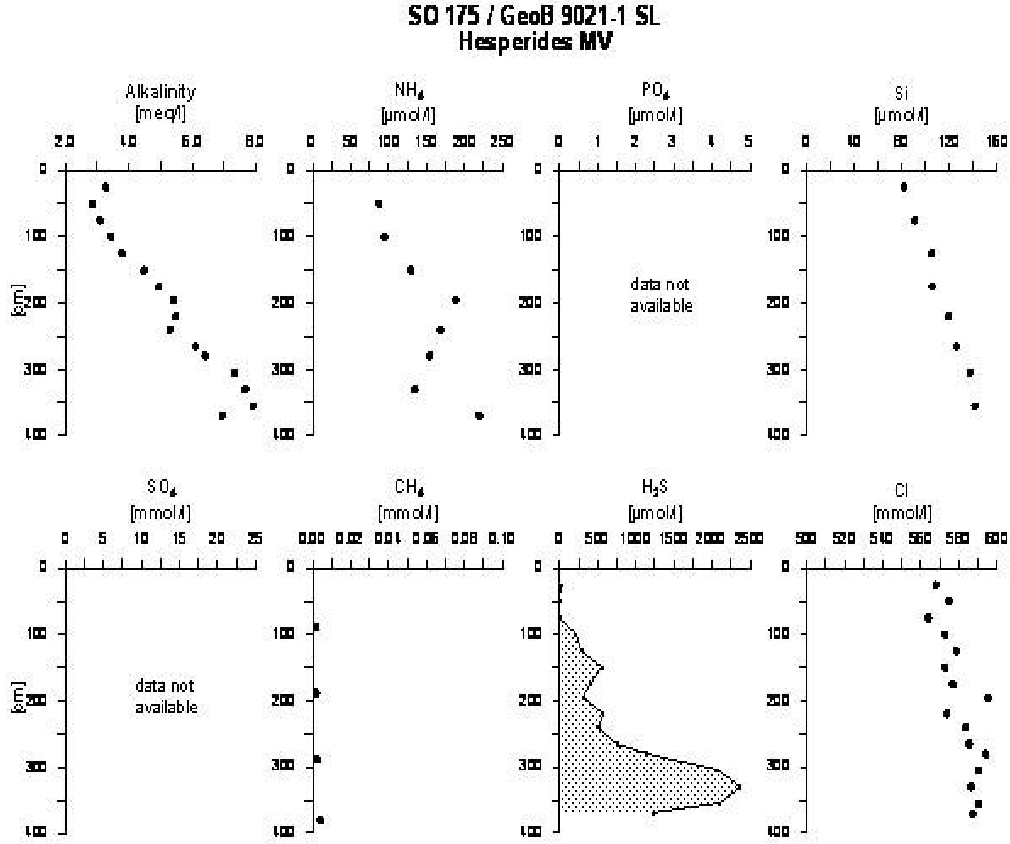


**Fig. 6.26.** Pore water geochemistry from station GeoB 9021-1, *Hesperides* MV.

Almazan *mud volcano*

Only one TV-MUC (GeoB 9029-2) was sampled in the *Faro / Almazan* MV area. The geochemical data obtained from this site do not show any indication for the rise of methane-rich fluids.

Captain Arutyunov *mud volcano*

The area around *Captain Arutyunov* mud volcano was intensively studied by pore water geochemistry. Samples were taken from one TV-Grab (GeoB 9036-1), one TV-MUC (GeoB 9036-2), and two gravity cores (GeoB 9041-1, 9072-1) that were directed to the central summit of the mud volcano. All cores contained small pieces of gas hydrate in discrete layers indicating intense advection of methane-rich fluids. Two additional cores (GeoB 9038-1, 9040-1) were taken from two adjacent topographic highs to the west and the east.

In **Figures 6.27 and 6.28** we present the pore water profiles of the MUC (GeoB 9036-2) providing a higher depth resolution for the upper 40 cm bsf of the sediment and one GC-core (GeoB 9072-1), respectively. High amounts of methane (1.2 mmol/l) and H2S (5 mmol/l) indicate that the zone of AOM is already reached at the base of the MUC-core (**Fig. 6.27**). Within the upper 20 cm pore water components do not show significant gradients, which is probably due to intense mixing of the superficial sediment layer. The concentration profiles of alkalinity and hydrogen sulfide (with a distinct peak in the topmost sample) in GC-core clearly show that the reaction horizon is restricted to the uppermost sediment section, which is confirmed by concentration profiles of ammonium and phosphate (**Fig. 6.28**). All parameters measured show hardly any variation over depth reflecting a rather undiluted fluid provided by active upward flow. However, even at this site there was no indication for seeps at the seafloor meaning that focused flow rates are at least only moderate (probably <10 cm/yr). The chloride concentrations at station GeoB 9072-1 increase significantly (up to 10%) above the normal seawater value (35‰ PSU) towards the base of the core (**Fig. 6.28**). The source for this chloride enrichment is not clear by now. Active gas hydrate formation or a deep brine source are likely explanations, which have to be proved by further analyses. The scatter in the chloride profile is probably caused by gas hydrate dissociation in distinct layers.

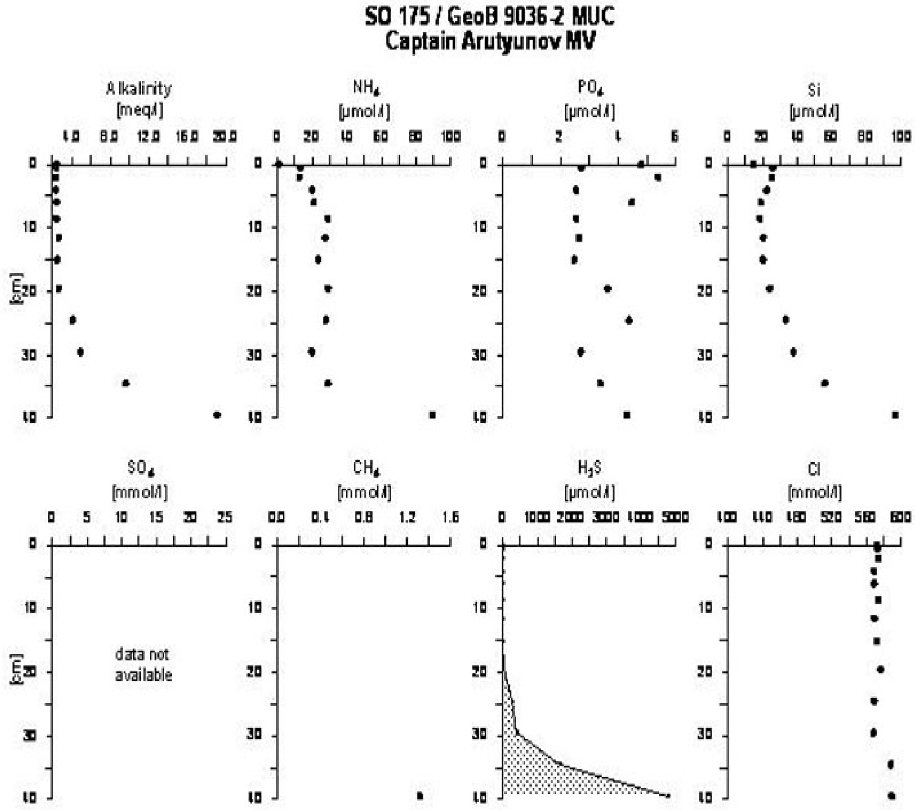


**Fig. 6.27.** Pore water geochemistry from gravity MUC GeoB 9036-2, *Capt. Arutyunov* MV.

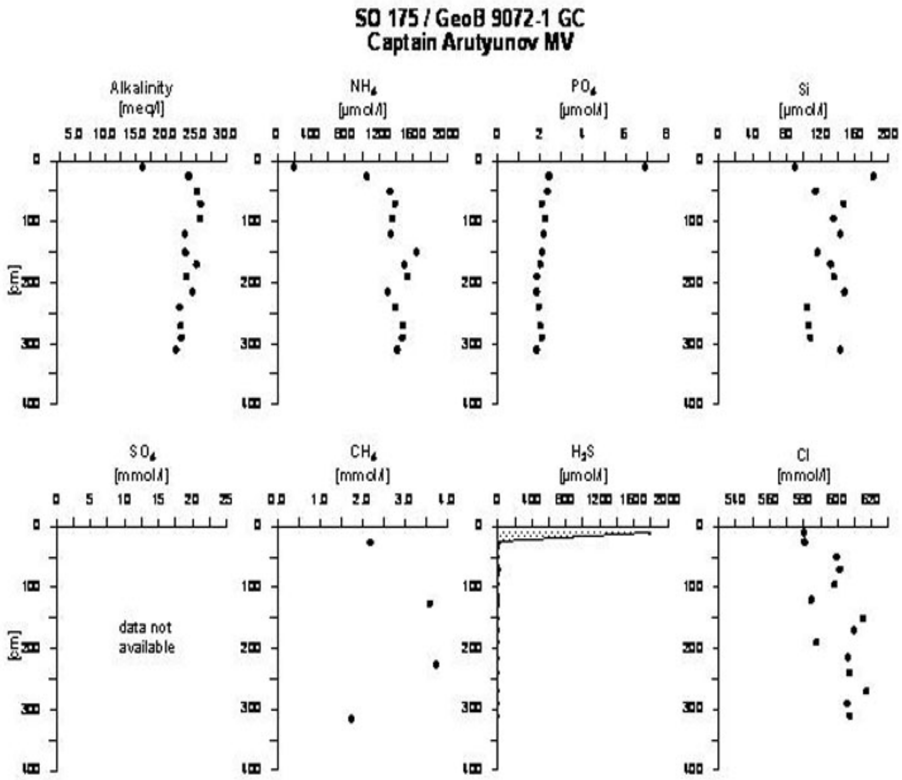


**Fig. 6.28.** Pore water geochemistry from gravity GeoB 9072-1, *Capt. Arutyunov* MV.

Both cores from the adjacent mounds are comparatively inactive. As shown in **Figure 6.29** (station GeoB 9040-1 east of *Captain Arutyunov* MV), the alkalinity increase is very low in upper 4 m and there was no smell of $H_2S$ indicating that the zone of AOM (anaerobic oxidation of methane) was not reached within the sampled sediment section.

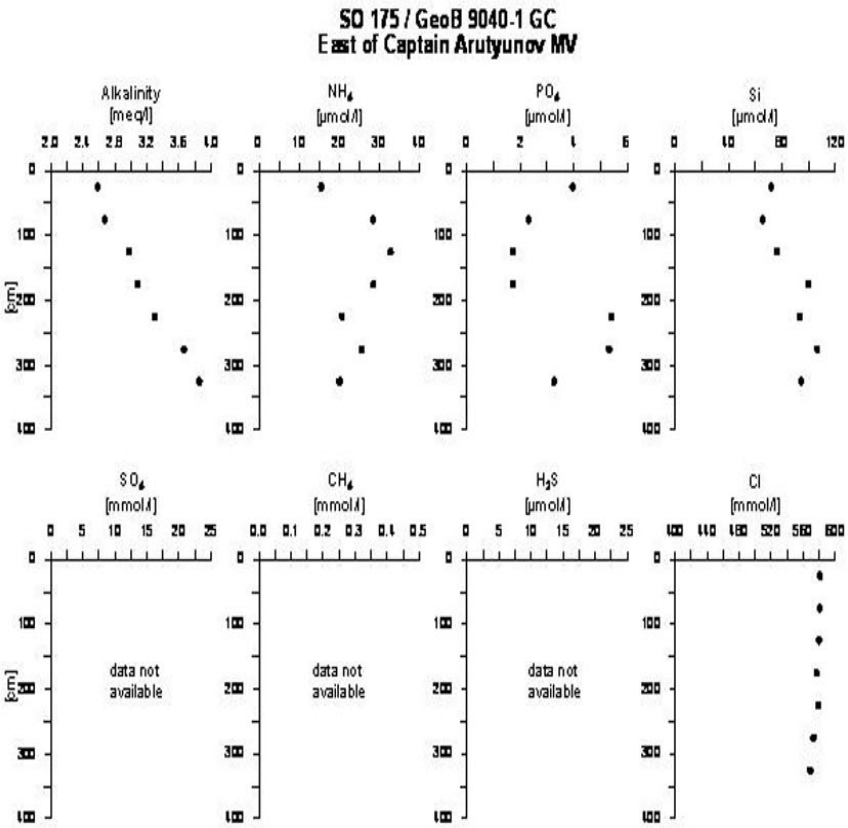


**Fig. 6.29.** Pore water geochemistry from gravity GeoB 9040-1, east of *Capt. Arutyunov* MV.

Bonjardim *mud volcano*

*Bonjardim* mud volcano is the geochemically most active site investigated at the lower slope (~3000 m water depth). One TV-MUC (GeoB 9051-1) and one gravity core (GeoB 9051-2) were sampled for pore water analyses. The concentration vs. depth profiles of the MUC-core (**Fig. 6.30**) are similar to site (GeoB 9036-2) at *Captain Arutyunov* (**Fig. 6.26**), although the alkalinity level is lower and only slightly enriched methane concentrations could be measured at the base of the core. The chloride profile shows a slight linear decrease over depth. This trend is continued in the GC core of this site (**Fig. 6.31**), reaching a final depletion of about 40% of the normal seawater value at about 2 mbsf. The continuous curve indicates that the pore water freshening is not caused by gas hydrate dissociation during core recovery, thus fluids fluids may originate from a deeper source.

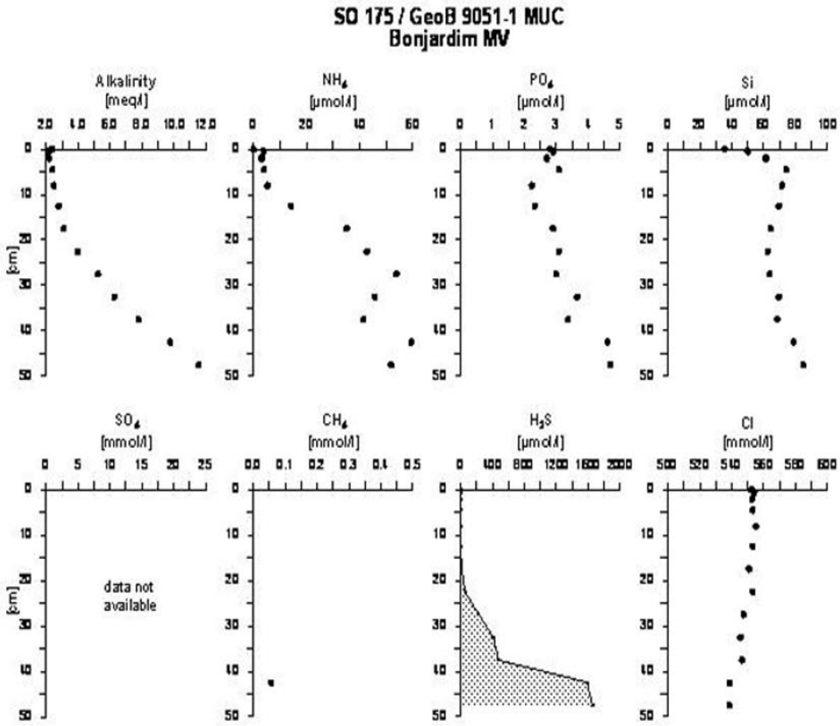


**Fig. 6.30.** Pore water geochemistry from MUC GeoB 9051-1, *Bonjardim* MV.

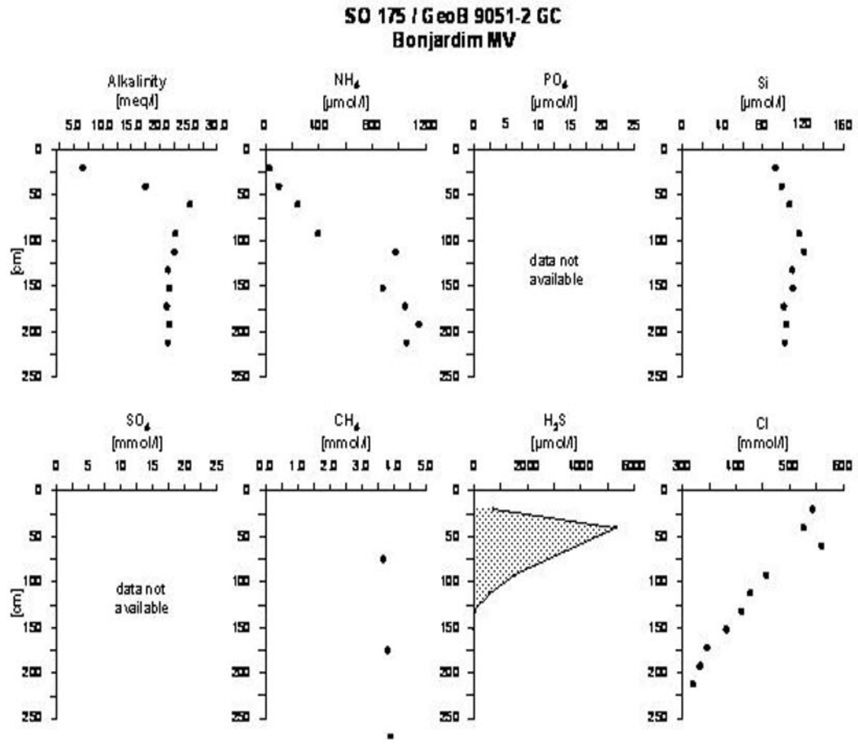


**Fig. 6.31.** Pore water geochemistry from gravity GeoB 9051-2, *Bonjardim* MV.

Similar results were obtained from two gravity cores (GeoB 9052-1, 9052-2) taken at a small mound located in close vicinity to *Bonjardim* MV. However, at this site the pore water freshening is less pronounced (<10%) and the depth-horizon of AOM is below 5 mbsf, indicating much lower fluid flow rates compared to *Bonjardim* and *Captain Arutyunov* MV.

Ginsburg and Gemini *mud volcanoes*

Three sites were sampled by gravity corer at the upper continental slope towards the Moroccan coast. GC GeoB 9061-1 at *Ginsburg* MV (**Fig. 6.32**), GC GeoB 9063-1 at a mound near *Ginsburg* MV (**Fig. 6.33**), and GeoB 9067-1 at *Gemini* MV (**Fig. 6.34**). All sites are indicative for fluid flow, whereas flow rates are much higher at *Ginsburg* and *Gemini* MV compared to the unnamed mound close to *Ginsburg* MV. Chlorinity profiles show a continuous freshening with increasing depth similar to those measured in the area around *Bonjardim* MV, although the degree of freshening only reaches values of up to 25% (**Fig. 6.34**). There were no indications for the occurrence of gas hydrates in these cores, being in good agreement with the smooth, continuous chlorinity profiles. Interestingly, concentrations of ammonia and phosphate are significantly lower in comparison to the *Bonjardim* MV stations, which indicates different fluid sources or processes of fluid and/or gas advection further upslope.

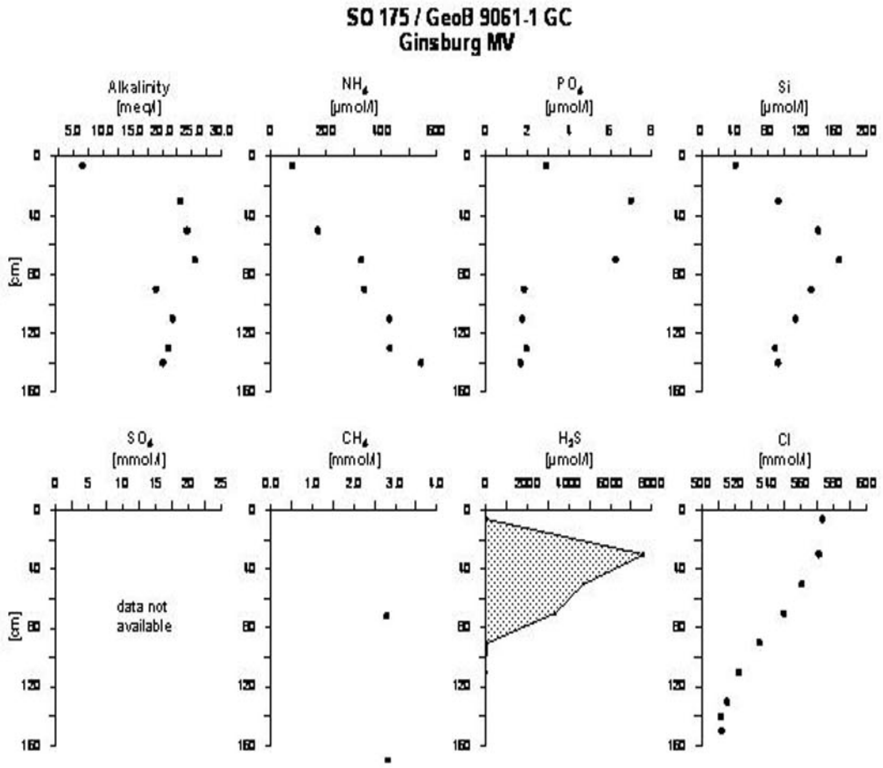


**Fig. 6.32.** Pore water geochemistry from gravity core GeoB 9061-1, *Ginsburg* MV.

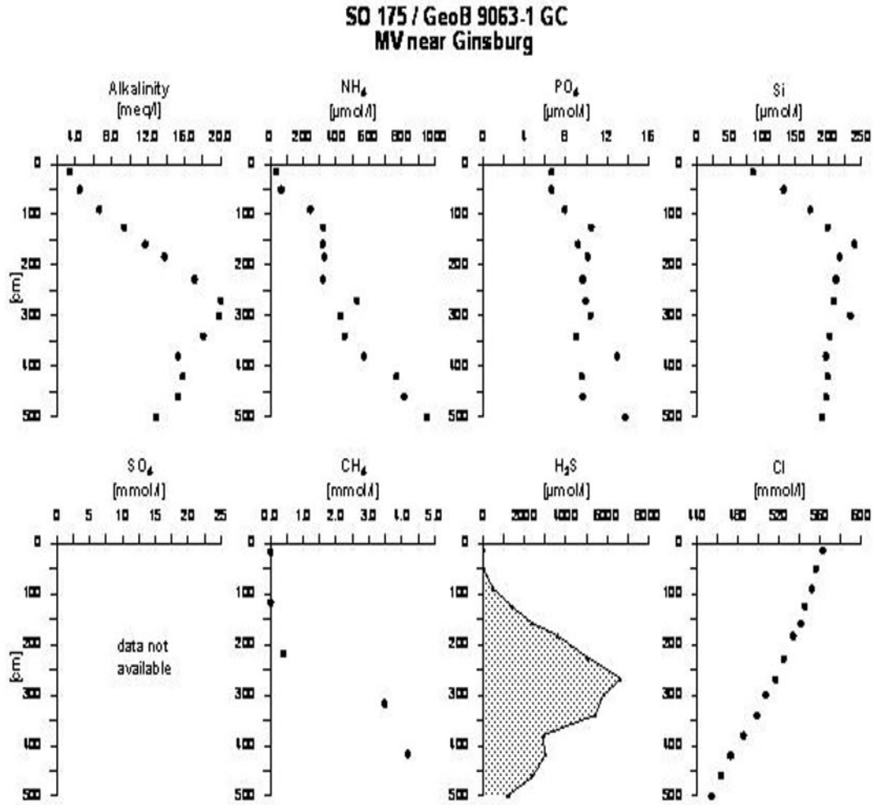


**Fig. 6.33.** Pore water geochemistry from gravity core GeoB 9063-1, near *Ginsburg* MV.

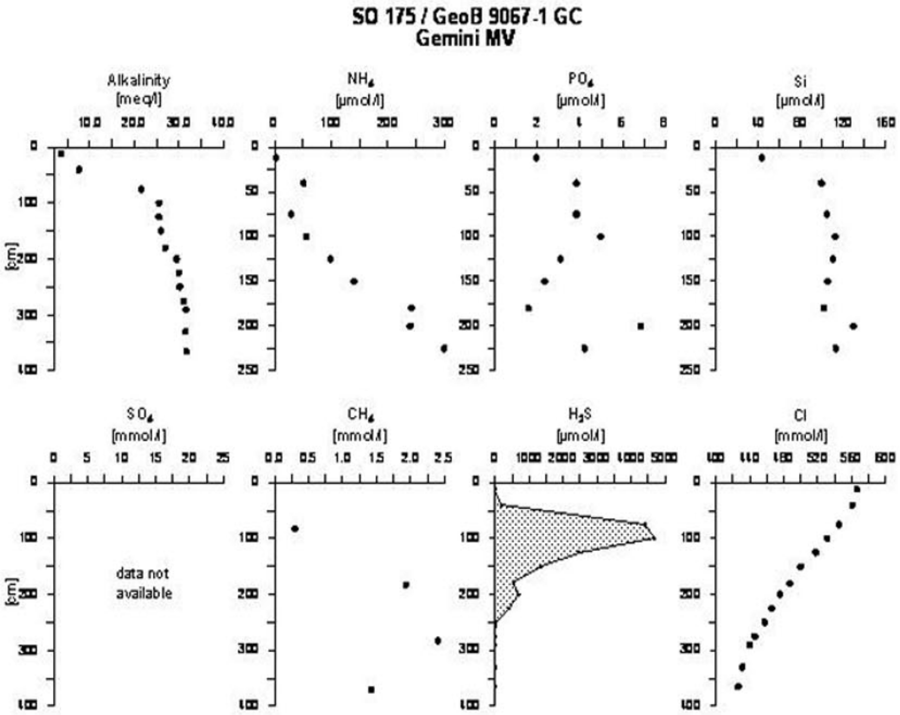


**Fig. 6.34.** Pore water geochemistry from gravity core GeoB 9067-1, *Gemini* MV.

### 6.3.7. Heat flow and pore pressure

(I. Grevemeyer, N. Kaul, J. Poort)

#### Heat flow anomalies over mud volcanoes

A secondary target of the heat flow surveys was to study the heat transfer through mud volcanoes in the Gulf of Cadiz. Mud volcanoes or diapirs show profound differences in the heat budget. A few spectacular features do vent fluids at high temperatures and hence provide high heat flow anomalies. The best know examples are the Haakon Mosby mud volcano offshore Norway (Eldholm et al., 1999) and mud volcanoes seaward of the deformation front of the Barbados prism (Henry et al., 1996). Other features, however, indicate only moderate thermal anomalies – like mud diapirs offshore Costa Rica (Grevemeyer et al., 2004) – or show only weak indications for significant heat transfer – like mud volcanoes on the Mediterranean Ridge

(Camerlenghi et al., 1995). However, only a few mud volcanoes world-wide have been studied by heat flow specialists.

In the Gulf of Cadiz we used two different approaches to survey mud volcanoes: (i) transects of heat flow station have been placed across the mounds, (ii) on some gravity cores we attached miniature temperature data loggers (MTLs). In total, six mounds were investigated (**Fig. 6.35**).

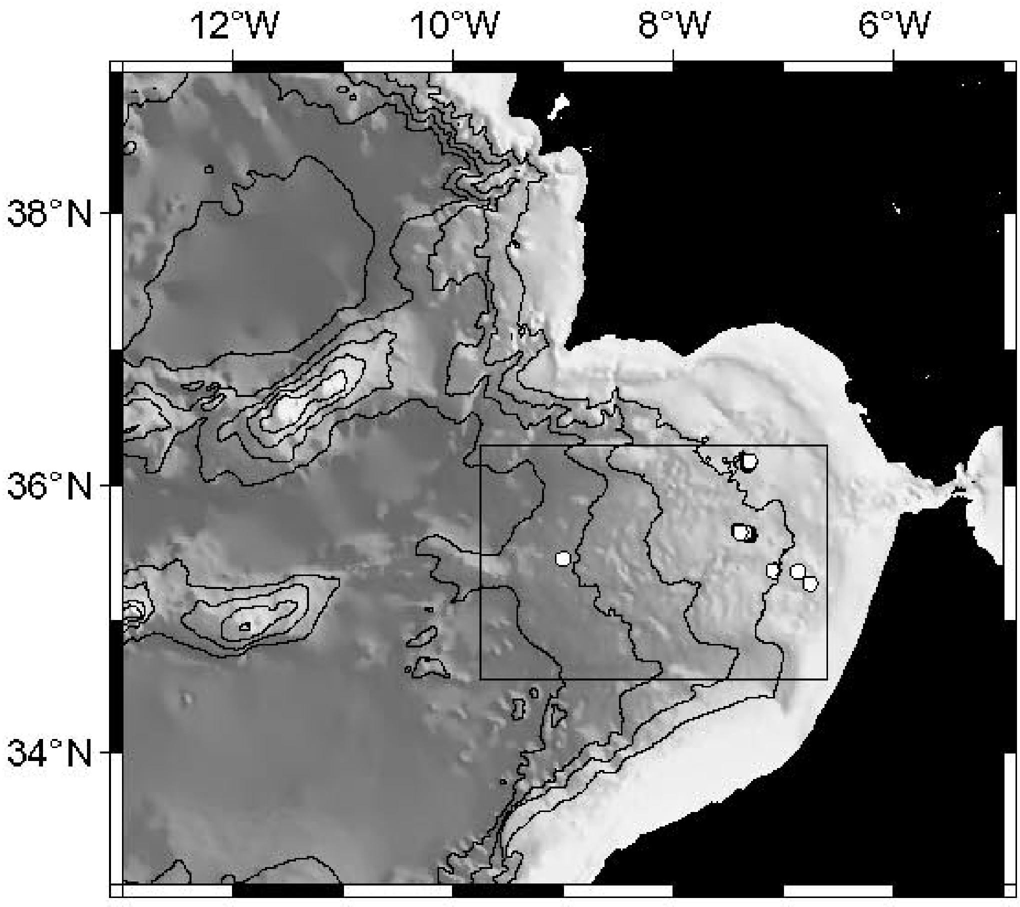


**Fig. 6.35.** Overview chart with heat flow sites on mud volcanoes during SO175.

A major problem in the survey area was that most mud volcanoes occurred in water depth of less than ~1500 m. The water column at depth of less than 1500-1000 m is generally affected by sessional variations of the bottom water temperature. In the Gulf of Cadiz, the problem might be exasperated by the outflow of the salty and very warm Mediterranean water. Transient changes in the water column will cause a temperature wave which runs from the seafloor down and may therefore overprint Earth's heat loss. An example is given for the *Hesperides* mud volcano (**Fig. 6.36**). Non-linear-gradients (NLG) are observed.

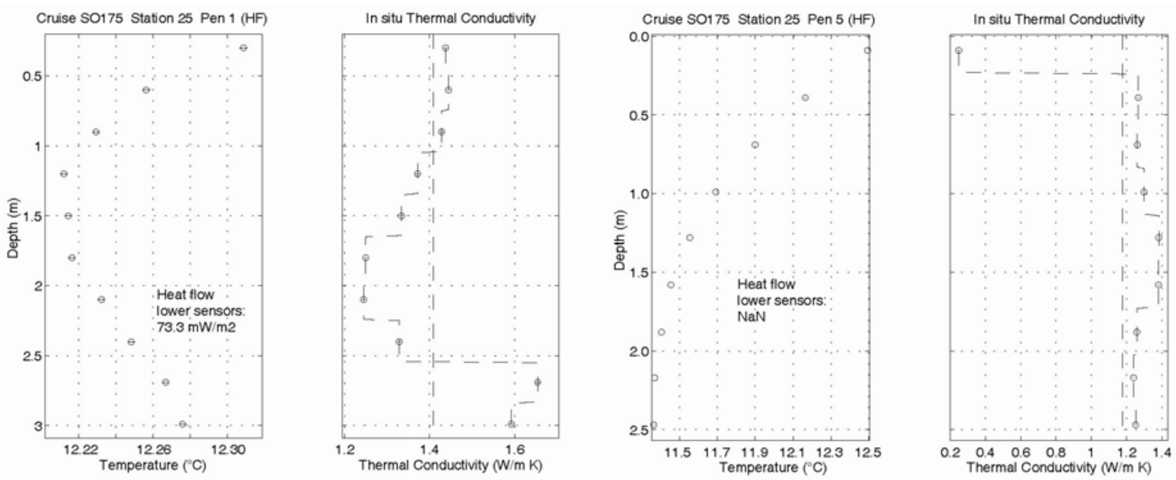


**Fig. 6.36.** Non-linear heat flow results from station GeoB 9025, *Hesperides* MV.

Nevertheless, transient features generally decay rapidly with depth. Thus, some penetrations provide linear trends for the lowermost sensors. Assuming that these sensors are not affected by transient temperature variations cause by the bottom water, we calculated the heat flow for theses sensors (**Fig. 6.37**). It is important to note that all data presented in this chapter are based on an initial assessment! A second problem might be caused by high sedimentation rates (Hutchison, 1985).

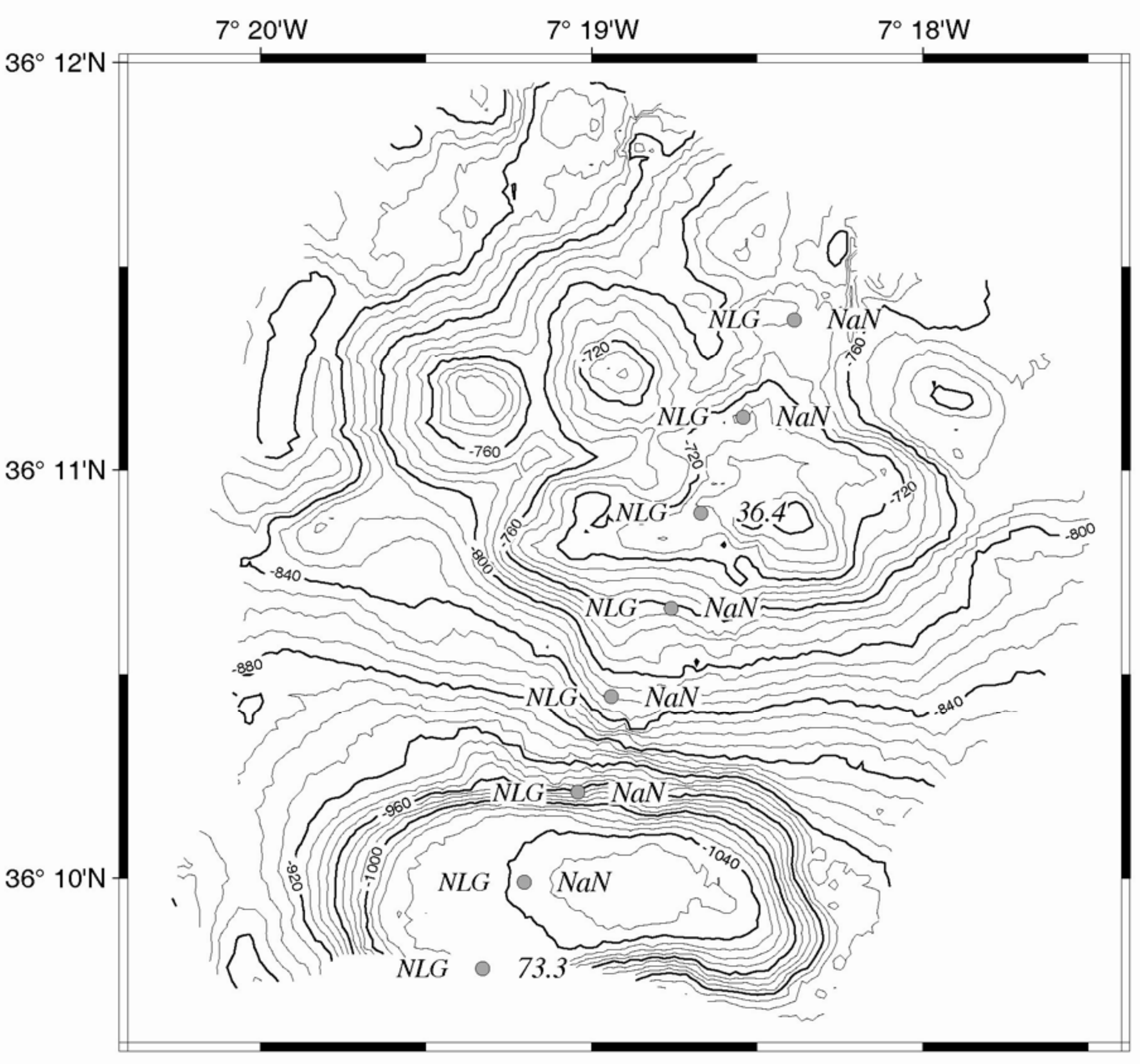


**Fig. 6.37.** Transect of heat flow measurements at station GeoB 9025, *Hesperides* MV.

*Captain Arutyunov* mud volcano is located in a pond like sedimentary basin. Heat flow is generally very low, even for the lowermost sensors (**Figs. 6.38 and 6.39**). We suspect that high sedimentation rates may cool the sedimentary blanket and hence lower the surface heat flow. Nevertheless, the insignificant temperature changes with depth and the low gradients obtained on the mound clearly support the fact that the features surveyed are reasonable inactive. This observation is not only valid for the *Captain Arutyunov* MV, but also for the *Hesperides* and *Ginsburg* MVs.

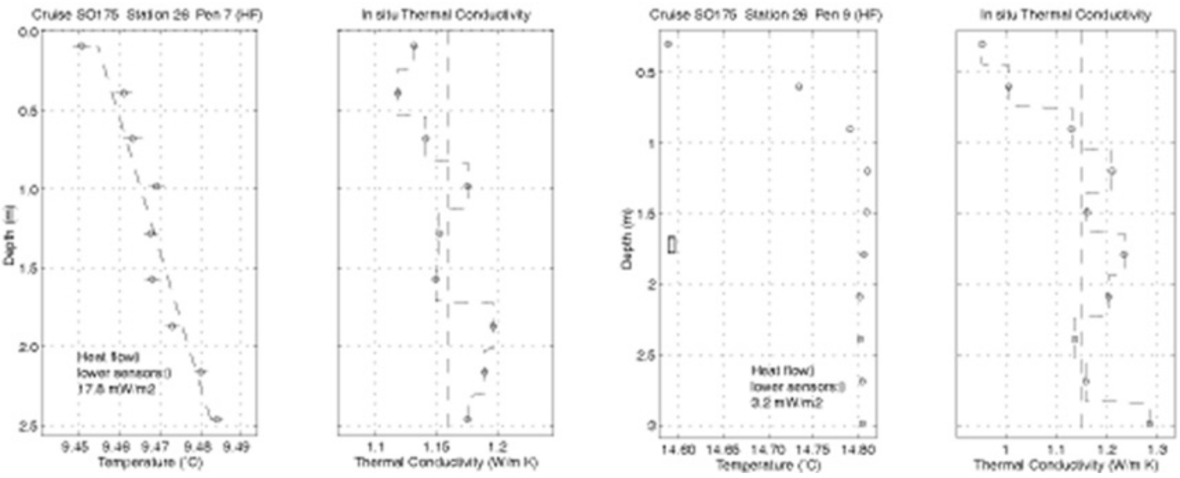


**Fig. 6.38.** Heat flow data at station GeoB 9042, *Captain Arutyunov* MV.

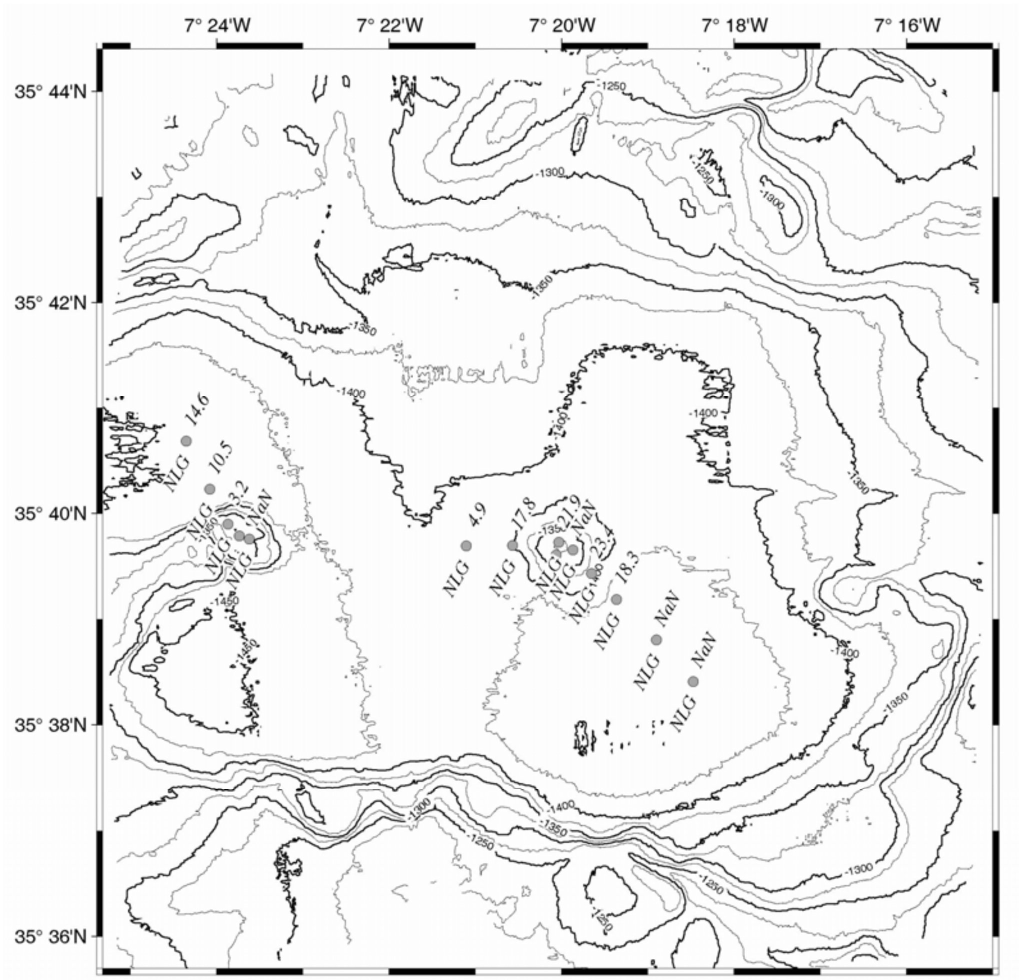


**Fig. 6.39.** Transect of heat flow measurements at station GeoB 9042, *Captain Arutyunov* MV.

The deepest mud volcano studied was *Bonjardin* with a crestal depth of ~3100 m. From stations surveyed for the regional transect we know that the feature was too depth to be affected by transient changes of the bottom water temperature. Thus, we were very surprised to observe non-linear gradients (**Fig. 6.40**). Measurements adjacent to the mound indicate that the temperature at these reference sites increase linearly with depth. Using the uppermost linear trend, we yield values much high than those obtained from the reference sites (**Fig. 6.41**). We therefore suggest that the mound is characterised by seepage. In addition, gas hydrates have been sampled on *Bonjardim*. Temperature excursions are linked to layers with low thermal conductivities. Laboratory experiments have shown that gas hydrates are characterised by the lowest thermal conductivities ever observed in nature. We therefore suspect that gas hydrate dissociation may cause the excursion of the temperature at individual sensors. A refined post cruise analysis of the temperature data is required to understand the impact of seasonal bottom water variations and of gas hydrate dissociation or generation.

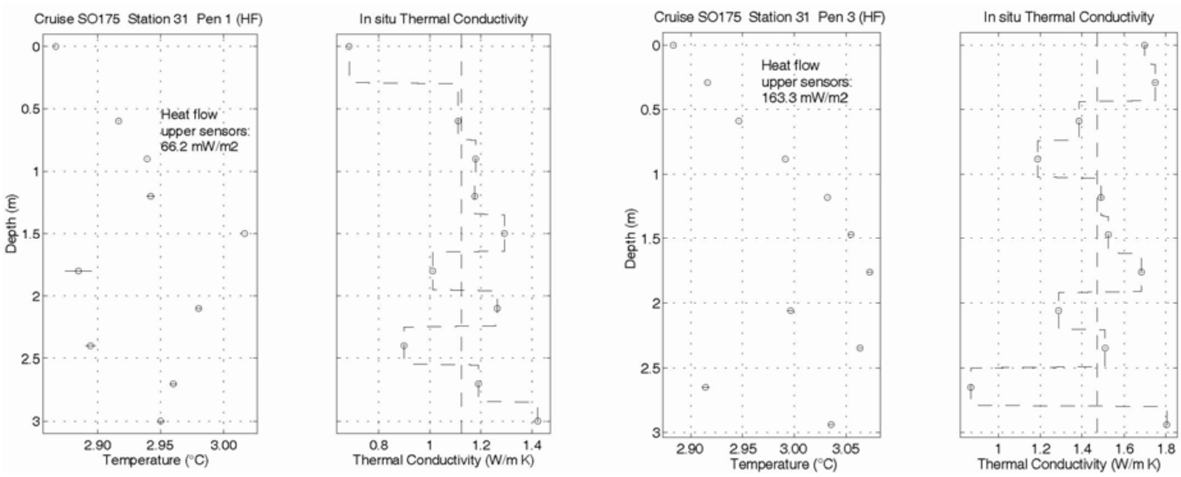


**Fig. 6.40.** Heat flow data at station GeoB 9053, *Bonjardim* MV.

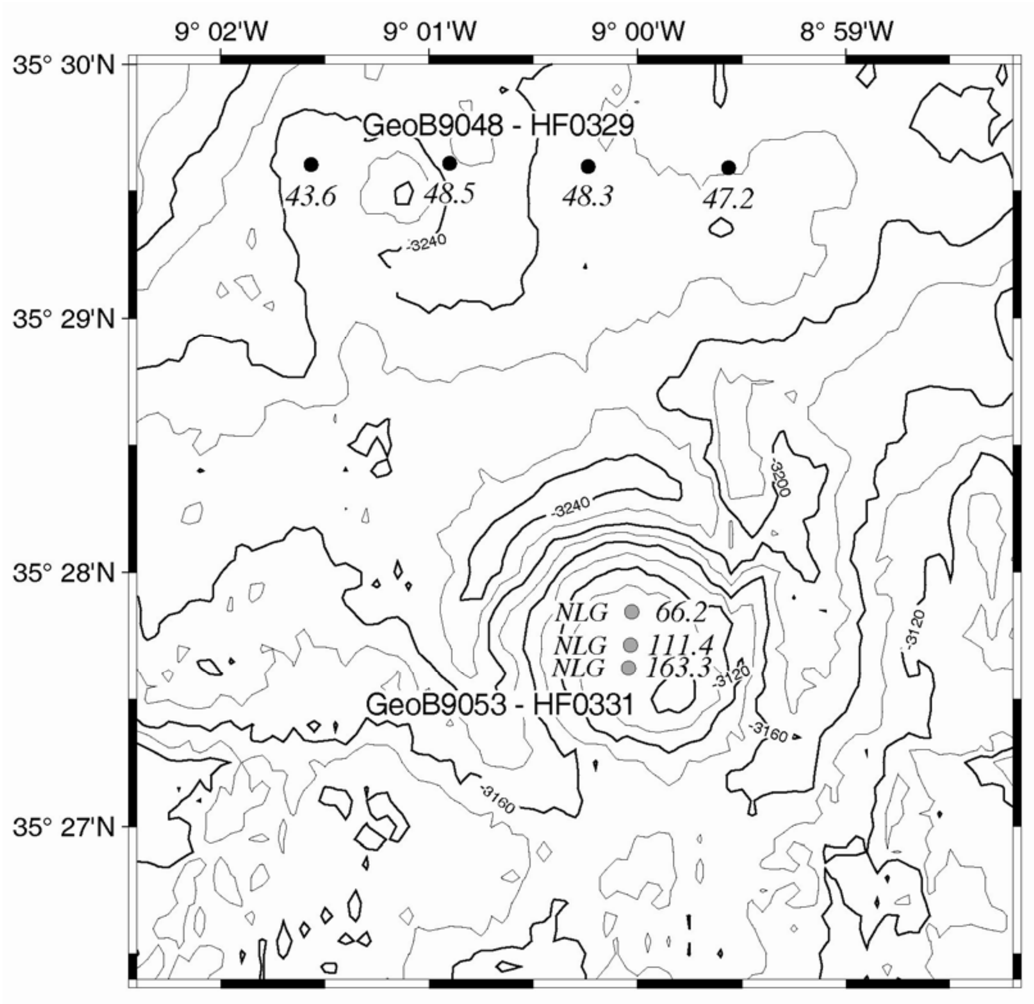


**Fig. 6.41.** Transect of heat flow measurements at station GeoB 9053, *Bonjardim* MV.

Pore pressure-temperature probe

After serious consideration of different possible targets, the mud volcano *Captain Arutyunov* was chosen for the deployment due to its activity and moderate water depth. This was done immediately after the recovery of a gravity corer, which contained obviously a considerable amount of gas hydrate. The instrument was lowered in free fall mode from the surface.

Deployment details:

- 35° 39.724' N
- 7° 20.044 'W
- approx. 1400 m water depth
- Time of deployment: 14.12.2003, 13:49 GMT
- Start time 14.12.2003, 18:17 GMT

- End time: 14.01.2004, 8:00 GMT

### 6.3.8. Microbiology

(H. Niemann, T. Wilkop)

Methane concentrations were measured on board from samples taken at the cut section of Gravity cores or at the lower part from MUC-cores. Mainly three different methane profiles can be distinguished: (1) high concentrations (>1 mM) where the methane transition zone is at between 1 and 3m (*Captain Arutyunov* MV, *Bonjardim* MV, *Ginsburg* MV, *Gemini* MV); ). (2) high concentrations and deep methane transition zone (unnamed dome GeoB9052-1 and -2, GeoB9063-1); and (3) low methane concentrations (<0.2 mM) (*Hesperides* MV). For plots refer to **Figures 6.42 through 6.48**. All cores/ TV grabs other than those mentioned above did not contain significant amounts of methane (>1 µM). Note that some decreases in methane concentration at the lowest core section (e.g. *Captain Arutyunov*) might be due to loss after coring. **Table 6.6.** lists all stations and sediment horizons sampled for AOM, SRR, methane, sulphate, molecular surveys, lipid analysis, life sediments organisms and carbonate structure. Our preliminary conclusion is that mud volcanoes and other geological structures in the Gulf of Cadiz seem to be rather inactive. The methane transition zone is usually deeper 1m below sea floor and seep associated organisms are rare; i.e., *Captain Arutyunov* MV sediments contain worms that could be related to *Pogonophora* sp. (worms with methanotrophic bacteria in their gastro-vascular system) and at *Faro* MV some mythilid bivalves likely to be related *Calyptogena* sp. (contain sulphide oxidizing bacteria in their gills). This directly indicates a low diffusive / low flux regime in sampled sediments.

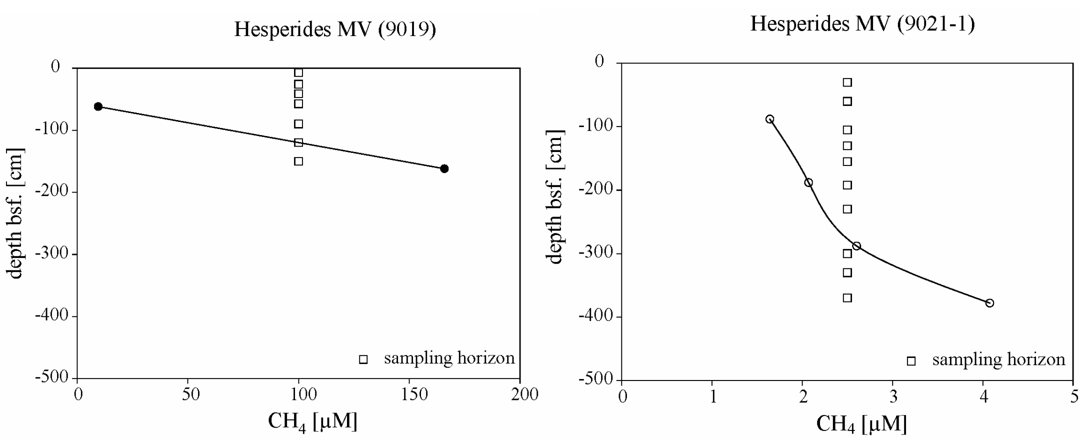


**Fig. 6.42.** Microbiology data from *Hesperides* MV: **A)** station GeoB 9019; **B)** GeoB 9021.

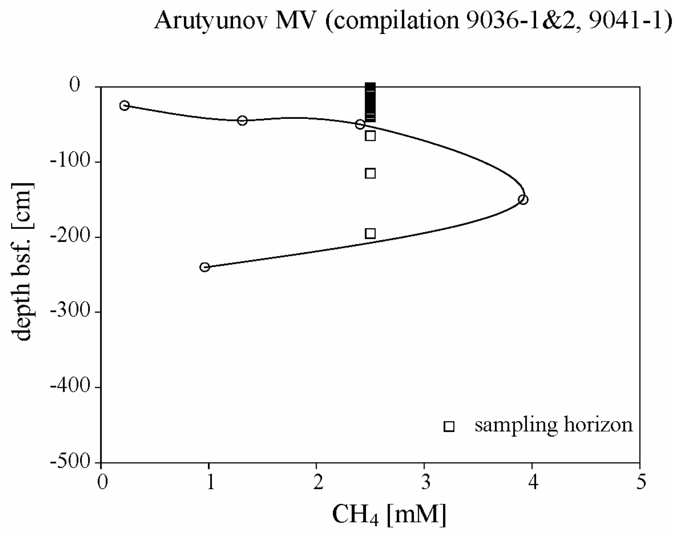


**Fig. 6.43.** Microbiology data from *Captain Arutyunov* MV: **A)** station GeoB 9036; **B)** GeoB 9041.

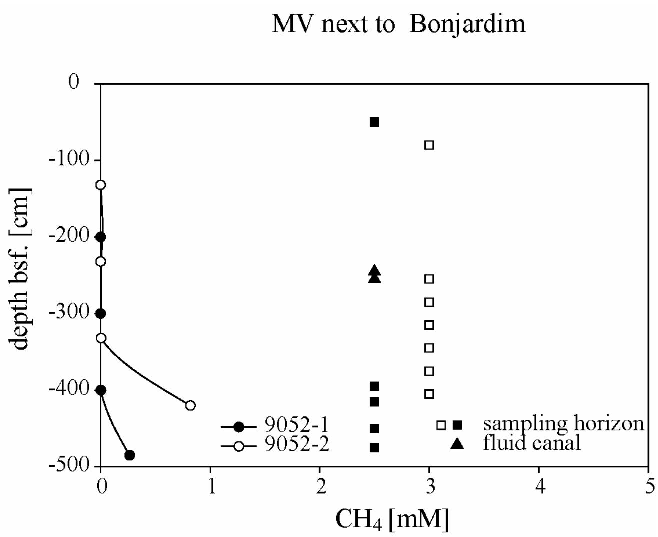


**Fig. 6.44.** Microbiology data from a mound near *Bonjardim* MV, station GeoB 9053.

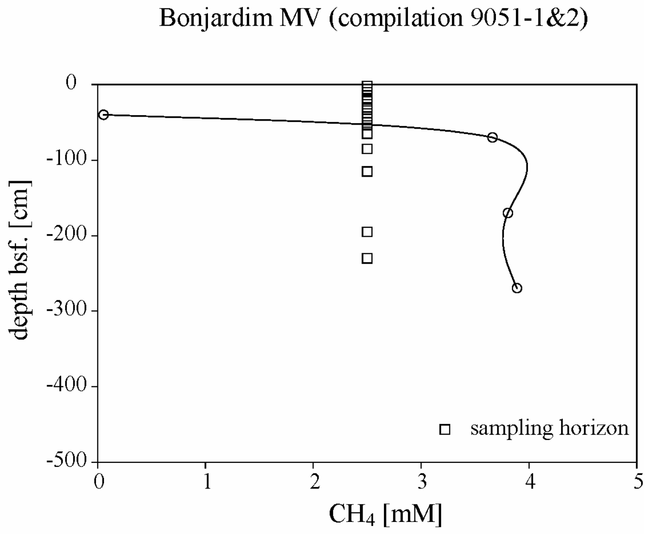


**Fig. 6.45.** Microbiology data from *Bonjardim* MV, station GeoB 9051.

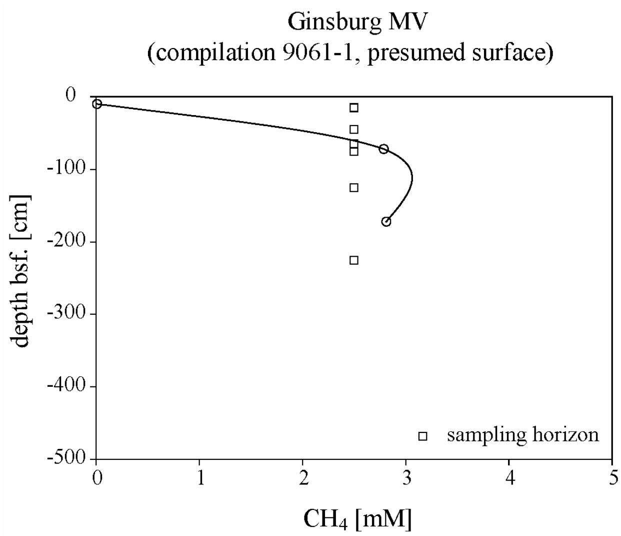


**Fig. 6.46.** Microbiology data from *Ginsburg* MV, station GeoB 9061.

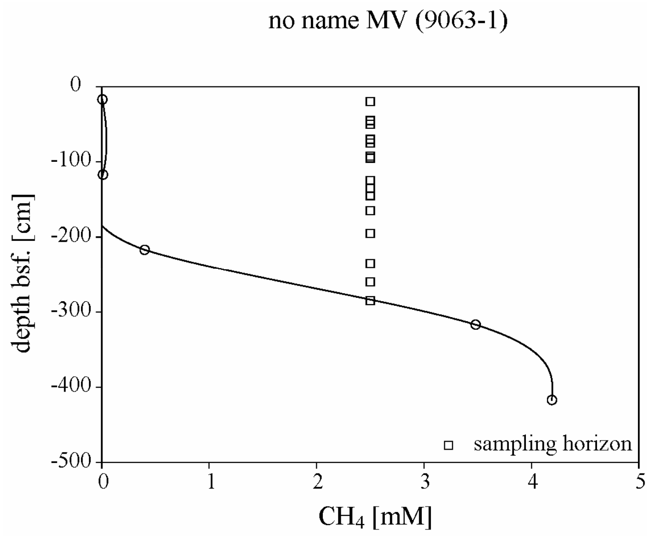


**Fig. 6.47.** Microbiology data from a mud mound at station GeoB 9063.

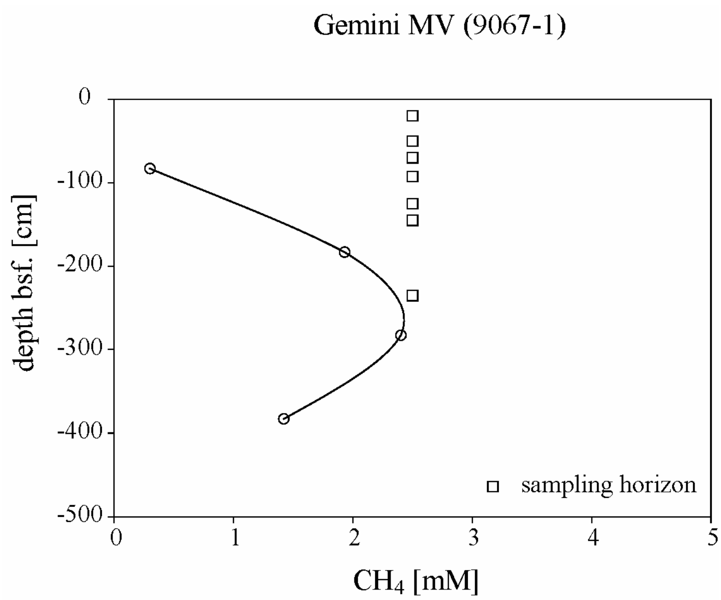


**Fig. 6.48.** Microbiology data from *Gemini* MV, station GeoB 9067.

| **Device**<br>**Name of Struct.** | **Station** | **AOM, SRR**<br>**SO4, CH4** | **FISH**<br>**DNA** | **Life**<br>**sediment** | **Bio-**<br>**marker** | **carb.**<br>**S. Noe´** |
|---|---|---|---|---|---|---|
| GC | 9019 | 5-10 | 5-10 | | 5-10 | |
| Hesperides MV | | 24-28 | 24-28 | | 24-28 | |
| | | 40-43 | 40-43 | | 40-43 | |
| | | 55-60 | 55-60 | | 55-60 | |
| | | 87-93 | 87-93 | | 87-93 | |
| | | 117-123 | 117-123 | | 117-123 | |
| | | 147-153 | 147-153 | | 147-153 | |
| GC | 9021-1 | 27-33 | 27-33 | 180-190 | 27-33 | |
| Hesperides MV | | 57-63 | 57-63 | | 57-63 | |
| | | 100-110 | 100-110 | | 100-110 | |
| | | 127-133 | 127-133 | | 127-133 | |
| | | 152-158 | 152-158 | | 152-158 | |
| | | 190-194 | 190-194 | | 190-194 | |
| | | 227-233 | 227-233 | | 227-233 | |
| | | 297-303 | 297-303 | | 297-303 | |
| | | 333-338 | 333-338 | | 333-338 | |
| | | 367-373 | 367-373 | | 367-373 | |
| TV Grab | 9023 | | | | crusts | x |
| Hesperides MV | | | | | | |
| TV Grab | 9024 | | | | chimney | x |
| Hesperides MV | | | | | | |
| TV Grab | 9029-3 | | | | crusts | x |
| Faro MV | | | | | bivalves | |
| TV Grab | 9036-1 | | bulk | | bulk | |
| Captn A | | | | | | |
| MUC | 9036-2 | 0-2 | 0-5 | 30-40 | 0-2 | |
| Captn A | | 2-4 | 5-10 | | 2-4 | |
| | | 4-6 | 10-15 | | 4-6 | |
| | | 6-8 | 15-20 | | 6-8 | |
| | | 8-10 | 20-25 | | 8-10 | |
| | | 10-12 | 25-30 | | 10-12 | |
| | | 12-14 | 30-35 | | 12-14 | |
| | | 14-16 | 35-40 | | 14-16 | |
| | | 16-18 | | | 16-18 | |
| | | 18-20 | | | 18-20 | |
| | | 20-22 | | | 20-22 | |
| | | 22-24 | | | 22-24 | |
| | | 24-26 | | | 24-26 | |
| | | 26-28 | | | 26-28 | |
| | | 28-30 | | | 28-30 | |
| | | 30-32 | | | 30-32 | |
| | | 34-36 | | | 32-34 | |
| | | 36-38 | | | 34-36 | |
| | | 38-40 | | | 36-38 | |
| | | 40-42 | | | 38-40 | |

| Device<br>Name of Struct. | Station | AOM, SRR<br>SO4, CH4 | FISH<br>DNA | Life<br>sediment | Bio-<br>marker | carb.<br>S. Noe´ |
|---|---|---|---|---|---|---|
| GC | 9041-1 | 2-6 | 2-6 | | 5-15 | |
| Captn A | | 20-30 | 20-30 | | 20-30 | |
| | | 40-50 | 40-50 | | 35-45 | |
| | | 60-70 | 60-70 | | 60-70 | |
| | | 110-120 | 110-120 | | 110-120 | |
| | | 190-200 | 190-200 | | 190-200 | |
| MUC | 9051-1 | 0-4 | 0-5 | 0-20 | 0-5 | |
| Bonjardim | | 4-8 | 5-10 | 20-40 | 5-10 | |
| | | 8-12 | 10-15 | 40-50 | 10-15 | |
| | | 12-16 | 15-20 | | 15-20 | |
| | | 16-20 | 20-25 | | 20-25 | |
| | | 20-24 | 25-30 | | 25-30 | |
| | | 24-28 | 30-35 | | 30-35 | |
| | | 28-32 | 35-40 | | 35-40 | |
| | | 36-40 | 40-45 | | 40-45 | |
| | | 40-44 | 45-50 | | 45-50 | |
| | | 44-48 | 50-55 | | 50-55 | |
| | | 48-52 | | | | |
| | | 52-56 | | | | |
| GC | 9051-2 | 15-25 | 15-25 | | 15-25 | |
| Bonjardim | | 40-50 | 40-50 | | 40-50 | |
| | | 60-70 | 60-70 | | 60-70 | |
| | | 80-90 | 80-90 | | 80-90 | |
| | | 110-120 | 110-120 | | 110-120 | |
| | | 190-200 | 190-200 | | 190-200 | |
| | | 240-250 | 240-250 | | 240-250 | |
| GC | 9052-1 | 45-55 | 45-55 | | 45-55 | |
| MV next Bonjardim | | 240-250 | 240-250 | | 240-250 | |
| | | 250-260 | 250-260 | | 250-260 | |
| | | 390-400 | 390-400 | | 390-400 | |
| | | 415-425 | 415-425 | | 415-425 | |
| | | 445-455 | 445-455 | | 445-455 | |
| | | 470-480 | 470-480 | | 470-480 | |
| GC | 9052-2 | 80 | 80 | | 80 | |
| MV next Bonjardim | | | 180 | | 180 | |
| | | 250-260 | 250-260 | | 250-260 | |
| | | 280-290 | 280-290 | | 280-290 | |
| | | 310-320 | 310-320 | | 310-320 | |
| | | 340-350 | 340-350 | | 340-350 | |
| | | 370-380 | 370-380 | | 370-380 | |
| | | 400-410 | 400-410 | | 400-410 | |
| GC | 9061-1 | 10-20 | 10-20 | 40-50 | 10-20 | |
| Ginsburg | | 70-80 | 70-80 | 70-170 | 70-80 | |
| | | 60-70 | 60-70 | | 60-70 | |
| | | 40-50 | 40-50 | | 40-50 | |
| | | 120-130 | 120-130 | | 120-130 | |
| | | 100-110 | 100-110 | | 100-110 | |

| Device<br>Name of Struct. | Station | AOM, SRR<br>SO4, CH4 | FISH<br>DNA | Life<br>sediment | Bio-<br>marker | carb.<br>S. Noe´ |
|---|---|---|---|---|---|---|
| GC | 9063-1 | 40-50 | 40-50 | | 40-50 | |
| MV no name | | 70-80 | 70-80 | | 70-80 | |
| | | 90-100 | 90-100 | | 90-100 | |
| | | 130-140 | 130-140 | | 130-140 | |
| | | 160-170 | 160-170 | | 160-170 | |
| | | 190-200 | 190-200 | | 190-200 | |
| | | 230-240 | 230-240 | | 230-240 | |
| | | 255-265 | 255-265 | | 255-265 | |
| | | 280-290 | 280-290 | | 280-290 | |
| | | | | | | |
| GC | 9067-1 | 15-25 | 15-25 | | 15-25 | |
| Gemini MV | | 45-55 | 45-55 | | 45-55 | |
| | | 65-75 | 65-75 | | 65-75 | |
| | | 85-100 | 85-100 | | 85-100 | |
| | | 120-130 | 120-130 | | 120-130 | |
| | | 140-150 | 140-150 | | 140-150 | |
| | | 230-240 | 230-240 | | 230-240 | |
| | | | | | | |
| TV grab | 9073 | | worms | | worms | |
| Captn A | | | | | | |

**Table 6.6.** Microbilogy data from GeoB stations into mud mounds. See text.

## 6.4 Deformation Front and Tectonics of the Deformed Wedge

### 6.4.1. Introduction

(M.-A. Gutscher, A. Kopf)

The study area offshore Iberia and NW Africa is situated in a complex tectonic scenario where a transform fault initiating at the MAR (Mid-Atlantic Ridge) meets the zone of African-Eurasian continental collision. The scenario is complicated by spreading in the W' Alboran Sea, salt diapirism, and massive erosion of the Betic Cordillera and Rif mountain range. Most recently, Gutscher et al. (2002) suggested that a (most likely ancient) subduction system with an eastward dipping slab exists beneath the Gibraltar sedimentary wedge.

The wedge is surrounded by three abyssal plains, known as *Tagus*, *Horseshoe*, and *Seine* (e.g. **Fig. 3.1**). Two major objectives of SO175 were (i) to sample material from these incoming sedimentary sections for post-cruise geotechnical characterization of its frictional properties, and (ii) to assess via seabed mapping, seismic reflection surveys, and heat flow measurements where active thrusting presently takes place.

### 6.4.2. Operations

(A. Kopf)

A total of eight stations have been dedicated to study the deformation front and upper portions of the wedge as far as tectonism (in the widest sense) is concerned. Methods included Parasound echography, Simrad mapping, seismic reflection profiling, OFOS, heat flow measurements, and coring.

The locations of the stations can be seen in **Figure 6.1**, and are listed in Appendix 8.1.

### *6.4.3. Mapping/geophysics and OFOS*

(M.-A. Gutscher, A. Kopf)

During SO175, the deformation front (DF) was surveyed along most of its length at its western extremity. Within this region the DF exhibits a general arcuate shape (convex to the west). It is deepest adjacent to the abyssal plains, at water depths of 4200 - 4300 m. East of 9°W, the DF shallows (< 3500 m water depth) at the base of the Portugese Margin and trends N70E to N90E. West of 9°15'W and adjacent to the Horseshoe Abyssal Plain, the general strike of the DF is NE. It veers gradually to a nearly NS orientation just north of the Coral Patch Ridge (**Fig. 6.49**). South of this ridge and adjacent to the Horseshoe Abyssal Plain, the shape of the DF is more complex, with several undulations but the overall orientation is SE. The southernmost portion of the DF (adjacent to the Rharb Valley at the base of the Moroccan Margin) was not surveyed, but based on existing digital bathymetric maps and available seismic reflection profiles it appears to follow a N70 E trend, shallowing to the east.

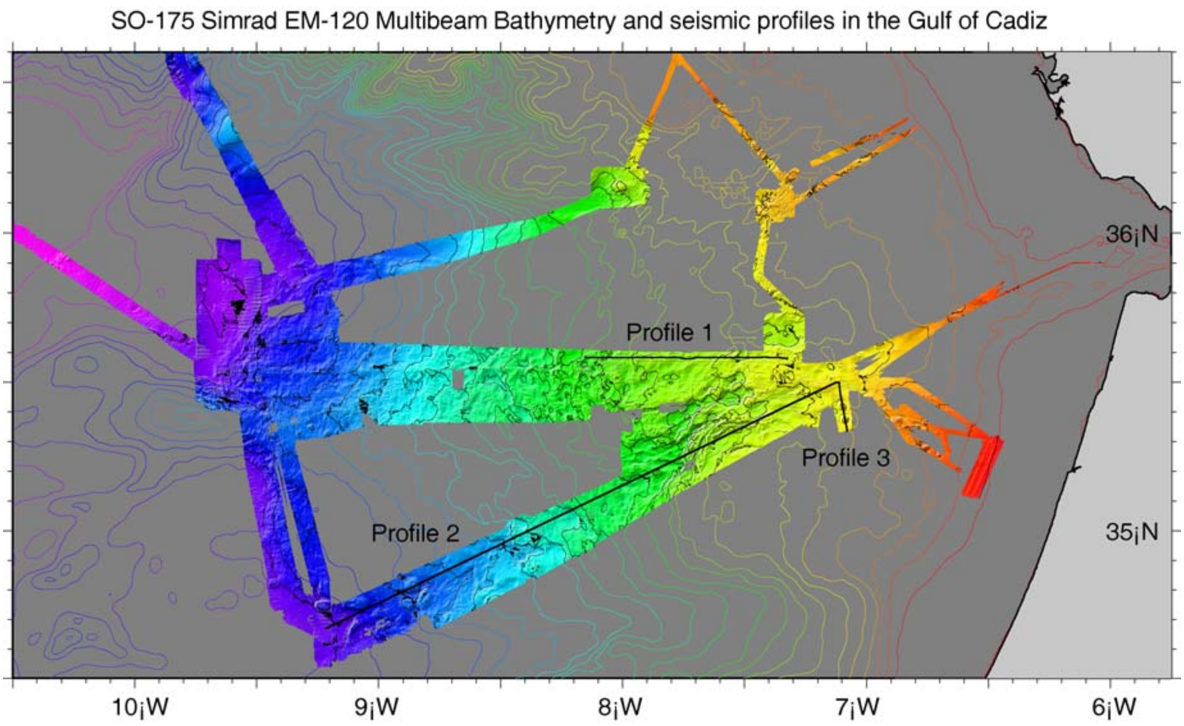


**Fig. 6.49.** General Bathymetric Map with newly acquired SO175 Simrad-EM120 Multibeam Data superposed on Gebco 1 min bathymetric contours. Location of SO175 seismic profiles 1 – 3 is shown.

***NW Deformation Front (adjacent to the Horseshoe Abyssal Plain)***

This region was well covered by our survey and shows a series of elongate ridges (dimensions typically 10 km x 2 km) oriented sub-parallel to the overall curved shape of the DF. These ridges are imaged in cross-section by the Parasound sub-bottom profiles and show folding of the entire visible sedimentary sequence (which consists of well laminated reflections alternating with thin, more transparent layers). Between the folds, steps are commonly observed with a vertical height typically of 80 m and which appear to represent reverse faults (**Fig. 6.50**).

This pattern was observed on profiles with orientations ranging from N 150 E to N 90 E to N 70 E and thus indicates NW and W vergent thrusting and folding here. The ridges typically show a spacing of 5 – 10 km and up to 5 – 6 are observed along any given profile. This pattern of seaward vergent thrusting and folding, adjacent to an abyssal plain, with a seafloor surface shallowing away from the sea (here to the E) is typical for an accretionary wedge. The fresh morphological appearance, as well as the Parasound images showing deformation of the uppermost (most recently deposited) layers suggests that deformation is active here today.

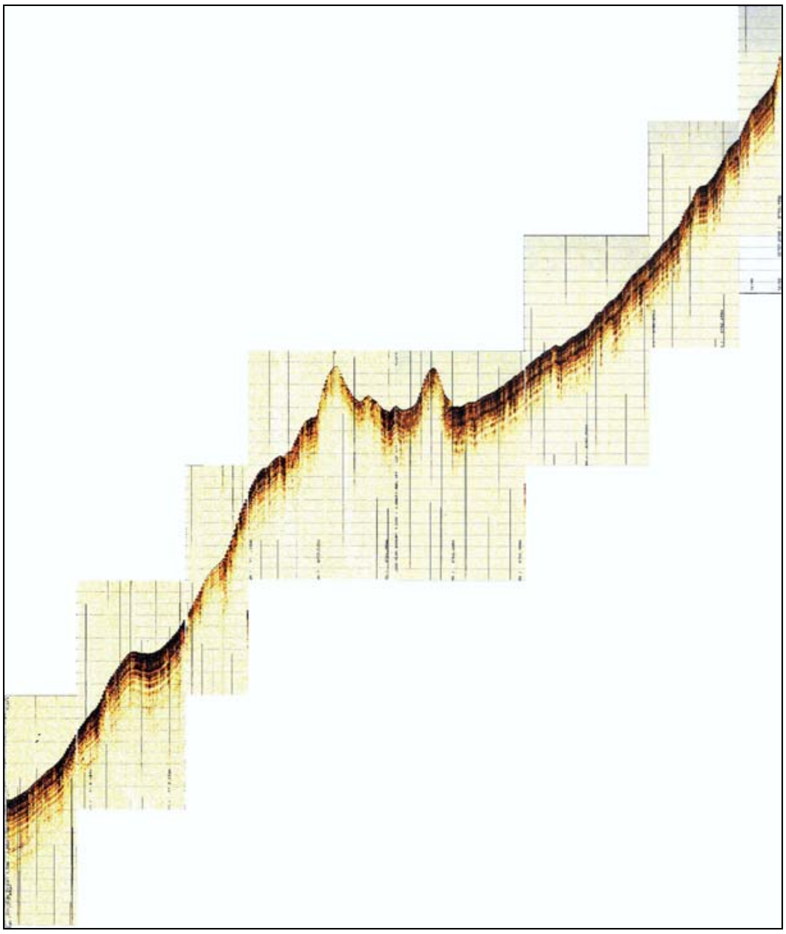

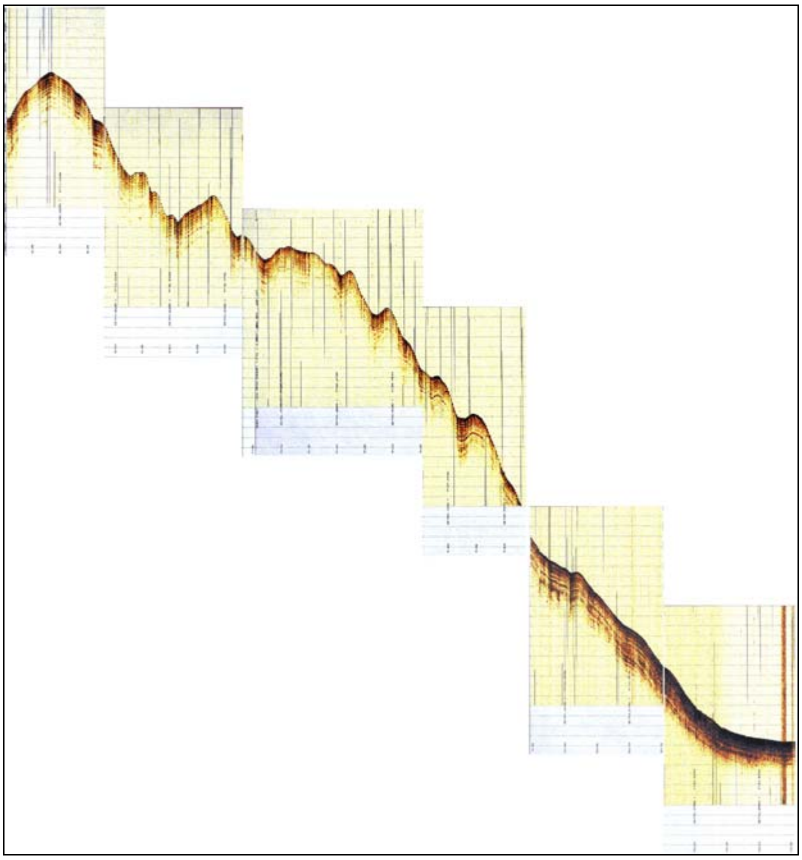

**Fig. 6.50.** Parasound images of the deformation front along
**a)** a NW-SE- profile (GeoB9009-2), and **b)** an E-W profile (GeoB 9050).

### *Deformation Front at Coral Patch Ridge*

Coral Patch Ridge is a bathymetric high known from published seismic profiles to exhibit NW and SE vergent reverse faulting of the entire sedimentary sequence with apparent involvement of the underlying basement. It forms a prominent positive free-air gravity anomaly (> +60 mGal) and thus appears to represent a structural basement high. The DF at the level of Coral Patch Ridge shallows by 300 – 500 m (to about 3800 m depth) and is offset to the E by 10 - 15 km. The DF appears to wrap around this basement high, with several anticlinal ridges sub-parallel to the depth contours of Coral Patch Ridge. This pattern of indentation into a deformation front of an accretionary wedge is commonly observed when asperities (seamounts, or ridges) are subducted beneath an accretionary wedge (Dominguez et al., 2000). Furthermore the eastward indentation provides a kinematic marker between the abyssal plain and the deforming accretionary wedge indicating relative E – W convergence between these two domains.

***SW Deformation Front (adjacent to the Seine Abyssal Plain)***

The DF south of 35°15'S shows undulations within an overall SE trend. South of 34°50' S, large circular and elongate bumps (≥5 km diameter, 200 m high) are observed at the DF, as well as within the lowermost portion of the accretionary wedge. Seaward (W and SW) of the DF similarly large bathymetric features are observed in the existing digital bathymetric map (**Fig. 6.51**). Some of these structures are imaged on SISMAR deep seismic reflection profiles and represent salt diapirs, seen to originate in structurally controlled syn-rift basins related to Mesozoic rifting of Africa and North America (Contrucci et al., in press). In order to determine the nature of these diapiric features a prominent bathymetric high, within the wedge (at the bottom of Line SISMAR-16 and on profile GeoB 9056, shot during this cruise) was sampled by two gravity cores with simultaneous heat flow measurements (GeoB 9085, 9086, 9087). Anomalously high heat flow values (120-170 mW/m$^2$) were observed. As salt has a very high thermal conductivity, the high heat flow suggests these may be salt domes (see Ch. 6.4.7. below). A geochemical analysis of the pore fluids indicated significantly elevated salinity (15%) and confirms the salt dome origin of this structure (see Ch. 6.4.6. below). This implies that the morphologically similar structures observed south of 34°50'N are a field of salt domes.

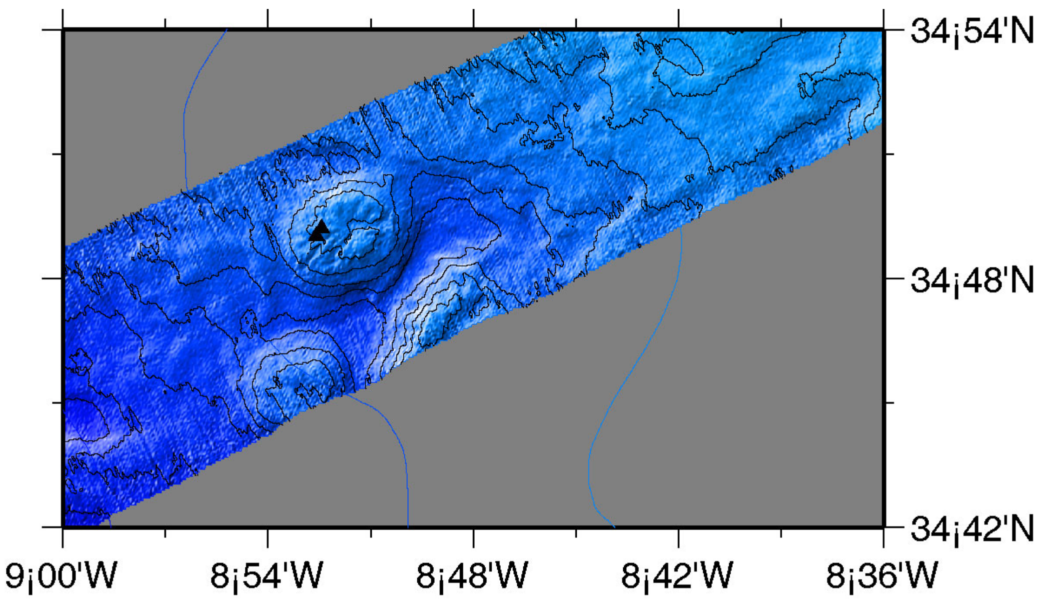


**Fig. 6.51.** Close-up of Poseidon salt dome with core locations

The deformation front itself (Fig. 6.52) is not dissimilar to the other two profiles further north (see **Fig. 6.50**).

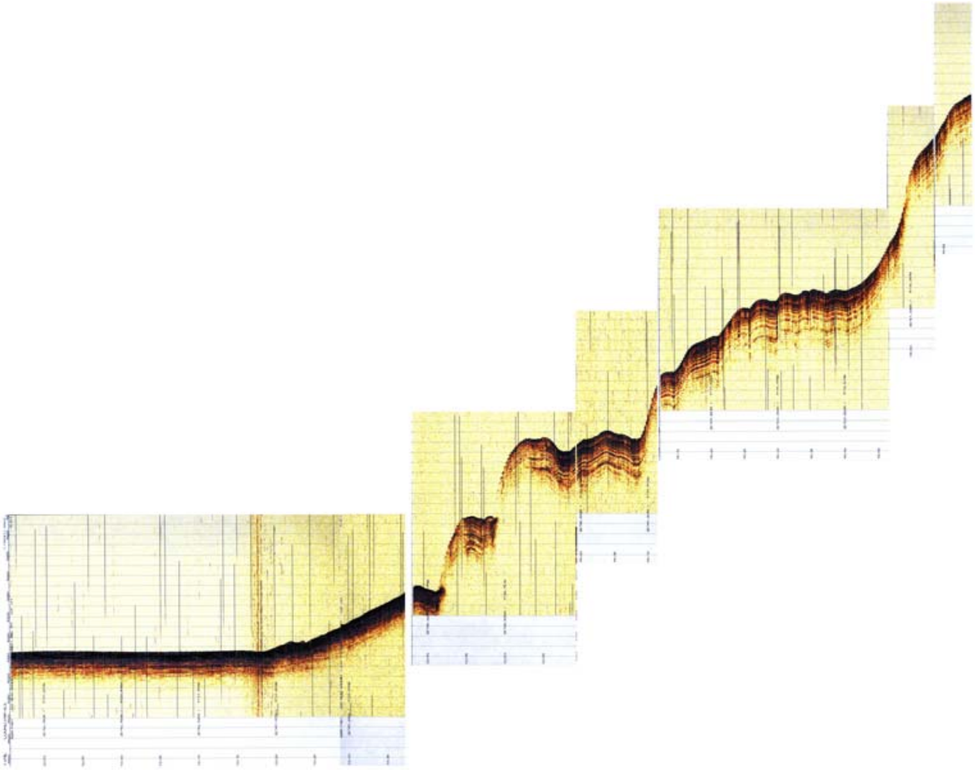

**Fig. 6.52.** Parasound images of the deformation front along a SW-NE- profile (GeoB 9088).

*General structural features of the wedge*

Two bands of bathymetric data coverage with 20 – 30 km width provide regional transects across the accretionary wedge with E-W and WSW-ENE orientations. Although correlations from one band to the other are difficult due to lack of data coverage, there appear to be 4 general morphological domains in the wedge. These are from W to E:

- a lowermost slope (from about 4200 - 3400 m depth) characterized by abundant low anticlinal ridges (well defined near the deformation front) and a flat surface slope (~0.5° surface slope)
- a lower slope (from 3400 – 2400 m depth), slightly steeper (1° mean slope), marked locally by 100 - 300 m high fault scarps
- a mid-slope region extending from approximately 8.5°W to 7.5°W (corresponding to water depths of 2400 - 1400 m), featuring abundant circular and elongate closed depressions [These depressions are very well imaged by published TASYO (Hernandez-Molina et al., 2003) and CADISAR (**Fig. 6.53**; cf. Mulder et al., 2003) multibeam data.

These structures were described as "ponded basins" by Mulder et al., 2003, though their precise origin remains unclear.]

- an upper slope (from 1400 - 600 m depth) with an almost horizontal slope (< 0.4°), characterized by a generally smooth seafloor morphology, with local basins and a high concentration of mud volcanoes.

Heat flow measurements conducted along these bands provide two regional heat flow transects and are reported below (see Ch. 6.4.7. below).

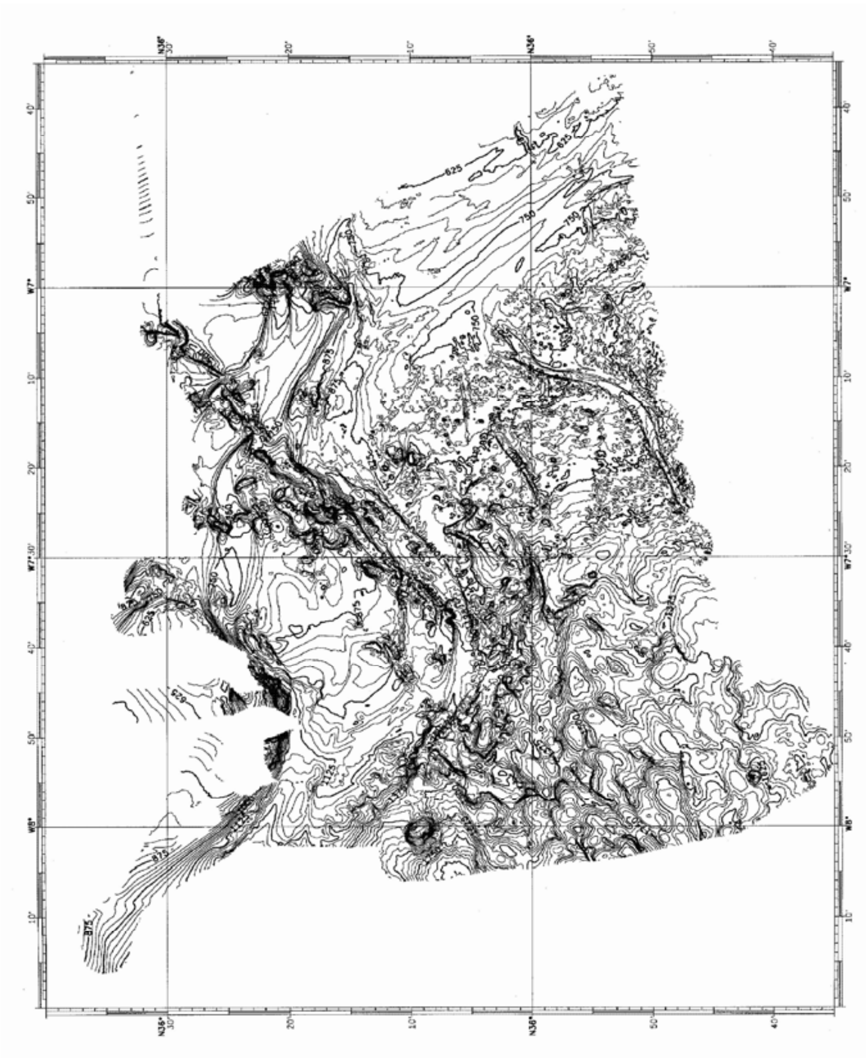

**Fig. 6.53.** CADISAR bathymetric map (Mulder et al., 2003).

**Additional observations of thrust faults and related scarps**

Additional heat flow and towed video camera (OFOS) surveys were conducted across the lowermost of 3 prominent fault scarps seen on SISMAR Line 16. The heat flow survey indicated elevated heat flow in the immediate vicinity of the bathymetric scarp, though a correction for the topographic effects must still be applied (see Ch. 6.4.7. below). The elevated heat flow raised the possibility of a contribution from enhanced fluid flow in proximity to the fault. The OFOS survey crossed the fault scarp where the heat flow data were acquired and crossed yet two more times further south and east along the scarp (**Fig. 6.54**). No signs of faunal communities associated with fluid venting were observed.

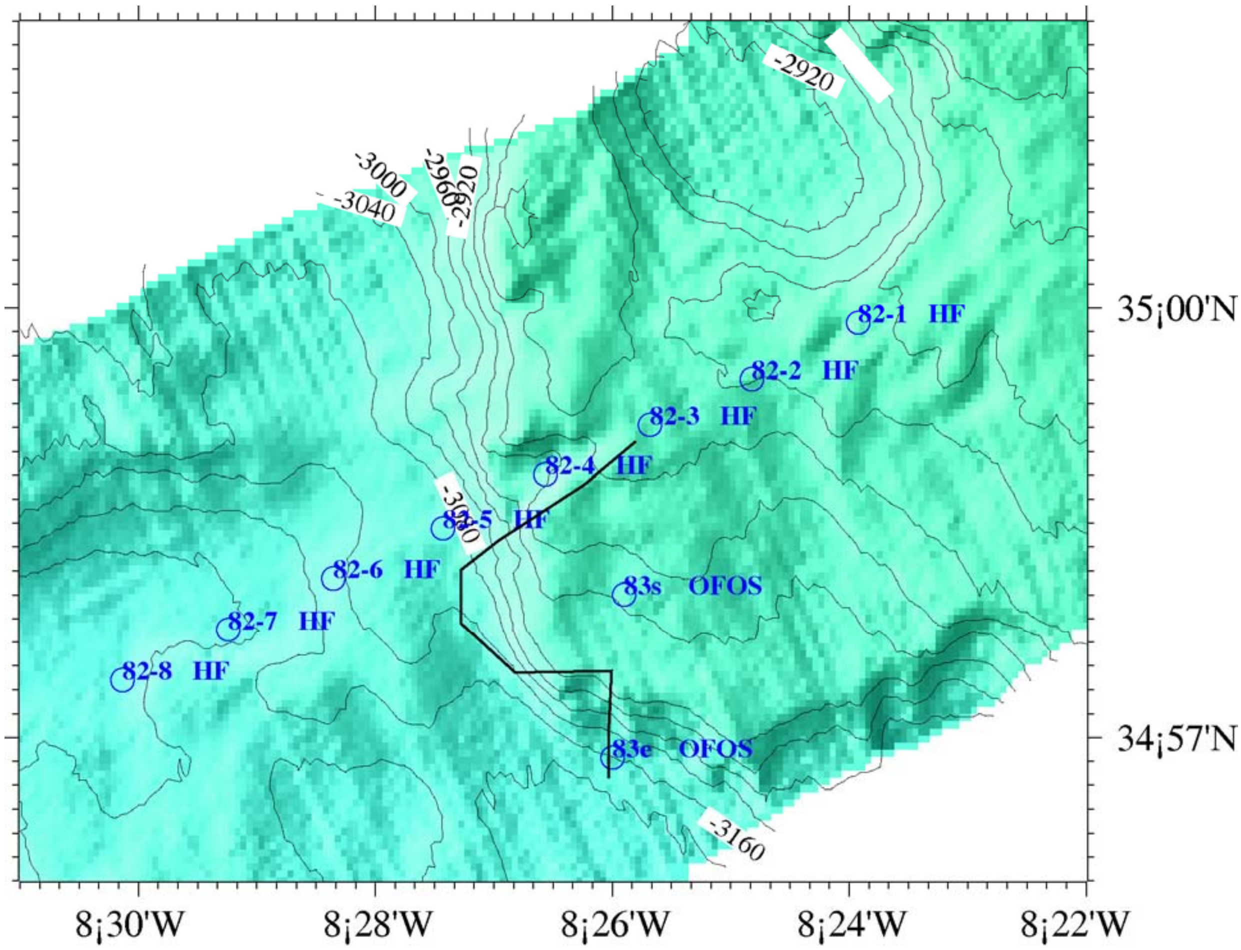


**Fig. 6.54.** Lower fault scarp on line *Sismar 16*, with the locations of heat flow measurements and the track of the OFOS Survey.

### 6.4.4. Lithology

(D. Hebbeln, B. Dorschel, A. Marti, M. Lutz)

Several sediment cores were taken in the uppermost portions of the abyssal plains and at the deformation front (**Table 6.7**). The cores from the three abyssal plains of the region, the *Horseshoe*, *Seine* and *Tagus* abyssal plains, were taken in order to describe the sediment of the incoming plate. The mostly hemipelagic sediments are generally fine grained, consisting of muddy clays and clayey muds. The uppermost 10 to 30 cm of these cores are marked by a light brown, oxidised sediment layer. Below, the sediment colour is mainly gray with some olive-coloured parts. Often the sediment is mottled with black spots, reflecting the accumulation of FeS in layers and/or spots formerly marked by enriched organic carbon contents.

The cores from the *Tagus* and *Seine* abyssal plains contain a number of turbidites, which form typical contributions in near-slope abyssal plain sediments. Only the *Horseshoe* abyssal plain gravity core (GeoB 9045-2) recovered no turbidites. However, this is probably due to the limited length of this record of only 53 cm, as e.g. core GeoB 9055-1 from the *Seine* abyssal plain has its uppermost turbidite starting at 130 cm core depth. This core contains four turbidites ranging in thickness between 4 and 10 cm. All of them have dark sands at their base and show a clear fining upward sequence. However, it appears that the turbidites do not grade in a final mud facies. In contrast, this can be observed in core GeoB 9095-1 from the *Tagus* abyssal plain, which in total has 6 turbidites. Here, some of the turbidites show a full sequence from a sandy basal part to a muddy or even clayey upper part. This is also reflected in the thickness of the turbidites, which in this core range from 4 to 36 cm. Core GeoB 9010-1 taken at the deformation front also consists of hemipelagic sediments with a number of turbidites. The background sedimentation provides a mainly gray muddy clay, which only in the uppermost 47 cm gets a sandy component. Close to the core top the sediment colour changes into light brown. The five turbidites in this core range in thickness from 2 to 14 cm and have dark sands at their base.

Two more sediment cores have been taken from the mound-like *Poseidon* dome. Core GeoB 9085-1 was taken close to its top, while GeoB 9086-1 has been retrieved from its flank. Interestingly, both cores show a marked offset.

| station no. | latitude °N | longitude °W | water depth (m) | recovery (m) | area | sediments |
|---|---|---|---|---|---|---|
| GeoB 9095-1 | 37:30.01 | 11:02.03 | 5161 | 3.10 | *Tagus* abyssal plain | hemipel. sedim. w/ turbidites |
| GeoB 9045-2 | 35:29.60 | 09:33.43 | 3951 | 0.53 | *Horseshoe* abyssal plain | hemipelagic sediments |
| GeoB 9055-1 | 34:39.98 | 09:10.00 | 4179 | 2.49 | *Seine* abyssal plain | hemipel. sedim. w/ turbidites |
| GeoB 9010-1 | 35:47.00 | 09:32.00 | 4365 | 2.32 | Deformation front | hemipel. sedim. w/ turbidites |
| GeoB 9086-1 | 34:49.21 | 08:51.00 | 3463 | 4.69 | Poseidon dome | hemipel. sedim. w/ turbidites |
| GeoB 9085-1 | 34:49.11 | 08:51.70 | 3457 | 5.70 | Poseidon dome | hemipelagic sediments |

**Table 6.7.** List of gravity cores taken during SO-175 from the abyssal plains and the deformation front area in the Gulf of Cadiz.

### 6.4.5. MST and Physical properties

(W. Brückmann, A. Foubert)

Cores taken at the seaward part of the deformation front sometimes show turbiditic sequences in the MST data. The fining upward of these sequences can be seen in a decrease in gamma density It is further suggested that the base of turbiditic sections is more frequently associated with higher magnetic susceptibility values. Cores at the toe and on the sedimentary wedge show no clear variations in either MST or physical properties data.

Full MST data are shown in **Appendix 8.4**, while physical property data from all cores studied with respect to index properties are shown in **Table 6.8**.

| sample ID | depth | section | tare | wet | dry | water | void | wet weight | colume | wet bulk | dry weight | volume | grain | salt corrected | salinity | mass of | mass | volume |
|---|---|---|---|---|---|---|---|---|---|---|---|---|---|---|---|---|---|---|
| | in section | | | weight | weight | content | ratio e | sample | wet sample | density | sample | dry sample | density | grain density | psu | water | of salt | of salt |
| GeoB 9001-1 | 50 | 1 | 1270 | 15781 | 8990 | 46,80 | 0,88 | 14,511 | 8,711 | 1,67 | 7720 | 2,781 | 2,78 | 2,826 | 34,50 | 6,791 | 0,548 | 0,2427 |
| GeoB 9001-1 | 50 | 2 | 1250 | 16359 | 9626 | 44,56 | 0,80 | 15,109 | 9,528 | 1,59 | 8376 | 3,171 | 2,64 | 2,673 | 34,50 | 6,733 | 0,543 | 0,2406 |
| GeoB 9001-1 | 50 | 3 | 1260 | 16379 | 10463 | 39,13 | 0,64 | 15,119 | 9,054 | 1,67 | 9203 | 3,395 | 2,71 | 2,741 | 34,50 | 5,916 | 0,477 | 0,2114 |
| GeoB 9001-1 | 50 | 4 | 1275 | 15492 | 9678 | 40,89 | 0,69 | 14,217 | 8,464 | 1,68 | 8403 | 3,125 | 2,69 | 2,720 | 34,50 | 5,814 | 0,469 | 0,2078 |
| GeoB 9001-1 | 50 | 5 | 1272 | 17105 | 11205 | 37,26 | 0,59 | 15,833 | 9,1 | 1,74 | 9933 | 3,719 | 2,67 | 2,696 | 34,50 | 5,9 | 0,476 | 0,2108 |
| GeoB 9008-2 | 50 | 1 | 1275 | 16499 | 10750 | 37,76 | 0,61 | 15,224 | 8,995 | 1,69 | 9475 | 3,535 | 2,68 | 2,706 | 34,50 | 5,749 | 0,464 | 0,2054 |
| GeoB 9008-2 | 64 | 2 | 1277 | 15139 | 10237 | 35,36 | 0,55 | 13,862 | 8,086 | 1,71 | 8960 | 3,27 | 2,74 | 2,767 | 34,50 | 4,902 | 0,395 | 0,1752 |
| GeoB 9008-2 | 54 | 3 | 1269 | 16502 | 11768 | 31,08 | 0,45 | 15,233 | 8,396 | 1,81 | 10499 | 3,842 | 2,73 | 2,755 | 34,50 | 4,734 | 0,382 | 0,1692 |
| GeoB 9010-1 | 2 | 1 | 1281 | 17004 | 10803 | 39,44 | 0,65 | 15,723 | 9,471 | 1,66 | 9522 | 3,474 | 2,74 | 2,774 | 34,50 | 6,201 | 0,500 | 0,2216 |
| GeoB 9010-1 | 20 | 2 | 1274 | 13996 | 9234 | 37,43 | 0,60 | 12,722 | 7,437 | 1,71 | 7960 | 2,931 | 2,72 | 2,744 | 34,50 | 4,762 | 0,384 | 0,1702 |
| GeoB 9010-1 | 70 | 2 | 1275 | 15530 | 10382 | 36,11 | 0,57 | 14,255 | 8,267 | 1,72 | 9107 | 3,413 | 2,67 | 2,692 | 34,50 | 5,148 | 0,415 | 0,1840 |
| GeoB 9010-1 | 20 | 3 | 1268 | 17187 | 11124 | 38,09 | 0,62 | 15,919 | 9,334 | 1,71 | 9856 | 3,684 | 2,68 | 2,701 | 34,50 | 6,063 | 0,489 | 0,2166 |
| GeoB 9010-1 | 90 | 3 | 1267 | 12606 | 8407 | 37,03 | 0,59 | 11,339 | 6,526 | 1,74 | 7140 | 2,694 | 2,65 | 2,674 | 34,50 | 4,199 | 0,339 | 0,1500 |
| GeoB 9014-2 | 48 | 1 | 1275 | 16628 | 10574 | 39,43 | 0,65 | 15,353 | 9,23 | 1,66 | 9299 | 2,694 | 3,45 | 3,556 | 34,50 | 6,054 | 0,488 | 0,2163 |
| GeoB 9014-2 | 50 | 2 | 1276 | 16003 | 9965 | 41,00 | 0,69 | 14,727 | 9,144 | 1,61 | 8689 | 2,694 | 3,23 | 3,310 | 34,50 | 6,038 | 0,487 | 0,2158 |
| GeoB 9019-1 | 43 | 1 | 1262 | 18454 | 11979 | 37,66 | 0,60 | 17,192 | 10,332 | 1,66 | 10717 | 3,83 | 2,80 | 2,833 | 34,50 | 6,475 | 0,522 | 0,2314 |
| GeoB 9019-1 | 72 | 2 | 1271 | 13770 | 9446 | 34,59 | 0,53 | 12,499 | 7,238 | 1,73 | 8175 | 3,675 | 2,22 | 2,223 | 34,50 | 4,324 | 0,349 | 0,1545 |
| GeoB 9021-1 | 56 | 1 | 1267 | 20510 | 13903 | 34,33 | 0,52 | 19,243 | 11,129 | 1,73 | 12636 | 4,679 | 2,70 | 2,724 | 34,50 | 6,607 | 0,533 | 0,2361 |
| GeoB 9021-1 | 75 | 2 | 1268 | 20251 | 14625 | 29,64 | 0,42 | 18,983 | 10,239 | 1,85 | 13357 | 4,884 | 2,73 | 2,755 | 34,50 | 5,626 | 0,454 | 0,2010 |
| GeoB 9038-1 | 40 | 1 | 1196 | 21103 | 13287 | 39,26 | 0,65 | 19,907 | 12,13 | 1,64 | 12091 | 4,419 | 2,74 | 2,768 | 34,50 | 7,816 | 0,630 | 0,2793 |
| GeoB 9038-1 | 70 | 2 | 1203 | 20162 | 13685 | 34,16 | 0,52 | 18,959 | 10,95 | 1,73 | 12482 | 4,586 | 2,72 | 2,746 | 34,50 | 6,477 | 0,522 | 0,2314 |
| GeoB 9038-1 | 60 | 3 | 1200 | 16872 | 12314 | 29,08 | 0,41 | 15,672 | 8,54 | 1,83 | 11114 | 4,026 | 2,76 | 2,782 | 34,50 | 4,558 | 0,368 | 0,1629 |
| GeoB 9039-1 | 40 | 1 | 1202 | 11721 | 7368 | 41,38 | 0,71 | 10,519 | 6,425 | 1,64 | 6166 | 2,222 | 2,77 | 2,814 | 34,50 | 4,353 | 0,351 | 0,1555 |
| GeoB 9039-1 | 60 | 2 | 1205 | 11475 | 8580 | 28,19 | 0,39 | 10,27 | 5,512 | 1,86 | 7375 | 2,706 | 2,73 | 2,744 | 34,50 | 2,895 | 0,233 | 0,1034 |
| GeoB 9039-1 | 20 | 3 | 1203 | 11933 | 8715 | 29,99 | 0,43 | 10,73 | 5,848 | 1,83 | 7512 | 2,758 | 2,72 | 2,744 | 34,50 | 3,218 | 0,260 | 0,1150 |
| GeoB 9039-1 | 40 | 4 | 1204 | 9578 | 7350 | 26,61 | 0,36 | 8,374 | 4,274 | 1,96 | 6146 | 2,231 | 2,75 | 2,773 | 34,50 | 2,228 | 0,180 | 0,0796 |
| GeoB 9040-1 | 40 | 1 | 1209 | 11069 | 7568 | 35,51 | 0,55 | 9,86 | 5,711 | 1,73 | 6359 | 2,274 | 2,80 | 2,828 | 34,50 | 3,501 | 0,282 | 0,1251 |
| GeoB 9040-1 | 15 | 2 | 1214 | 16703 | 10953 | 37,12 | 0,59 | 15,489 | 9,341 | 1,66 | 9739 | 3,602 | 2,70 | 2,731 | 34,50 | 5,75 | 0,464 | 0,2055 |
| GeoB 9040-1 | 60 | 3 | 1207 | 19236 | 12383 | 38,01 | 0,61 | 18,029 | 10,697 | 1,69 | 11176 | 4,126 | 2,71 | 2,737 | 34,50 | 6,853 | 0,553 | 0,2449 |
| GeoB 9040-1 | 60 | 4 | 1206 | 21806 | 14313 | 36,37 | 0,57 | 20,6 | 12,158 | 1,69 | 13107 | 4,83 | 2,71 | 2,740 | 34,50 | 7,493 | 0,604 | 0,2677 |
| GeoB 9041-1 | 40 | 1 | 1261 | 12400 | 8671 | 33,48 | 0,50 | 11,139 | 6,523 | 1,71 | 7410 | 2,632 | 2,82 | 2,845 | 34,50 | 3,729 | 0,301 | 0,1332 |
| GeoB 9041-1 | 20 | 2 | 1268 | 19593 | 13822 | 31,49 | 0,46 | 18,325 | 10,444 | 1,75 | 12554 | 4,492 | 2,79 | 2,821 | 34,50 | 5,771 | 0,465 | 0,2062 |
| GeoB 9041-1 | 50 | 3 | 1264 | 14700 | 10363 | 32,28 | 0,48 | 13,436 | 7,83 | 1,72 | 9099 | 3,296 | 2,76 | 2,785 | 34,50 | 4,337 | 0,350 | 0,1550 |
| GeoB 9045-2 | 25 | 1 | 1206 | 10462 | 6831 | 39,23 | 0,65 | 9,256 | 5,678 | 1,63 | 5625 | 4,842 | 1,16 | 1,132 | 34,50 | 3,631 | 0,293 | 0,1297 |
| GeoB 9051-2 | 40 | 1 | 1205 | 11148 | 7539 | 36,30 | 0,57 | 9,943 | 5,587 | 1,78 | 6334 | 2,199 | 2,88 | 2,919 | 34,50 | 3,609 | 0,291 | 0,1290 |
| GeoB 9051-2 | 40 | 2 | 1216 | 13198 | 9578 | 30,21 | 0,43 | 11,982 | 6,585 | 1,82 | 8362 | 2,849 | 2,94 | 2,967 | 34,50 | 3,62 | 0,292 | 0,1294 |
| GeoB 9051-2 | 40 | 3 | 1205 | 13647 | 9759 | 31,25 | 0,45 | 12,442 | 7,006 | 1,78 | 8554 | 3,079 | 2,78 | 2,803 | 34,50 | 3,888 | 0,314 | 0,1389 |
| GeoB 9052-1 | 60 | 1 | 1200 | 15238 | 8886 | 45,25 | 0,83 | 14,038 | 8,872 | 1,58 | 7686 | 2,819 | 2,73 | 2,768 | 34,50 | 6,352 | 0,512 | 0,2270 |
| GeoB 9052-1 | 80 | 2 | 1216 | 13831 | 8678 | 40,85 | 0,69 | 12,615 | 8,034 | 1,57 | 7462 | 2,734 | 2,73 | 2,763 | 34,50 | 5,153 | 0,416 | 0,1841 |
| GeoB 9052-1 | 30 | 3 | 1208 | 16352 | 9922 | 42,46 | 0,74 | 15,144 | 9,448 | 1,60 | 8714 | 3,245 | 2,69 | 2,718 | 34,50 | 6,43 | 0,519 | 0,2298 |
| GeoB 9052-1 | 40 | 4 | 1188 | 18751 | 11785 | 39,66 | 0,66 | 17,563 | 10,782 | 1,63 | 10597 | 3,867 | 2,74 | 2,774 | 34,50 | 6,966 | 0,562 | 0,2489 |
| GeoB 9052-1 | 50 | 5 | 1203 | 15452 | 10148 | 37,22 | 0,59 | 14,249 | 8,312 | 1,71 | 8945 | 3,32 | 2,69 | 2,721 | 34,50 | 5,304 | 0,428 | 0,1895 |
| GeoB 9052-2 | 10 | 1 | 1167 | 14303 | 8965 | 40,64 | 0,68 | 13,136 | 8,087 | 1,62 | 7798 | 2,78 | 2,81 | 2,845 | 34,50 | 5,338 | 0,431 | 0,1907 |
| GeoB 9052-2 | 70 | 2 | 1204 | 16079 | 9695 | 42,92 | 0,75 | 14,875 | 9,128 | 1,63 | 8491 | 3,124 | 2,72 | 2,754 | 34,50 | 6,384 | 0,515 | 0,2281 |
| GeoB 9052-2 | 30 | 3 | 1202 | 12054 | 10478 | 14,52 | 0,17 | 10,852 | 10,134 | 1,07 | 9276 | 3,408 | 2,72 | 2,730 | 34,50 | 1,576 | 0,127 | 0,0563 |
| GeoB 9052-2 | 30 | 4 | 1213 | 15450 | 10005 | 38,25 | 0,62 | 14,237 | 8,532 | 1,67 | 8792 | 3,165 | 2,78 | 2,812 | 34,50 | 5,445 | 0,439 | 0,1946 |
| GeoB 9052-2 | 30 | 5 | 1195 | 10692 | 7098 | 37,84 | 0,61 | 9,497 | 5,445 | 1,74 | 5903 | 2,127 | 2,78 | 2,809 | 34,50 | 3,594 | 0,290 | 0,1284 |
| GeoB 9055-1 | 10 | 1 | 1205 | 13926 | 8647 | 41,50 | 0,71 | 12,721 | 7,843 | 1,62 | 7442 | 2,727 | 2,73 | 2,764 | 34,50 | 5,279 | 0,426 | 0,1886 |
| GeoB 9055-1 | 50 | 2 | 1206 | 14172 | 8745 | 41,86 | 0,72 | 12,966 | 8,117 | 1,60 | 7539 | 2,72 | 2,77 | 2,811 | 34,50 | 5,427 | 0,438 | 0,1939 |
| GeoB 9055-1 | 60 | 3 | 1213 | 11909 | 7641 | 39,90 | 0,66 | 10,696 | 6,375 | 1,68 | 6428 | 2,309 | 2,78 | 2,821 | 34,50 | 4,268 | 0,344 | 0,1525 |
| GeoB 9063-1 | 30 | 4 | 1285 | 14299 | 10068 | 32,51 | 0,48 | 13,014 | 5,718 | 2,28 | 8783 | 3,172 | 2,77 | 2,795 | 34,50 | 4,231 | 0,341 | 0,1512 |
| GeoB 9063-1 | 20 | 5 | 1285 | 11560 | 8004 | 34,61 | 0,53 | 10,275 | 7,077 | 1,45 | 6719 | 2,417 | 2,78 | 2,809 | 34,50 | 3,556 | 0,287 | 0,1271 |

| sample ID | depth | section | tare | wet | dry | water | void | wet weight | colume | wet bulk | dry weight | volume | grain | salt corrected | salinity | mass of | mass | volume |
|---|---|---|---|---|---|---|---|---|---|---|---|---|---|---|---|---|---|---|
| | in section | | | weight | weight | content | ratio e | sample | wet sample | density | sample | dry sample | density | grain density | psu | water | of salt | of salt |
| GeoB 9064-1 | 50 | 1 | 1278 | 17190 | 9856 | 46,09 | 0,85 | 15,912 | 9,493 | 1,68 | 8578 | 3,082 | 2,78 | 2,832 | 34,50 | 7,334 | 0,591 | 0,2621 |
| GeoB 9064-1 | 50 | 2 | 1276 | 14746 | 10944 | 28,23 | 0,39 | 13,47 | 7,887 | 1,71 | 9668 | 3,575 | 2,70 | 2,722 | 34,50 | 3,802 | 0,307 | 0,1359 |
| GeoB 9064-1 | 30 | 3 | 1263 | 16664 | 11445 | 33,89 | 0,51 | 15,401 | 8,88 | 1,73 | 10182 | 3,723 | 2,73 | 2,760 | 34,50 | 5,219 | 0,421 | 0,1865 |
| GeoB 9064-1 | 20 | 4 | 1273 | 12272 | 8888 | 30,77 | 0,44 | 10,999 | 5,978 | 1,84 | 7615 | 2,729 | 2,79 | 2,815 | 34,50 | 3,384 | 0,273 | 0,1209 |
| GeoB 9064-1 | 50 | 5 | 1281 | 13024 | 9020 | 34,10 | 0,52 | 11,743 | 6,668 | 1,76 | 7739 | 2,735 | 2,83 | 2,861 | 34,50 | 4,004 | 0,323 | 0,1431 |
| GeoB 9064-1 | 10 | 6 | 1274 | 17549 | 11706 | 35,90 | 0,56 | 16,275 | 9,565 | 1,70 | 10432 | 3,826 | 2,73 | 2,754 | 34,50 | 5,843 | 0,471 | 0,2088 |
| GeoB 9065-1 | 20 | 1 | 1282 | 18793 | 12702 | 34,78 | 0,53 | 17,511 | 9,826 | 1,78 | 11420 | 4,152 | 2,75 | 2,778 | 34,50 | 6,091 | 0,491 | 0,2176 |
| GeoB 9065-1 | 20 | 2 | 1279 | 15292 | 10521 | 34,05 | 0,52 | 14,013 | 7,901 | 1,77 | 9242 | 3,385 | 2,73 | 2,755 | 34,50 | 4,771 | 0,385 | 0,1705 |
| GeoB 9065-1 | 20 | 3 | 1280 | 14491 | 10099 | 33,25 | 0,50 | 13,211 | 7,368 | 1,79 | 8819 | 3,205 | 2,75 | 2,777 | 34,50 | 4,392 | 0,354 | 0,1569 |
| GeoB 9065-1 | 20 | 4 | 1284 | 16147 | 11127 | 33,78 | 0,51 | 14,863 | 8,388 | 1,77 | 9843 | 3,576 | 2,75 | 2,779 | 34,50 | 5,02 | 0,405 | 0,1794 |
| GeoB 9065-1 | | 5 | 1276 | 19159 | 13417 | 32,11 | 0,47 | 17,883 | 9,843 | 1,82 | 12141 | 4,447 | 2,73 | 2,753 | 34,50 | 5,742 | 0,463 | 0,2052 |
| GeoB 9066-1 | 10 | 1 | 1280 | 15113 | 9157 | 43,06 | 0,76 | 13,833 | 8,692 | 1,59 | 7877 | 2,859 | 2,76 | 2,795 | 34,50 | 5,956 | 0,480 | 0,2128 |
| GeoB 9066-1 | 20 | 2 | 1278 | 17788 | 14746 | 18,43 | 0,23 | 16,51 | 8,698 | 1,90 | 13468 | 4,398 | 3,06 | 3,083 | 34,50 | 3,042 | 0,245 | 0,1087 |
| GeoB 9066-1 | 40 | 3 | 1280 | 17882 | 13244 | 27,94 | 0,39 | 16,602 | 8,485 | 1,96 | 11964 | 4,704 | 2,54 | 2,554 | 34,50 | 4,638 | 0,374 | 0,1657 |
| GeoB 9066-1 | 50 | 4 | 1284 | 19207 | 14098 | 28,51 | 0,40 | 17,923 | 9,457 | 1,90 | 12814 | 4,959 | 2,58 | 2,596 | 34,50 | 5,109 | 0,412 | 0,1826 |
| GeoB 9068-1 | 30 | 1 | 1276 | 17407 | 12892 | 27,99 | 0,39 | 16,131 | 8,828 | 1,83 | 11616 | 4,18 | 2,78 | 2,800 | 34,50 | 4,515 | 0,364 | 0,1613 |
| GeoB 9068-1 | 10 | 2 | 1279 | 14124 | 10155 | 30,90 | 0,45 | 12,845 | 10,534 | 1,22 | 8876 | 4,679 | 1,90 | 1,886 | 34,50 | 3,969 | 0,320 | 0,1418 |
| GeoB 9068-1 | 40 | 3 | 1277 | 18807 | 13966 | 27,62 | 0,38 | 17,53 | 9,353 | 1,87 | 12689 | 4,554 | 2,79 | 2,807 | 34,50 | 4,841 | 0,390 | 0,1730 |
| GeoB 9068-1 | 50 | 4 | 1279 | 18320 | 12992 | 31,27 | 0,45 | 17,041 | 9,286 | 1,84 | 11713 | 4,463 | 2,62 | 2,641 | 34,50 | 5,328 | 0,430 | 0,1904 |
| GeoB 9069-1 | 10 | 4 | 1280 | 16210 | 11451 | 31,88 | 0,47 | 14,93 | 8,621 | 1,73 | 10171 | 3,737 | 2,72 | 2,744 | 34,50 | 4,759 | 0,384 | 0,1701 |
| GeoB 9069-1 | 10 | 5 | 1280 | 14983 | 9841 | 37,52 | 0,60 | 13,703 | 8,131 | 1,69 | 8561 | 3,312 | 2,58 | 2,604 | 34,50 | 5,142 | 0,415 | 0,1837 |
| GeoB 9069-1 | 10 | 6 | 1280 | 15389 | 11446 | 27,95 | 0,39 | 14,109 | 7,723 | 1,83 | 10166 | 3,761 | 2,70 | 2,720 | 34,50 | 3,943 | 0,318 | 0,1409 |
| GeoB 9081-1 | 15 | 5 | 1250 | 17273 | 10650 | 41,33 | 0,70 | 16,023 | 9,54 | 1,68 | 9400 | 3,526 | 2,67 | 2,695 | 34,50 | 6,623 | 0,534 | 0,2367 |
| GeoB 9085-1 | 10 | 1 | 1281 | 15025 | 9474 | 40,39 | 0,68 | 13,744 | 8,419 | 1,63 | 8193 | 3,031 | 2,70 | 2,734 | 34,50 | 5,551 | 0,448 | 0,1984 |
| GeoB 9085-1 | 40 | 2 | 1279 | 15828 | 9677 | 42,28 | 0,73 | 14,549 | 9,149 | 1,59 | 8398 | 3,058 | 2,75 | 2,784 | 34,50 | 6,151 | 0,496 | 0,2198 |
| GeoB 9085-1 | 10 | 3 | 1281 | 16362 | 11940 | 29,32 | 0,41 | 15,081 | 9,173 | 1,64 | 10659 | 3,905 | 2,73 | 2,750 | 34,50 | 4,422 | 0,357 | 0,1580 |
| GeoB 9085-1 | 10 | 4 | 1280 | 16476 | 10500 | 39,33 | 0,65 | 15,196 | 9,133 | 1,66 | 9220 | 3,402 | 2,71 | 2,741 | 34,50 | 5,976 | 0,482 | 0,2135 |
| GeoB 9085-1 | 10 | 5 | 1280 | 17138 | 10673 | 40,77 | 0,69 | 15,858 | 9,092 | 1,74 | 9393 | 3,454 | 2,72 | 2,753 | 34,50 | 6,465 | 0,521 | 0,2310 |
| GeoB 9086-1 | 10 | 1 | | 14738 | 9219 | 37,45 | 0,60 | 14,738 | 8,419 | 1,75 | 9219 | 2,874 | 3,21 | 3,278 | 34,50 | 5,519 | 0,445 | 0,1972 |
| GeoB 9086-1 | 10 | 2 | 1250 | 14567 | 9664 | 36,82 | 0,58 | 13,317 | 8,249 | 1,61 | 8414 | 2,76 | 3,05 | 3,102 | 34,50 | 4,903 | 0,395 | 0,1752 |
| GeoB 9086-1 | 10 | 3 | 1250 | 14781 | 11713 | 22,67 | 0,29 | 13,531 | 8,239 | 1,64 | 10463 | | | | | | | |
| GeoB 9086-1 | 40 | 4 | 1250 | 16248 | 10655 | 37,29 | 0,59 | 14,998 | 3,143 | 4,77 | 9405 | 3,132 | 3,00 | 3,054 | 34,50 | 5,593 | 0,451 | 0,1999 |
| GeoB 9091-1 | 30 | 1 | 1250 | 12095 | 6966 | 47,29 | 0,90 | 10,845 | 7,341 | 1,48 | 5716 | 2,087 | 2,74 | 2,785 | 34,50 | 5,129 | 0,414 | 0,1833 |
| GeoB 9091-1 | 70 | 2 | 1250 | 14005 | 8694 | 41,64 | 0,71 | 12,755 | 8,589 | 1,49 | 7444 | 2,773 | 2,68 | 2,716 | 34,50 | 5,311 | 0,428 | 0,1898 |
| GeoB 9091-1 | 40 | 3 | 1250 | 13308 | 8498 | 39,89 | 0,66 | 12,058 | 7,244 | 1,66 | 7248 | 2,617 | 2,77 | 2,806 | 34,50 | 4,81 | 0,388 | 0,1719 |
| GeoB 9091-1 | 50 | 4 | 1250 | 16272 | 10173 | 40,60 | 0,68 | 15,022 | 9,072 | 1,66 | 8923 | 3,356 | 2,66 | 2,687 | 34,50 | 6,099 | 0,492 | 0,2179 |
| GeoB 9092-1 | 60 | 2 | 1280 | 11547 | 7426 | 40,14 | 0,67 | 10,267 | 5,91 | 1,74 | 6146 | 2,248 | 2,73 | 2,767 | 34,50 | 4,121 | 0,332 | 0,1473 |
| GeoB 9092-1 | 60 | 3 | 1280 | 11833 | 8092 | 35,45 | 0,55 | 10,553 | 5,99 | 1,76 | 6812 | 2,533 | 2,69 | 2,713 | 34,50 | 3,741 | 0,302 | 0,1337 |
| GeoB 9092-1 | 60 | 4 | 1280 | 13599 | 9141 | 36,19 | 0,57 | 12,319 | 6,974 | 1,77 | 7861 | 2,959 | 2,66 | 2,679 | 34,50 | 4,458 | 0,360 | 0,1593 |
| GeoB 9092-1 | 50 | 5 | 1280 | 14054 | 9965 | 32,01 | 0,47 | 12,774 | 7,276 | 1,76 | 8685 | 3,13 | 2,77 | 2,800 | 34,50 | 4,089 | 0,330 | 0,1461 |
| GeoB 9093-1 | 20 | 1 | 1280 | 14309 | 8513 | 44,49 | 0,80 | 13,029 | 8,181 | 1,59 | 7233 | 2,626 | 2,75 | 2,797 | 34,50 | 5,796 | 0,467 | 0,2071 |
| GeoB 9093-1 | 60 | 2 | 1280 | 14117 | 8687 | 42,30 | 0,73 | 12,837 | 8,133 | 1,58 | 7407 | 2,689 | 2,75 | 2,793 | 34,50 | 5,43 | 0,438 | 0,1940 |
| GeoB 9093-1 | 50 | 3 | 1280 | 9893 | 6800 | 35,91 | 0,56 | 8,613 | 4,751 | 1,81 | 5520 | 1,996 | 2,77 | 2,795 | 34,50 | 3,093 | 0,249 | 0,1105 |
| GeoB 9093-1 | 50 | 4 | 1280 | 11290 | 7640 | 36,46 | 0,57 | 10,01 | 5,641 | 1,77 | 6360 | 2,385 | 2,67 | 2,690 | 34,50 | 3,65 | 0,294 | 0,1304 |
| GeoB 9093-1 | 50 | 5 | 1280 | 12283 | 8406 | 35,24 | 0,54 | 11,003 | 6,321 | 1,74 | 7126 | 2,666 | 2,67 | 2,696 | 34,50 | 3,877 | 0,313 | 0,1385 |
| GeoB 9093-1 | 50 | 6 | 1280 | 10783 | 7817 | 31,21 | 0,45 | 9,503 | 5,528 | 1,72 | 6537 | 2,399 | 2,72 | 2,747 | 34,50 | 2,966 | 0,239 | 0,1060 |

**Table 6.8.** Physical property data from all core sections sampled during SO175. Please refer to the respective chapters for further information on corresponding lithologies.

### 6.4.6. Pore water geochemistry

(C. Hensen, K. Nass, M. Marquardt)

Two gravity cores (GeoB 9085-1 and GeoB 9086-1) were taken at the summit and the flank of Poseidon, a large mound-shaped structure located close to the supposed deformation front, in order to test the hypotheses, whether it was formed by salt diapirism or any different process (i.e., mud volcanism). Both cores did not contain methane concentrations above the atmospheric background level and did not smell of $H_2S$. Furthermore, profiles of alkalinity and dissolved nutrients indicate only very low mineralization activity (**Fig. 6.55**). However, a significant increase of the chlorinity of more than 10% at the base of gravity core GeoB 9085-1 strongly supports the idea that highly saline brines are diffusing upwards to the seafloor.

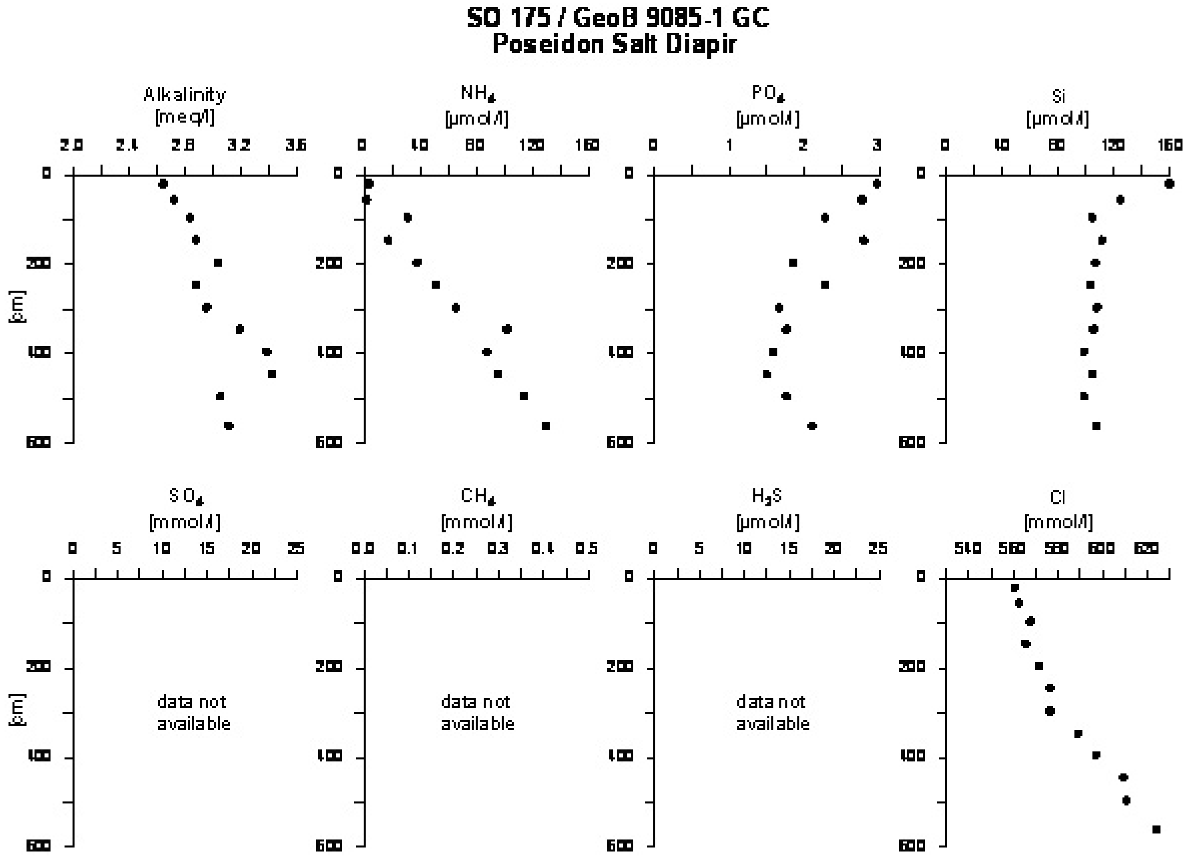


**Fig. 6.55.** Pore water geochemistry from station GeoB 9085, *Poseidon* salt dome.

### 6.4.7. Heat flow and pore pressure

(I. Grevemeyer, N. Kaul, J. Poort)

As pointed out earlier, the nature of the Gibraltar sedimentary prism is still under discussion. Authors either believe that the wedge is an olistostrome caused by sediment input from the

Mediterranean Sea (e.g., Torelli et al., 1997) or suggest that the wedge might be caused by slab retreat and hence active subduction (Gutscher et al., 2002). Like for the Marques de Pombal fault, heat flow data may reveal the processes governing the Gibraltar prism. Advection of heat into the deep subduction zone would cause low fore-arc heat flow, which tends to decrease eastward, if shear heating in the subduction thrust can be neglected (e.g., Molnar and England, 1990; Grevemeyer et al., 2003).

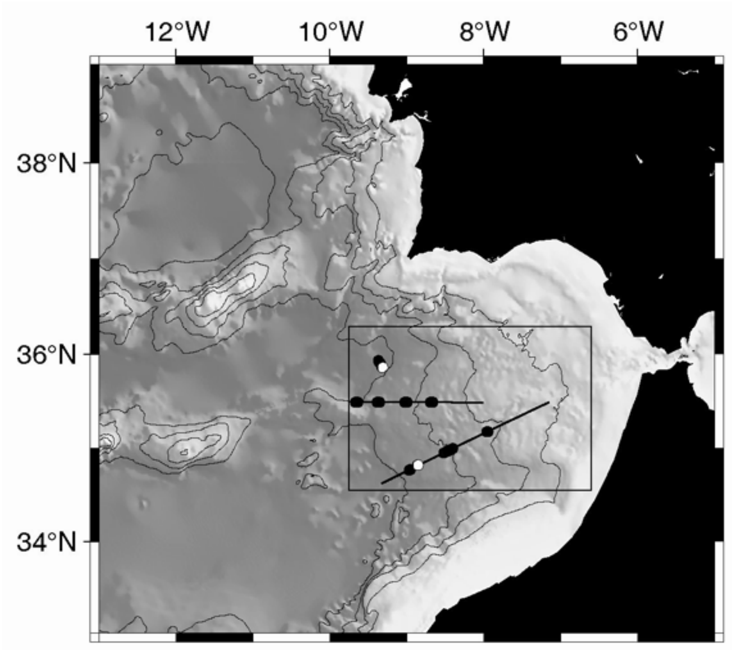


**Fig. 6.56.** Deformation front and Gibraltar sedimentary prism with location of heat flow stations.

A total of eight heat flow stations (**Figs. 6.54 and 6.56**) with 36 penetrations surveyed the deformation front and wedge area. Station GeoB9009 (H0323) crossed the deformation front at the NW terminus of the wedge (**Fig. 6.57**). Heat flow data vary very little (52-60 mW/m$^2$), though they increase by 5-7 mW/m$^2$ over the first accretionary ridge, which may indicate dewatering at slow rates. The stations GeoB9046 to GeoB9049 (H0327-H0330) surveyed a roughly 90 km long transect across the toe and western part of the prism (**Fig. 6.58**) near 35°N. Values clearly decrease towards Gibraltar and therefore indicate active under-thrusting. Thus, may support the idea of subduction. A second transect was placed along the SW-NE trending *SISMAR* 16 line (Gutscher et al., 2002; Thiebot and Gutscher, 2004).

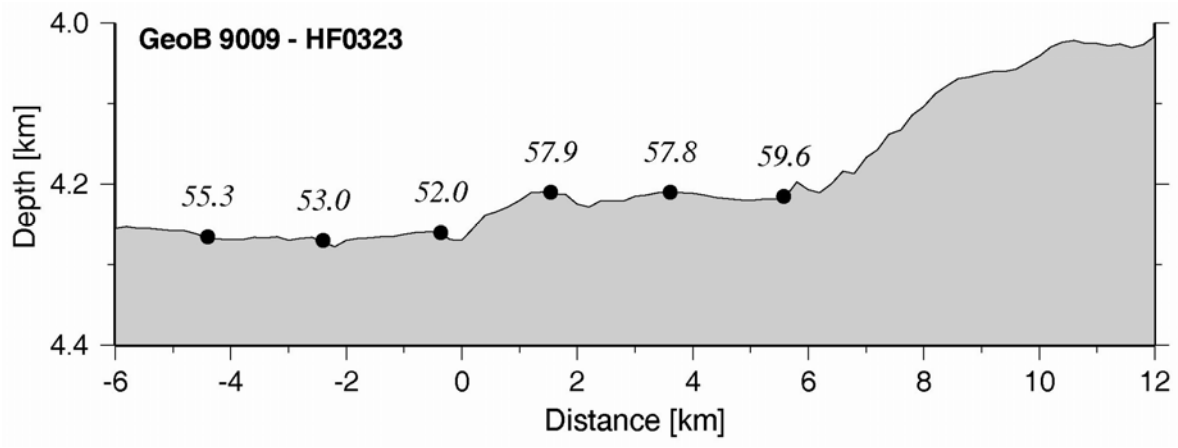


**Fig. 6.57.** *Tagus* abyssal plain - Gorringe Bank - *Horseshoe* Abyssal Plain transect heat flow locations at station GeoB 9009. See text.

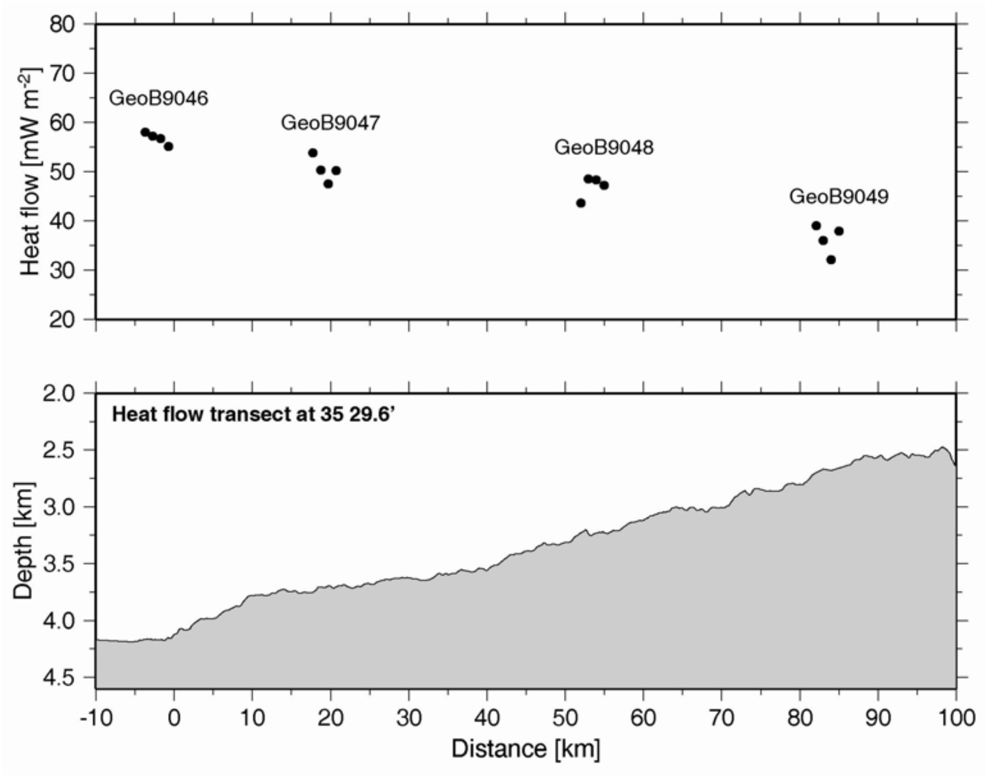


**Fig. 6.58.** Heat flow locations and data at stations GeoB 9046 to GeoB 9049. See text for interpretation.

Compared to the 35°N-transect, heat flow data show a much flatter trend (**Fig. 6.59**). Nevertheless, the overall trend of both lines suggest values decreasing eastward (**Fig. 6.60**). The higher values at 120 km from the deformation front on the *SISMAR* 16 line may indicate the onset of shear heating in the suspected under-thrust fault and may therefore be related to a (temperature-dependent) change in the frictional properties of the fault.

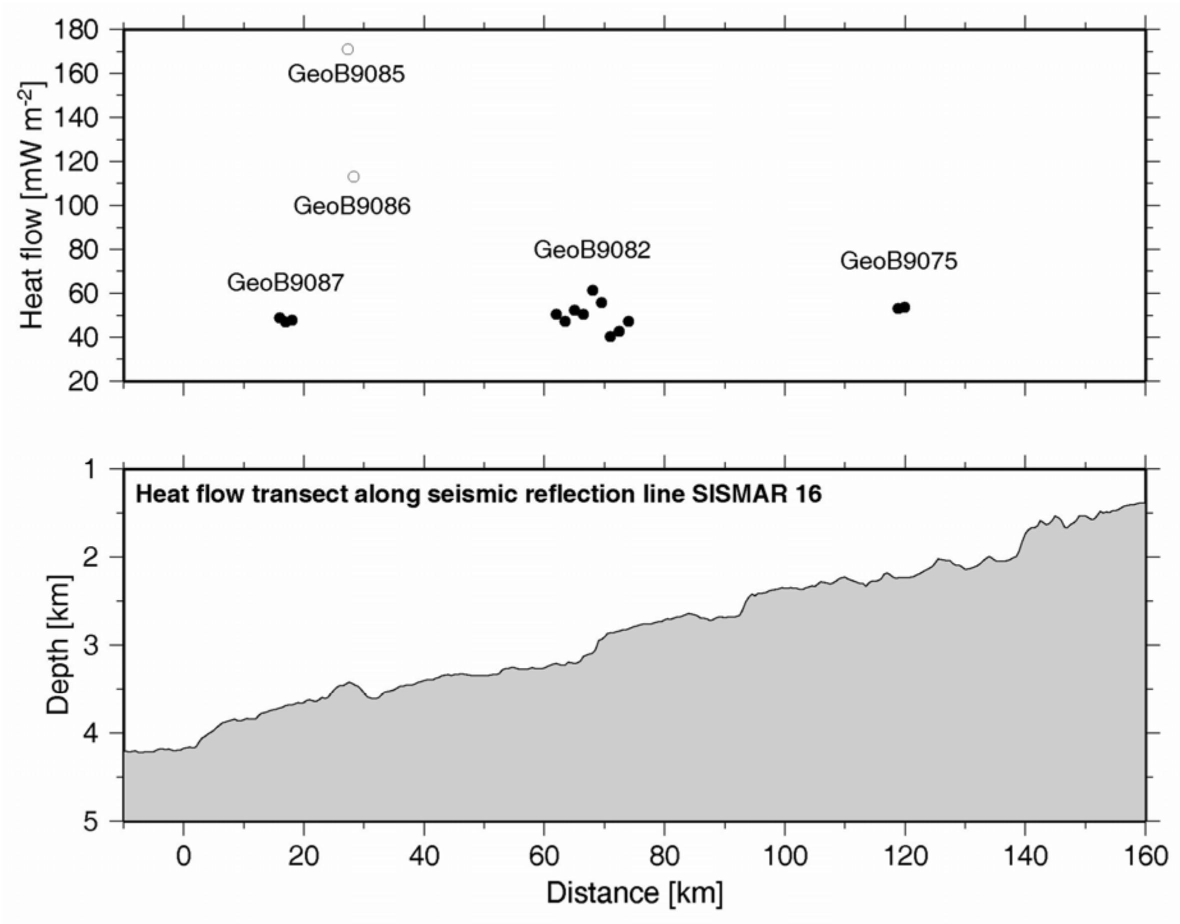


**Fig. 6.59.** Topography (bottom) and heat flow data (top) along line *SISMAR*-16; stations GeoB 9075, 9082, and 9085-9087. See text for interpretation.

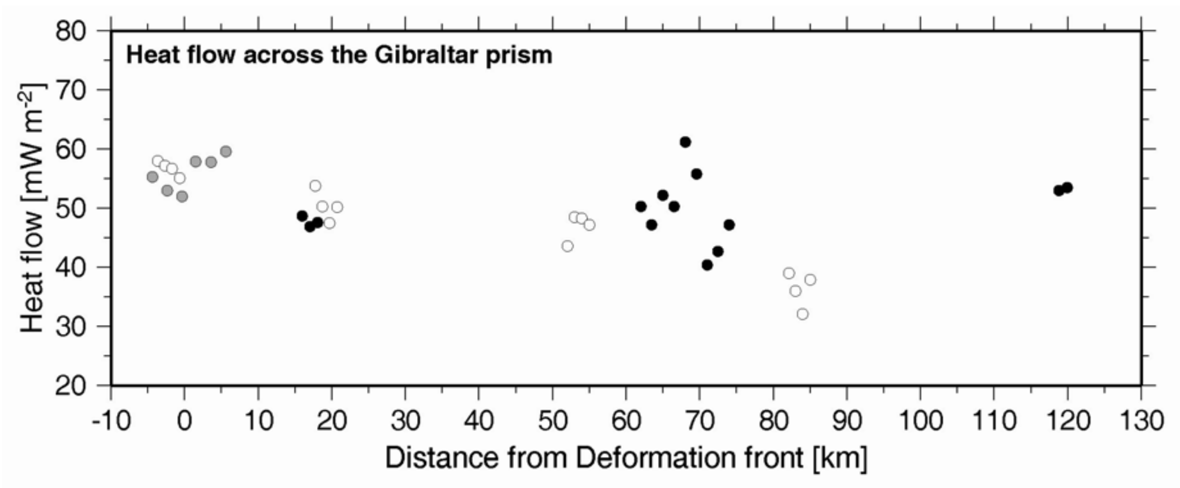


**Fig. 6.60.** Combined heat flow data from Figures 6.58 and 6.59 overlain with respect to distance to the deformation front of the prism. See text.

The Gorringe Ridge is a major topographic feature SW of Portugal and it is believed to be caused by over- or under-trusting at crustal scale (Galindo-Zaldívar et al., 2003). Earthquake activity under Gorringe Ridge suggest that it is part of the suture zone where the Eurasian and African plate meet. In the last days of the cruise the regional heat flow pattern of the region were surveyed (**Figs. 6.61 and 6.62**). Station GeoB9096 (H0342) was located on the Tagus abyssal plain. Values of 65 mW/m$^2$ were measured. In the Horseshoe abyssal plain values are 4-5 mW/m$^2$ lower (Stations GeoB9090/H0340 and GeoB9097/H0343). The trend seems to be systematic. However, the difference in absolute values is very low. Thus, is is difficult to reveal if large-scale thrusting occurs at a crustal-scale, as for example suggested by Galindo-Zaldívar et al. (2003).

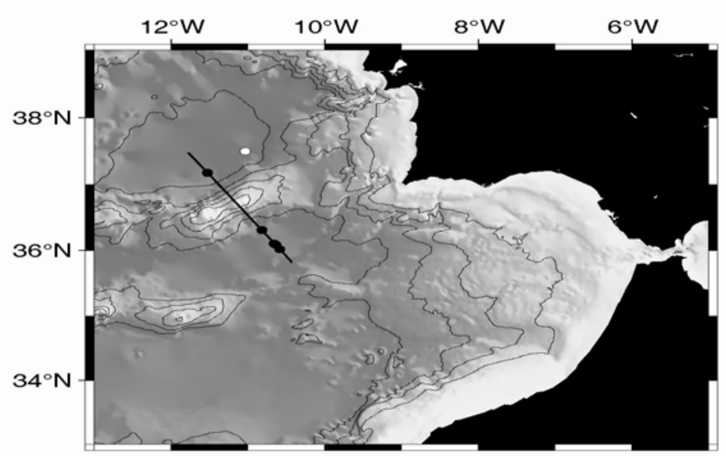


**Fig. 6.61.** Map with locations of heat flow stations in the Gorringe Bank area.

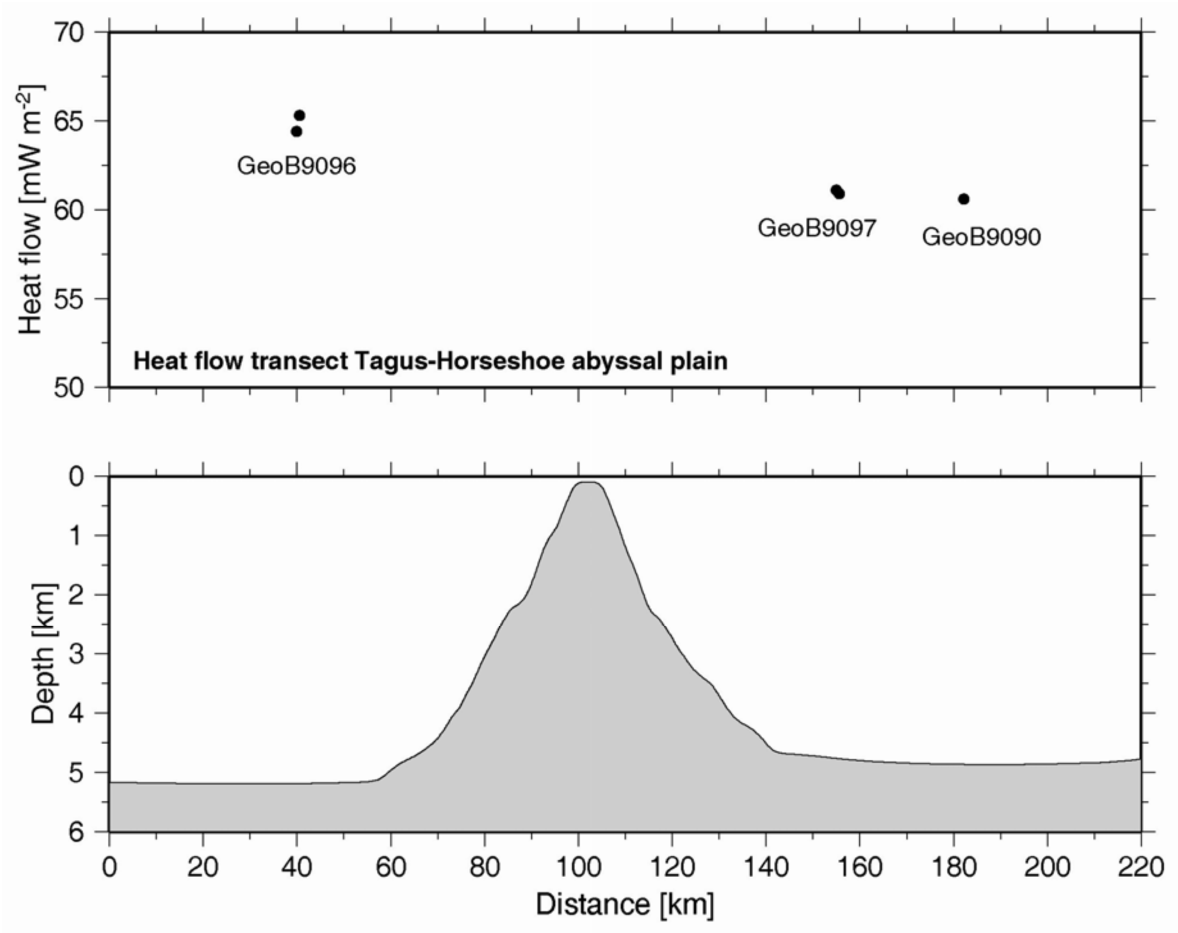


**Fig. 6.62.** Heat flow data across the Grringe Bank from *Tagus* to *Horseshoe* abyssal plain; stations GeoB 9090, 9096 (*Tagus*), and 9097 (*Horseshoe*). See text for interpretation.

## 6.5 Miscellaneous sites

(A. Foubert, M.-A. Gutscher, D. Hebbeln, A. Kopf)

During leg SO175-3, we explored two small areas close to the Moroccan margin, which cannot easily be placed into the three main research fields of the *GAP* cruise (i.e., Chapters 6.2. through 6.4.). They are the paleoceanographic sites within the Al Arraiche mud volcano province, and the subsided island west of Gibraltar, known on maps as "The Ridge", "Banco de Majuan", or "Banc de Spartel" (for location, see **Fig. 6.63.**). These two sites will be described in some detail in this chapter.

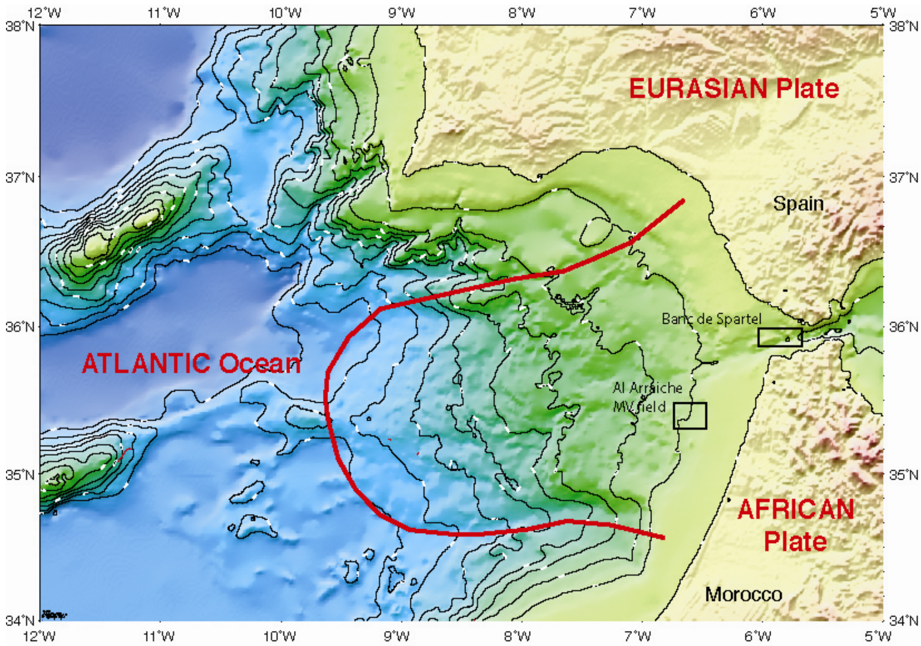


**Fig. 6.63.**: Location of the Al Arraiche MV field (W' Moroccan margin) and Banc de Spartel topographic high (W' Straits of Gibraltar) within the *GAP* study area.

### 6.5.1. Driftsediments and the influence of MOW in Al Arraiche Mud Volcano Field (W of the Moroccan margin)

(A. Foubert, D. Hebbeln)

The present sedimentation in the Gulf of Cadiz is strongly controlled by the Mediterranean Outflow Water, a strong current which has been active since the Pliocene, after the Mediterranean basin was flooded after the Messinian salinity crisis (Mougenot et al., 1986). Presently the MOW is a strong, warm (13°C) and saline (38 g $l^{-1}$) current which flows out of the Mediterranean below the Atlantic Waters. A current named the Atlantic inflow (Nelson et al., 1999) flows back from the Atlantic into the Mediterranean. When reaching the Gulf, the MOW is mainly deflected towards the north due to the Coriolis force. However, west of 06°20'W, it splits into two cores which flows along the seabed at water depths of 300 to 1500 m. The upper core is a geostrophic current which follows a northerly path, bending westwards along the Spanish and the Portuguese continental slopes at depths of 300-600 m. The lower core is an ageostrophic current and flow southwest-westwards from the Strait of Gibraltar. It divides into an intermediate core flowing between 550 and 900 m water depths and a deep core flowing between 900 and 1500 m water depths

. Probably this lower branch of the MOW influences also the upper part of the Moroccan margin on depths in between 500 and 900 m. The sediments on this part of the margin are probably partly shaped by the influence of the MOW, resulting in contouritic drift deposits. Large contourite drifts build-up and shaped by the MOW are already well-known along the Spanish and the Portuguese margins (Faugeres et al., 1985; Stow et al., 1986; Mulder et al., 2003).

***Operations and Sedimentology***

Three cores, localized on three different depths, are taken in the sediments W of the Moroccan margin (**Fig. 6.5.2.**). Core GeoB9064 is localized in the sediments W of Vernadsky Ridge and Renard Ridge at a depth of 702 m and provided an undisturbed record of muddy clayey sediments. Core GeoB9065 at a water depth of 507 m was taken in the sediments in between the two ridges and bears witness of the presence of some turbidites, probably originating from the two ridges and from the shelf. Core GeoB9066 is localized in the sediments S of MV Al Idrisi on a waterdepth of 376 m and is characterized by really coarse, compact material, probably corresponding with drift deposits. These cores will be analyzed on isotopic signature, foraminiferal associations, geochemical element composition (CORTEX), clay mineralogy, grain size variations and paleomagnetic intensity changes.

The two other gravity cores (**Fig.6.64**) were taken in the sediments in the neighbourhood of the presence of deepwater corals and carbonate mounds, one in the sediments in between some carbonate mounds on Pen Duick Escarpment (GeoB9068) and one in the sediments next to Pen Duick Escarpment (GeoB9069). The core on the Escarpment consists in the upper part of muddy sand with an abrupt change in colour and sediment composition to more clayey material on a depth of 2 m. The core next to the Escarpment consists of muddy clays with some turbidites.

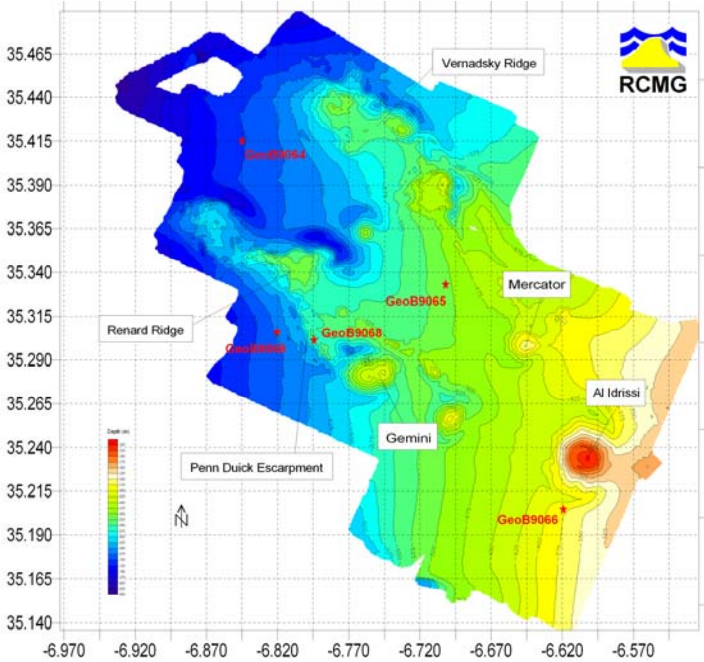


**Fig. 6.64.** Location of the cores in Al Arraiche MV field (W of Moroccan margin)

### 6.5.2. West Gibraltar Site

(M.-A. Gutscher, A. Kopf)

A bathymetric high in the western Straits of Gibraltar was investigated on December 15, 2003. It is located along the N70°E trending Gibraltar lineament, which controls the geometry of the strait of Gibraltar and appears to continue into the accretionary wedge to the WSW. This lineament has been proposed to be a dextral strike-slip fault, and the 5 x 10 km lozenge shaped high appears to be a pop-up formed in this context. This shoal (rising to 51 m water depth) was the target of a bathymetric survey in July 2003 by M.-A. Gutscher with R/V Suroit and the resulting high resolution bathymetric map was used as a basis for our investigations (**Fig. 6.65**).

The objectives were to obtain samples from this high, located mid-way between Inner Betic allochthonous units to the north and Inner Rif units to the south. An additional objective was to find evidence for paleobeach facies, as this shoal was a subaerially exposed island during the last glacial maximum. Dating of these facies can help determine the relative amounts of tectonic vs. eustatic subsidence for this location, and this has important implications for the assessment of the activity of the Gibraltar Arc system as a whole.

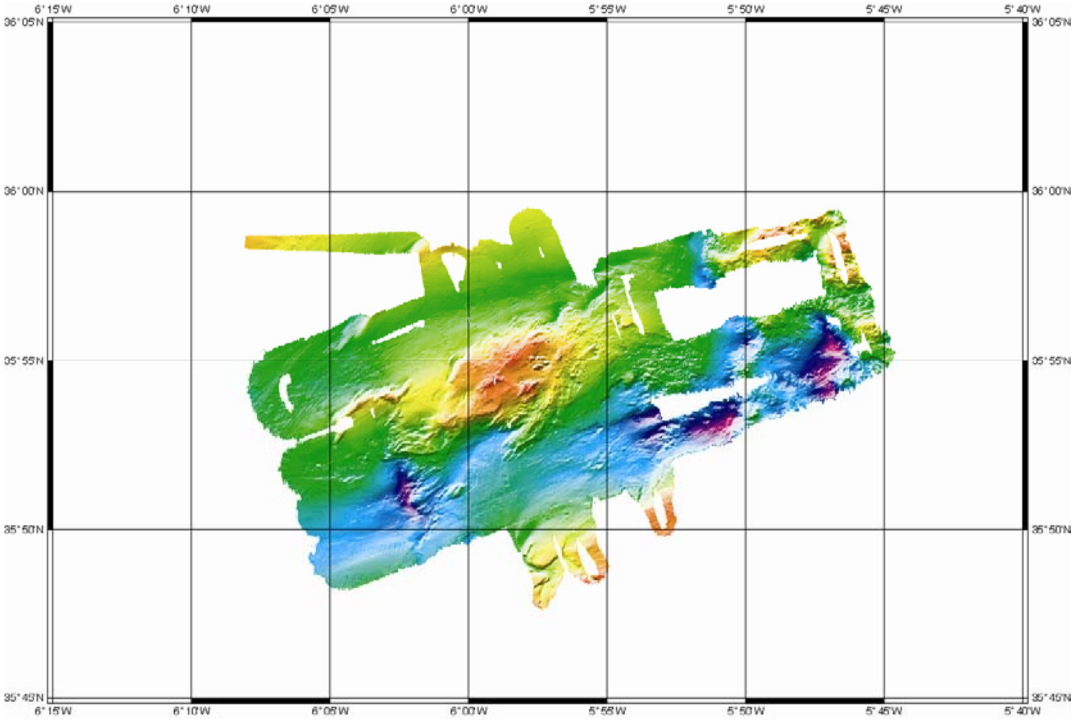


**Figure 6.65.** High resolution Simrad EM300 multibeam bathymetric map (unpublished data from R/V *Suroit*, courtesy of M.-A. Gutscher)

*Video Camera (OFOS) observations*

Track 1 began near the summit of the shoal at roughly 60 m water depth. The seafloor was very rugged, consisting of steeply dipping and highly fractured beds of hard bedrock. Bedding orientation appeared to be predominantly NW-SE, reflecting parallel bands seen in the bathymetric map. Deep clefts in the stone commonly cross-cut these layers and were oriented principally E-W to NE-SW. The summit region was in the photic zone and marked by abundant marine vegetation, including kelp up to 3 m in length (a sample attached to the OFOS was recovered). The track continued to the west, descending to a broad plateau (several km wide) at about 110 m water depth. Gravel, sand and cobbles at the lower edge of the plateau suggested erosional processes due to wave action, and thus a paleo-beach facies. The dive was interrupted to remove 2 large pieces of kelp obscuring the camera view.

Track 2 began at the northern edge of the plateau and followed the slope break to the SW. Finer-grained sands and gravels were observed on the plateau, becoming coarser grained at the slope break. Large clasts and blocks were observed near the slope break.

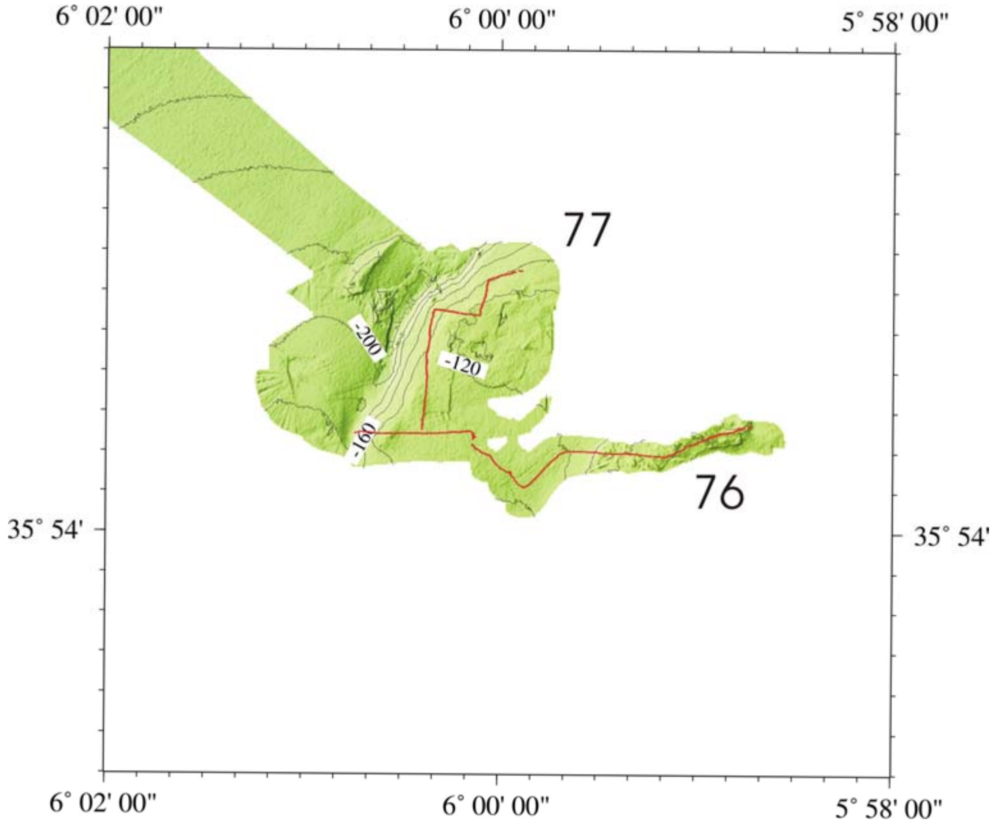


**Figure 6.66.** OFOS track across Banc de Spartel.

*TV grabs*

Three TV grabs were taken, one just above the slope break in a region with medium sized blocky rock fragments, one on the plateau with finer grained sediments and one just beneath the slope break with large rock slabs. For location, see **Figure 6.67**.

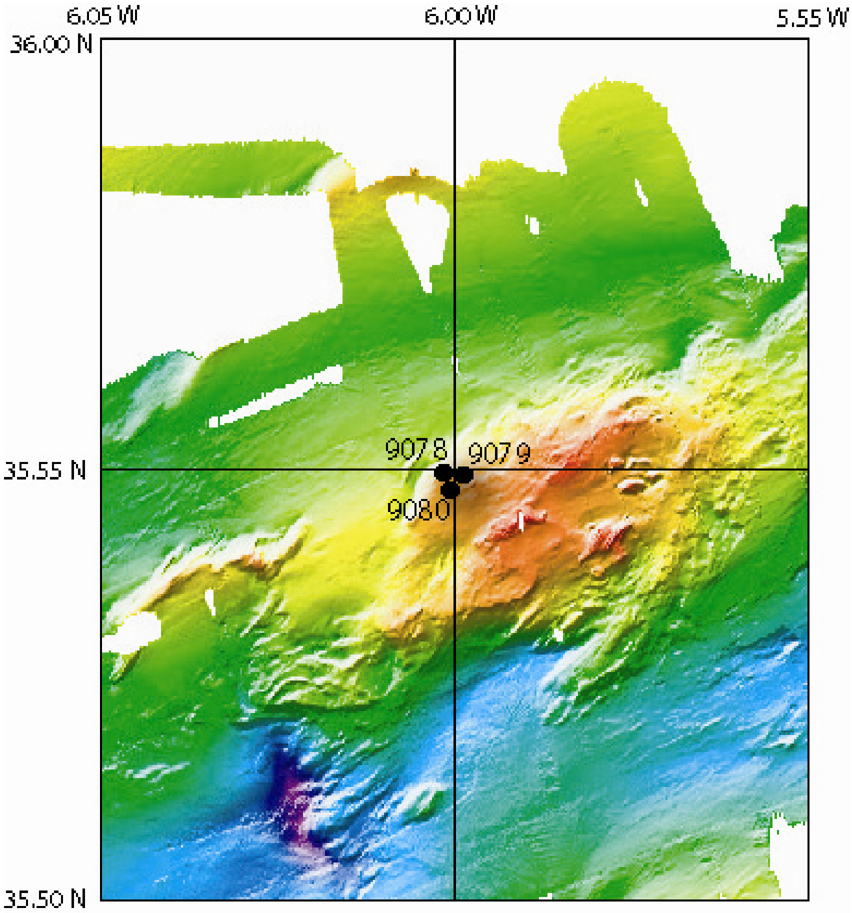


**Figure 6.67.** Detail of high resolution Simrad EM300 multibeam bathymetric map (unpublished data from R/V *Suroit*, courtesy of M.-A. Gutscher), as shown in **Fig. 6.65**. Positions of TV grabs are marked as black dots.

*TV grab 1: station GeoB 9078*

The first TV grab at the *Banc de Spartel* aimed for rocks and sediments juxtaposing the escarpment at approximately120 m water depth. Video footage from OFOS surveys indicates that this area near the edge of the plateau-like area of the western shoal comprises hard rocks, pebbles, fine sand, and possibly artifacts. The grab was closed at 113 m bsl and brought to deck. It recovered about a ton of material consisting of mainly hard rocks and pebbles in a bryozoa-sand matrix. The cobbles and rocks were largely carbonates (supposed beach-rock; see TV grab 3) and greenish clay- and siltstones. Some rocks show joints and veins, and appear to have been fragmented by tectonic forces. Specimens with white calcitic encrustment up to several millimeters thick have been found among the rocks recovered. Examples of the recovery are shown in **Figure 6.68**.

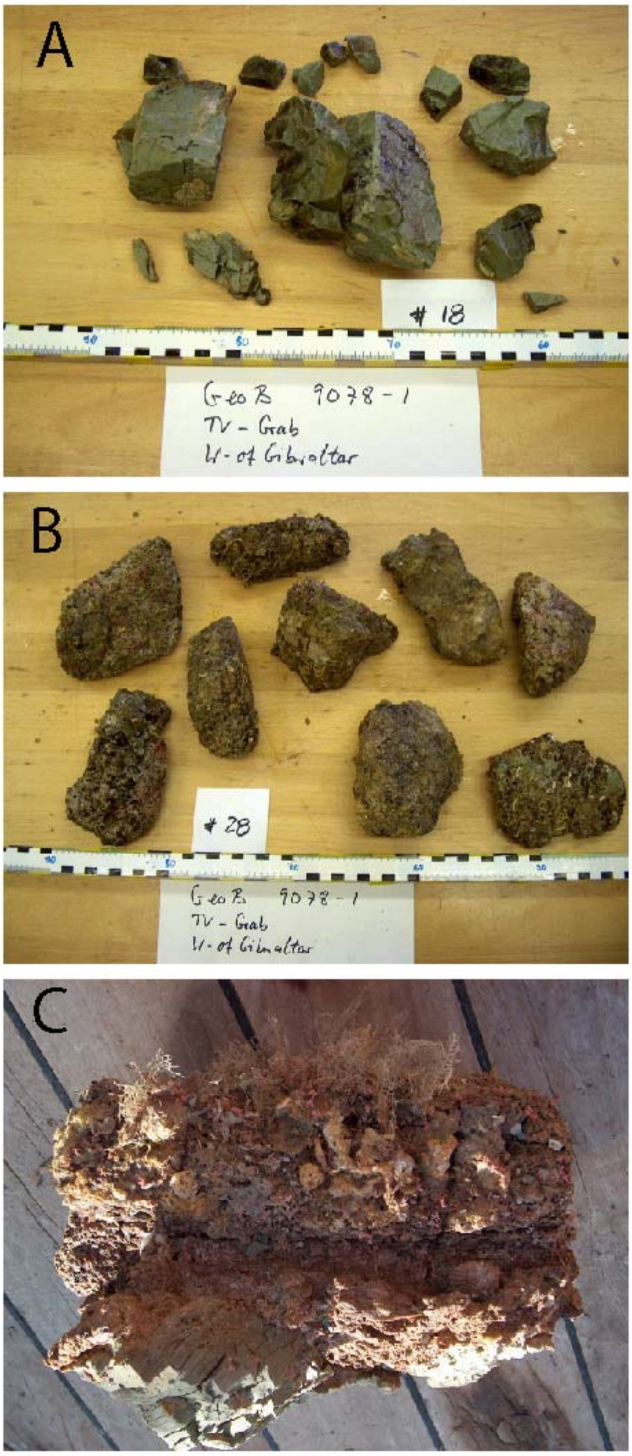


**Figure 6.68.** Rocks and pebbles recovered from station GeoB 9078. **a)** Green clayey siltstones; **b)** cobbles of a calcareous beach-rock; **c)** larger boulder (45 cm across) of beach rock grown on (the supposedly autochthonous) green clayey siltstones. See text.

*TV grab 2: station GeoB 9079*

The second grab was taken slightly east at a water depth of 116 mbsl (see **Fig. 6.67**). It aimed for the background sediment on the plateu-like area dominating the western part of the shoal. The operation was successful and gained a lot of fairly coarse-grained sands and fine gravels. Main components include carbonate, quartz, and bryozoa. Small amounts of organic-rich material have also been recovered, which may represent paleo-soils. Plant material and other biogenic debris (echinoderm fragments, annelida, foraminifera, etc.; see **Fig. 6.69**) was also frequently found in the sandy matrix.


**Figure 6.69.** Sandy sediment recovered from station GeoB 9079.
**a)** length of x-axis of photograph is ca. 60 mm; **b)** length of x-axis of photograph is ca. 10 mm.

*TV grab 3: station GeoB 9080*

The third grab was lowered right at the edge of the escarpment separating the plateau of the shoal from the surrounding seafloor. From OFOS surveying it appeared as if the escarpment is built of massive carbonate rocks. However, we managed to recover three large pieces of these rocks which were previously been broken off the platform due to tectonic movements. Material was taken in 125 meters of water depth (**Fig. 6.67**). The porous carbonates are overgrown with various plants and microorganisms, as can be seen on the largest rock we got on deck. It is about 70 cm long, 40 cm wide, and 25-30 cm thick (**Fig. 6.70**). The carbonate has incorporated mollusc shells, mud clasts, and other organisms and rock fragments. It is tentatively interpreted as a beach rock deposit (see above). Dating is planned as a first post-cruise study.

**Figure 6.70.** One of a total of three big pieces of beach rock recovered from station GeoB 9080. See text.

All material recovered was tentatively described and archived. No geochemical or microbiological work was carried out on the samples. This will be attempted post cruise.

## 7. References

Argus, D.F., Gordon, R.G., Demets, C., Stein, S., 1989. Closure of the Africa-Eurasia-North America plate motion circuit and tectonics of the Gloria fault, J. Geophys. Res. 94, 5585-5602.

Baptista, M.A., Heitor, S., Miranda, J.M., Miranda P.M.A., and Mendes Victor, L., 1998. The 1755 Lisbon; Evaluation of the tsunami parameters, J. Geodynamics 25, 143-157.

Baraza, J., Ercilla, G., 1996. Gas-charged sediments and large pockmark-like features in the Gulf of Cadiz (SW Spain). Mar. Petrol. Geol. 13, 253-261.

Battista, B.M., Lowrie, A., Makarov, V., and Somoza, L., 2000. Lateral tectonics in the Gulf of Mexico, Gulf of Cadiz, and the Middle America Trench; impacts on hydrocarbon accumulations. Proc. AAPG, 2000, p.11

Berastegui, X., Banks, C.J., Puig, C., Taberner, C., Waltham, D., and Fernandez, M., 1998. Lateral diapiric emplacement of Triassic evaporites at the southern margin of the Guadalquivir Basin, Spain. Proc. 23rd EGS meeting; Annales Geophysicae,16 (supplement), p.59.

Blanco, M.J., and Spakman, W., 1993. The P-wave velocity structure of the mantle below the Iberian Peninsula: Evidence for a subducted lithosphere beneath southern Spain: Tectonophysics, 221, 13–34.

Blankenship, C.L., 1992. Structure and palaeogeography of the External Betic Cordillera, southern Spain. Mar. Petrol. Geol. 9, 256-264.

Blum, P., 1997. Physical properties handbook: A guide to shipboard measurements of physical properties of deep-sea cores. *ODP Technical Note*, 26.

Boetius, A., Ravenschlag, K., Schubert, C., Rickert, D., Widdel, F., Gieseke, A., Amann, R., Jørgensen, B.B., Witte, U., Pfannkuche, O., (2000) A marine microbial consortium apparently mediating anaerobic methane of oxidation. *Nature*, 407, 623-626.#

Brown, K.M., and Westbrook, G.K., 1988. Mud diapirism and subcretion in the Barbados Ridge Complex. *Tectonics*, 7: 613-640

Brown, K.M., 1990. The nature and hydrogeologic significance of mud diapirs and diatremes for accretionary systems. *J. Geophys. Res*., 95, 8969-8982

BS 1377, 1991. Methods of test for soils for civil engineering purposes. *Brit. Stand. Inst.*

Buforn, E., Udias, A., and Madariaga, R., 1991, Intermediate and deep earthquakes in Spain, Pure Appl. Geophys. 136, p. 375-393.

Bullard, E.C., 1939. Heat flow is South Africa, Proc. R. Soc. London Series A, 173, 474-503.

Calvert, A., Sandvol, E., Seber, D., Barazangi, M., Roecker, S., Mourabit, T., Vidal, F., Alguacil, G., and Jabour, N., 2000, Geodynamic evolution of the lithosphere and upper mantle beneath the Alboran region of the western Mediterranean: Constraints from travel time tomography: Journal of Geophysical Research, 105, 10,871–10,898.

Camerlenghi, A., Cita, M.B., Della Vedova, B., Fusi, N., Mirabile, L., Pellis, G., 1995. Geophysical evidence of mud diapirism on the Mediterreanean Ridge accretionary complex. *Mar. Geophys. Res*., 17: 115-141

Casado, C., Sanz de Galdeano, C., Palacios, S., and Romero, J., 2001. The structure of the Alboran Sea: an interpretation from seismological and geological data. Tectonophysics 338, 79-95.

Cragg, B. A., Parkes, R. J., Fry, J. C., Weightman, A. J., Rochelle, P. A., Maxwell, J. R., Kastner, M., Hovland, M., Whiticar, M. J., and Sample, J. C. (1995). The impact of fluid and gas venting on bacterial populations and processes in sediments from the Cascadia Margin accretionary system (sites 888-892) and the geochemical consequences, *Proceedings of the Ocean Drilling Program, Scientific Results*, Vol. 146 (Pt. 1), 399-410.

Diaz del Rio, V., Somoza, L., Martinez, F.J., Mata, M.P., Delgado, A., Hernandez-Molina, F.J., Lunar, R., Martin-Rubi, J.A., Maestro, A. Fernandez-Puga, M.C., Leon, R., Llave, E., Medialdea, T., and Vazquez, J.T., 2003. Vast fields of hydrocarbon-derived carbonate chimneys related to the accretionary wedge/ olistostrome of the Gulf of Cadiz. Marine Geology, 195, 177-200.

Docherty, C., and Banda, E., 1995. Evidence for the eastward migration of the Alboran Sea based on regional subsidence analysis: A case for basin formation by delamination of the subcrustal lithosphere?. Tectonics 14, 804-818.

Dominguez, S., Malavieille, J., and Lallemand, S.E., 2000. Deformation of margins in response to seamount subduction: Insights from sandbox experiments. Tectonics, v. 19, p. 182-196.

Duggen, S., Hoernle, K., van den Bogaard, P., Ruepke, L., Phipps-Morgan, J., 2003. Deep roots of the Messinian Salinity Crisis. Nature 422, 602-606.

Duggen, S., Hoernle, K., van den Bogaard, P., Harris, C., 2004. Magmatic evolution of the Alboran Region: The role of subduction in forming the western Mediterranean and causing the Messinian Salinity Crisis. Earth Planet. Sci. Lett. (in press).

Eldholm, O., Sundvor, E., Vogt, P.R., Hjelstuen, B.O., Crane, K., Nilsen, A.K., Gladczenko, T.P., 1999. SW Barents sea continental
margin heat flow and Hakon Mosby mud volcano. Geo-Mar. Lett. 19, 29– 37.

Faccenna, C., Becker, T.W., Pio Lucente, F., Jolivet, L., and Rosetti, F., 2001. History of subduction and back-arc extension in the Central Mediterranean. Geophysical Journal International 145, 809-820.

Faugeres, J.C., Frappa, M., Gonthier, E. de-Resseguier, A., and Stow, D.A.V., 1985. Modele et facies de type contourite a la surface d'une ride sedimentaire edifiee par des courants issus de la veine d'eau mediterraneenne (ride du Faro, Golfe de Cadix). Bull. Soc. Geol. France, 1: 35-47.

Galindo-Zaldívar, J., A. Maldonado, and A.A. Schreider, 2003.Gorringe Ridge gravity and magnetic anomalies are compatible with thrusting at a crustal scale, *Geophys. J. Int., 153*, 586-594.

Gardner, J.M., 2001, Mud volcanoes revealed and sampled on the Western Moroccan continental margin: Geophysical Research Letters, 28, 339–342.

Gieskes, J. M., Garno, T., and Brumsack, H., 1991. Chemical methods for interstitial water analysis aboard Joides Resolution. Ocean Drilling Program, Texas A & M Univ.

Gràcia, E., Dañobeitia, J.J., Vergés, J., an Bartolomé, R., 2003a. Crustal architecture and tectonic evolution of the Gulf of Cadiz (SW Iberian Margin) at the convergence of the Eurasian and African plates. *Tectonics*, 22 (4): 1033-1057

Gracia, E., Danobeitia, J.J., Verges, J., PARSIFAL Team, 2003b. Mapping active faults offshore Portugal (36°N-38°N): Implications for seismic hazard assessment along the southwest Iberian margin. Geology 31, 83-86.

Grasshoff, K., Ehrhardt, M., and Kremling, K., 1997. Methods of seawater analysis. Verlag Chemie.

Grevemeyer I., J.L. Diaz-Naveas C.R. Ranero, H. Villinger, and Ocean Drilling Program Leg 202 Scientific Party, 2003. Heat flow over the descending Nazca plate in Central Chile, 32°S to 41°S: evidence from ODP Leg 202 and the occurrence of natural gas hydrates, *Earth Planet. Sci. Lett. 213,* 285-298.

Grevemeyer I., A.J. Kopf, N. Fekete, N. Kaul, H.W. Villinger, M. Heesemann, K. Wallmann, V. Spiesz, H.-H. Gennerich, M. Müller, W. Weinrebe, 2004. Fluid flow through active mud dome Mound Culebra offshore Nicoya Peninsula, Costa Rica: evidence from heat flow surveying. Mar. Geol., 207, 145-157.

Grimison, N.L. and Chen, W.P., 1986. The Azores-Gibraltar Plate Boundary: Focal Mechanisms, Dephts of Earthquakes and their Tectonic Implications. *Journal of Geophysical Research*, 91, B2, 2029-2047.

Gutscher, M.-A., Malod, J., Rehault, J.-P., Contrucci, I., Klingelhoefer, F., Mendes-Victor, L., Spakman, W., 2002. Evidence for active subduction beneath Gibraltar. Geology 30, 1071-1074.

Gutscher, M.-A., Baptista, M.A., Miranda, J.M., 2004. The Gibraltar Arc seismogenic zone (part 2): constraints on a shallow east dipping fault plane source for the 1755 Lisbon earthquake provided by tsunami modeling and seismic intensity. Tectonophysics, in press.

Hampton, M.A., H.J. Lee, and J. Locat, 1996. Submarine landslides, Rev. Geophys., 34, 33-59.

Hartmann, A, and H. Villinger (2002) Inversion of marine heat flow mwasurements by expansion of the temperature decay function, Geophys. J. Int., 148, 628-636.

Hedberg, H., 1974. Relation of methane generation to undercompacted shales, shale diapirs and mud volcanoes. *AAPG Bull*., 58: 661-673

Henry, P., Le Pichon, X., Lallemant, S., Lance, S., Martin, J. B., Foucher, J.-P., Fiala-Médioni, A., Rostek, F., Guilhaumou, N., Pranal, V., and Castrec, M., 1996. Fluid flow in and around a mud volcano field seaward of the Barbados accretionary wedge: Results from Manon cruise. *Journal of Geophysical Research 101(B9*), 20297-20323.

Hensen C., Zabel M., Pfeifer K., Schwenk T., Kasten S., Riedinger N., Schulz H. D., and Boetius A., 2003. Control of sulfate pore water profiles by sedimentary events and the significance of anaerobic oxidation of methane for the burial of sulfur in marine sediments. Geochim. Cosmochim. Acta 67(14), 2631-2647.

Hernandez-Molina, J., Llave, E., Somoza, L., Renandez-Puga, M., Maestro, A., Leon, R., Medialdea, T., Barnolas, A., Garcia, M., Diaz del Rio, V., Fernandez-Sala, L.M., Vazquez, J.T., Lobo, F., Alveirinho-Dias, J.M., Rodero, J., Gardner, J., 2003. Looking for clues to paleoceanographic imprints: A diagnosis of the Gulf of Cadiz contourite depositional systems. Geology, v. 31, p.19-22.

Higgins, G.E., and Saunders, J.B., 1974. Mud volcanoes – Their nature and origin. *Verhandlungen der Naturforschenden Gesellschaft Basel*, 84: 101–152

Hoppie, B.W., et al., 1994. Natural gamma-ray measurements on ODP cores; introduction to procedures with examples from Leg 150. In: Proc. Ocean Drilling Program, Initial reports, 150: 63-127

Hornibrook, E. R. C., Longstaffe, F. J., and Fyfe, W. S., 1997. Spatial distribution of microbial methane production pathways in temperate zone wetland soils: stable carbon and hydrogen isotope evidence, *Geochimica et Cosmochimica Acta*, Vol. 61, No. 4, 745-753.

Hutchinson, I., 1985. The effects of sedimentation and compaction on oceanic heat flow. Geophys. J. Royal Astron. Soc., 82, 439-459.

Ivanenkov, V. N. and Lyakhin, Y. I., 1978. Determination of total alkalinity in seawater. In: Bordovsky, O.K. and Ivenenkov, V. N. (eds.): Methods of hydrochemical investigations in the ocean, Nauka Publ. House, Moscow, 110-114 (in Russian).

Jimenez-Munt, I., Fernandez, M., Torne, M., Bird, P., 2001. The transition from linear to diffuse plate boundary in the Azores-Gibraltar region. Earth Planet. Sci. Lett. 192, 175-189.

Johnston, A., 1996. Seismic moment assessment of earthquakes in stable continental regions – III. New Madrid, 1811-1812, Charleston 1886 and Lisbon 1755. Geophys. J. Int. 126, 314-344.

Kenyon, N.H., Ivanov, M.K., Akhmetzhanov, A.M., Akhmanov, G.G., 2000. Multidisciplinary Study of Geological Processes on the North East Atlantic and Western Mediterranean Margins. IOC Technical Series No. 56, UNESCO, 2000

Kenyon, N.H., Ivanov, M.K., Akhmetzhanov, A.M., Akhmanov, G.G., 2001. Interdisciplinary Approaches to Geoscience on the North East Atlantic Margin and Mid-Atlantic Ridge. IOC Technical Series No. 60, UNESCO, 2001

Kenyon, N.H., Ivanov, M.K., Akhmetzhanov, A.M., Akhmanov, G.G., 2002. Geological Processes in the Mediterranean and Black Seas and North East Atlantic. IOC Technical Series No. 62, UNESCO, 2002

Kopf, A., Klaeschen, D. and Mascle, J., 2001. Extreme efficiency of mud volcanism in dewatering accretionary prisms. Earth and Planetary Science Letters 189, 295-313.

Kopf, A.J., 2002. Significance of mud volcanism. *Reviews of Geophysics*, 40/2, 52pp. [DOI 10.1029/2000RG000093]

Kopf., A.J., 2003. Important global impact of methane degassing through mud volcanoes on past and present Earth climate. *Int. J. Earth Sciences 92/5: 806-816*

Lavrushin, V.U., Polyak, B.G., Prasolov, R.M., and Kamenskii, I.L., 1996. Sources of material in mud volcano products (based on isotopic, hydrochemical, and geological data). *Lithology Min. Resources,* 31/6: 557-578

Lonergan, L. and White, N., 1997. Origin of the Betic-Rif mountain belt. Tectonics 16, 504-522.

Lovley, D. R. and Goodwin, S. (1988). Hydrogen concentrations as an indicator of the predominant terminal electron-accepting reactions in aquatic sediments, *Geochimica et Cosmochimica Acta*, Vol. 52, 2993-3003.

Lowrie, A., Battista, B., Somoza, L., Moffet, S., and Makarov, V., 1999. Hydrocarbon accumulations and continental margin tectonics; lateral motions of the Gulf of Mexico, Gulf of Cadiz, and the Middle America Trench. NOGS Log, 39, 9.

Martinez-Solares, J.M., Lopez A., and Mezcua, J., 1979. Isoseismal map of the 1755 Lisbon earthquake obtained from Spanish data. Tectonophysics 53, 301-313.

Mascle, J., Huguen, C., Benkhelil, J., Chamot-Rooke, N. Chaumillon, E., Foucher, J.-P., Griboulard, R., Kopf, A., Lamarche, G., Volkonskaia, A., Woodside, J., and Zitter, T., 1999. Images may show start of European-African Plate collision. EOS Trans. AGU, 80/37: 421-428.

Mazurenko, L. L., Soloviev, V. A., Belenkaya, I., Ivanov, M. K., and Pinheiro, L. M. (2002). Mud volcano gas hydrates in the Gulf of Cadiz, *Terra Nova* 14, 321-329.

McAullife, C. (1971). GC determination of solutes by multiple phase equilibration, *Chem. Tech.* 1, 46-51.

Maldonado, A., L. Somoza, and L. Pallare´s, 1999. The Betic orogen and the Iberian-African boundary in the Gulf of Cadiz: Geological evolution (central North Atlantic), Mar. Geol., 155, 9 – 43.

Molnar, P., and P. England, Temperature, heat flux, and frictional stress near major thrust faults, *J. Geophys. Res.*, 95, 4833-4856, 1990.

Morales, J., Serrano, I., Jabaloy, A., Galindo-Saldivar, J., Zhao, D., Torcal, F., Vidal, F., and Gonzales-Lodeiro, F., 1999. Active continental subduction beneath the Betic Cordillera and Alboran Sea. Geology, 27, 735–738.

Mougenot, D., Vanney, J.-R., Mauret, A., Kidd, R., 1986. Les montagnes sous-marines de la marge continentale nord-portugaise: morphologie et e volution structurale. Bull. Soc. Geol. Fr. 2, 401-412.

Mulder, T., and Cochonat, P., 1996. Classification of offshore mass movements. J. Sed. Res., 66, 43-57.

Mulder, T., Voisset, M., Lecroart, P., Le Drezen, E., Gonthier, E., Hanquiez, V. Faugeres, J.-C., Habgood, E., Hernandez-Molina, F.J., Estrada, F., Llave-Barranco, E., Poirier, D., Gorini, C., Fuchey, Y., Volcker, A., Freitas, P., Lobo Sanchez, F., Fernandez, L. M., Kenyon, N., and Morel, J., 2003. The Gulf of Cadiz: an unstable giant contouritic levee, Geo-Marine Letters , v. 23, p. 7-18

Negredo, A., Bird, P., Sanz de Galdeano, C., and Buforn, E., 2002. Neotectonic modeling of the Ibero-Maghrebian region. Journal Geophys. Res., 107, 11,229.

Nelson, C. H., and A. Maldonado, 1999. The Cadiz margin study off Spain: An introduction, Mar. Geol., 155, 3 – 9.

Niewöhner, C., Hensen, C., Kasten, S., Zabel, M., and Schulz, H. D., 1998. Deep sulfate reduction completely mediated by anaerobic methane oxidation in sediments of the upwelling area off Namibia. *Geochim. Cosmochim. Acta* 62 (3), 455-464.

Perconig, E., 1962. Sur la constitution geologique de l'Andalousie occidentale, en particulier du bassin du Guadalquivir (Espagne meridionale). Fallot Memorial Vol., Soc. Geol. France, 1: 229-256.

Pfender, M., and H. Villinger, 2002. Miniaturized data logger for deep sea sediment temperature measurements, Mar. Geol., 186, 557-570.

Pinheiro, L.M., Ivanov, M.K., Sautkin, A., Akhmanov, G., Magalhaes, V.H., Volkonskaya, A., Monteiro, J.H., Somoza, L ., Gardner, J., Hamouni, N., Cunha, M.R., 2003. Mud volcanism in the Gulf of Cadiz: results from the TTR-10 cruise. Marine Geology 3269, 1-21.

Platt, J.P., and Vissers, R.L.M., 1989. Extensional collapse of thickened continental lithosphere: A working hy-pothesis for the Alboran Sea and Gibraltar arc: Geology, 17, 540–543.

Rehault, J.-P., Boillot, G., and Mauffret, A., 1985. The western Mediterranean Basin, in Stanley, D.J., and Wezel, F.C., eds., Geological Evolution of the Mediterranean Basin, Springer, Berlin, p. 101-129.

Royden, L.H., 1993. Evolution of retreating subduction boundaries formed during continental collision. Tectonics, v. 12, p. 629-638.

Sanz de Galdeano, C., 1990. Geologic evolution of the Betic Cordilleras in the Western Mediterranean, Miocene to present, Tectonophysics, 172, 107 – 119.

Sartori, R., Torelli, L., Zitellini, N., Peis, D., Lodolo, E., 1994. Eastern segment of the Azores-Gibraltar line (central-eastern Atlantic): An oceanic plate boundary with diffuse compressional deformation. Geology 22, 555-558.

Seber, D., M. Barazangi, A. Ibenbrahim, and A. Demnati, 2996.Geophysical evidence for lithospheric delamination beneath the Alboran Sea and Rif-Betic mountains, Nature, 379, 785 – 790.

Somoza, L., A. Maestro, and A. Lowrie, 2001. Allochthonous blocks as hydrocarbons traps in the Gulf of Cadiz. Proc. 1999 Offshore Technology Conference, Houston, Tex., 1999.

Somoza, L., Diaz-del-Rio, V., Leon, R., Ivanov, M.K., Fernandez-Puga, M.C., Lobato, A., Maestro, A., Hernandez-Molina, F.J., Gardner, J.M., Rodero, J., Pinheiro, L.M., Vasquez, J.T., Medialdea, T., Fernandez-Salas, L.M., 2003. Seabed morphology and hydrocarbon seepage in the the Gulf of Cadiz mudvolcano area:imagery of multibeam data and ultra-high resolution data. Mar.Geology, 195, 153-176.

Spiess, V., 1993. Digitale Sedimenttomographie. Neue Wege zu einer hochauflösenden Akustostratigraphie. Berichgte aus dem FB Geowissenschaften der Univ. Bremen, 35: 199pp.

Stich, D., Ammon, C.J., Morales, J., 2003. Moment-tensor solutions for small and moderate earthquakes in the Ibero-Maghreb region. J. Geophys. Res. 108, 2148.

Stow, D.A.V., Faugeres, J.C., and Gonthier, E., 1986.Facies distribution and textural variation in Faro Drift contourites; velocity fluctuation and drift growth. Marine Geology, 72, 71-100.

Terrinha, P., Pinheiro, L.M., Henriet, J.-P., Matia, L., Ivanov, A.K., Monteiro, J.H., Akhmetzhanov, A., Volkonskaya, Cunha, M.R., Shaskin, P., Rovere, M., 2003. Tsunamigenic-seismogenic structures, neotectonics, sedimentary processes and slope instability on the Southwest Portugese Margin. Marine Geology 3266, 1-19.

Thiebot, E., and Gutscher, M.-A., 2004. The Gibraltar Arc seismogenic zone (part1): constraints on a shallow east dipping fault plane source for the 1755 Lisbon earthquake provided by seismic data, gravity and thermal modeling. Tectonophysics, in press.

Tobias, H. J. and Brenna, J. T. (1997). On-line pyrolysis as a limitless reduction source for high-precision isotopic analysis of organic-derived hydrogen, *Analytical Chemistry* 69, 3148-3152.

Torelli, L., R. Sartori, and N. Zitellini, 1997. The giant chaotic body in the Atlantic Ocean off Gibraltar: new results from deep seismic reflection survey, *Mar. Petrol. Geol., 14*, 125-138.

Tortella, D., Torne, M, and Perez-Estaun, A., 1997. Geodynamic evolution of the eastern segment of the Azores-Gibraltar Zone: the Gorringe Bank and Gulf of Cadiz region, Marine Geophys. Res. 19, 211-230.

Urgeles, R., Masson, D.G., Canals, M., Watts, A.B., and Le Bas, T., 1999. Recurrent large-scale landsliding on the west flank of La Palma, Canary Islands. J. Geophys. Res. 104, 25,331-25,348.

Watts, A.B., Platt, J.P., and Buhl, P., 1993. Tectonic evolution of the Alboran Sea Basin. Basin Res. 5, 153-177.

Wellsbury, P., Herbert, R. A., and Parkes, R. J. (1996). Bacterial activity and production in near surface estuarine and freshwater sediments, *FEMS Microbiology Ecology* 19, 203-214.

Zeck, H.P., 1997, Mantle peridotites outlining the Gibraltar Arc: Centrifugal extensional allocthons derived from the earlier Alpine, westward subducted nappe pile. Tectonophysics, 281, 195–207.

Zitellini, N., L. Mendes-Victor, D. Co´ rdoba, J. J. Danobeitia, R. Nicolich, G. Pellis, A. Ribeiro, R. Sartori, L. Torelli, and BIGSETS Team, 2001. Source of 1755 Lisbon earthquake and tsunami investigated. Eos (Transactions, American Geophysical Union) 82, 285-291.

Zitillini, N., F. Chierici, R. Sartori, and L. Torelli, The tectonic source of the 1755 Lisbon earthquake and tsunami, Ann. Geofisica, 42, 49-55, 1999.

## 8. Appendix

### Appendix 8.1. Station list SO-175

| SO175 | | | | | | | | | | | | | | | |
|---|---|---|---|---|---|---|---|---|---|---|---|---|---|---|---|
| | | | Time (UTC) | | | | | Begin / on seafloor | | End / off seafloor | | | | | |
| Date | St. No. | Instrument | Begin | Start Sci. Program | End Sci. Program | End | Durati h:mm | Latitude N° | Longitude W° | Latitude N° | Longitude W° | Water depth (m) | Recovery x | Supervisor | Area |
| 27.11.2003 | GeoB9001-1 | CTD | 08:35 | 08:35 | 09:11 | 09:57 | | 36:52.79 | 10:05.07 | 0,025611 | 10:05.09 | 3560 | max = 2000 m, Sound-velocity profile | | Marques de Pombal - Fault |
| 27.11.2003 | GeoB9002-1 | HS | 10:13 | 10:13 | 10:22 | 10:22 | | 36:52.76 | 10:04.89 | 36:53.70 | 10:05.60 | | v=5 kn | Sahling | Marques de Pombal - Fault |
| 27.11.2003 | GeoB9002-2 | OFOS | 10:46 | 11:54 | 13:01 | 14:17 | | 36:52.78 | 10:04.96 | 36:53.01 | 10:05.63 | 3910 | | Sahling | Marques de Pombal - Fault |
| 27.11.2003 | GeoB9003-1 | HS | 15:03 | 15:03 | 15:09 | 15:09 | | 36:50.50 | 09:57.22 | 36:50.35 | 09:57.80 | 2688 | v=5 kn | Sahling | Marques de Pombal - Headwall |
| 27.11.2003 | GeoB9003-2 | OFOS | 15:42 | 16:28 | 18:10 | 19:03 | | 36:50.33 | 09:57.79 | 36:50.17 | 09:50.30 | 2730 | | Sahling | Marques de Pombal - Headwall |
| 27.11.2003 | GeoB9004-1 | HF | 20:11 | 21:02 | 11:38 | n.d. 12:52:00 PM | | 36:52.98 | 09:54.73 | 36:57.05 | 10:05.68 | 2500 | 11 Profiles | Grevemeye | Marques de Pombal |
| 28.11.2003 | GeoB9005-1 | TV-MUC | 13:45 | 15:10 | 15:14 | 16:52 | | 37:00.94 | 10:10.89 | 37:00.96 | 10:10.91 | 3928 | 4 cores, 26-36 cm | Hebbeln | Marques de Pombal |
| 28.11.2003 | GeoB9006-1 | GC + MTL | 17:42 | 18:58 | 18:59 | 20:20 | | 36:54.99 | 10:05.55 | 36:54.99 | 10:05.55 | 3926 | 4.3 m | Hebbeln | Marques de Pombal |
| 29.11.2003 | GeoB9007-1 | HS/PS | 21:45 | 21:45 | n.d. 8:38 | n.d. 8:38:00 AM | | 37:00.96 | 10:10.92 | 36:50.00 | 09:59.56 | | v=6 kn, 5 Profiles | Gutscher | Marques de Pombal |
| 29.11.2003 | GeoB9008-1 | TV-MUC | 09:02 | 10:02 | 10:09 | 11:10 | | 36:50.29 | 09:58.54 | 36:50.29 | 09:58.56 | 2708 | 4 cores, 17 cm | Hensen | Marques de Pombal |
| 29.11.2003 | GeoB9008-2 | GC + MTL | 11:37 | 12:24 | 12:24 | 13:43 | | 36:50.27 | 09:58.54 | 36:50.27 | 09:58.54 | 2708 | 2.68 m | Hebbeln | Marques de Pombal |
| 29.11.2003 | GeoB9009-1 | HF | 20:14 | 21:28 | 06:02 | 07:22 | | 35:56.09 | 09:22.20 | 35:51.58 | 09:18.58 | 4268 | 6 temperature profiles | Kaul | Deformation front |
| 30.11.2003 | GeoB9009-2 | HS/PS | 08:32 | 08:32 | 10:30 | 10:30 | | 35:42.00 | 09:12.00 | 35:46.83 | 09:31.84 | | v=12 kn | Gutscher | Deformation front |
| 30.11.2003 | GeoB9010-1 | GC + MTL | 10:35 | 11:45 | 11:45 | 13:13 | | 35:47.00 | 09:32.01 | 35:47.00 | 09:32.01 | 4376 | 2.32 m | Hebbeln | Deformation front |
| 30.11.2003 | GeoB9011-1 | HS/PS | 18:04 | 18:04 | 23:52 | 23:52 | | 36:01.00 | 8:22.00 | 36:12.00 | 07:55.00 | | v=8 kn | Gutscher | Transit |
| 01.12.2003 | GeoB9012-1 | OFOS | 00:31 | 01:18 | 06:44 | 08:40 | | 36:9.52 | 7:59.959 | 36:07.75 | 8:00.86 | 1317 | | Sahling | Lolita MV |
| 01.12.2003 | GeoB9013 | OFOS | 12:13 | 12:36 | 13:59 | 14:22 | | 36:36.56 | 7:47.13 | 36:35.59 | 7:46.74 | 763 | | Sahling | leaky faults |
| 01.12.2003 | GeoB9014-1 | TV-MUC | 14:59 | 15:21 | 15:26 | 15:55 | | 36:35.81 | 7:46.82 | 36:35.81 | 7:46.82 | 716 | 4 cores , max depth 33cm | Kopf | leaky faults |
| 01.12.2003 | GeoB9014-2 | GC | 14:59 | | | 15:55 | | 36:35.81 | 7:46.82 | 36:35.81 | 7:46.82 | 758 | 1.44 m | Hebbeln | leaky faults |
| 01.12.2003 | GeoB9015 | GC | 16:13 | 16:17 | 16:51 | 17:22 | | 36:35.81 | 7:46.81 | 36:35.81 | 7:46.80 | 769 | | Hebbeln | |
| 01.12.2003 | GeoB9016 | OFOS | 22:02 | 22:19 | 02:11 | 02:35 | | 36:11.86 | 7:17.52 | 36:11.06 | 7:19.95 | 760 | | Sahling | Hesperides MV |
| 02.12.2003 | GeoB9017 | OFOS | 03:05 | 03:20 | 07:31 | 08:00 | | 36:12.05 | 7:18.36 | 36:09.93 | 07:18.91 | 819 | | Bueckmann | Hesperides MV |
| 02.12.2003 | GeoB9018 | GC | 08:30 | 08:45 | 08:45 | 09:05 | | 36:10.98 | 7:18.37 | 36:10.98 | 7:18.37 | 702 | 3.47m | Hebbeln | Hesperides MV |
| 02.12.2003 | GeoB9019 | GC | 09:30 | 09:48 | 09:48 | 10:05 | | 36:11.18 | 7:19.15 | 36:11.18 | 7:19.15 | 767 | 1.62m | Hebbeln | Hesperides MV |
| 02.12.2003 | GeoB9020 | GC | 10:40 | 10:56 | 10:56 | 11:21 | | 36:11.16 | 7:19.29 | 36:11.16 | 7:19.29 | 730 | 0.19m | Hebbeln | Hesperides MV |
| 02.12.2003 | GeoB9021-1 | GC | 11:53 | 12:12 | 12:12 | 12:45 | | 36:10.99 | 7:18.38 | 36:10.99 | 7:18.38 | 701 | 3.78m | Hebbeln | Hesperides MV |
| 02.12.2003 | GeoB9021-2 | INNGAS | | | | | | | | | | | Gerätetest | Kaul | Hesperides MV |
| 02.12.2003 | GeoB9022 | TV-G | 13:05 | 13:39 | 14:25 | 15:00 | | 36:10.94 | 7:18.37 | 36:10.89 | 07:18.35 | 676 | corals | Brueckman | Hesperides MV |
| 02.12.2003 | GeoB9023 | TV-G | 15:40 | 16:00 | 16:12 | 16:40 | | 36:10.80 | 7:18.35 | 36:10.80 | 07:18.35 | 761 | chimneys | Brueckman | Hesperides MV |
| 02.12.2003 | GeoB9024 | TV-G | 16:52 | 17:15 | 17:57 | 18:42 | | 36:11.34 | 7:18.45 | 36:11.42 | 7:18.44 | 727 | crusts | Brueckman | Hesperides MV |
| 02.12.2003 | GeoB9025 | HF | 19:07 | 19:35 | n.d 01:44 | n.d. 02:06 | | 36:09.78 | 7:19.32 | 36:11.81 | 7:18.11 | 1034 | 10 temperatur profiles | Grevemeyer | |
| 02.12.2003 | GeoB9026 | CTD | 16:32 | 16:34 | 16:53 | 17:19 | | 36:03.99 | 7:22.02 | 36:03.99 | 7:22.02 | 942 | | | |
| 03.12.2003 | GeoB9027 | HS | 17:48 | 17:48 | 22:12 | 22:12 | | 36:02.94 | 7:26.22 | 36:2.811 | 7:18.828 | 902 | | Gutscher | Faro Almazan |
| 03.12.2003 | GeoB9028 | OFOS | 22:50 | 23:10 | 7:00 AM | n.d. 08:18 | | 36:5.77 | 7:23.19 | 36:05.17 | 7:24.09 | 885 | | Brueckman | Faro Almazan |
| 04.12.2003 | GeoB9029-1 | TV-MUC | 08:50 | 09:16 | 09:32 | 10:08 | | 36:5.69 | 7:24.14 | 36:05.66 | 7:24.18 | 904 | 0 cm | Hensen | Faro Almazan |
| 04.12.2003 | GeoB9029-2 | TV-MUC | 08:50 | 10:34 | 11:15 | 11:40 | | 36:5.69 | 7:24.18 | 36:05.60 | 7:24.04 | 921 | 4 cores max depth 12cm | Hensen | Faro Almazan |
| 04.12.2003 | GeoB9029-3 | TV-G | 08:50 | 12:34 | 13:50 | 10:08 | | 36:5.68 | 7:24.17 | 36:5.68 | 7:24.18 | 907 | evt Bakterienmatten | Brueckman | Faro Almazan |
| 04.12.2003 | GeoB9030-1 | TV-G | 14:40 | 14:59 | 16:35 | 17:00 | | 36:5.43 | 7:24.26 | 36:5.10 | 7:24.52 | 908 | kein Gewinn | Brueckman | Faro Almazan |
| 04.12.2003 | GeoB9030-2 | TV-G | 14:40 | 15:51 | 16:35 | 17:00 | | 36:5.68 | 7:24.17 | 36:5.30 | 7:24.46 | 949 | kein Gewinn | Brueckman | Faro Almazan |
| 04.12.2003 | GeoB9030-3 | TV-G | 14:40 | 16:34 | 16:35 | 17:00 | | 36:5.43 | 7:24.26 | 36:5.10 | 7:24.52 | 980 | ????? | Brueckman | Faro Almazan |
| 04.12.2003 | GeoB9031 | GC | 17:35 | 17:52 | 17:52 | 18:20 | | 36:5.68 | 7:24.17 | 36:5.75 | 7:23.28 | 897 | 4.84m | Hebbeln | Faro Almazan |
| 04.12.2003 | GeoB9032 | GC | 18:30 | 18:51 | 18:51 | 19:09 | | 36:5.43 | 7:24.26 | 36:5.55 | 7:23.57 | 843 | 2.20m | Hebbeln | Faro Almazan |
| 04.12.2003 | GeoB9033 | HS/PS | 21:00 | 21:00 | n.d. 1:50 | n.d. 1:50 | | 35:53.40 | 7:26.44 | 35:42.59 | 7:19.94 | | v=6 kn | Gutscher | |
| 04.12.2003 | GeoB9034 | HS/PS | 02:18 | 02:18 | 02:18 | 03:26 | | 35:42.66 | 7:23.33 | 35:35.90 | 7:23.38 | | v=6 kn | Gutscher | |
| 05.12.2003 | GeoB9035 | OFOS | 04:00 | | | 08:00 | | 35:40.11 | 7:20.04 | 35:39.35 | 7:19.76 | 1400 | | Brueckman | Arutyunov |
| 05.12.2003 | GeoB9036-1 | TV-G | 08:40 | 09:05 | 09:07 | 10:30 | | 35:39.69 | 7:19.99 | 35:29.68 | 7:19.96 | 1320 | voll | Brueckman | Arutyunov |

| SO175 | | | | | | | | | | | | | | | |
|---|---|---|---|---|---|---|---|---|---|---|---|---|---|---|---|
| | | | Time (UTC) | | | | | Begin / on seafloor | | End / off seafloor | | | | | |
| Date | St. No. | Instrument | Begin | Start Sci. Program | End Sci. Program | End | Durati h:m | Latitude N° | Longitude W° | Latitude N° | Longitude W° | Water depth (m) | Recovery x | Supervisor | Area |
| 05.12.2003 | GeoB 9036-2 | TV-MUC | 10:53 | 11:23 | 11:25 | 12:07 | | 35:39.717 | 7:19.98 | 35:39.71 | 7:19.98 | 1326 | 6 cores, max depth 38cm | Hensen | Arutyunov |
| 05.12.2003 | GeoB 9037 | GC | 12:22 | 13:05 | 13:05 | 13:35 | | 35:39.928 | 7:20.081 | 35:39.928 | 7:20.081 | 1371 | 3.76m | Hebbeln | Arutyunov |
| 05.12.2003 | GeoB 9038 | GC | 14:10 | 14:28 | 14:28 | 14:50 | | 35:39.295 | 7:16.47 | 35:39.295 | 7:16.47 | 1313 | | Hebbeln | Arutyunov |
| 05.12.2003 | GeoB 9039 | GC | 15:10 | 15:33 | 15:33 | 16:06 | | 35:41.21 | 7:16.52 | 35:41.21 | 7:16.52 | 1331 | 4.50m | Hebbeln | Arutyunov |
| 05.12.2003 | GeoB 9040 | GC | 16:49 | 17:09 | 17:09 | 17:45 | | 35:39.56 | 7:23.38 | 35:39.56 | 7:23.38 | 1380 | | Hebbeln | Arutyunov |
| 05.12.2003 | GeoB 9041 | GC | 18:15 | 18:43 | 18:43 | 19:09 | | 35:39.70 | 7:19.97 | 35:39.70 | 7:19.97 | 1316 | 2.35m | Hebbeln | Arutyunov |
| 05.12.2003 | GeoB 9042 | HF | 19:30 | 20:20 | n.d. 8:12 | 08:42 | | 35:38.40 | 7:28.45 | 35:39.76 | 7:23.65 | 1443 | 14 temperature profiles | Grevemeyer | |
| 06.12.2003 | GeoB 9043 | Seismik HS/PS | 09:55 | 09:55 | nextday | nextday 2:56:00 A | | 35:35.06 | 7:17.73 | 35:34.99 | 09:10.85 | 1240 | | Kaul | Arutyunov |
| 07.12.2003 | GeoB 9044 | HS/PS | 02:56 | 02:56 | 08:32 | 08:32 | | 35:35.00 | 9:40.01 | 35:34.97 | 9:33.44 | | v=8 kn | Gutscher | Transit |
| 07.12.2003 | GeoB 9045-1 | TV-MUC | 09:15 | 10:34 | 10:35 | 15:20 | | 35:29.60 | 9:33.44 | 35:29.59 | 9:33.46 | 3991 | 4 cores, max depth 31cm | Hensen | Bonjardim |
| 07.12.2003 | GeoB 9045-2 | GC | 13:00 | 14:15 | 14:15 | 15:08 | | 35:29.60 | 9:33.43 | 35:29.60 | 9:33.43 | 3951 | 0.60m | Hebbeln | Bonjardim |
| 07.12.2003 | GeoB 9046 | HF | 15:53 | 17:08 | 20:48 | 22:01 | | 35:29.62 | 9:39.85 | 35:29.60 | 9:22.76 | 4222 | 4 temperature profiles | Kaul | Bonjardim |
| 07.12.2003 | GeoB 9047 | HF | 23:32 | n.d. 0:36 | n.d3:45 | 04:54 | | 35:29.60 | 9:20.78 | 35:29.60 | 9:22.76 | 3717 | 4 temperature profiles | Kaul | Bonjardim |
| 08.12.2003 | GeoB 9048 | HF | 06:32 | 07:32 | 11:08 | 12:07 | | 35:29.60 | 9:01.56 | 35:29.59 | 8:59.56 | 3236 | 4 temperature profiles | Kaul | Bonjardim |
| 08.12.2003 | GeoB 9049 | HF | 13:34 | 14:24 | 17:43 | 18:36 | | 35:29.58 | 8:41.68 | 35:29.59 | 8:39.70 | 2697 | 4 temperature profiles | Kaul | Bonjardim |
| 08.12.2003 | GeoB 9050-1 | HS/PS | 18:45 | 18:45 | 22:43 | 22:43 | | 35:29.60 | 8:39.00 | 35:29.60 | 8:00.00 | | v=8 kn | Gutscher | |
| 12/82003 | GeoB 9050-2 | HS/PS | 23:05 | 23:05 | 06:24 | 06:24 | | 35:32.25 | 8:00.19 | 35:25.00 | 9:00.00 | | v=8 kn | Gutscher | |
| 09.12.2003 | GeoB 9051-1 | TV-MUC | 08:00 | 09:08 | 09:36 | 10:44 | | 35:27.61 | 9:00.02 | 35:27.72 | 8:59.98 | 3088 | 5 cores max depth 60cm | Hebbeln | Bonjardim |
| 09.12.2003 | GeoB 9051-2 | GC | 11:04 | 11:54 | 11:54 | 13:00 | | 35:27.61 | 9:00.03 | 35:27.61 | 9:00.03 | 3087 | | Hebbeln | Bonjardim |
| 09.12.2003 | GeoB 9052-1 | GC | 14:15 | 15:05 | 15:05 | 16:20 | | 35:31.08 | 8:47.00 | 35:31.08 | 8:47.00 | 2747 | | Hebbeln | Bonjardim |
| 09.12.2003 | GeoB 9052-2 | GC | 17:08 | 17:57 | 17:57 | 19:05 | | 35:31.12 | 8:47.01 | 35:31.12 | 8:47.01 | 2744 | | Hebbeln | Bonjardim |
| 09.12.2003 | GeoB 9053 | HF | 20:42 | 21:37 | 22:52 | 00:00 | | 35:27.82 | 9:00.00 | 35:27.62 | 09:00.00 | 3068 | 3 temperature profiles | Kaul | Bonjardim |
| 10.12.2003 | GeoB 9054 | HS/PS | 00:10 | 00:10 | 12:05 | 12:05 | | 35:25.00 | 09:00.00 | 34:39.99 | 09:09.98 | 3142 | v=7.5 kn | Gutscher | Transit |
| 10.12.2003 | GeoB 9055-1 | GC | 12:07 | 13:20 | 13:20 | 15:03 | | 34:39.98 | 9:10.00 | 34:39.98 | 9:10.00 | 4179 | 2.49m | Hebbeln | Abyssal plain |
| 10.12.2003 | GeoB 9055-2 | TV-MUC | 15:03 | 16:36 | 16:39 | 18:18 | | 34:39.97 | 9:10.01 | 34:39.98 | 9:10.00 | 4205 | 1 core, max depth 10cm | Hensen | Abyssal plain |
| 10.12.2003 | GeoB 9056 | Seismik | 18:48 | 19:08 | n.d. 17:12 | | | 34:39.98 | 09:15.00 | 35:29.41 | 07:08.90 | | v=5 kn | Kaul | Poseidon --> Ginsburg |
| 11.12.2003 | GeoB 9057 | OFOS | 21:15 | 21:43 | 03:34 | n.d. 3:55:00 AM | | 35:24.68 | 07:06.10 | 35:25.00 | 07:05.62 | 1058 | | Brueckman | Ginsburg |
| 12.12.2003 | GeoB 9058 | OFOS | 04:26 | 04:47 | 08:00 | 08:25 | | 35:24.68 | 07:06.10 | 35:25.00 | 07:05.62 | 1023 | | Brueckman | Yuma MV |
| 12.12.2003 | GeoB 9059-1 | TV-MUC | 08:56 | 09:18 | 09:19 | 09:42 | | 35:22.42 | 07:05.28 | 35:22.42 | 07:05.28 | 911 | 3 cores, max depth 0.35m | Hensen | Ginsburg MV |
| 12.12.2003 | GeoB 9059-2 | TV-G | 09:59 | 10:39 | 10:49 | 11:09 | | 35:22.42 | 07:05.30 | 35:22.39 | 07:05.31 | 910 | Abbruch, Greifer schließt | Brueckman | Ginsburg MV |
| 12.12.2003 | GeoB 9059-3 | TV-G | 11:30 | 11:47 | 11:51 | 12:30 | | 35:22.40 | 07:05.31 | 35:22.40 | 7:05.33 | 909 | | Brueckman | Ginsburg MV |
| 12.12.2003 | GeoB 9060 | TV-G | 12:52 | 13:24 | 14:49 | 15:54 | | 35:22.77 | 07:05.24 | 35:22.82 | 07:05.25 | 991 | some corals | Brueckman | Ginsburg MV |
| 12.12.2003 | GeoB 9061 | GC | 16:49 | 17:07 | 17:07 | 17:40 | | 35:22.42 | 07:05.29 | 35:22.42 | 07:05.29 | 912 | 1.54 m | Hebbeln | Ginsburg MV |
| 12.12.2003 | GeoB 9062 | HS/PS | 19:07 | 19:07 | n.d. 07:3 | n.d. 07:30 | | 35:20.04 | 07:10.05 | 35:32.00 | 07:05.00 | | v=8 kn | Gutscher | Transit |
| 13.12.2003 | GeoB 9063 | GC | 08:51 | 09:03 | | 09:23 | | 35:21.99 | 06:51.92 | 35:21.99 | 06:51.92 | 598 | 5.00 m | Hebbeln | Belgica area off Morocco |
| 13.12.2003 | GeoB 9064 | GC | 09:50 | 10:05 | 10:05 | 10:24 | | 35:24.91 | 06:50.71 | 35:24.91 | 06:50.71 | 702 | 5.50 m | Hebbeln | Belgica area off Morocco |
| 13.12.2003 | GeoB 9065 | GC | 11:28 | 11:39 | 11:39 | 11:55 | | 35:19.60 | 06:42.08 | 35:19.60 | 06:42.08 | 507 | 6.29 m | Hebbeln | Belgica area off Morocco |
| 13.12.2003 | GeoB 9066 | GC | 12:56 | 13:08 | 13:08 | 13:25 | | 35:12.19 | 06:37.09 | 35:12.19 | 06:37.09 | 376 | 3.20 m | Hebbeln | Belgica area off Morocco |
| 13.12.2003 | GeoB 9067 | GC | 14:26 | 14:55 | 14:55 | 15:21 | | 35:16.92 | 06:45.47 | 35:16.92 | 06:45.47 | 435 | 3.70 m | Hebbeln | Belgica area off Morocco |
| 13.12.2003 | GeoB 9068 | GC | 15:45 | 16:02 | 16:02 | 16:23 | | 35:18.03 | 06:47.42 | 35:18.03 | 06:47.42 | 567 | 4.38 m | Hebbeln | Belgica area off Morocco |
| 13.12.2003 | GeoB 9069 | GC | 16:45 | 17:03 | 17:03 | 17:26 | | 35:18.21 | 06:49.14 | 35:18.21 | 06:49.14 | 669 | 5.13 m | Hebbeln | Belgica area off Morocco |
| 13.12.2003 | GeoB 9070 | GC | 18:02 | 18:21 | 18:21 | 18:55 | | 35:22.00 | 06:51.90 | 35:22.00 | 06:51.90 | 594 | | Hebbeln | Belgica area off Morocco |
| 13.12.2003 | GeoB 9071 | HS/PS | 21:10 | 21:10 | n.d. 8:54 | n.d. 8:54 | | 35:18.00 | 6.26.20 | 35:39.69 | 7:19.97 | 137 | v=8 kn | Gutscher | Morocco continental shelf |
| 13.12.2003 | GeoB 9072-1 | GC | 08:55 | 09:23 | 09:23 | 10:00 | | 35:39.71 | 7:19.95 | 35:39.71 | 7:19.95 | 1321 | 3.15 m | Hebbeln | |
| 14.12.2003 | GeoB 9072-2 | TV-MUC | 10:39 | 11:11 | 11:12 | 12:00 | | 35:39.70 | 7:19.98 | 35:39.71 | 7:19.98 | 1322 | | | |
| 14.12.2003 | GeoB 9072-3 | TV-G | 12:10 | 12:53 | 12:54 | 13:47 | | 35:39.72 | 7:20.03 | 35:39.71 | 7:19.99 | 1324 | mud breccia | Brueckmann | |
| 14.12.2003 | GeoB 9074 | HS/PS | 13:51 | 13:51 | 20:00 | 20:00 | | 35:39.73 | 7:20.00 | 35:10.52 | 7:57.24 | | v=8 kn | Gutscher | |
| 14.12.2003 | GeoN 9075 | HF | 20:00 | 20:54 | 22:08 | 22:52 | | 35:10.51 | 7:57.23 | 35:10.74 | 7:56.66 | 2239 | 2 temperature profiles | Kaul | |
| 15:12.03 | GeoB 9076 | OFOS | 08:30 | 08:36 | 11:21 | 11:27 | | 35:54.43 | 05:58.77 | 35:54.39 | 06:00.76 | 71 | | | Banc de Spartel |
| 15.12.2003 | GeoB 9077 | OFOS | 12:08 | 12:16 | 13:50 | 14:15 | | 35:55.06 | 05:59.94 | 35:54.39 | 06:00.39 | 134 | | | Banc de Spartel |

**SO175**

| Date | St. No. | Instrument | Time (UTC) Begin | Start Sci. Program | End Sci. Program | End | Durati h:m | Begin / on seafloor Latitude N° | Longitude W° | End / off seafloor Latitude N° | Longitude W° | Water depth (m) | Recovery x | Supervisor | Area |
|---|---|---|---|---|---|---|---|---|---|---|---|---|---|---|---|
| 15.12.2003 | GeoB 9078 | TV-G | 14:34 | 14:42 | 14:53 | 15:12 | | 35:54.69 | 06:00.35 | 35:54.67 | 06:00.35 | 113 | | Brueckman | Banc de Spartel |
| 15.12.2003 | GeoB 9079 | TV-G | 15:29 | 15:38 | 15:49 | 16:00 | | 35:54.71 | 05:59.99 | 35:54.71 | 06:00.00 | 116 | | Brueckman | Banc de Spartel |
| 15.12.2003 | GeoB 9080 | TV-G | 16:14 | 16:32 | 17:00 | 17:27 | | 35:54.91 | 06:00.16 | 35:54.91 | 06:00.22 | 125 | | Brueckman | Banc de Spartel |
| 16.12.2003 | GeoB 9081 | HS/PS | 00:07 | 00:07 | 07:33 | 07:33 | | 35:21.24 | 97:19.03 | 34:53.00 | 8:23.00 | | v=8 kn | Gutscher | Banc de Spartel |
| 16.12.2003 | GeoB 9082 | HF | 08:15 | 09:08 | 20:22 | 21:26 | | 34:59.94 | 8:23.95 | 34:57.04 | 8:31.01 | 2816 | 9 temperature profiles | Kaul | Deformation front scarp |
| 16.12.2003 | GeoB 9083 | OFOS | 22:00 | 22:52 | n.d. 4:00 | n.d. 04:57 | | 34:58.26 | 8:25.88 | 34:56.87 | 8:26.00 | 2908 | | Brueckman | Deformation front scarp |
| 17.12.2003 | GeoB 9084 | HS/PS | 05:24 | 05:24 | 08:00 | 08:00 | | 34:52.50 | 8:26.00 | 34:43.00 | 8:48.00 | | v=8 kn | Gutscher | Transit |
| 17.12.2003 | GeoB 9085 | GC/MTL | 08:44 | 09:41 | 09:48 | 11:00 | | 34:49.11 | 8:51.70 | 34:49.11 | 8:51.70 | 3457 | | Hebbeln | Poseidon |
| 17.12.2003 | GeoB 9086 | GC/MTL | 11:19 | 12:17 | 12:24 | 13:24 | | 34:49.21 | 8:51.00 | 34:49.21 | 8:51.00 | 3463 | | Hebbeln | Transit |
| 17.12.2003 | GeoB 9087 | HF | 14:09 | 15:14 | 17:49 | 19:00 | | 34:46.54 | 8:56.96 | 34:46.06 | 8:58.12 | 3710 | | Kaul | Transit |
| 17.12.2003 | GeoB 9088 | HS/PS | 19:46 | 19:46 | n.d. 11.1 | n.d. 11.18 | | 34:42.00 | 8:51.00 | 35:34.98 | 9:43.01 | | v=8 kn | Gutscher | |
| 18.12.2003 | GeoB 9089 | TV-MUC | 16:56 | 18:41 | 18:41 | 20:00 | | 36:06.27 | 10:40.00 | 36:06.27 | 10:40.00 | 4897 | 2 cores, max. depth 31 cm | Hebbeln | |
| 18.12.2003 | GeoB 9090 | HF | 20:44 | 22:25 | n.d. 1:59 | n.d. 03:37:00 | | 36:06.72 | 10:39.37 | 36:05.33 | 10:38.23 | 4894 | 4 temperature profiles | Grevemeyer | |
| 19.12.2003 | GeoB 9091 | GC | 08:03 | 09:07 | 09:07 | 10:19 | | 36:50.02 | 10:08.68 | 36:50.02 | 10:08.68 | 3957 | 3.47 m | Hebbeln | |
| 19.12.2003 | GeoB 9092 | GC | 10:58 | 11:50 | 11:50 | 13:11 | | 36:48.01 | 10:04.00 | 36:47.99 | 10:04.00 | 3229 | 4.05 m | Hebbeln | |
| 19.12.2003 | GeoB 9093 | GC | 13:41 | 14:30 | 14:30 | 15:20 | | 36:49.03 | 10:02.01 | 36:49.03 | 10:02.01 | 3006 | | Hebbeln | |
| 19.12.2003 | GeoB 9094 | Seismik | 16:32 | 16:54 | n.d. 211 | n.d. 2:29 | | 36:56.11 | 10:00.97 | 36:52.25 | 9:52.69 | | v=5 kn | Kaul | |
| 20.12.2003 | GeoB 9095-1 | GC/MTL | 08:45 | 09:59 | 10:05 | 11:43 | | 37:30.01 | 11:02.03 | 37:30.01 | 11:02.03 | 5123 | | Hebbeln | |

| Abbreviations: |
|---|
| CTD (Conductivity temperature depth) |
| TV–MUC (TV–Multicorer) |
| GC (Gravity Corer) |
| TV–G (TV–Grab sampler) |
| OFOS (Ocean floor observation system) |
| HF (Heat Flow detector) |
| MTL (Miniatur Temperature Logger) |
| PS-survey (Parasound, Simrad) |
| n.d. (next day) |

## Appendix 8.2. OFOS (Ocean Floor Observation System) track list SO 175

During SO175, a total of 12 OFOS video-sled stations were carried out:

GeoB 9002-1 : Marquis de Pombal landslide area, upper slope area across headwall

GeoB 9003-1 : Marquis de Pombal landslide area, lower slope

GeoB 9012-1 : Lolita mud volcano

GeoB 9013-1 : Leaky faults area

GeoB 9016-1 : Hesperides mud volcano

GeoB 9017-1 : Hesperides mud volcano

GeoB 9028-1 : Faro mud volcano

GeoB 9035-1 : Capitan Arutyunov mud volcano

GeoB 9057-1 : Ginsburg mud volcano

GeoB 9058-1 : Yuma mud volcano

GeoB 9076-1 : Banc de Spartel

GeoB 9077-1 : Banc de Spartel

GeoB 9083-1 : Scarp along SISMAR16 seismic profile

## Appendix 8.3.1. Gravity core list SO175

| station no. | latitude °N | longitude °W | water depth (m) | recovery (m) | desciption | colour logging | porewater | phys. prop. | core penetrom. | MSCL | area | sediments | remarks |
|---|---|---|---|---|---|---|---|---|---|---|---|---|---|
| GeoB 9006-1 | 36:55.00 | 10:05.56 | 3949 | 4.30 | X | X* | X | X | X | X | Marques de Pombal | hemipelagic & turbidites | |
| GeoB 9008-2 | 36:50.29 | 09:58.57 | 2734 | 2.68 | X | X* | X | X | X | X | Marques de Pombal | hemipelagic & slideplane | |
| GeoB 9010-1 | 35:47.00 | 09:32.00 | 4365 | 2.32 | X | X* | | X | X | X | Deformation front | hemipelagic & turbidites | |
| GeoB 9014-2 | 36:35.81 | 07:46.81 | 759 | 1.44 | X | X* | X | X | X | X | Leaky faults | hemipelagic | |
| GeoB 9018-1 | 36:10.98 | 07:18.37 | 702 | 3.47 | uno | pen | ed | | | X | Hesperides MV | hemipleagic & corals | |
| GeoB 9019-1 | 36:11.18 | 07:19.15 | 767 | 1.62 | X | X* | X | X | X | X | Hesperides MV | mud breccia | |
| GeoB 9020-1 | 36:11.16 | 07:19.29 | 730 | 0.19 | uno | pen | ed | | | X | Hesperides MV | mud breccia (core bent) | |
| GeoB 9021-1 | 36:10.99 | 07:18.38 | 701 | 3.78 | X | X* | X | X | X | X | Hesperides MV | hemipleagic & corals | = GeoB 9018 |
| GeoB 9031-1 | 36:05.75 | 07:23.28 | 897 | 4.84 | uno | pen | ed | | | X | Faro MV | hemipleagic & corals | |
| GeoB 9032-1 | 36:05.55 | 07:23.57 | 843 | 2.20 | uno | pen | ed | | | X | Faro MV | hemipleagic & corals | |
| GeoB 9037-1 | 35:39.93 | 07:20.08 | 1381 | 3.76 | X | X | | X | X | X | Capt. Arutyunov MV | mud breccia | |
| GeoB 9038-1 | 35:39.30 | 07:16.52 | 1313 | 2.63 | X | X | X | X | X | X | unnamed MV #1 | mud breccia | |
| GeoB 9039-1 | 35:41.21 | 07:16.52 | 1331 | 4.50 | X | X | | X | X | X | N of unnamed MV #1 | hemipleagic sediments | |
| GeoB 9040-1 | 35:39.56 | 07:23.38 | 1380 | 3.43 | X | X | X | X | X | X | unnamed MV #2 | hemipleagic & mud breccia | |
| GeoB 9041-1 | 35:39.70 | 07:19.97 | 1316 | 2.35 | X | X | X | X | X | X | Capt. Arutyunov MV | mud breccia & gas hydrates | |
| GeoB 9045-2 | 35:29.60 | 09:33.43 | 3951 | 0.53 | X | X | | X | X | X | Horseshoe abyssal plain | hemipelagic sediments | |
| GeoB 9051-2 | 35:27.61 | 09:00.03 | 3087 | 2.63 | X | X | X | X | X | X | Bonjardim MV | mud breccia | |
| GeoB 9052-1 | 35:31.08 | 08:47.00 | 2747 | 4.86 | X | X | X | X | X | X | unnamed dome | hemipelagic sediments | |
| GeoB 9052-2 | 35:31.12 | 08:47.01 | 2744 | 4.20 | X | X | X | X | X | X | unnamed dome | hemipelagic sediments | |
| GeoB 9055-1 | 34:39.98 | 09:10.00 | 4179 | 2.49 | X | X | X | X | X | X | Seine abyssal plain | hemipel. sedim. w/ turbidites | |
| GeoB 9061-1 | 35:22.42 | 07:05.29 | 912 | 1.54 | X | X | X | X | X | X | Ginsburg MV | mud breccia | |
| GeoB 9063-1 | 35:21.99 | 06:51.92 | 598 | 5.00 | X | X | X | X | X | X | unnamed MV E of TTR | hemipleagic & corals | |
| GeoB 9064-1 | 35:24.91 | 06:50.71 | 702 | 5.44 | X | X | | X | X | X | cont. slope/paleoc. | hemipelagic sediments | |
| GeoB 9065-1 | 35:19.60 | 06:42.08 | 507 | 6.29 | X | X | | X | X | X | cont. slope/paleoc. | hemipel. sedim. w/ turbidites | |
| GeoB 9066-1 | 35:12.19 | 06:37.09 | 376 | 3.09 | X | X | | X | X | X | cont. slope/paleoc. | hemipelagic s. (core bent) | |
| GeoB 9067-1 | 35:16.92 | 06:45.47 | 435 | 3.70 | X | X | X | X | X | X | Gemini MV | mud breccia | |
| GeoB 9068-1 | 35:18.03 | 06:47.42 | 567 | 4.38 | X | X | | X | X | X | Pen Duick Escarpm. | hemipelagic sediments | |
| GeoB 9069-1 | 35:18.21 | 06:49.14 | 669 | 5.13 | X | X | | X | X | X | Pen Duick Escarpm. | hemipel. sedim. w/ turbidites | |
| GeoB 9070-1 | 35:22.00 | 06:51.90 | 594 | 6.00 | uno | pen | ed | | | X | unnamed MV E of TTR | hemipleagic & corals | = GeoB 9063 |
| GeoB 9072-1 | 35:39.71 | 07:19.95 | 1321 | 3.25 | | | X | | | | Capt. Arutyunov MV | mud breccia & gas hydrates | = GeoB 9041 |
| GeoB 9085-1 | 34:49.11 | 08:51.70 | 3457 | 5.70 | X | X | X | X | X | X | Poseidon dome | hemipelagic sediments | |
| GeoB 9086-1 | 34:49.21 | 08:51.00 | 3463 | 4.69 | X | X | X | X | X | X | Poseidon dome | hemipel. sedim. w/ turbidites | |
| GeoB 9091-1 | 36:50.02 | 10:08.68 | 3957 | 3.47 | X | X | X | X | X | X | Marques de Pombal | hemipelagic sediments | |
| GeoB 9092-1 | 36:48.01 | 10:04.00 | 3229 | 4.05 | X | X | | X | X | X | Marques de Pombal | hemipelagic sediments | |
| GeoB 9093-1 | 36:49.03 | 10:02.01 | 3006 | 3.32 | X | X | | X | X | X | Marques de Pombal | hemipelagic sediments | |
| GeoB 9095-1 | 37:30.01 | 11:02.03 | 5123 | 3.10 | X | X | | | | X | Tagus abyssal plain | hemipel. sedim. w/ turbidites | |

X* = Colour scanning has been carried out only after the protcall in Cadiz

**Appendix 8.3.2. TV Grabs List SO-175**

| St. No. | Latitude N° | Longitude W° | Water depth (m) | Area |
|---|---|---|---|---|
| GeoB 9022-1 | 36:10.98 | 07:18.36 | 676 | Hesperides MV |
| GeoB 9023-1 | 36:10.73 | 07:18.39 | 761 | Hesperides MV |
| GeoB 9024-1 | 36:11.32 | 07:18.45 | 727 | Hesperides MV |
| GeoB 9029-3 | 36:05.68 | 07:24.12 | 907 | Faro MV |
| GeoB 9030-1 | 36:05.36 | 07:24.39 | 908 | Faro MV |
| GeoB 9030-2 | 36:05.30 | 07:24.46 | 949 | Faro MV |
| GeoB 9030-3 | 36:05.10 | 07:24.52 | 980 | Faro MV |
| GeoB 9036-1 | 35:39.69 | 07:19.99 | 1320 | Capt. Arutyunov MV |
| GeoB 9059-2 | 35:22.42 | 07:05.30 | 910 | Ginsburg MV |
| GeoB 9059-3 | 35:22.40 | 07:05.33 | 909 | Ginsburg MV |
| GeoB 9060-1 | 35:22.82 | 07:05.25 | 991 | Ginsburg MV |
| GeoB 9072-3 | 35:39.71 | 07:19.99 | 1324 | Capt. Arutyunov MV |
| GeoB 9078-1 | 35:54.69 | 06:00.35 | 113 | Banc de Spartel |
| GeoB 9079-1 | 35:54.71 | 05:59.99 | 116 | Banc de Spartel |
| GeoB 9080-1 | 35:54.91 | 06:00.16 | 125 | Banc de Spartel |

## Appendix 8.3.3. MUC Sampling list SO-175

| station no. | latitude N° | longitude W° | water depth (m) | recovery (cm) | description | bottom water | core #1 | core #2 | core #3 | core #4 | core #5 | core #6 | area |
|---|---|---|---|---|---|---|---|---|---|---|---|---|---|
| GeoB 9005-1 | 37:00.96 | 10:10.91 | 3919 | 26-36 | X | X | C/S | F | S/T | S/T | - | - | Marques de Pombal |
| GeoB 9008-1 | 36:50.29 | 09:58.54 | 2708 | 17 | X | X | C/S | S/T | BG | BG | - | - | Marques de Pombal |
| GeoB 9014-1 | 36:35.81 | 07:46.81 | 758 | 30 | X | X | C/S | F | GT | PW | - | - | Leaky faults |
| GeoB 9029-1 | 36:05.69 | 07:24.14 | 904 | - | - | - | - | - | - | - | - | - | Faro MV |
| GeoB 9029-2 | 36:05.61 | 07:24.04 | 921 | 12 | X | X | C/S | F | PW | - | - | - | Faro MV |
| GeoB 9036-2 | 35:39.72 | 07:19.98 | 1326 | 38 | X | - | F/S | BG | BG | BG | GT | PW | Capt. Arutjonov MV |
| GeoB 9045-1 | 35:29.59 | 09:33.46 | 3991 | 30 | X | X | F | C/S | PW | GT | - | - | Horseshoe abyssal plain |
| GeoB 9051-1 | 35:27.72 | 08:59.98 | 3088 | 55 | X | - | F/GT | BG | BG | PW | - | - | Bonjardim MV |
| GeoB 9055-2 | 34:39.99 | 09:10.00 | 4205 | 10 | X | - | S/T | - | - | - | - | - | Seine abyssal plain |
| GeoB 9059-1 | 35:22.42 | 07:05.28 | 911 | 39 | X | X | C/S | F/GT | PW | - | - | - | Ginsburg MV |
| GeoB 9072-2 | 35:39.71 | 07:19.98 | 1322 | 60 | - | - | PW | PW | PW | PW | - | - | Capt. Arutjonov MV |
| GeoB 9089-1 | 36:06.27 | 10:40.00 | 4897 | 31 | X | - | S/T | S/T | - | - | - | - | Horseshoe abyssal plain |
| GeoB 9095-2 | 37:30.03 | 11:02.05 | 5162 | 30 | X | - | C | S/T | S/T | - | - | - | Tagus abyssal plain |
| GeoB 9099-1 | 36:02.23 | 10:34.80 | 4900 | 32 | - | - | S/T | S/T | - | - | - | - | Horseshoe abyssal plain |

Sampling GeoB Bremen: C: Corg, S:Sedimentology, F: Foraminifera, GT: Geotechnics
MPI Bremen: BG: Biogeochemistry
Geomar Kiel: PW: Porewater
Barcelona: S/T: Sedimentology/Turbidites

## Chapter 8.4. Lithologs and MST sheets

*see pages 165-198*

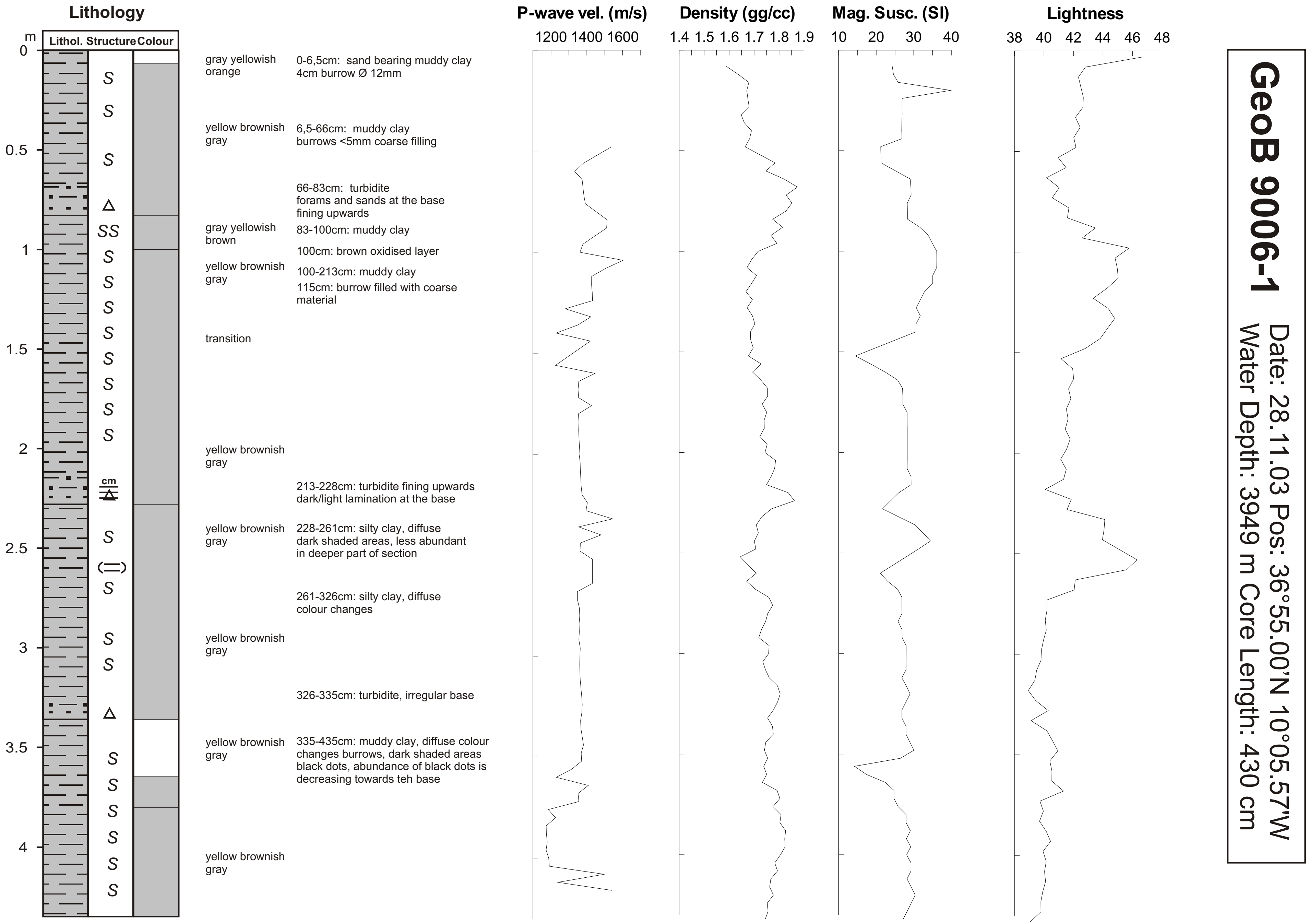


Core description, MST data and colour scanner data of core GeoB9006-1

Core description, MST data and colour scanner data of core GeoB9008-2

# GeoB 9008-2

Date: 29.11.03 Pos: 36°5.29'N 9°58.57'W
Water Depth: 2711 m Core Length: 268 cm

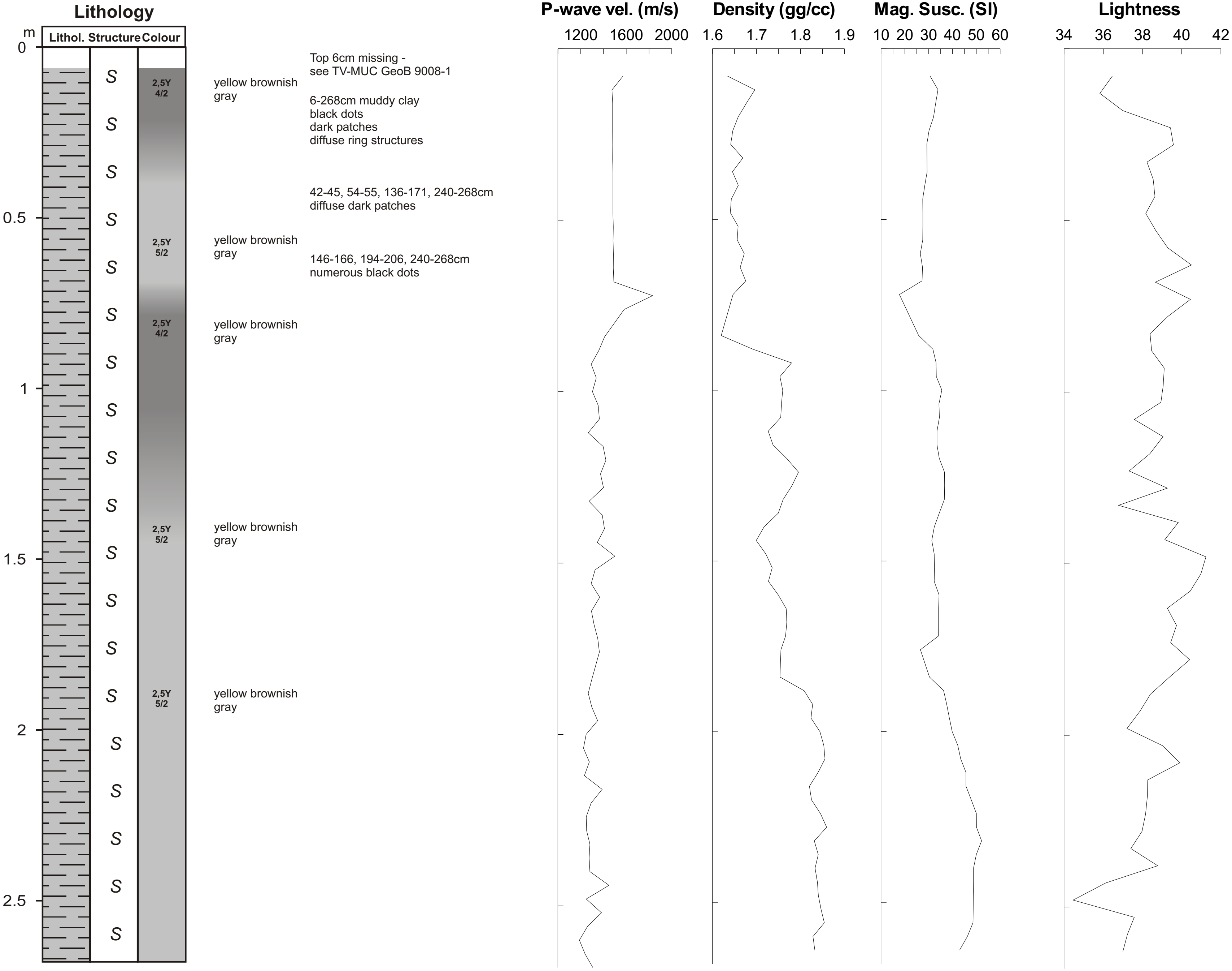

Core description, MST data and colour scanner data of core GeoB9010-1

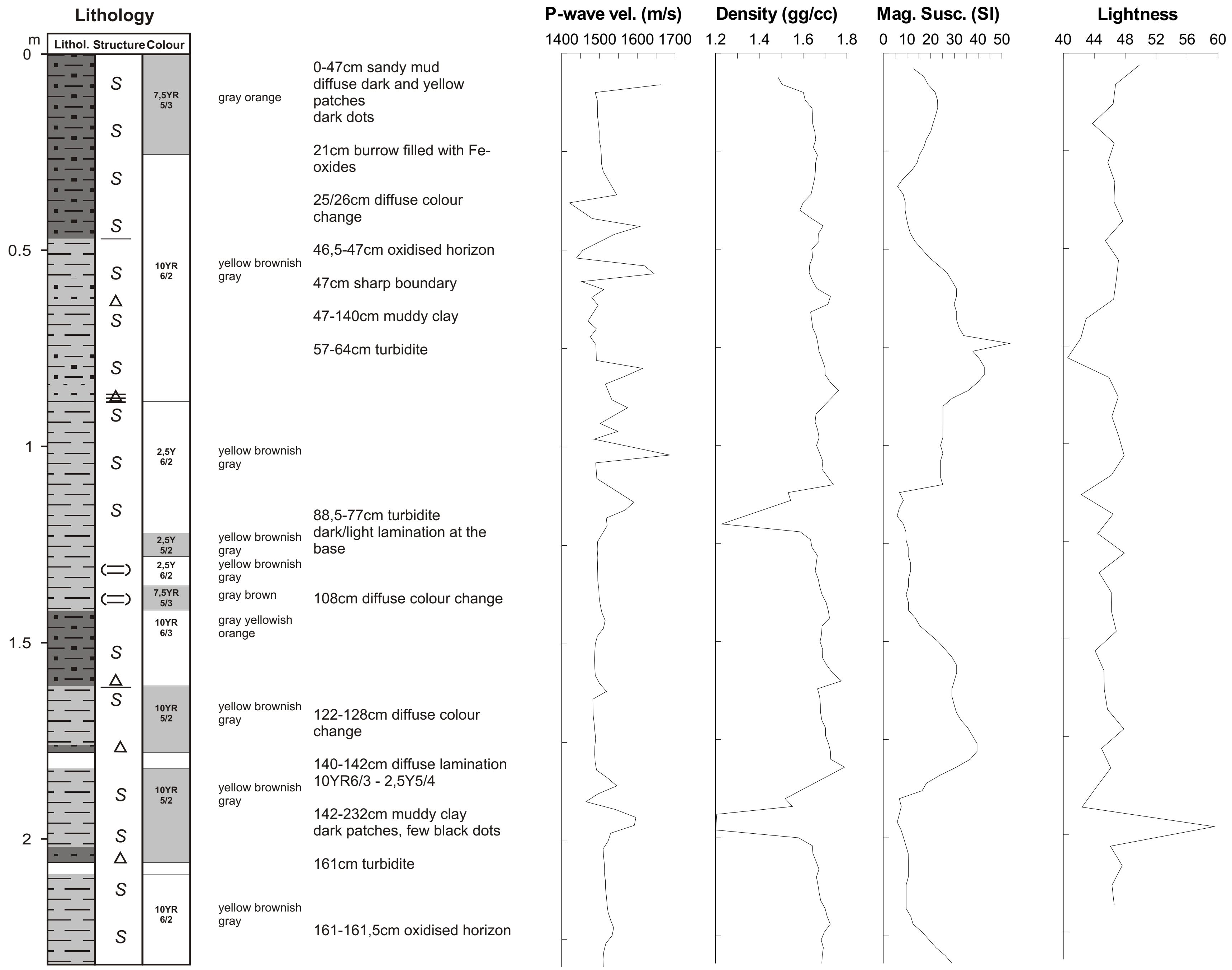


**GeoB 9010-1**

Date: 30.11.03 Pos: 35°47.00'N 9°32.00'W

Water Depth: 4365 m Core Length: 232 cm

Core description, MST data and colour scanner data of core GeoB9014-2

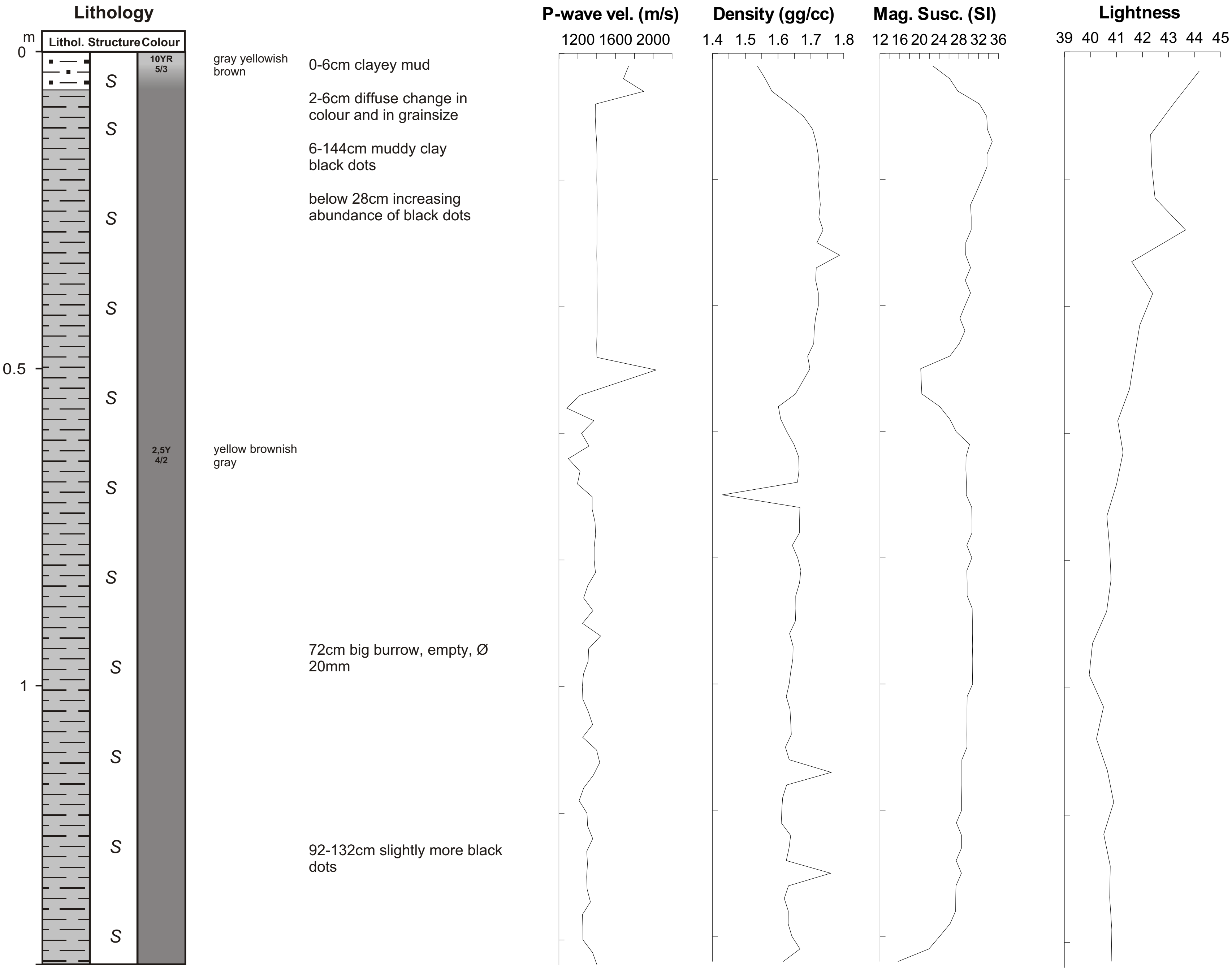


**GeoB 9014-2**

Date: 01.12.03 Pos: 36°35.81'N 7°46.81'W

Water Depth: 759 m Core Length: 132 cm

**GeoB 9018-1** Date: 02.12.03 Pos: 36°10.98'N 7°18.37'W
Water Depth:702 m Core Length: 347 cm

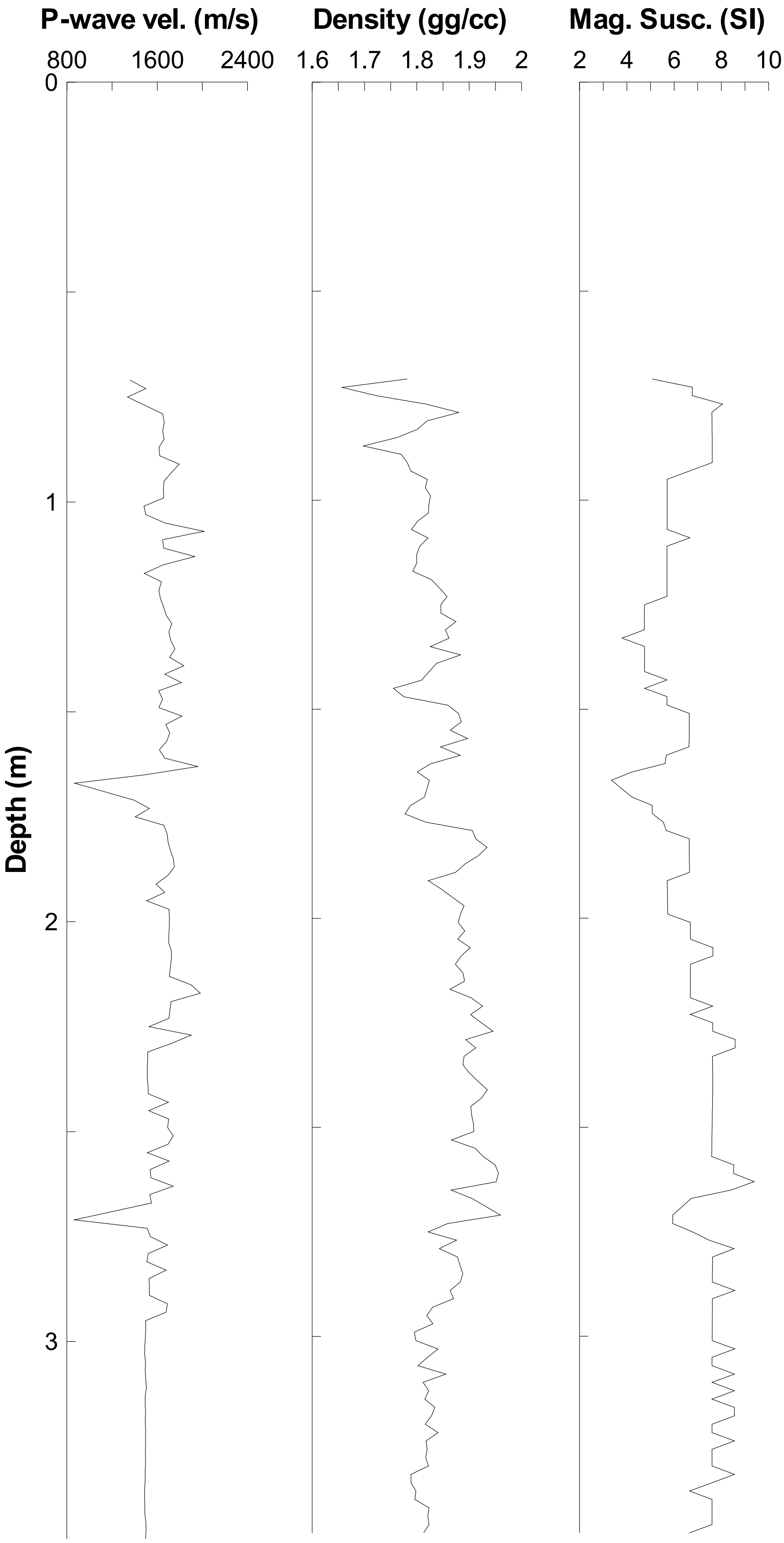


MST data of core GeoB9018-1

Core description, MST data and colour scanner data of core GeoB9019-1

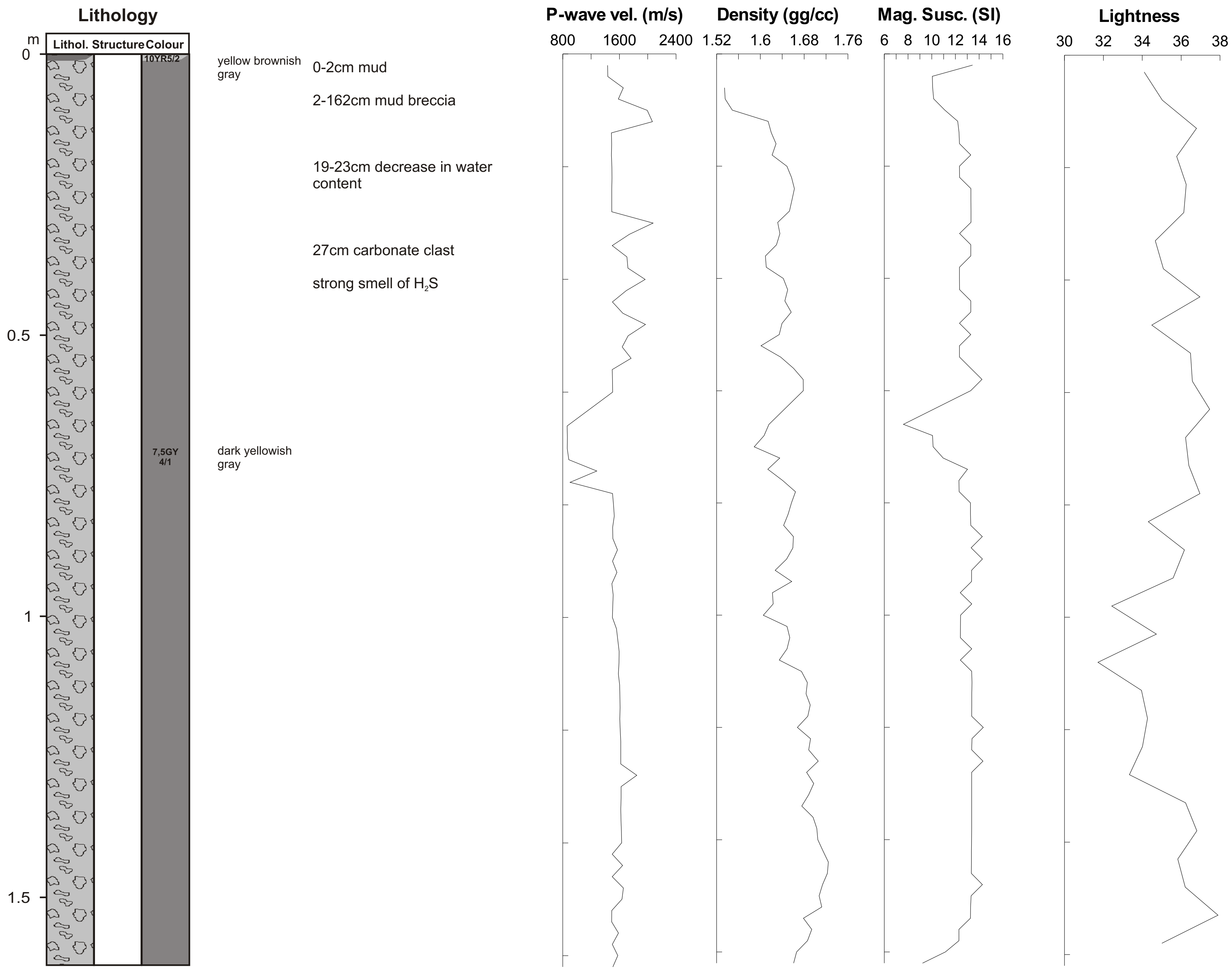


**GeoB 9019-1**

Date: 02.12.03 Pos: 36°11.18'N 7°19.15'W

Water Depth: 767 m Core Length: 162 cm

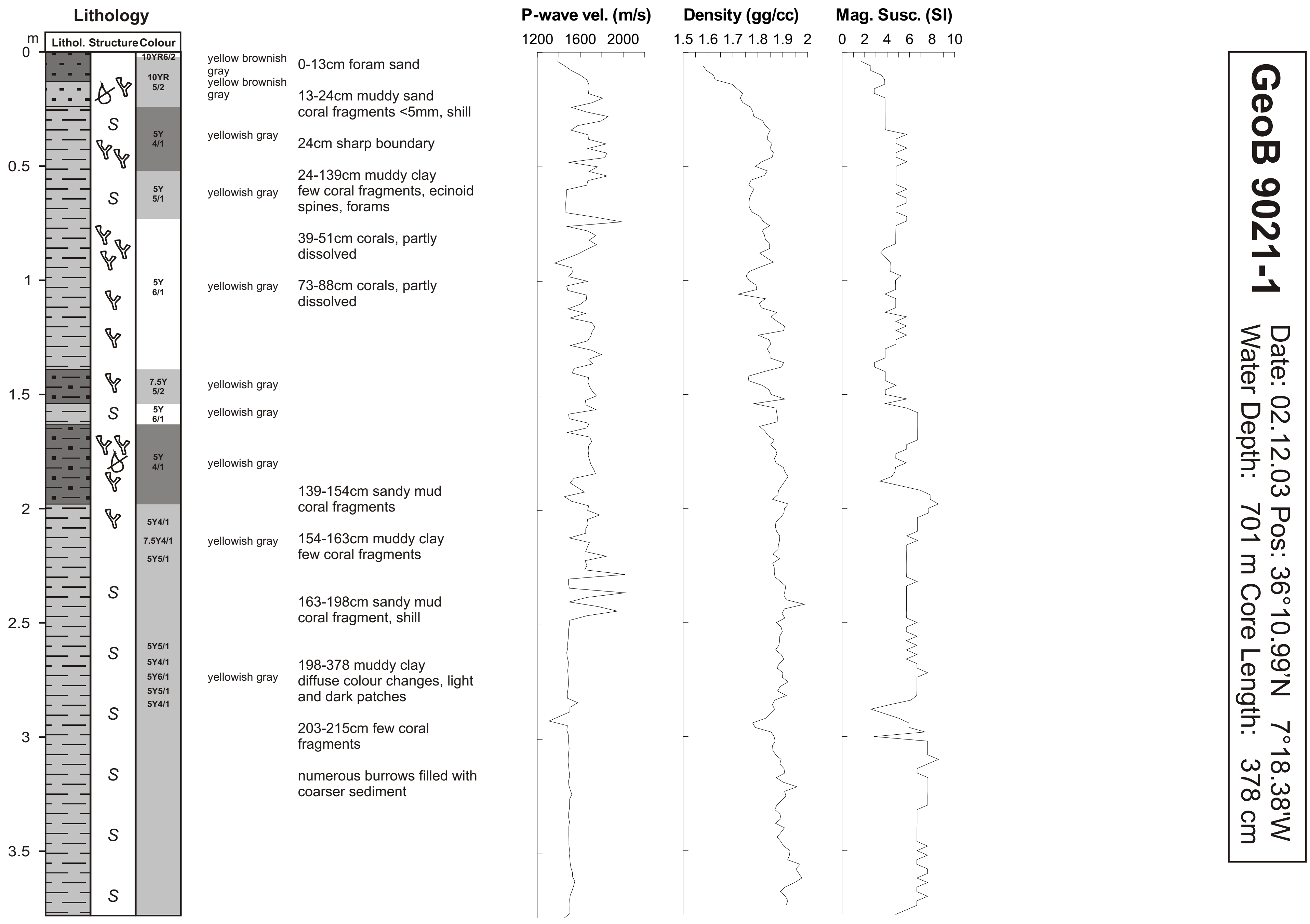


Core description, MST data and colour scanner data of core GeoB9021-1

**GeoB 9031-1** Date: 04.12.03 Pos: 36°5.750'N 7°23.28'W
Water Depth: 897 m Core Length: 484 cm

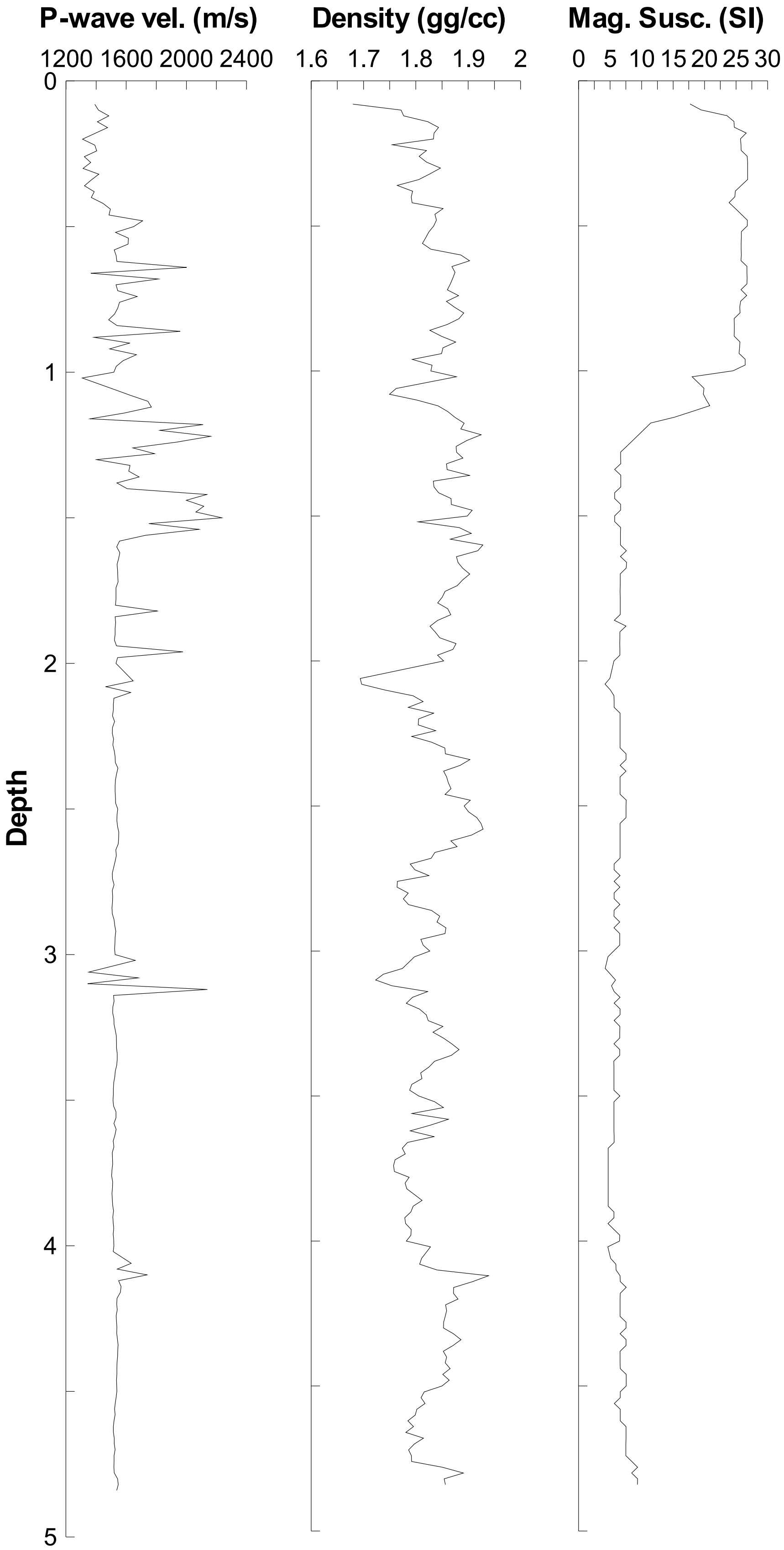


MST data of core GeoB9031-1

**GeoB 9032-1** Date: 04.12.03 Pos: 36°5.55'N 7°23.57'W
Water Depth: 843 m Core Length: 220 cm

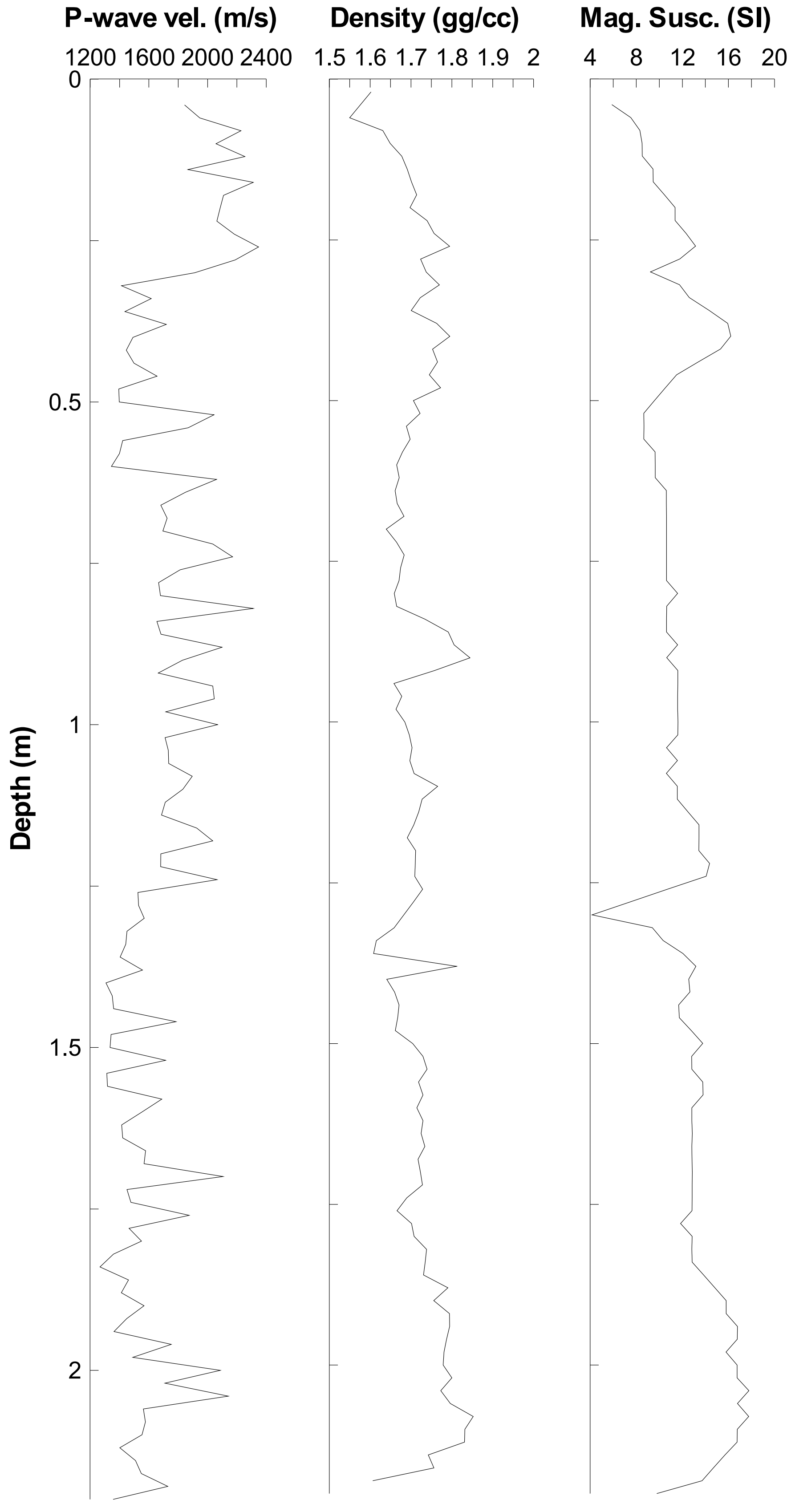


MST data of core GeoB9032-1

Core description, MST data and colour scanner data of core GeoB9037-1

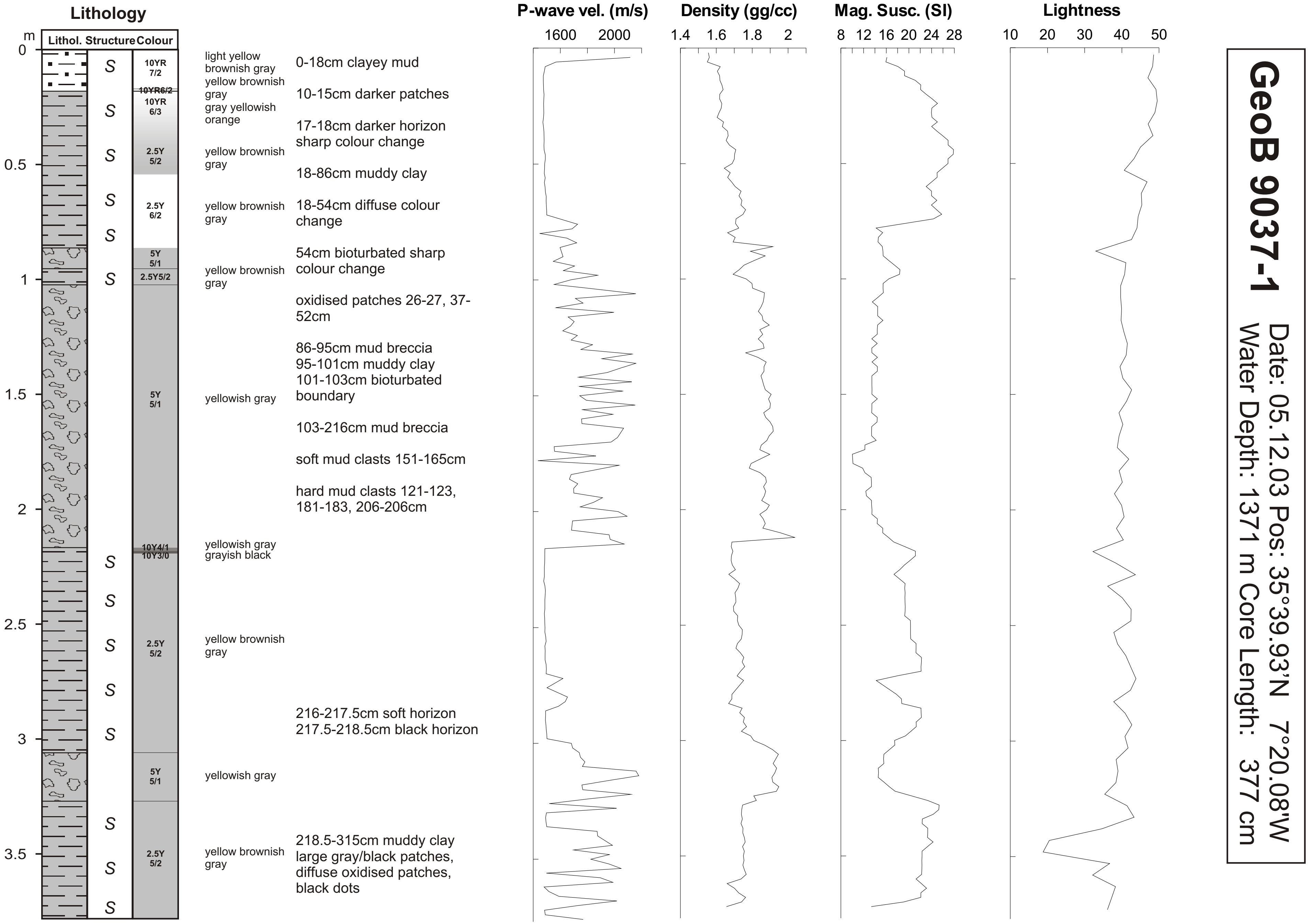

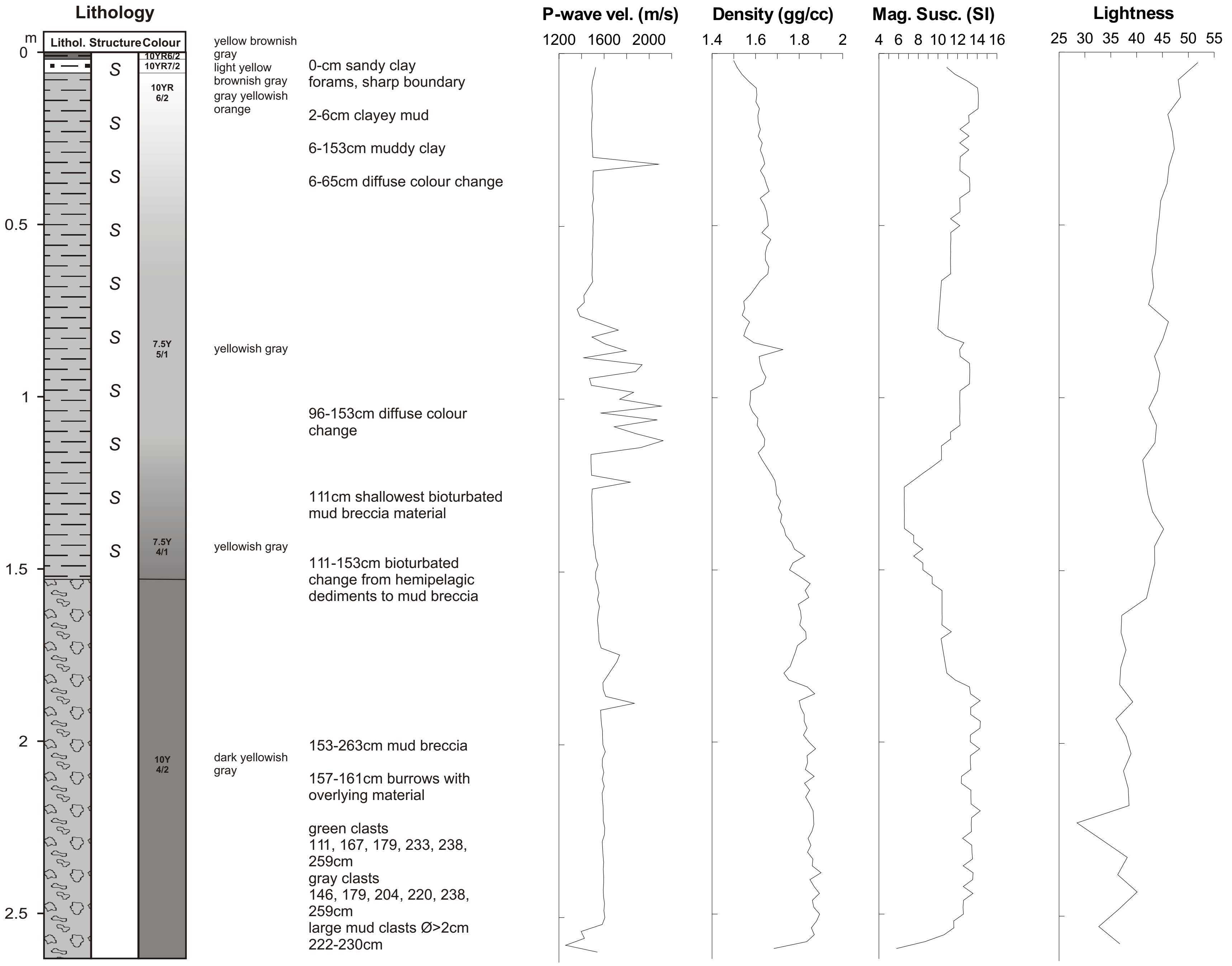


Core description, MST data and colour scanner data of core GeoB9038-1

**GeoB 9038-1**

Date: 05.12.03 Pos: 35°39.30'N 7°16.52'W

Water Depth: 1313 m Core Length: 263 cm

Core description, MST data and colour scanner data of core GeoB9039-1

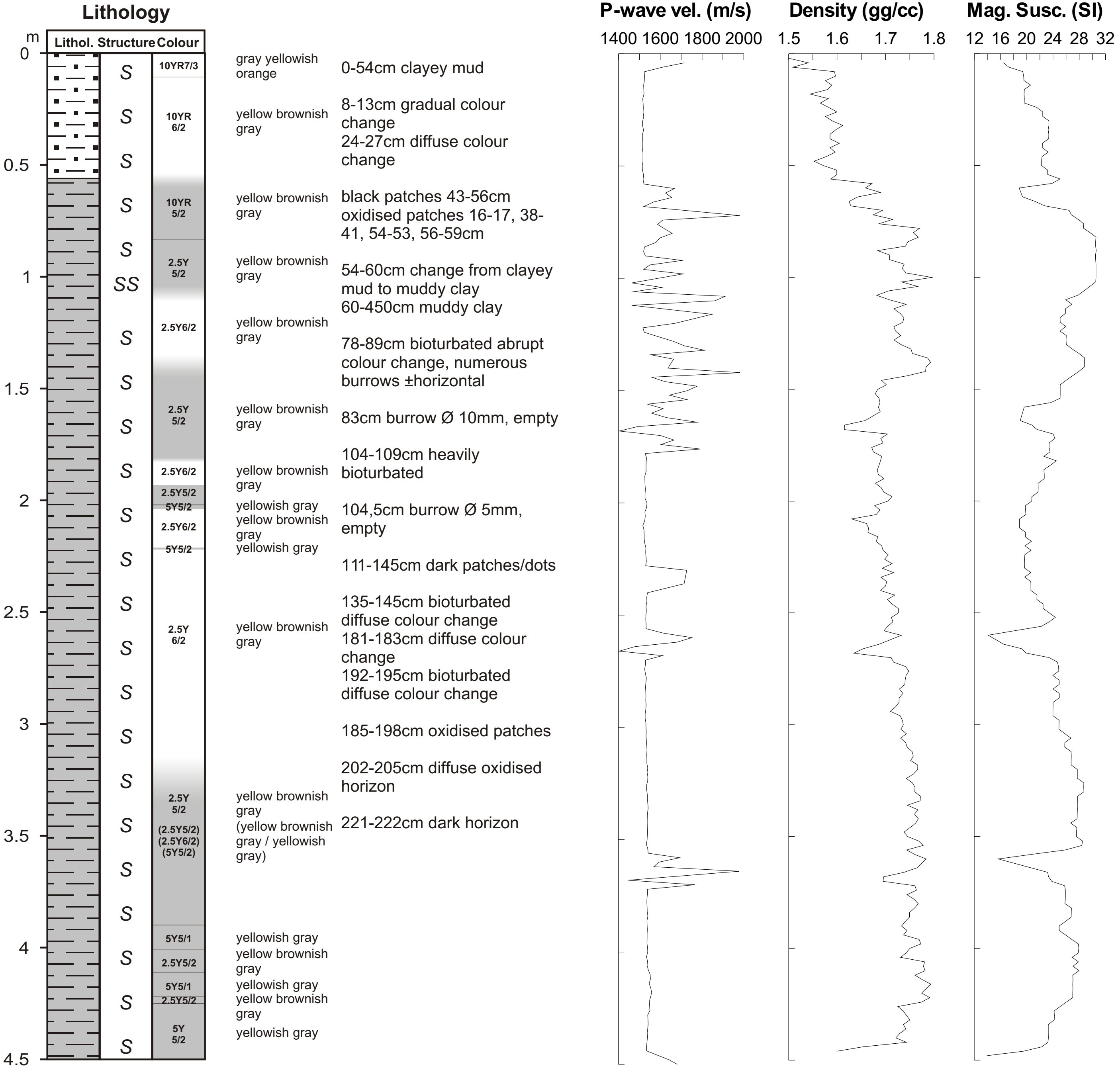


**GeoB 9039-1**

Date: 05.12.03 Pos: 35°41.21'N 7°16.52'W

Water Depth: 1331 m Core Length: 450 cm

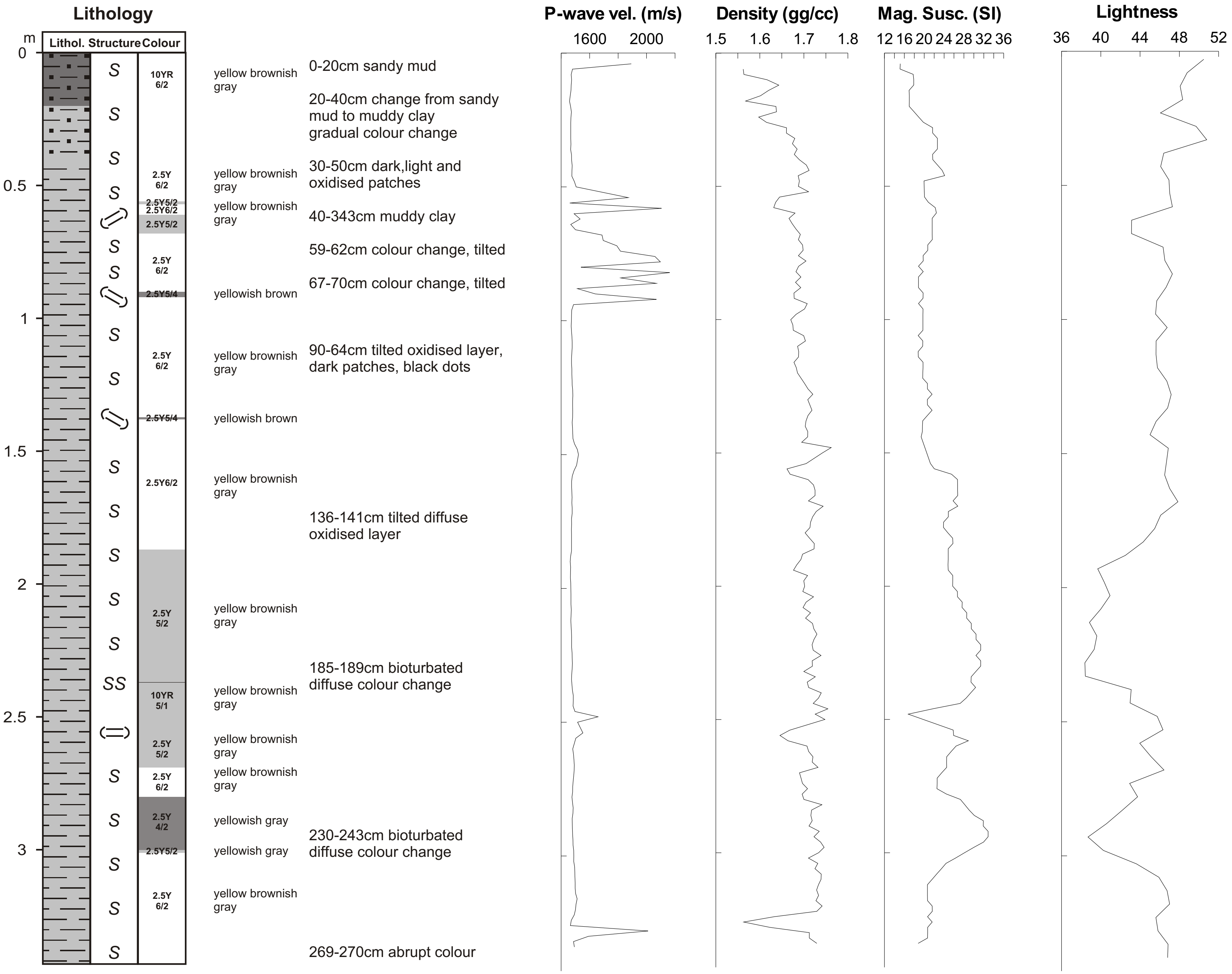


**GeoB 9040-1**

Date: 05.12.03 Pos: 35°39.56'N 7°23.38'W

Water Depth: 1380 m Core Length: 343 cm

Core description, MST data and colour scanner data of core GeoB9040-1

Core description and colour scanner data of core GeoB9041-1

# GeoB 9041-1

Date: 05.12.03 Pos: 35°39.70'N 7°19.97'W
Water Depth: 1316 m Core Length: 235 cm

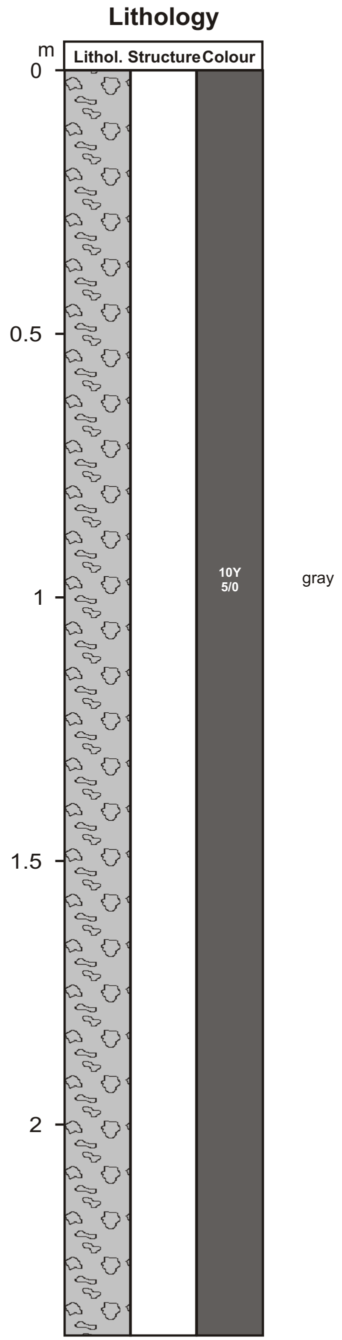


0-240cm homogenious mud breccia with gas hydrates

clasts >10mm at 14, 44, 91, 136, 161, 146, 180, 212, 221cm

holes >20mm at 15, 44, 60, 65-70, 94, 106, 110, 144-148, 174-180, 190-197, 207-210, 218-223cm

Core description, MST data and colour scanner data of core GeoB9045-2

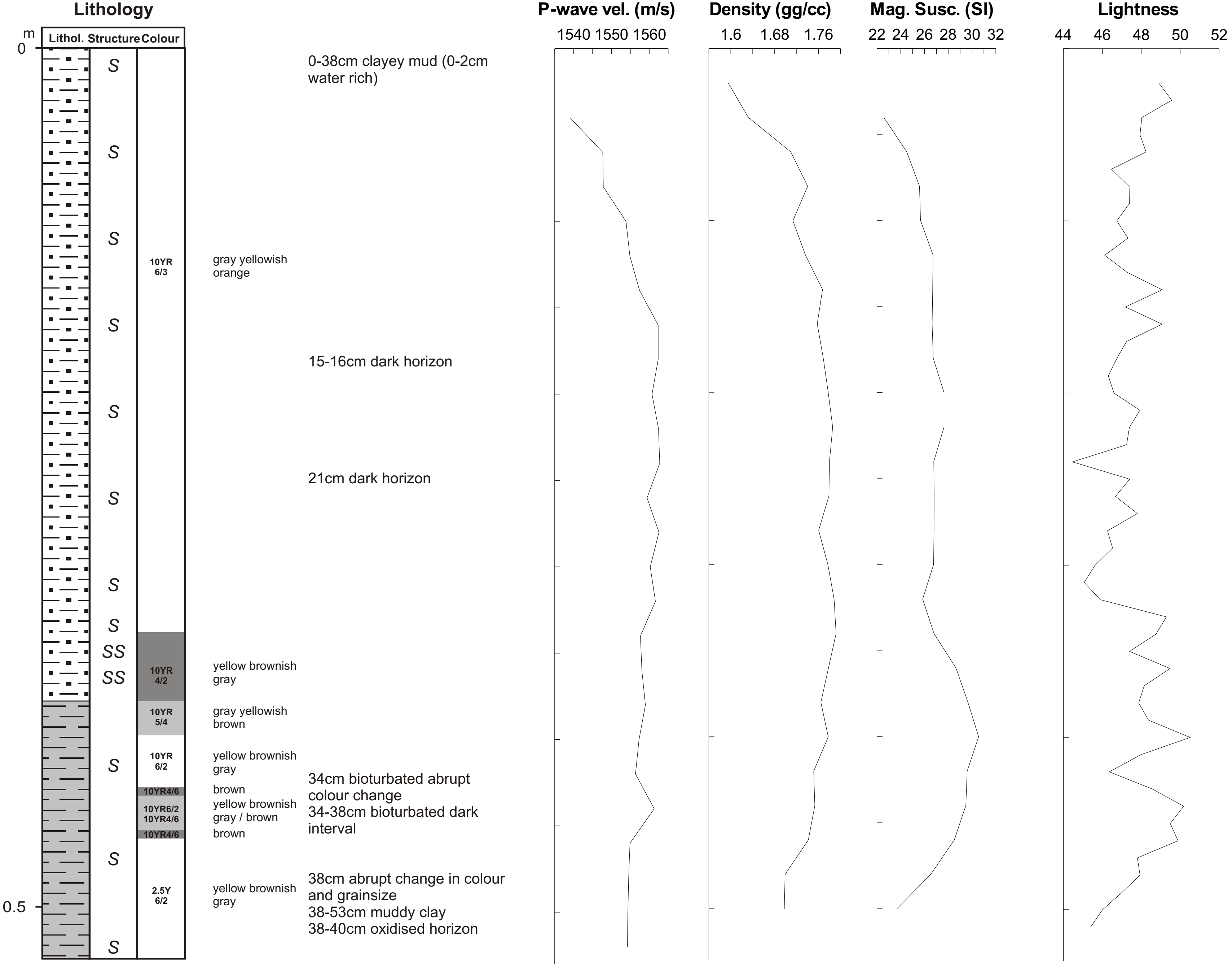


**GeoB 9045-2**
Date: 07.12.03 Pos: 35°29.60'N 9°33.43'W
Water Depth: 3951 m Core Length: 53 cm

Core description, MST data and colour scanner data of core GeoB9051-2

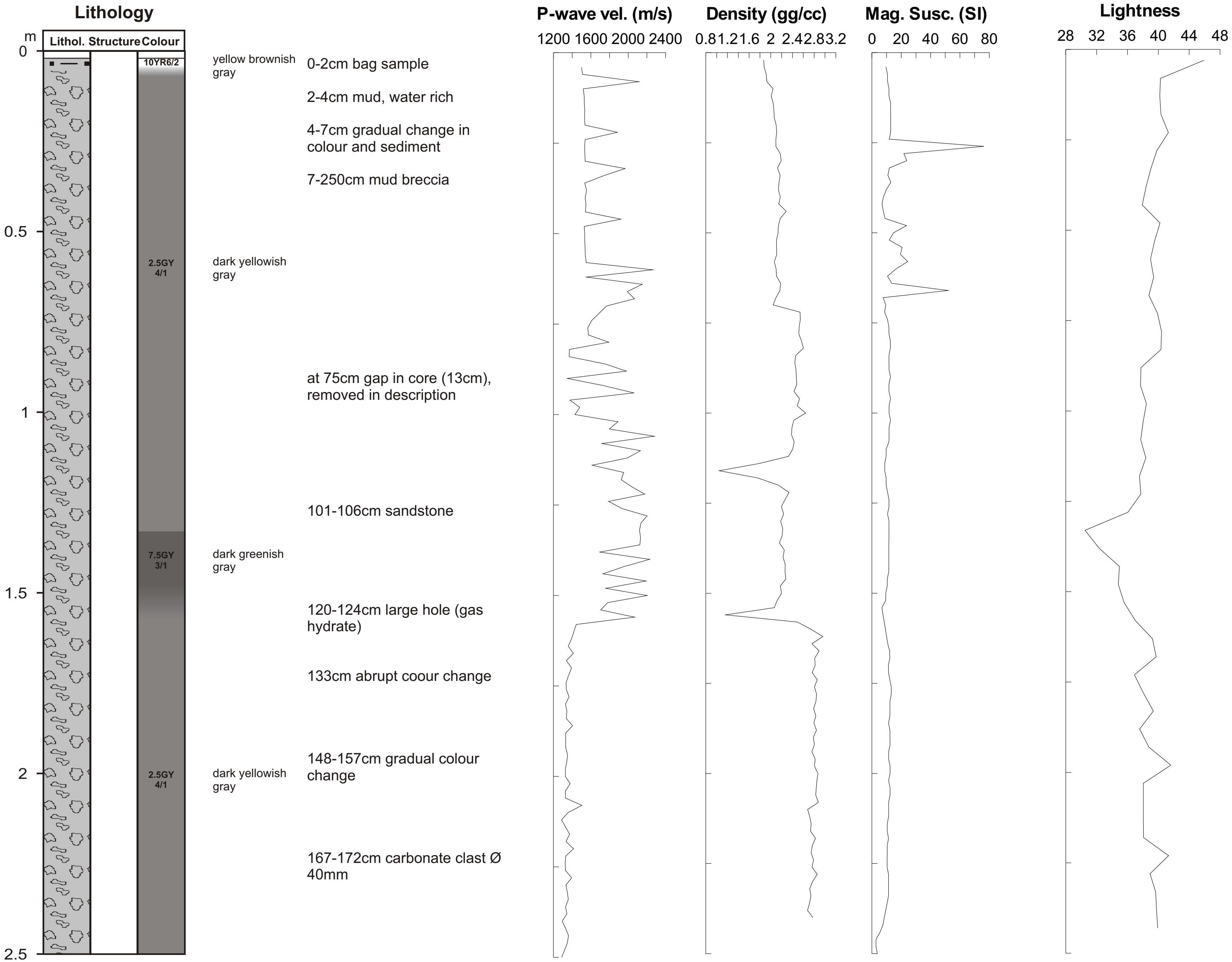


**GeoB 9051-2**

Date: 09.12.03 Pos: 35°27.61'N 9°00.03'W

Water Depth: 3087m Core Length: 263 cm

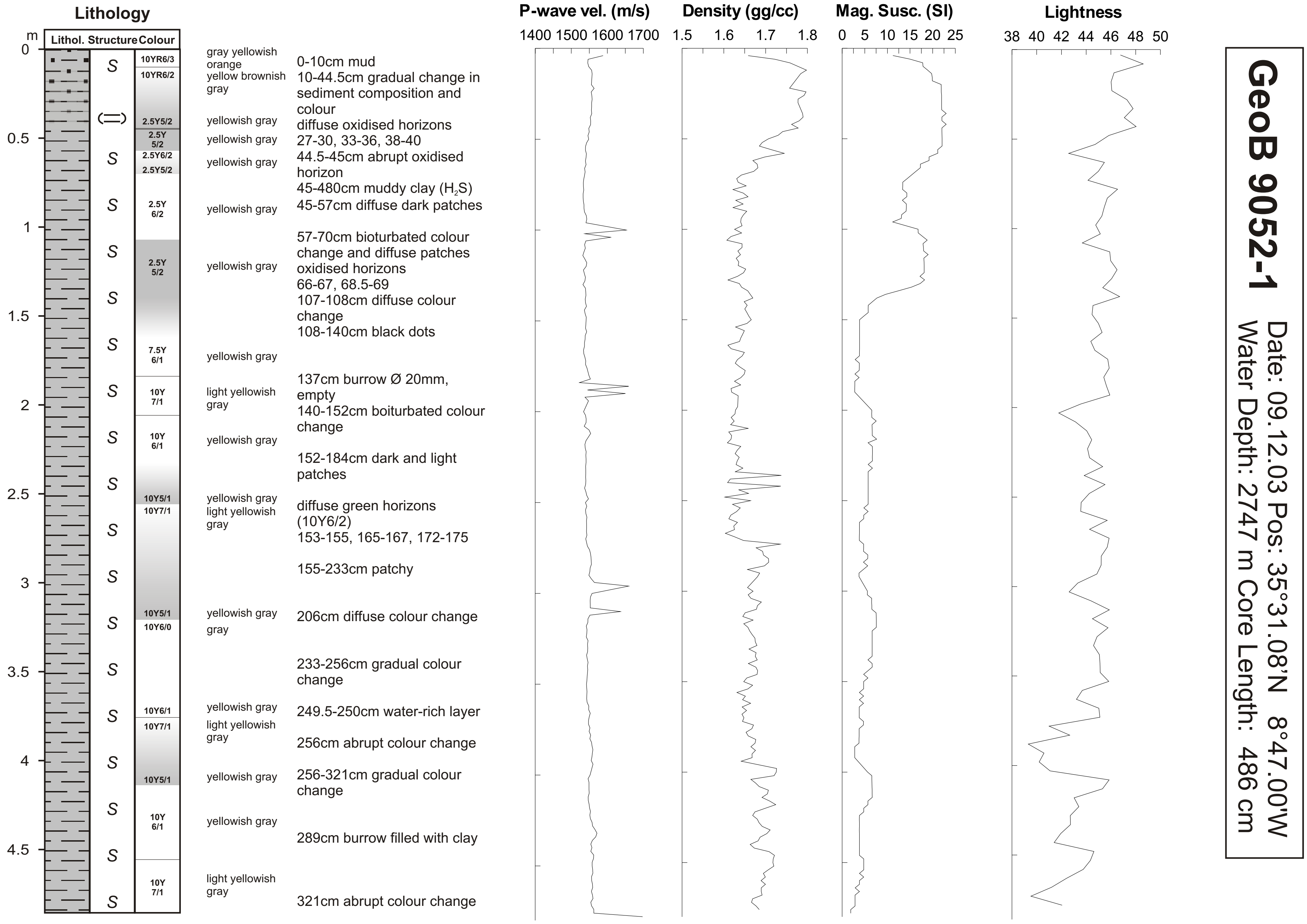


Core description, MST data and colour scanner data of core GeoB9052-1

Core description, MST data and colour scanner data of core GeoB9052-2

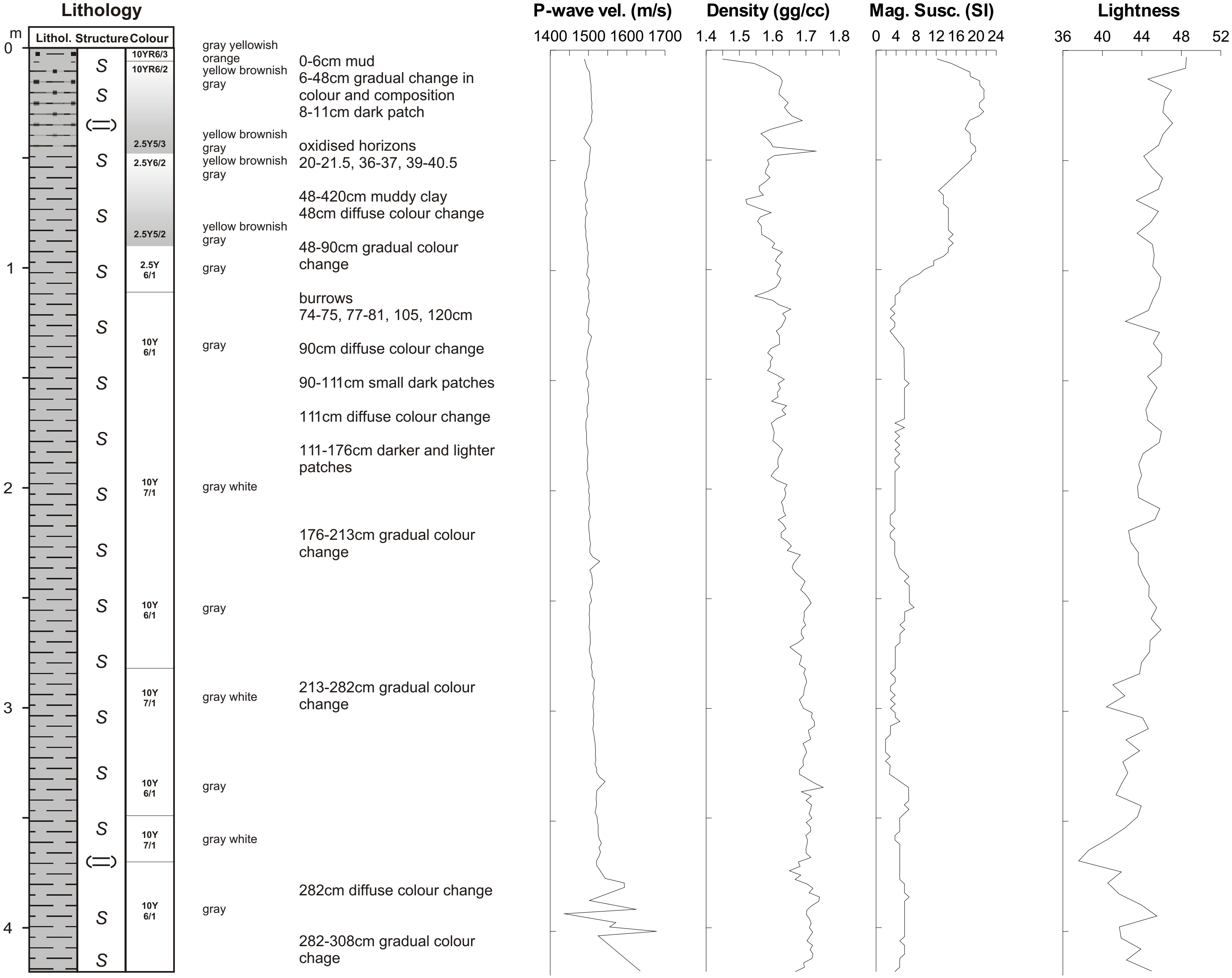


**GeoB 9052-2**

Date: 09.12.03 Pos: 35°31.12'N 8°47.01'W

Water Depth: 2753 m Core Length: 420 cm

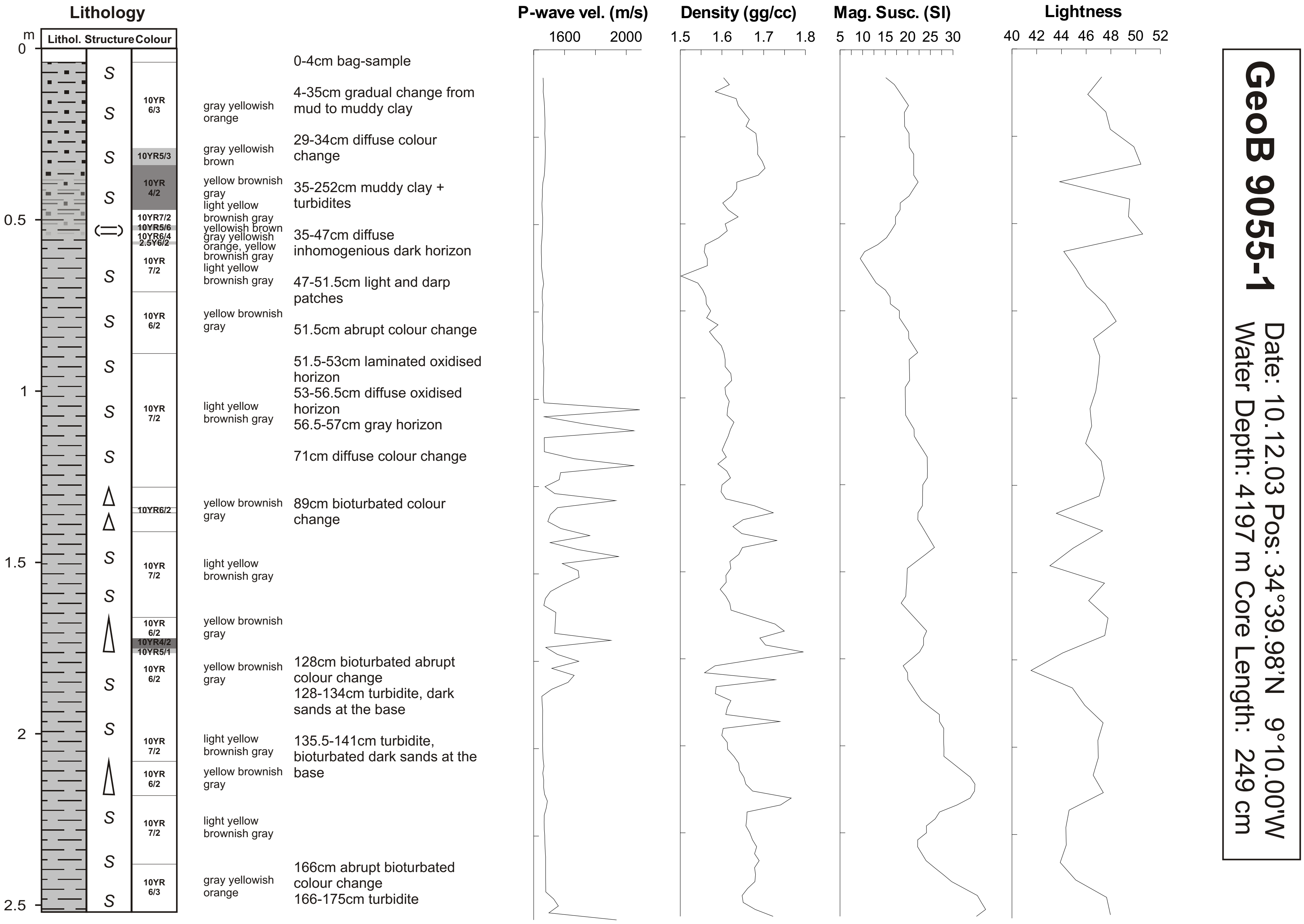


Core description, MST data and colour scanner data of core GeoB9055-1

**GeoB 9061-1**

Date: 12.12.03 Pos: 35°22.42'N 7°05.29'W

Water Depth: 911 m Core Length: 154 cm

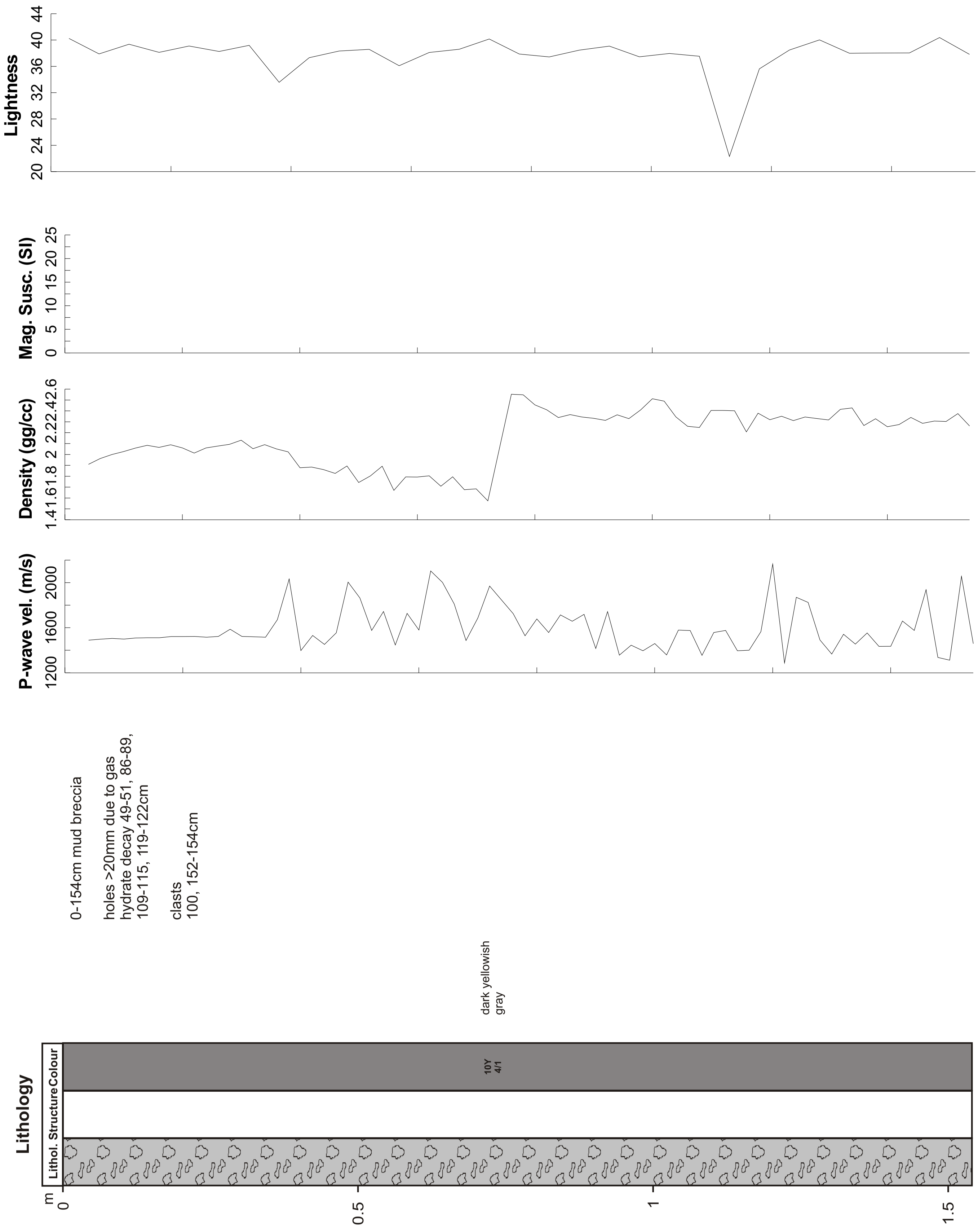


Core description, MST data and colour scanner data of core GeoB9061-1

Core description, MST data and colour scanner data of core GeoB9063-1

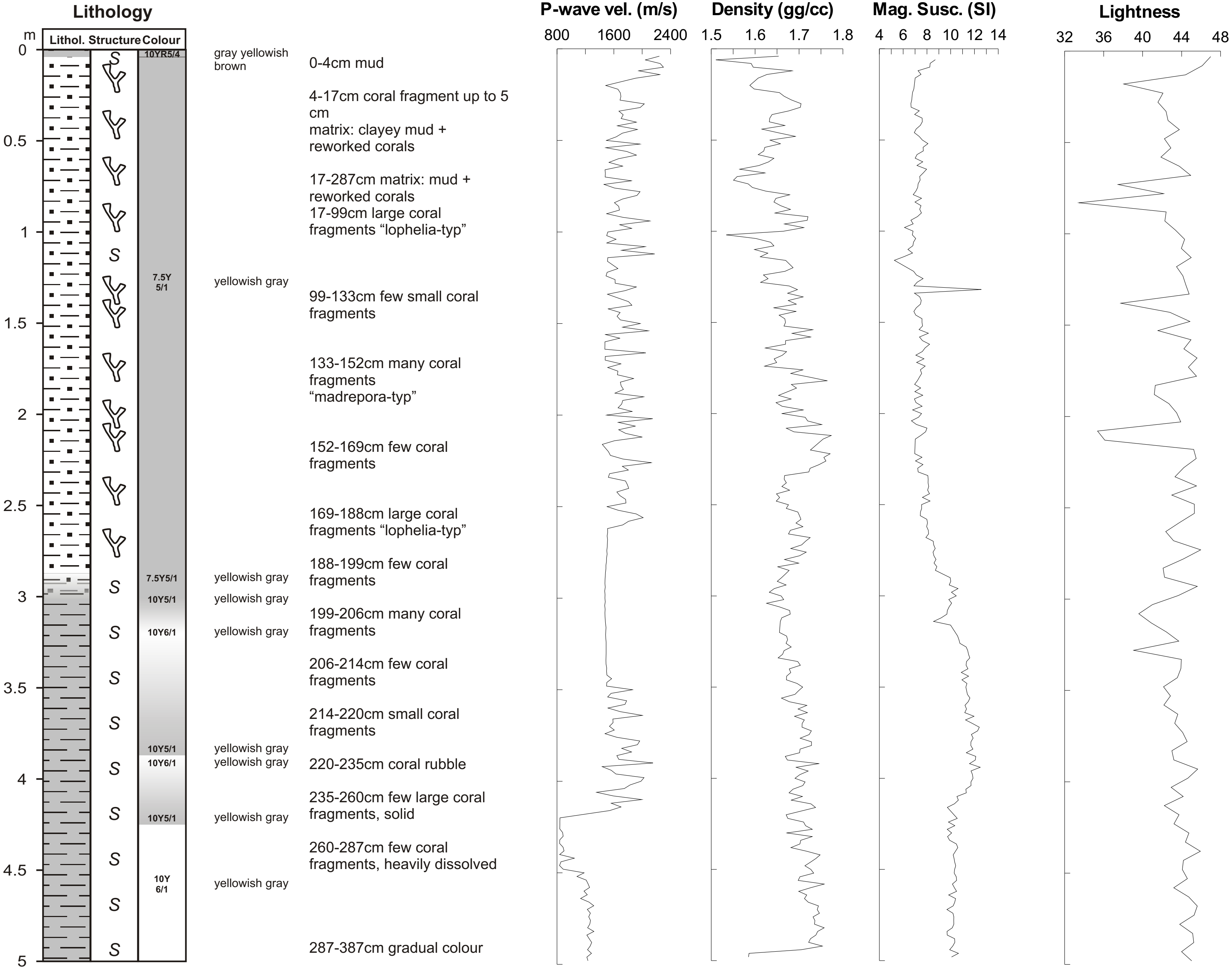


**GeoB 9063-1**

Date: 13.12.03 Pos: 35°21.99'N 6°51.99'W

Water Depth: 599 m Core Length: 500 cm

Core description, MST data and colour scanner data of core GeoB9064-1

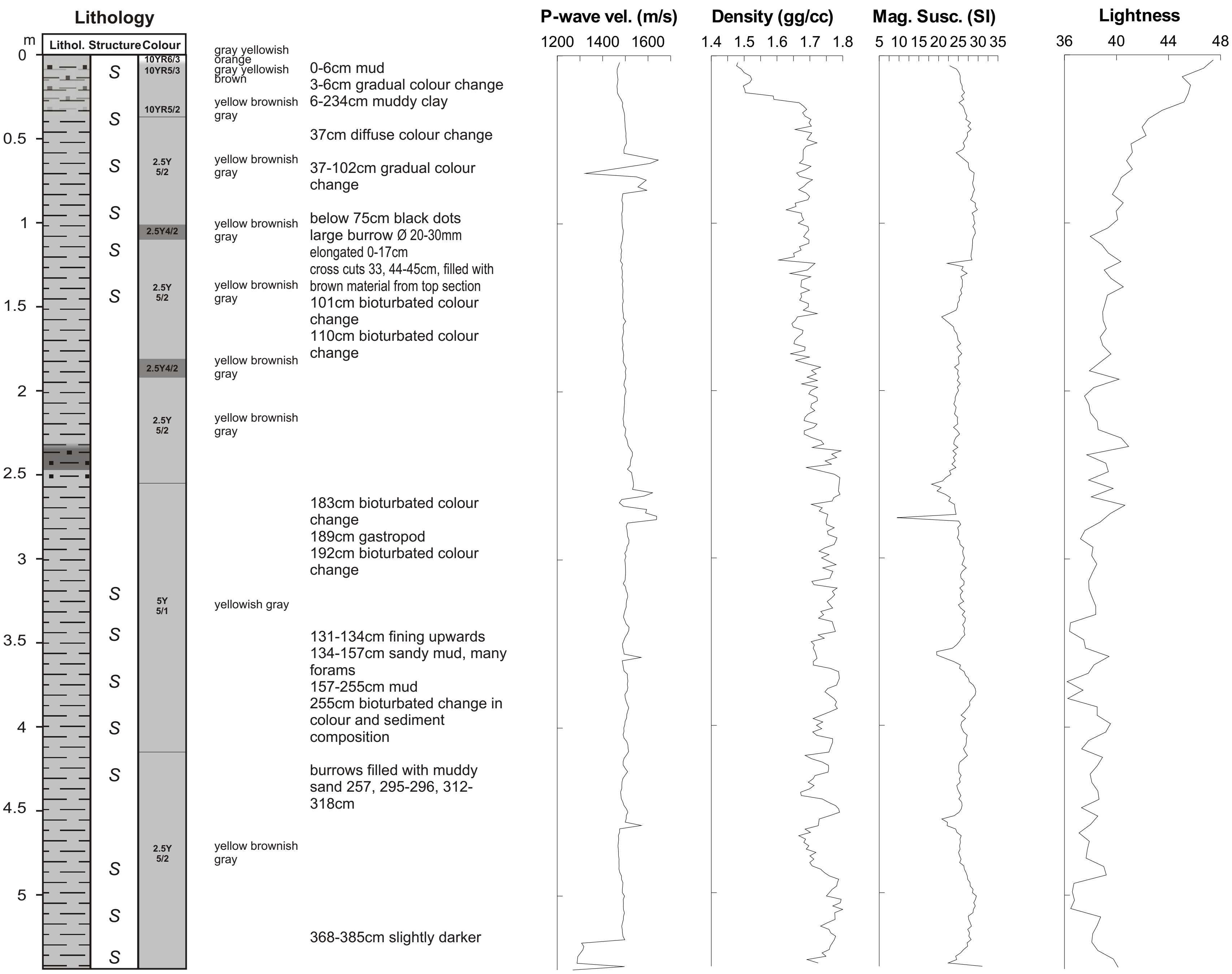


**GeoB 9064-1**

Date: 13.12.03 Pos: 35°24.91'N 6°50.72'W

Water Depth: 700 m Core Length: 544 cm

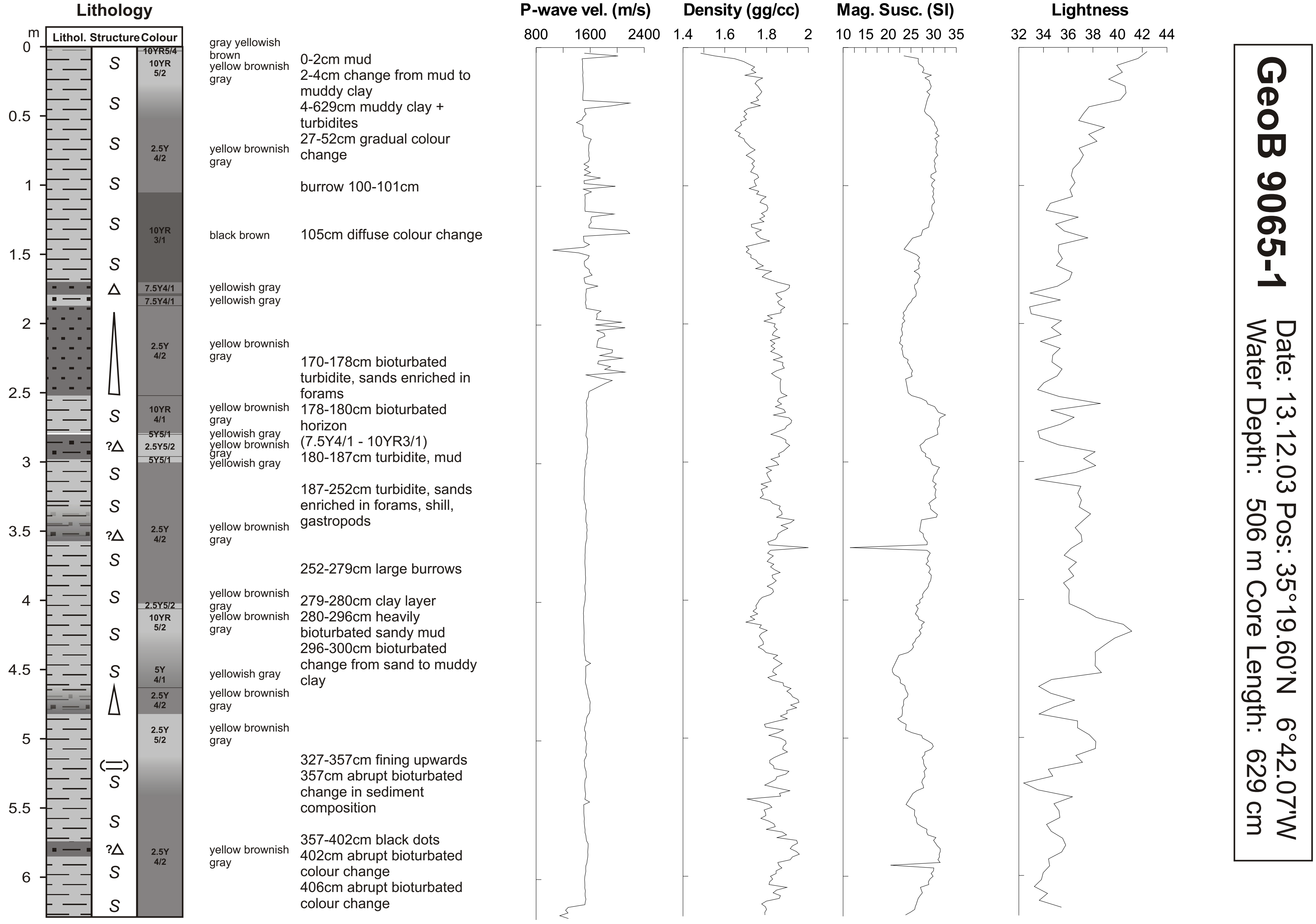


Core description, MST data and colour scanner data of core GeoB9065-1

Core description, MST data and colour scanner data of core GeoB9066F-1

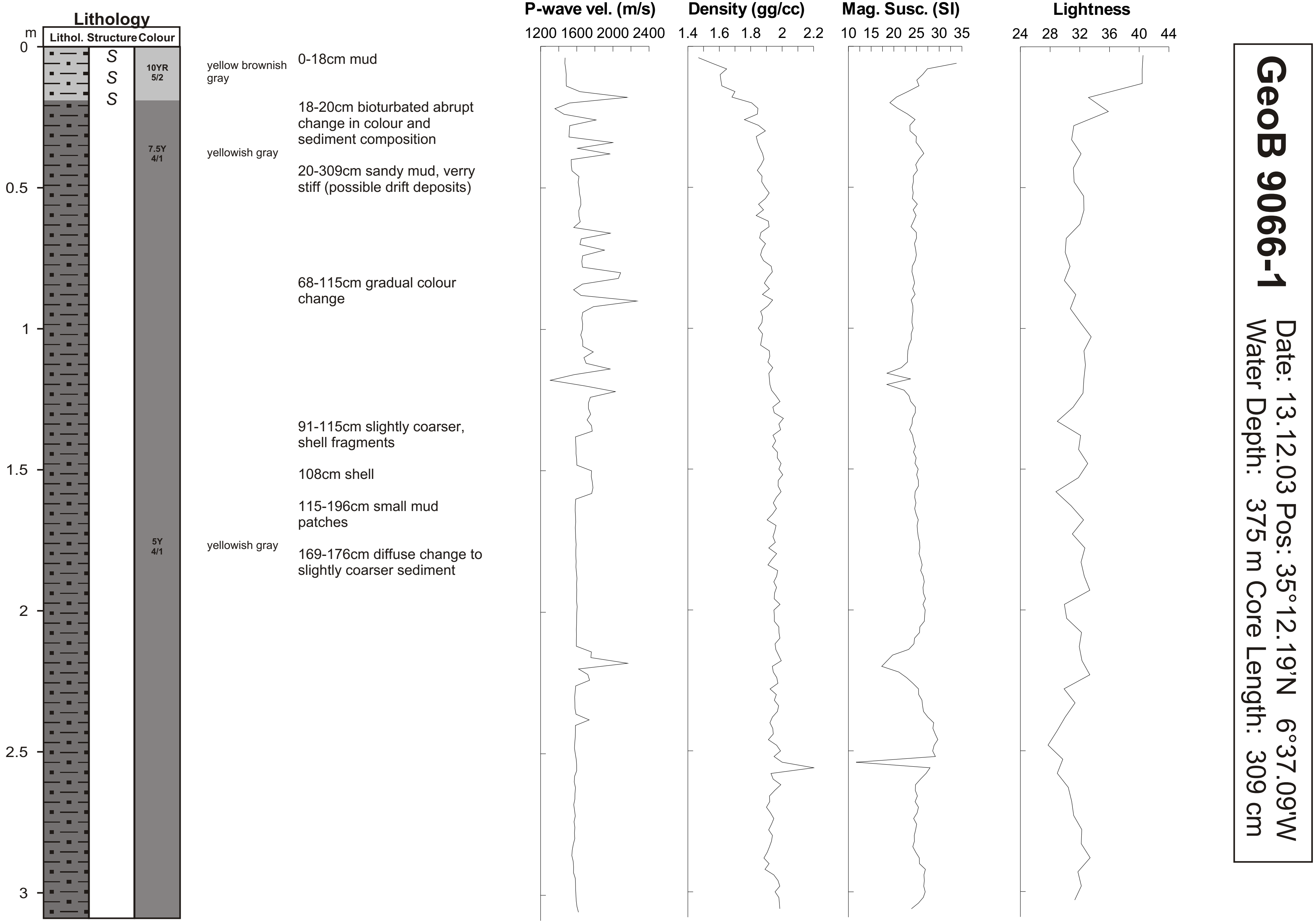

Core description, MST data and colour scanner data of core GeoB9067-1

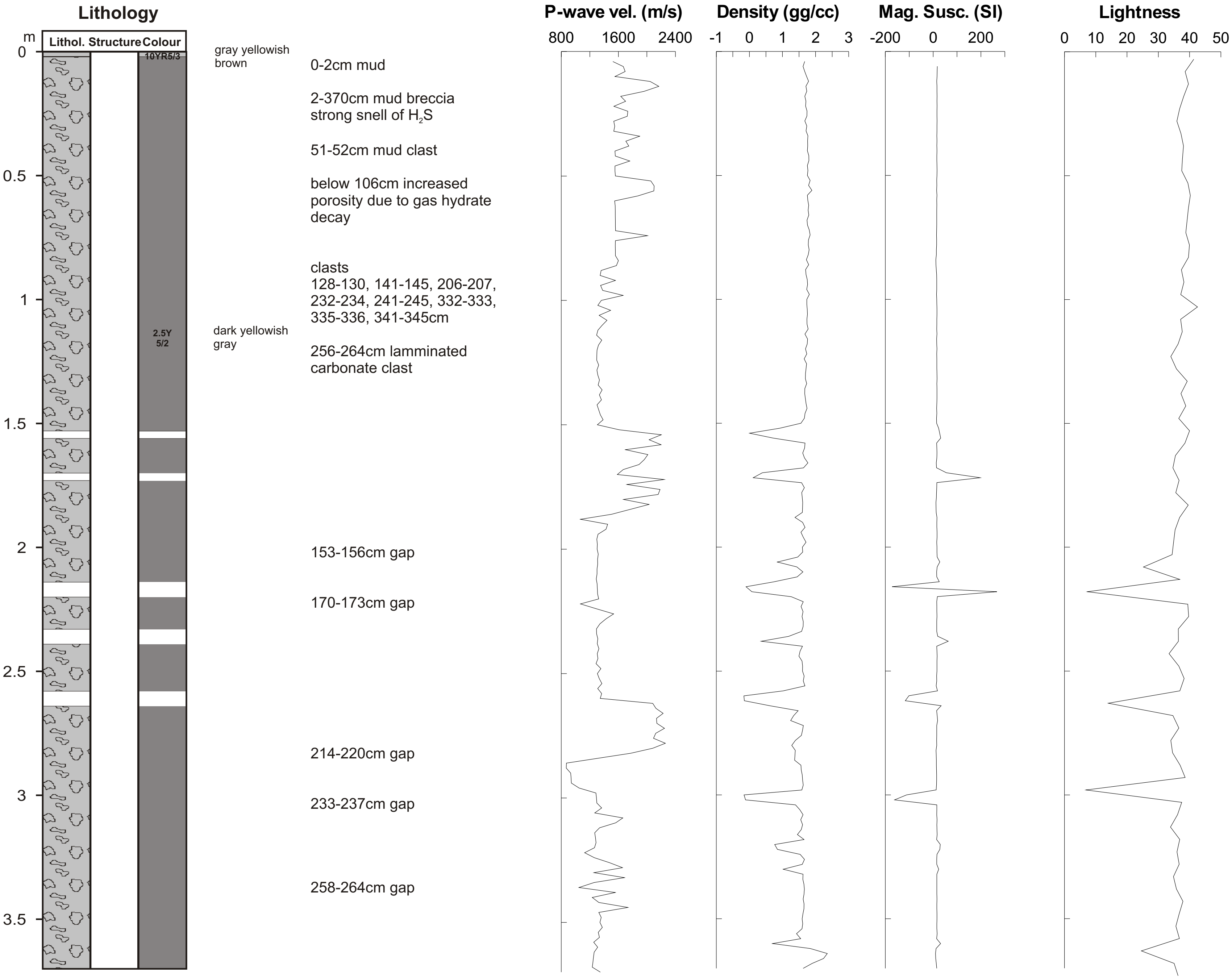


**GeoB 9067-1**

Date: 13.12.03 Pos: 35°16.92'N 6°45.47'W

Water Depth: 434 m Core Length: 370 cm

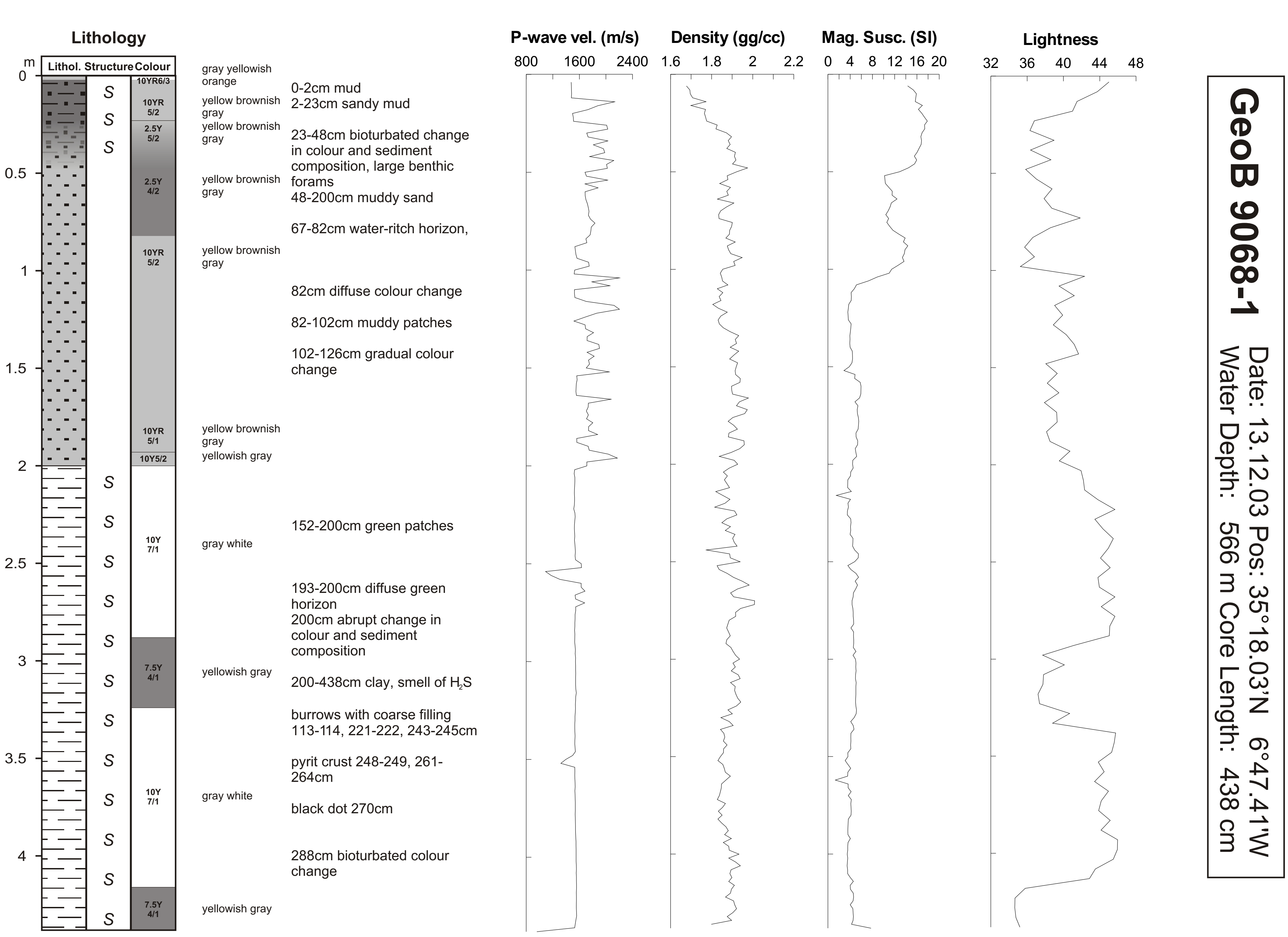


Core description, MST data and colour scanner data of core GeoB9068-1

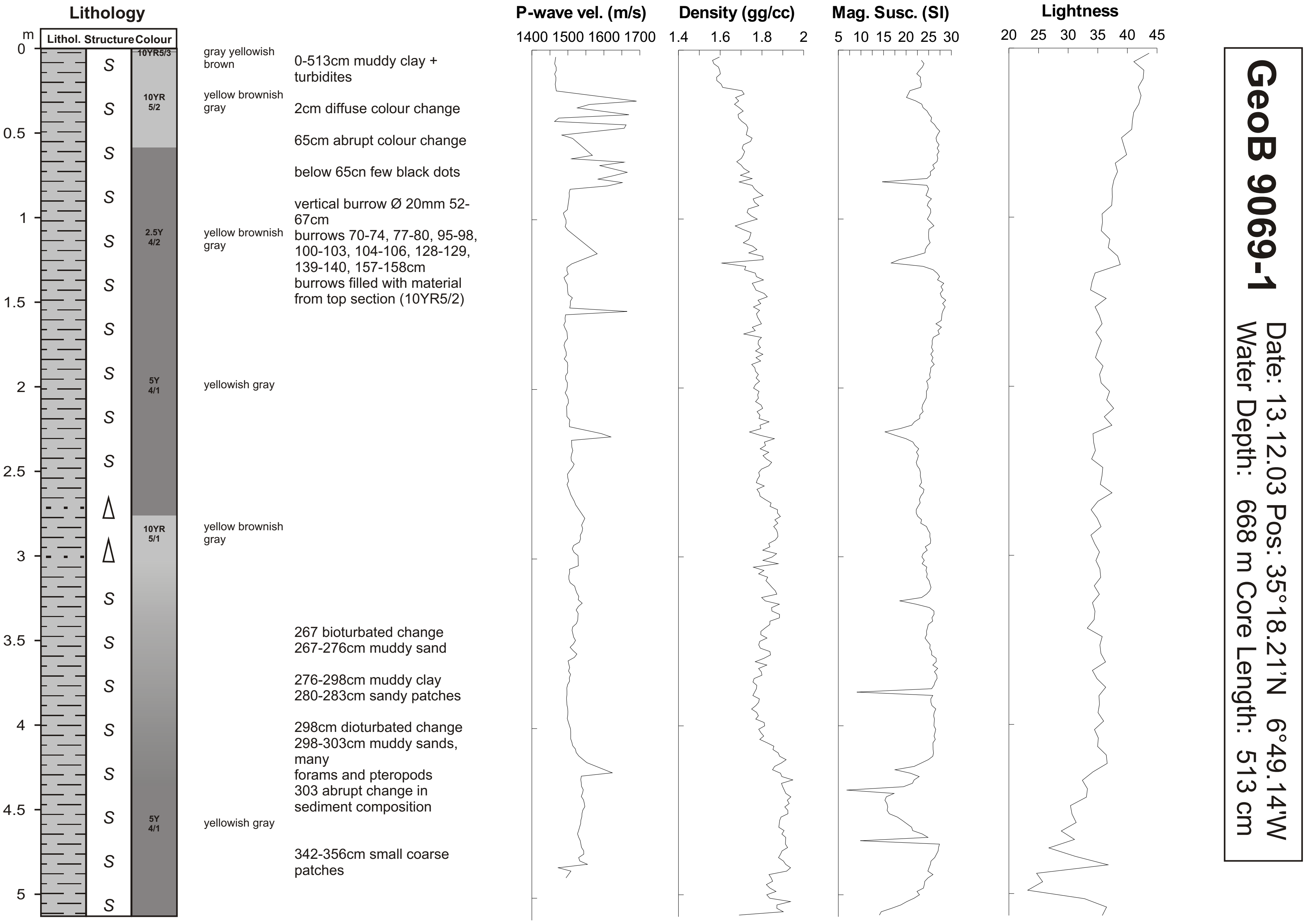


Core description, MST data and colour scanner data of core GeoB9069F-1

**GeoB 9070-1** Date: 13.12.03 Pos: 35°22.00'N 06°51.90'W
Water Depth: 594 m Core Length: 600 cm

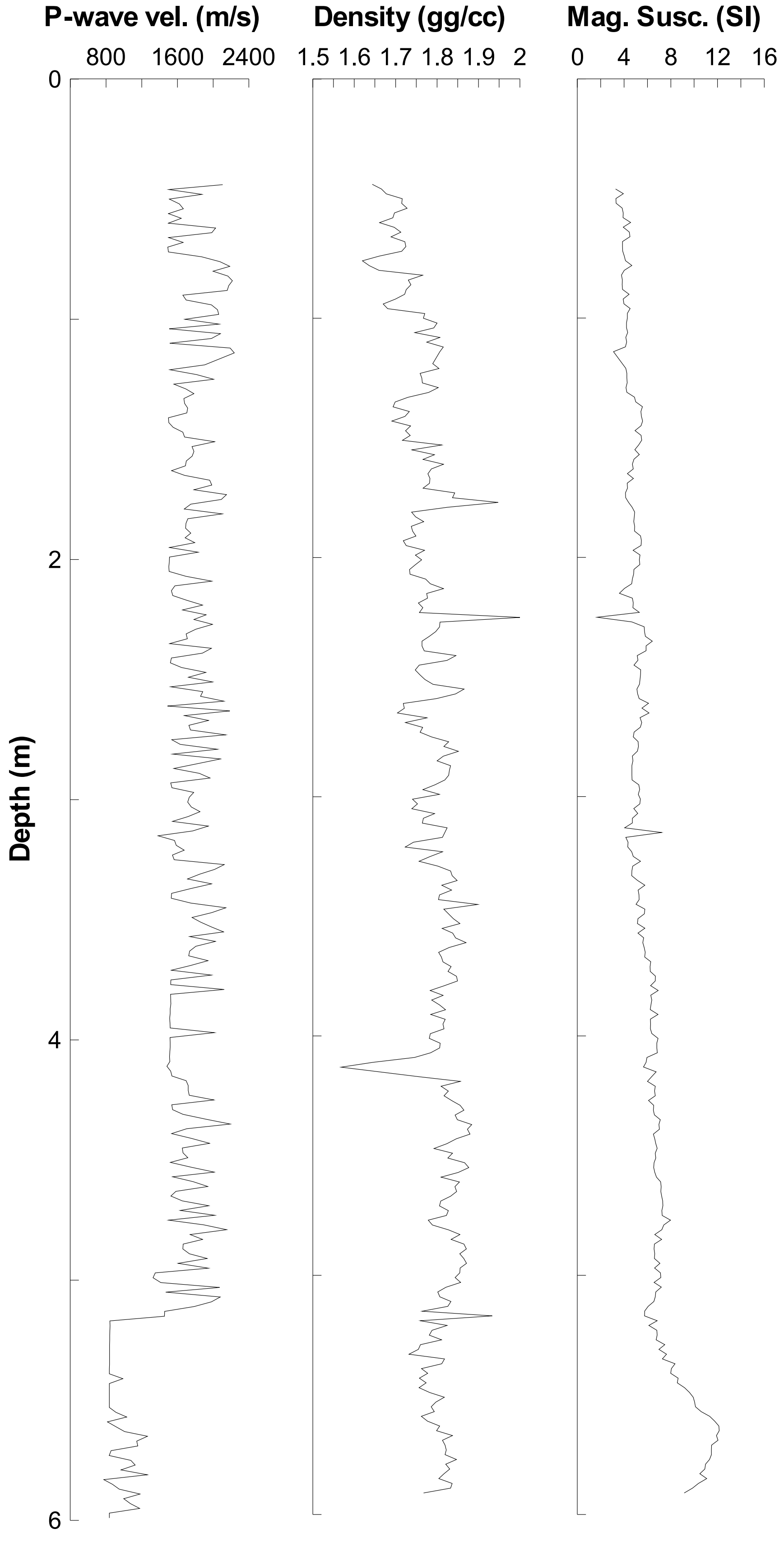


MST data of core GeoB9070-1

Core description, MST data and colour scanner data of core GeoB9085-1

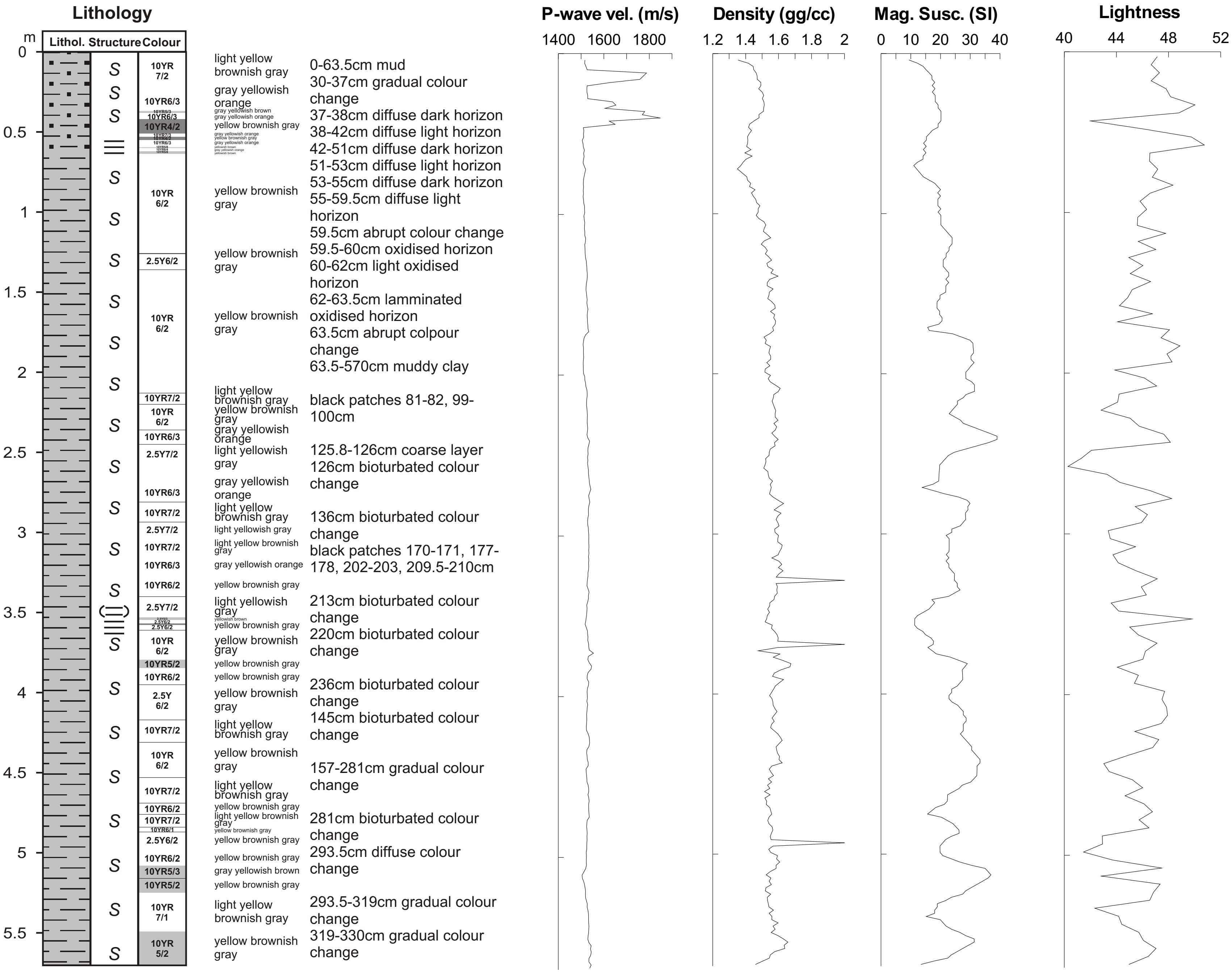


**GeoB 9085-1**

Date: 17.12.03 Pos: 34°49.13'N 8°51.70'W

Water Depth: 3442 m Core Length: 570 cm

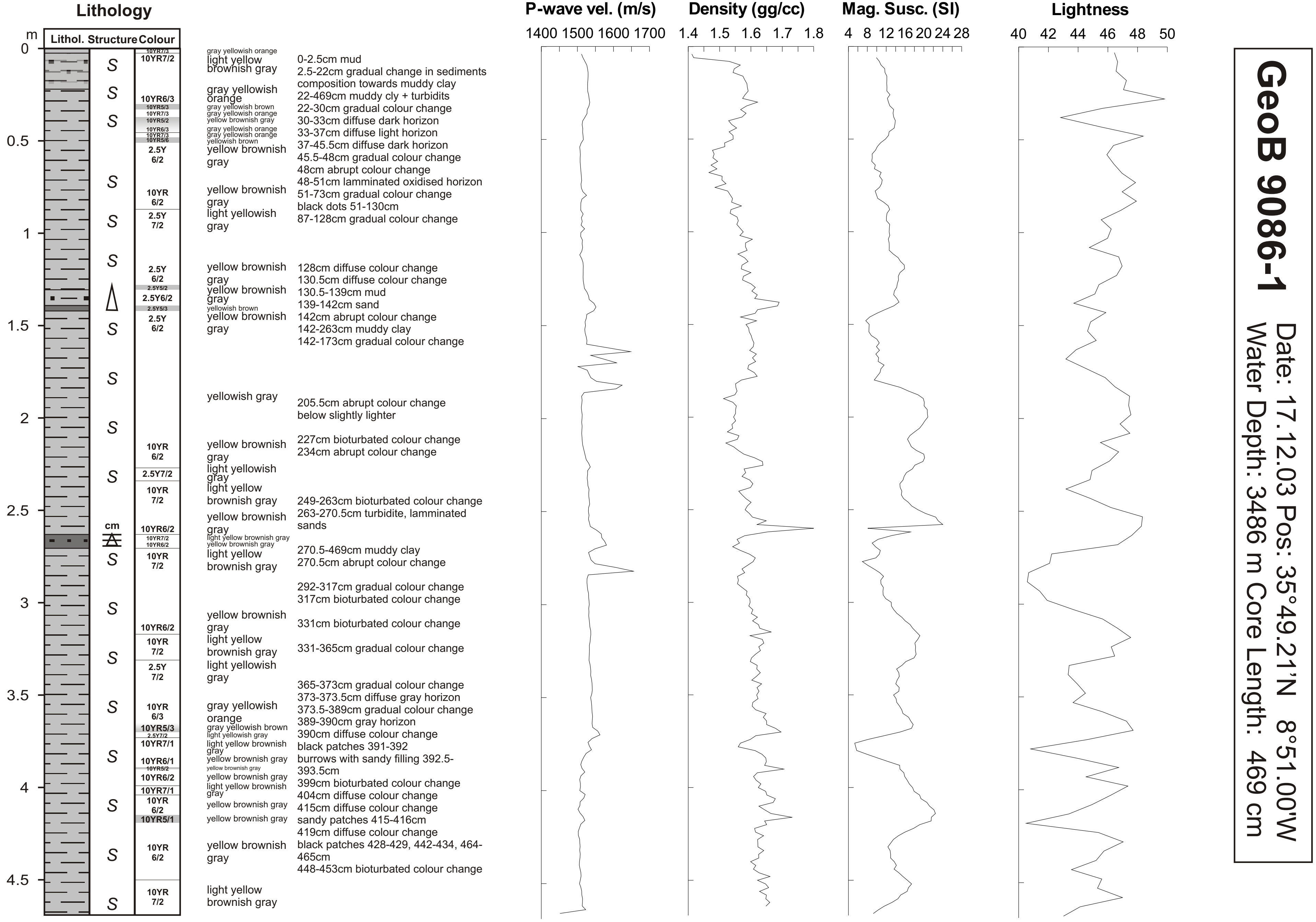


Core description, MST data and colour scanner data of core GeoB9086-1

**GeoB 9091-1**

Date: 19.12.03 Pos: 35°50.02'N 10°08.72'W
Water Depth: 3921 m Core Length: 347 cm

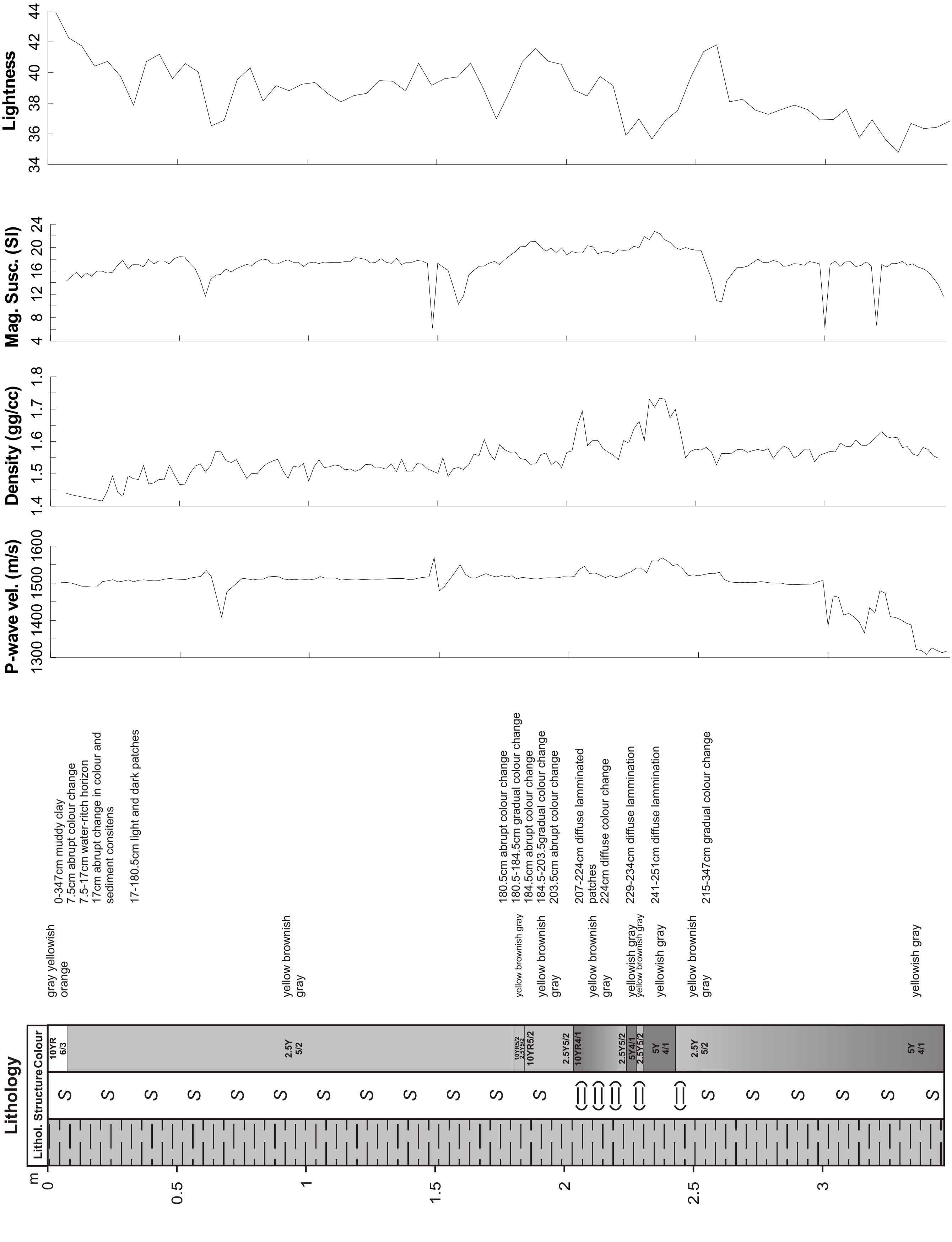


Core description, MST data and colour scanner data of core GeoB9091-1

Core description, MST data and  colour scanner data of core GeoB9092-1

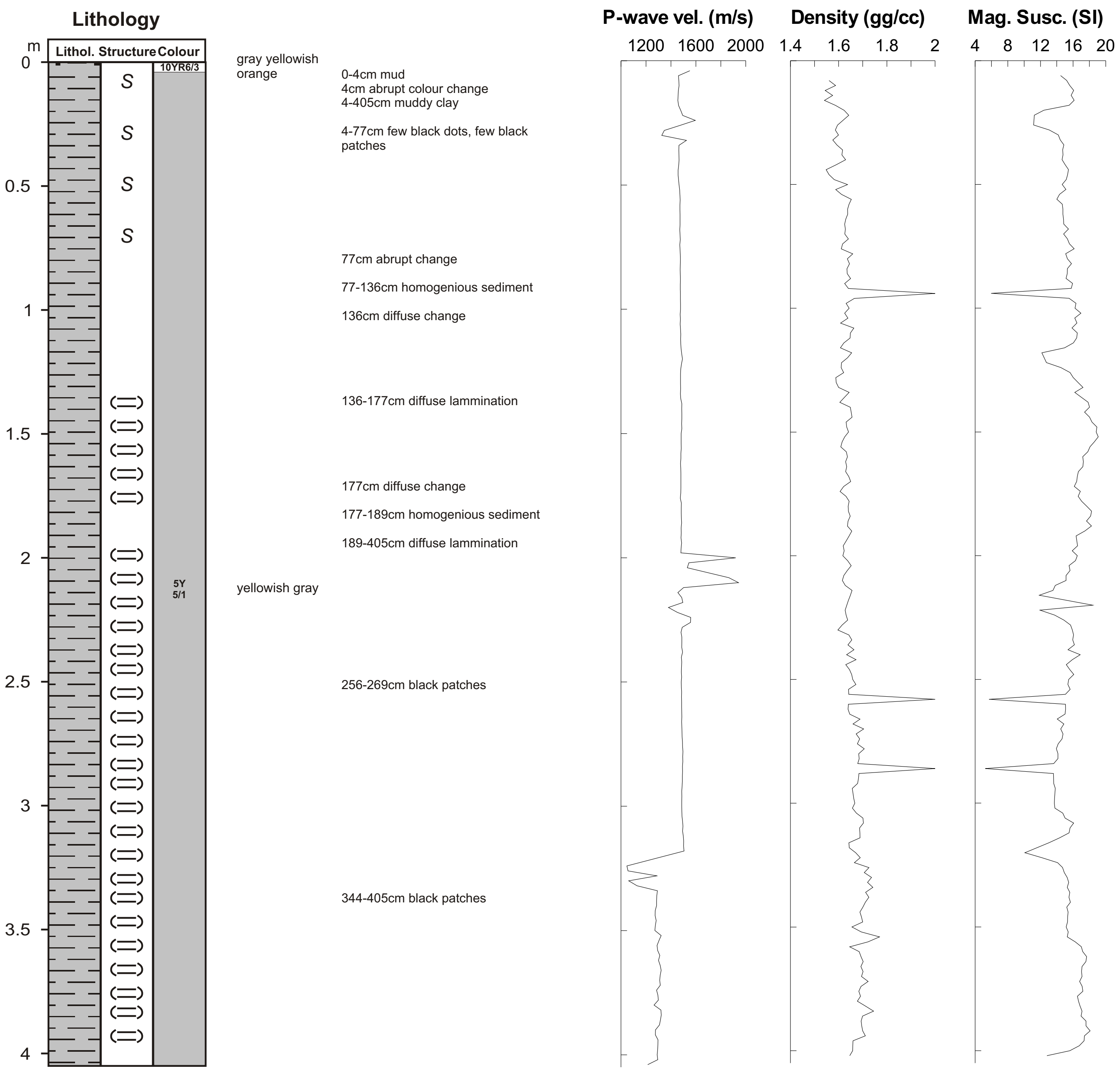


**GeoB 9092-1**

Date: 19.12.03 Pos: 36°47.99'N 10°04.00'W
Water Depth: 3230 m Core Length:  405 cm

Core description, MST data and colour scanner data of core GeoB9093-1

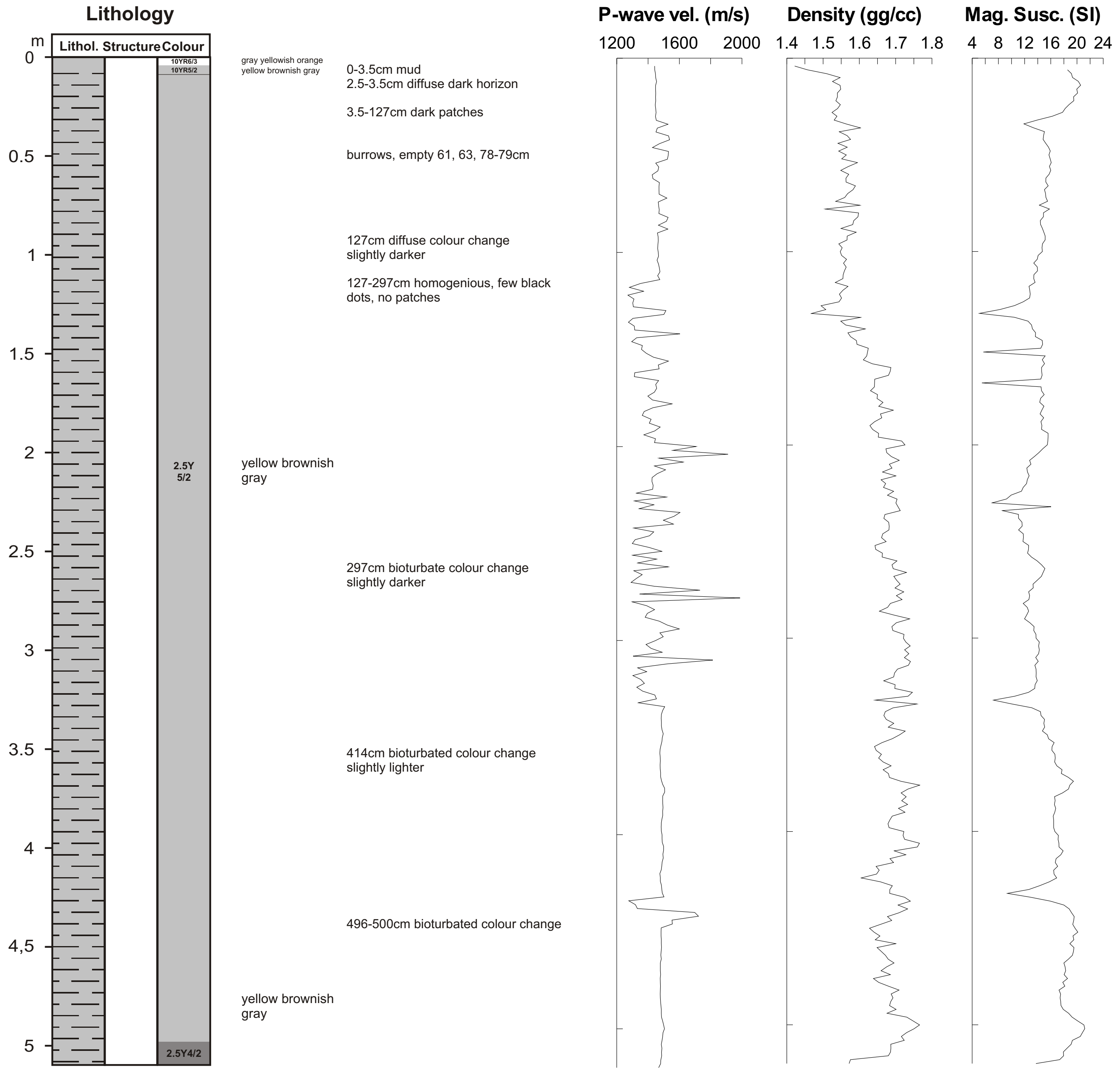


**GeoB 9093-1**

Date: 19.12.03 Pos: 36°4.08'N 10°01.95'W
Water Depth: 3003 m Core Length: 520 cm

Core description, MST data and colour scanner data of core GeoB9095-1

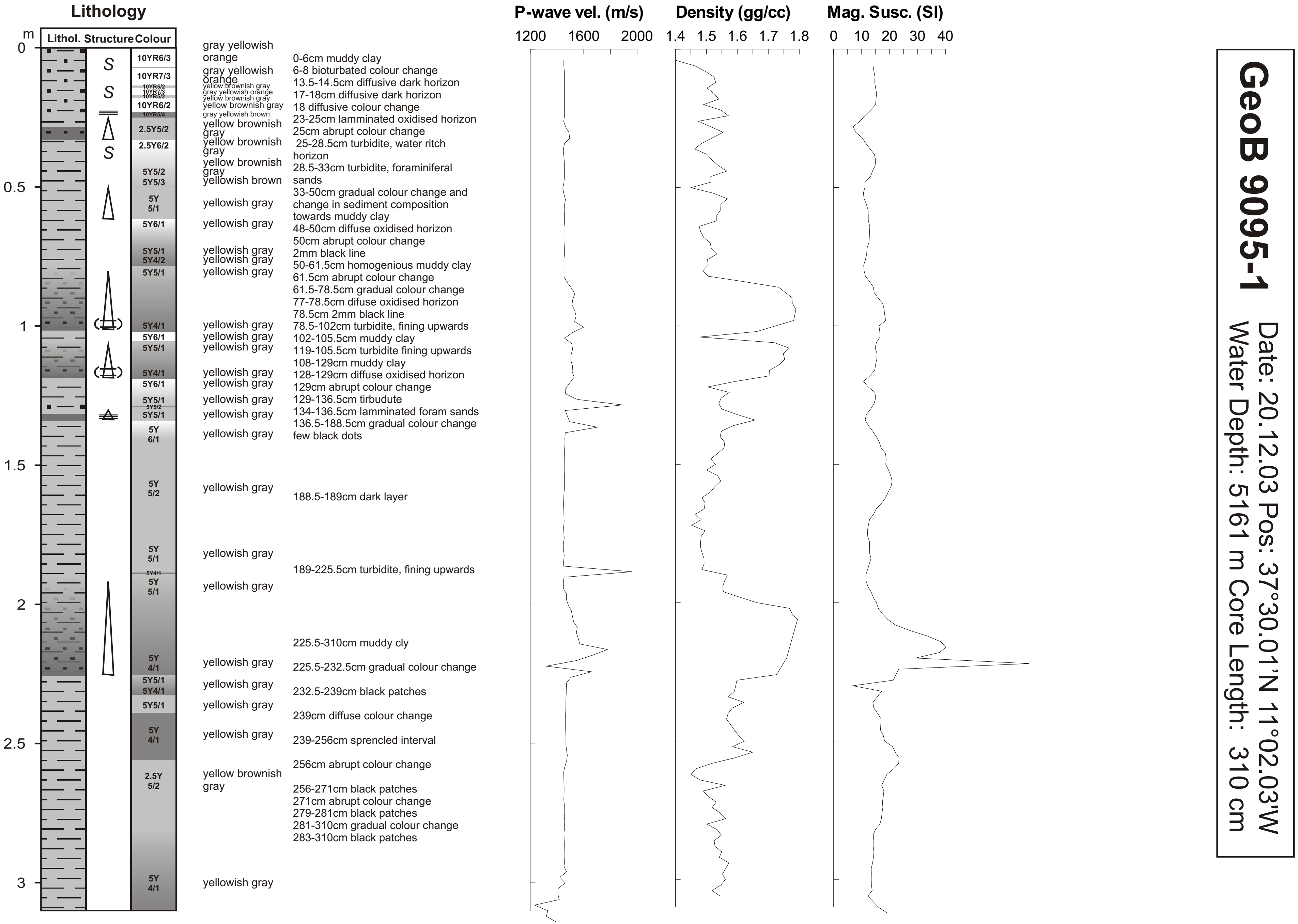

## 8.5. Weekly RCOM reports (website), in German

**EXPEDITION FS *Sonne* SO-175**
**"GAP (Gibraltar Arc Processes)"**

***(as submitted to RCOM website)***

25./26.11., Lissabon

SONNE läuft zum Sonnenuntergang pünktlich in Portugals Hauptstadt ein und wird vis-a-vis der Christusstatue vertäut. Der Geschäftsführer der Reederei Forschungsschifffahrt, Dr. von Seck, sowie Mannschaft der Gastwissenschaftler während der Atlantiküberquerung waren von der rauhen See und Tagen der Tatenlosigkeit gezeichnet. Stattdessen genoss das Team der GAP-Expedition die letzte Nacht im komfortablen Hotel in der Altstadt Lissabons, ehe es dann hieß, bis Weihnachten in eine schaukelnde Koje umzusteigen.

Tags darauf halfen zwei Dutzend Wissenschaftler aus 5 europäischen Staaten beim Löschen und Beladen für die Expedition. Trotz einiger kurzfristiger Umbesetzungen der Mannschaft hat sich eine Gruppe mit breiter Expertise gefunden, die Region des großen Erdbebens von Lissabons im Jahre 1755 zu studieren. Zwecks eines Briefings kamen zudem Drs. Pinheiro (Universität Aveiro, Portugal) und Hornibrook (Universität Bristol, UK) an Bord, um in einer angeregten Diskussion noch Input für GAP zu leisten.

Um 21 Uhr legte SONNE schließlich ab, um bei reichlich Wind und Swell den Weg nach Süden ins Arbeitsgebiet anzutreten. Die Truppe wird begleitet von einem Team von Spiegel-TV, das eine Reportage über sedimentkern-gestützte Erdbebenforschung zu senden gedenkt.

28.11., 36 53 N / 9 45 W

An der ersten Untersuchungsstation der Reise, der Marques de Pombal-Störung, wurde mit tiefgeschlepptem Videoschlitten, Wärmestromlanzen, Video-MUC und Schwerelot in 2 Tagen charakterisiert, ob der Überschiebungskörper und zwei südlich abgegangene Rutschungen mit Erdbebenaktivität in Verbindung stehen. Im Ostteil der Rutschung wurde die 20-25 m-hohe Abbruchkante der zweiten Rutschung mit Video und Seismik überfahren und abgebildet, ehe mehrere Kerne genommen wurden, deren Datierung den Bezug zu den jüngsten Erdbebenereignissen herstellen kann. Weiter westlich wurden ebenfalls seismisch ausgelöste Turbidite gewonnen, die auf der aktiv unterschobenen Platte mit höheren Wärmestromwerten absedimentierten.

Das Leben an Bord wurde von einigen "Ausfällen" durch Seekrankheit gekennzeichnet, die in starkem Kontrast zu den delikaten Lachssteaks des Küchenteams um Chefkoch Willi standen.

29.11., 35 54 N / 9 20 W

An einem Tag mit nahezu fehlendem Wellengang verliefen alle wissenschaftlichen Manöver reibungslos. Ausgenommen davon war das Zuwasserlassen eines Beiboots, dessen ölqualmender Motor zum ersten Mal für "blauen" Himmel sorgte und zudem dem Fernsehteam Außenaufnahmen von SONNE bescherte.

Eine ausgedehnte Wärmestromuntersuchung über die Deformationsfront des kontrovers diskutierten Sedimentkeils vor Gibraltar soll nun klären helfen, ob die Sedimente entlang der Plattengrenze in der Lage sind, verheerende Erdbeben hoher Magnitude zu erzeugen.

Alle Konzentration fokussiert sich nun auf die Entenbrust mit Orangen am Sonntag und das milde Wetter.

30.11., 35 47 N / 9 12 W

Bei für Ende November zu warmen Wetter und zu ruhigem Seegang nahmen wir Sediment-Schwerelot und Wärmestromdaten über den Nordwestteil der Deformationsfront des kontrovers diskutierten Schuppenkeils vor Gibraltar auf. Die Sedimente, eine Serie dezimetermächtiger Turbidite, wurden möglicherweise durch Erdbeben ausgelöst und nach Westen hangab geschüttet. Datierungen hierzu stehen nach der Expedition an.

01.12., 36 09 N / 7 47 W

Eine eher ereignisarme Nacht am tiefgeschleppten Videoschlitten (OFOS) endete dramatisch. Nachdem die Videotransekte über den über 500 m hohen *Lolita* Schlammvulkan wenig spektakuläres Bildmaterial lieferten, war plötzlich der Schlitten manövrierunfähig. Nachdem die schiffseigene Winde das Gerät nur mit Mühe wieder an deck zurückbringen konnte, weil sich ein Tiefseekabel darum verfangen hatte, befreite die geistesgegenwärtige Schiffscrew den Schlitten von der unfreiwilligen Last. Dabei schlug der kubikmetergroße Metallschlitten jedoch vehement um sich, schlug mehrfach gegen die Schiffswand von SONNE, konnte aber letztlich sicher an Bord gebracht werden.

Tagsüber wurden wegen der offensichtlichen Inaktivität des Schlammvulkans einige tiefwurzelnde Störungen weiter nördlich beprobt. Der dann wieder einsatzbereite Videoschlitten wurde dann in der Folgenacht neuerlich eingesetzt, diesmal erfolgreicher.

02.12., 36 11 N / 7 19 W

Am Hesperides Schlammvulkankomplex, der aus mehreren Gipfelkratern zusammengesetzt ist, sah man mit den Videokameras Gebiete mit Gasaustritten, Karbonatschloten, Schwämmen und Kaltwasserkorallen. Von vier Schwereloten traf nur eines unglücklich auf Karbonat und kam verbogen zurück, während drei Sedimentkerne Schlammbrekzien mit Tonsteinklasten aus der Tiefe förderten. Die Stimmung unter den Wissenschaftlern stieg noch deutlich. Zunächst wurde die Porendrucklanze erfolgreich getestet. Danach brachten drei erfolgreiche TV-Greifereinsätze einige Zentner Material an Deck. Darunter fanden sich Korallen in allen Farben und Formen, zementierter Schlamm, Holzfragmente und Karbonatschlote und -konkretionen.

Der Tag endete mit einem gelungenen Fest, um das Spiegel-TV Fernsehteam zu verabschieden. Mannschaft von SONNE und wissenschaftliche Besatzung mischten sich harmonisch bei einem wohlverdienten Bier vor dem sozialen Dreh- und Angelpunkt auf SONNE, dem roten Kühlschrank unter dem Arbeitsdeck im Rumpf des Schiffes.

03.12., Cadiz Hafenstop

Nachdem nachts die harten Karbonate die Wärmestromlanze beschädigten, liefen wir in Richtung Hafen von Cadiz, einer der ältesten Städte Spaniens, die ca. 1100 v.Chr. gegründet wurde. Im großen Hafen der beinahe landumschlossenen Bucht findet viel Handel mit Süd- und Nordamerika, aber auch SONNE fand hier für eine gute Stunde Platz. Da lediglich das TV-Team gegen Wissenschaftler ausgetauscht wurde, gab es keinen Landgang.

Wir sind derzeit auf dem Weg zurück ins Forschungsgebiet.

03.12., 36 05.68 N / 7 24.18 W

Nach dem kurzen Hafenaufenthalt in Cadiz fuhren wir in regnerisches, rauheres Wetter und arbeiteten am *Cibeles* Schlammvulkan, der auf einer interessanten sichelförmigen Störungsstruktur sitzt. Die Bilder der Videountersuchung aus der Folgenacht waren viel versprechend, um aktiven Fluidausstoss am Meeresboden beproben zu können. Die Nachtschicht hatte trotz der Ringe unter den Augen zuversichtliche Mienen.

04.12., 36 05.56 N / 7 23.57 W

Wider Erwarten konnten am *Cibeles* Schlammvulkan dann aber schwer Proben gegriffen werden. Aufgrund des offenbar langfristig stattgefundenen Fluidausstroms war das siltig-tonige Sediment weitestgehend zementiert, sodass mit dem Greifer nur einige Kilogramm an Deck gebracht werden konnten. Dem entgegen platzierten wir am Abend zwei Stossrohre in Regionen mit Korallenbeständen, die extrem guten Kerngewinn bescherten. Diesen versöhnlichen Tagesausklang zum Tag der Hl. Barbara, der Schutzgöttin aller Geologen und Bergleute, waren wir jedoch zu müde zu feiern, denn auch in dieser Nacht waren Videountersuchungen angesetzt.

05.12., 35 39.75 N / 7 19.95 W

Der *Capt. Arutyunov*-Schlammvulkan war schon vor unserer Expedition als einer der aktivsten Entwässerungspunkte auf dem Gibraltar-Schuppenkeil bekannt. nichtsdestotrotz galt es mit Beprobung und Wärmeflussmessungen zu belegen, wie effektiv diese Struktur im hydrogeologischen Kontext ist. Nachdem gleich am Morgen ein TV-Greifer eine knappe Tonne blubbernden, übelriechenden Matsch auf das Deck ergoss, schlug das Herz der Gashydratexperten höher. Einige Lote in diesen sowie zwei neu entdeckte Schlammvulkane sorgten für reichlich Arbeit sowie geologisch für Überraschungen, fand man beispielsweise feste, stark zerscherte und wieder verheilte Tonsteine, die als Klasten aus der tiefe des Keils mit an den Meeresboden gerissen wurden beim Schlammvulkanausbruch. Der Schlamm hatte dagegen ähnliche Konsistenz wie die Mohnsauce der Germknödel zu Mittag...

Nikolaus, auf Schleichfahrt gen Westen (35 35 N Breite)

Nachdem nachts auch eine Wärmestrom-Anomalie über *Capt. Arutyunov*-Schlammvulkan gemessen wurde, sind wir nun langsam gen Westen unterwegs, um ein reflexionsseismisches Profil über den gesamten Keil aufzunehmen. Dies gibt uns gleichsam Zeit für wissenschaftliche Diskussionen, Aufarbeitung des Kernmaterials von gestern, sowie für eine kleine Nikolaus-Party am Abend.

07.12., 35 29.6 N / 9 21.4 W

Nach einem Fest am Nikolausabend, das sich auf der sog. Kegelbahn (dem langen Flur mit den ganzen Laboren eine Etage unter dem Hauptdeck befindet) abspielte, nehmen wir uns die Tiefseeebene zum Ziel, um Sedimentkerne zu ziehen. Ziel ist, die Turbiditablagerungen zu untersuchen. Sie sind Sedimentschüttungen oder Ströme von Sedimentsuspension, die an Kontinentalhängen abwärts fliessen. Sie entstehen unter anderem durch Erdbeben, wie das schwere Lissabon-Erdbeben von 1755. Erstauinlicherweise fand sich in den Sedimentkernen aber kein Turbidit, sondern ausschliesslich sehr fester Ton.

08.12., 35 46.02 N / 9 00.05 W

Nachts als auch tagsüber kartierten wir den Ozeanboden, um geeignete Fluidaustrittsstellen zu finden. Ein solcher Ort ist der *Bonjardim*-Schlammvulkan, der etwa 3 km Durchmesser misst und sich als untermeerischer Berg über den umliegenden Meeresboden erhebt. Weitere kleine Hügel tauchten auf unserer Ozeanbodenkarte auf, die eventuell auf Sediment- oder Schlammvulkane hindeuten. Um dies zu beweisen wird sofort der Videoschlitten zu Wasser gelassen, der in einigen Metern über dem Meeresgrund hinter SONNE hergezogen wird und Fernsehbilder vom Bodensediment und seinen Organismen liefert.

09.12., 35 39.75 N / 7 19.95 W

Auf der Basis dieser Filmaufnahmen der Nacht ziehen wir tagsüber sedimentlote in über 3100 m Wassertiefe. Die Sedimente riechen hier stark nach Hydrogensulfid (d.h. wie faule Eier), was zwar unangenehm ist, aber ein indiz für die Aktivität von Mikroorganismen und den Ausstoss von Gas und Wasser ist. Die Entdeckung eines weiteren untermeerischen Hügels auf der Ozeanbodenkarte einige Seemeilen entfernt erwies sich als Enttäuschung: Die Sedimente sind homogen und geben uns keine Anzeichen schlammvulkanischer Aktivität.

Freude kommt trotzdem auf, denn das Nachtprogramm ist "locker", da weitere Strukturen am Meeresgrund kartiert werden. Nebenbei wird das traditionelle "Bergfest" begangen, das die Mitte der 28-tägigen Expedition darstellt. Zu Musik und Erfrischungsgetränken treffen sich Matrosen und Wissenschaftler von SONNE zum Tanzen und Feiern bis in den frühen Morgen. Getrübt wird alles von schwerer See, die nicht nur zu wackligen Tanzbeinen, sondern auch zu Wassereinbruch in die Labore führt, wenn Brecher über Deck gehen. Der Wind hat bis dato auf über 20 m/s zugenommen, und das Schiff schaukelt beängstigend.

10.-11.12.,

Umso erstaunlicher ist es, dass Petrus und Neptun schon tags darauf ganz andere Laune haben. Der Nordatlantik hier im Golf von cadiz ist glatt wie ein Ententeich, und man wird von der warmen Wintersonne regelrecht verwöhnt. das wissenschaftliche Programm sieht neben Sedimentkernen ein langes seismisches Profil vor. Dabei werden über 200 km Strecke mit Schallwellen einer Unterwasserkanone beschossen, die in den Meeresboden eindringen und dessen Untergrund reflektieren und zum Schiff zurücksenden. Auf diese Art gewinnen wir Informationen, die tiefer im Meeresgrund liegen als es mit Loten zu beproben ist. Während unter uns die schallwellen liefen, findet an Deck die wöchentliche Sicherheitsübung statt, um stets füt alle Fälle gerüstet zu sein.

Am östlichen Ende des seismischen Profils befindet sich der *Ginsburg*-Schlammvulkan, der vermutlich Gashydrat enthält. Diese Struktur wird gerade mit Videoschlitten befahren, um eventuell Sediment und das eisartige Methangas-Wasser-Gemisch zu beproben.

13.12., 35 18.1 N / 6 47.41 W

Nach dem erfolgreichen Abschluss der seismischen Profilaufnahme studieren wir weitere Schlammvulkane. Gleich morgens beproben wir einen bisher nicht bekannten untermeerischen Hügel. Die Sedimentkerne weisen unter einer dünnen Deckschicht die klassischen dunkelgrauen Tonbrekzien auf. Das sind Schlämme in Schlammvulkanen, die beim Aufstieg aus grosser Tiefe Brocken des darüberliegenden Gesteins mitrissen. Dieser neue Schlammvulkan als auch ein schon bekannter Vertreter, *Gemini,* weisen auf mehr oder minder starke Fluidaktivität hin. Den Rest des Tages nehmen wir zahlreiche Kerne auf dem marokkanischen Schelf, wo die Sedimente und nach der Expedition erlauben werden, den Einfluss des warmen Mittelmneerwassers in den Atlantik in der jüngsten Erdgeschichte zu rekonstruieren.

14.12., 35 37.32 N / 7 08.8 W

Kartierungen über Nacht brachten uns so dicht an die Küste Nordafrikas, dass wir nach Wochen der Abgeschiedenheit auf See endlich wieder mit den Lieben daheim telefonieren können mit den Handys. Morgens geht es nichtsdestotrotz weiter mit der Schlammvulkanforschung.

Der *Ginsburg* Schlammkegel, der einen mehrere hundert Meter weiten Kraterbereich hat, zeigt in unserem TV-Greifer kleine Gashydratchips. Insgesamt zählt er zu den aktiveren Vertretern der Schlammvulkane. Umgekehrt vermag keine unserer Videoschlitten-Untersuchungen direkt Hinweise auf bakterielle oder anderweitige Besiedelung aufgrund starken Gasausstosses zu geben. Um die Fluiddynamik quantitativ und längerfristig zu erfassen, liessen wir heute in den *Captain Arutyunov*-Schlammvulkan eine Lanze fallen, die über den Zeitraum von 4 Wochen Wärmestrom und Porendruck misst, aufzeichnet, und diese Daten dann mit Satellitentelefon am 14. Januar 2004 ins Heimatlabor nach Bremen sendet. Auch diese Installation wurde von der Hitze und Windstille begünstigt.

15.12., 35 55.2 N / 6 00.1 W

Aufgrund des herrlichen Wetters während fast der gesamten Fahrt haben wir etliche Ziele der Expedition schon erreicht und schieben einen Extraprogrammpunkt ein. In der Strasse von Gibraltar ganz im Osten unseres Untersuchungsgebioets existiert ein untermeerischer Rücken, der nur 50 Meter unter dem Meeresspiegel liegt. Diese Untiefe war vor der letzten Eiszeit eine Insel, deren Herkunft nicht gut bekannt ist. Unsere Videoschlittenuntersuchungen zeigen, dass sie einen magmatischen Kern hat im Zentrum, dass aber die Flanken von Weichsediment bedeckt sind. An den Rändern der ehemaligen Insel befinden sich Terrassen, die aus verbackenen Sedimenten bestehen. Sie sind mit allerlei Tieren und Pflanzen bewachsen. Eine Aufgabe nach der Expedition wird sein, diese sog. "beach rocks" zu datieren.

16.12., 34 58.3 N / 8 26.58 W

Nach der Rückkehr ins südliche Arbeitsgebiet massen wir den Wärmefluss über einige tektonische Störungen, da durch Reibung der Gesteins- und Sedimentblöcke Hitze entsteht, die durch das Wasser im Sediment abgeführt wird zum Meeresboden. Die Studien setzen sich bis zum kommenden Tag fort, da wir mittlerweile wieder in über 3000 m Wassertiefe operieren.

17.12., 34 49 N / 8 50.4 W

Erhöhte Wärmestromwerte haben wir heute an einem mehrere Kilometer weiten Kegel gemessen. Sie könnten entweder auf hohen Fluidfluss oder aber Salzstöcke im Untergrund hindeuten. Um diese Frage zu beantworten, haben wir zwei Sedimentkerne gezogen, die gerade im Labor untersucht werden. Nach Abschluss dieser Arbeit geht es langsam weiter nach Norden.

18.12., 36 06.3 N / 10 40.09 W

Die letzten Expeditionstage verbringen wir mit dem Sammeln von referenzsedimenten in den verschiedenen Tiefseebenen um den Gibraltarkeil. Diese Arbeiten sind zeitaufwendig, das grosse wassertiefen vorherrschen und unsere Geräte lange bis zum Meeresgrund unterwegs sind. Auf der Horseshoe-Tiefseeebene finden wir heute interessant geschichtete Sedimente, die durch hangrutschungen und Trübeströme verursacht wurden.

19.12., 36 48 N / 10 02 W

Eine solche Rutschung nehmen wir uns dann für eine Detailstudie vor. dabei wird zuerst reflexionsseismisch vermessen, um die Untergrudnstruktur abzubilden. Danach kann gezielt gekernt werden, und es gelingt uns perfekt, die nördlichste Zunge des Rutschungskörpers zu durchstossen. Die Porenwässer zeigen Anomalien, die darauf hindeuten, dass das Ereignis noch nicht lange zurück liegen kann.

20.12., 37 30 N / 11 01 W

Auf der Tagus-Tiefseeebene im Norden des Studiengebiets nehmen wir heute den tiefsten Kern der Expedition in über 5.1 km unter dem Meeresspiegel. Das 5-stündige manöver lohnt sich, denn wiederum geben gut geschichtete Sedimente Aufschluss über Trübeströme der jüngsten Erdgeschichte.

21.12., 36 02 N / 10 34.8 W

Während danach alle Labore abgebaut und in Container verpackt werden, wird nochmal für einige Stunden die Wärmestromlanze über Gorringe Bank und in der Horseshoe-Tiefseeebene in den Grund gerammt. Am Nachmittag machen wir uns dann gen Norden auf, um nach etwa 4 Wochen wieder in der portugiesischen Metropole einzulaufen.

22.-23.12., LISSABON (38 40 N / 8 15 W)

Grosse Erleichterung beim Grossteil der wissenschaftlichen Truppe: Es geht nach Hause in die Weihnachtsferien! Vorher muss freilich noch Container gepackt werden, um später in Deutschland leicht und systematisch löschen zu können. Gegen Mittag macht sich SONNE mit reduzierter Mannschaft auf die letzte Etappe von Lissabon ins heimatliche Deutschland.

Heiligabend, Biskaya

Wider Erwarten empfängt uns die (zu dieser Jahreszeit sonst extrem rauhe) Biskaya mit niederen Wellen, und mit drei Schiffsdieseln und günstigen Wind- und Strömungsverhältnissen durchkreuzen wir diesen gefährlichsten Reiseabschnitt unerwartet schnell. Die nach einer Rede des Kapitäns vorgenommene Einbescherung bedenkt die Mannschaft mit Fliessjacken der Reederei. Da die Temperaturen merklich abnehmen gen Norden ein wahrlich passendes Geschenk!

26.12./27.12., Ärmelkanal bei Calais/Frankreich

Nach voller Fahrt bis hinein in den Ärmelkanal kann heute eine Maschione abgeschaltet und auch die anderen beiden gedrosselt werden. Nichts steht einem pünktlichen Eintreffen in Deutschland mehr entgegen, und so dampfen wir gemütlich an der französischen und dann belgischen Küste entlang. Der Expeditionsbericht ist zum grössten Teil verfasst, und die Mannschaft verschönert auf der Überfahrt das Schiff für die Rückkehr nach Deutschland.

## 8.5 Weekly reports (in German)

**EXPEDITION FS *Sonne* SO-175 "*GAP* (Gibraltar Arc Processes)"**

***1. Wochenbericht***

Die Expedition *GAP* verfolgt primär das Ziel, die Frage zu erörtern, was die Ursache des historisch größten Erdbebens Europas ist, das sich am 01.11.1755 ereignete. In der auch heute seismisch aktiven Region des Golfes von Cadiz gibt es verschiedene Erdbebenherde, die auf tektonisch unterschiedliche Mechanismen zurückgehen und potentielle Risikogebiete.

Am 25.11. läuft SONNE zum Sonnenuntergang pünktlich in Portugals Hauptstadt Lissabon ein und macht vis-a-vis der Christusstatue fest. Da die Gastwissenschaftler, die während der Atlantiküberquerung (Leg SO175-1) unter der rauhen See litten, noch an Bord blieben, begann das Borden für SO175-2 erst am 26.11. ab 8 Uhr. Gleichzeitig wurden 2 Container gelöscht, andere umgestellt, und gebunkert. Um 21 Uhr legte SONNE schließlich ab, um bei reichlich Wind und Swell den Weg nach Süden ins Arbeitsgebiet anzutreten. Die Truppe wird begleitet von einem Team von Spiegel-TV, das 2004 eine Reportage über sedimentkern-gestützte Erdbebenforschung senden wird.

Nach nur 11 Stunden Transit gen Süden wurde an der ersten Untersuchungsstation der Reise, der Marques de Pombal-Störung, mit tiefgeschlepptem Videoschlitten, Wärmestromlanze, Video-MUC und Schwerelot 2 Tage gearbeitet. Hauptaugenmerk galt der Frage, ob der Überschiebungskörper und zwei südlich abgegangene Rutschungen mit Erdbebenaktivität in Verbindung stehen. Im Ostteil der Rutschung wurde die 20-25 m hohe Abbruchkante der zweiten Rutschung mit Video und Parasound überfahren und abgebildet, ehe mehrere Kerne genommen wurden, deren Datierung den Bezug zu den jüngsten Erdbebenereignissen herstellen kann. Weiter westlich wurden ebenfalls gradierte, möglicherweise seismisch ausgelöste Turbiditsequenzen gewonnen, die auf der aktiv unterschobenen Platte mit höheren Wärmestromwerten abgelagert wurden.

Das Leben an Bord wurde in den ersten beiden Tagen von einigen Fällen Seekrankheit beeinträchtigt, ehe der Wind erstaunlich abflaute und optimale Bedingungen zum Arbeiten angetroffen wurden. Die Stimmung an Bord ist gut und wurde durch eine Rettungsbootübung aufgelockert.

Eine ausgedehnte Wärmestromuntersuchung über die nordwestliche Deformationsfront des kontrovers diskutierten Sedimentkeils vor Gibraltar soll nun klären helfen, ob die Sedimente entlang der Plattengrenze in der Lage sind, verheerende Erdbeben hoher Magnitude zu erzeugen. Ein Schwerelotkern zeigte wiederum eine Serie dezimeter-mächtiger Turbidite mit grobsandiger Basis, aber ansonsten hohen Tongehalten. Bei der Überfahrung mit Sedimentechographie und SIMRAD wurden als Highlight des 1. Advent zwei bisher unbekannte Schlammvulkane entdeckt.

Das nächste Untersuchungsziel, der über 500 m hohe Schlammdiapir *Lolita*, wurde in der Nacht zum heutigen Montag mit dem tiefgeschleppten Videosystem studiert. Allem Anschein nach scheint die Struktur derzeit inaktiv, sodass von einer Kernbeprobung abgesehen wurde.

Alle an Bord sind munter und harren nun der beiden nächsten Zielgebiete, einer tiefwurzelnden "leaky fault" und dem Almazan Schlammvulkan, ehe am 3.12. Cadiz die Endstation von Leg SO175-2 darstellen wird.

Herzliche Grüsse aus dem Golf von Cadiz in die Heimat vom *GAP*-Team um Expeditionsleiter Achim Kopf

***2. Wochenbericht***

Nach einem nur einstündigen Hafenstopp in Cadiz am 03.12., der dazu diente, 4 Leute auszutauschen und etwas Luftfracht aufzunehmen, fuhr *SONNE* wieder westwärts, um die Untersuchungen im oberen Teil des Gibraltar-Schuppenkeils fortzusetzen. Die Fahrt führte uns erstmals in regnerisches, rauheres Wetter, wo wir am *Faro* Schlammvulkan, der auf einer interessanten sichelförmigen Störungsstruktur sitzt, arbeiteten. Die Bilder der Videountersuchung aus der Folgenacht waren viel versprechend, um aktiven Fluidausstoss am Meeresboden beproben zu können. Wider Erwarten konnten am *Faro* Schlammvulkan dann aber schwer Proben gegriffen werden. Aufgrund des offenbar langfristig stattgefundenen Fluidausstroms war das siltig-tonige Sediment weitestgehend zementiert, sodass mit dem Greifer nur einige Kilogramm an Deck gebracht werden konnten. Dem entgegen platzierten wir am Abend zwei Stossrohre in Regionen mit Korallenbeständen, die extrem guten Kerngewinn bescherten. Tags darauf war der *Capt. Arutyunov*-Schlammvulkan, der schon vor unserer Expedition als einer der aktivsten Entwässerungspunkte auf dem Gibraltar-Schuppenkeil bekannt war, unser Arbeitsziel. Gleich am Morgen förderte der TV-Greifer eine knappe Tonne blubbernden, übelriechenden Tonschlamm mit bis zu handtellergrossen Gashydratstücken an Deck. Einige Lote in diesen sowie zwei neu entdeckte Schlammvulkane sorgten für reichlich Arbeit sowie geologisch für Überraschungen. Man fand feste, stark zerscherte und wieder verheilte Tonsteine, die als Klasten aus der Tiefe des Keils mit an den Meeresboden gerissen wurden. Die Schlammvulkanausbrüche finden episodisch und mit langen Pausen eruptiver Inaktivität statt, wie ein Kern belegte, in dem drei Ausflussereignisse von jeweils mehreren Dezimetern hemipelagischen Hintergrundsediments unterbrochen wurden. Nachdem nachts auch eine Wärmestrom-Anomalie über *Capt. Arutyunov*-Schlammvulkan gemessen wurde, nahmen wir gen Westen ein reflexionsseismisches Profil über den gesamten Keil auf. Probleme mit der Airgun zwangen uns, dieses Profil abzubrechen; nach einer kurzen Reparatur ist das System nun aber wieder einsatzbereit. Am Nikolaustag beprobten wir an der westlichen Deformationsfront das unter den Keil abtauchende Sedimente, das extrem tonreich und zäh war. Im Gegensatz zur Deformationsfront weiter nordöstlich kamen hier keine Turbiditabfolgen vor. Ein Geothermic. Programm charakterisiert nun die frontalen etwa 100 km des Keils, ehe sich Kartierarbeiten in Schlammvulkanregionen des Mittelkeils anschließen.

Am morgigen 09. Dezember, der bereits die Fahrtmitte darstellt und mit dem traditionellen Bergfest begangen wird, wird einer dieser Schlammvulkane genauer untersucht und beprobt.

Sonnige Grüsse aus dem spiegelglatten Atlantik, das GAP-Team um Achim Kopf

### *3. Wochenbericht*

Zur Mitte der 4-wöchigen GAP-Expedition untersuchten wir in der Nacht zum 09. Dezember den etwa 3 km Durchmesser messenden *Bonjardim*-Schlammvulkan. Weitere kleine Hügel tauchten auf unserer Ozeanbodenkarte auf, die eventuell auf Sediment- oder Schlammvulkane hindeuten. Auf der Basis von Videoaufnahmen mit einem tiefgeschleppten Schlitten (OFOS) in über 3100 m Wassertiefe fanden wir Fluidaustrittstellen, die mit verschiedenen Geräten beprobt wurden. Die Entdeckung eines weiteren untermeerischen Hügels auf der Ozeanbodenkarte einige Seemeilen entfernt erwies sich als Enttäuschung: Die Sedimente sind homogen und geben uns keine Anzeichen schlammvulkanischer Aktivität, obwohl sie stark nach Hydrogensulfid rochen. Am Abend trafen sich dann Matrosen und Wissenschaftler von SONNE zum traditionellen Bergfest, um bis in den frühen Morgen zu Tanzen und zu Feiern. Während in jener Nacht der Wind hat bis dato auf über 20 m/s zugenommen hat und das Schiff beängstigend zum Schaukeln bringt, ist am Morgen bereits bestes Wetter und glatte See.

Am 10.-11.12. nehmen wir ein über 200 km langes reflexionsseismisches Profil über den gesamten Gibraltar-Schuppenkeil auf, bei dem uns das gute Wetter zu qualitativ hochwertigen Daten verhilft. Auf dem weniger als 1000 m tiefen Ostteil des Keils standen dann in den kommenden beiden Tagen verschiedene Schlammvulkane auf dem Forschungsprogramm. Dazu zählte die Probennahme am *Ginsburg, Captain Arutyunov, Gemini* und einem bisher unbekannten Schlammvulkan statt. Alle Kerne weisen auf mehr oder minder starke Fluidaktivität; zudem findet man stellenweise Gashydrat. Kartierungen während der Nacht belegen, dass potentiell mehr Schlammdome in der Region existieren, als man bisher dachte. Umgekehrt vermag keine unserer OFOS-Untersuchungen direkt Hinweise auf bakterielle oder anderweitige Besiedelung aufgrund starken Ventings zu geben. Um die Fluiddynamik quantitativ und längerfristig zu erfassen, ließen wir in den *Captain Arutyunov*-Schlammvulkan eine Lanze fallen, die über den Zeitraum von 4 Wochen Wärmestrom und Porendruck misst, aufzeichnet, und diese Daten dann via Satellitentelefon ins Heimatlabor nach Bremen sendet. Auch diese Installation wurde von der Hitze und Windstille begünstigt.

Wärmestrommessungen schließen nachts die arbeiten in dieser Region ab, sodass SONNE am 15.12. zu weiteren Zielen aufbrechen kann.

Herzliche Grüsse zum 3. Advent wünscht das GAP-Team um Achim Kopf

*4. Wochenbericht*

Aufgrund des herrlichen Wetters während fast der gesamten Fahrt haben wir etliche Ziele der Expedition schon erreicht und schieben einen Extraprogrammpunkt ein. In der Strasse von Gibraltar ganz im Osten unseres Untersuchungsgebiets existiert ein untermeerischer Rücken, der nur 50 Meter unter dem Meeresspiegel liegt. Diese Untiefe war vor der letzten Eiszeit eine Insel, deren Herkunft nicht gut bekannt ist. Unsere Videoschlittenuntersuchungen zeigen, dass sie einen magmatischen Kern hat im Zentrum, dass aber die Flanken von Weichsediment bedeckt sind. An den Rändern der ehemaligen Insel befinden sich Beachrock-Terrassen. Nach der Rückkehr ins südliche Arbeitsgebiet folgten Wärmestrommessungen über einige tektonische Störungen und einen Dom. Letzterer weist erhöhte Wärmestromwerte auf, die (genau wie erhöhte Porenwasserchlorinitäten) auf Salzstöcke im Untergrund hindeuten.

Während der Folgezeit ist unsere Hauptaufgabe, die Horseshoe und tagus Tiefseeebenen zu studieren. Das geschieht mit einer Serie von TV-MUCs und Schwereloten, um die Turbiditsequenzen zu datieren, die vermutlich mit den episodischen Erdbeben in der Region zusammenhängen. Wärmestrommessungen komplementieren diese Studien, wobei erste Ergebnisse suggerieren, dass es sich beim Gibraltarkeil tatsächlich um eine nach Osten einfallende Überschiebungszone handelt.

Um die Rutschungen nahe der Marques de Pombal-Störung, die wir in der ersten Woche untersuchten, besser verstehen und in den tektonischen wie zeitlichen Rahmen einhängen zu können, wurde abermals Sediment gekernt sowie Reflexionsseismik akquiriert. Hierbei gelang es uns, die jüngst mobilisierten Ablagerungen einer Hangrutschung zu durchörtern. Die Porenwasserchemie des Untergrundes und des remobilisierten Materials belegt, dass das Ereignis noch nicht lange zurückliegt. Diese Daten sollen zu Hause ergänzt und für Modellierungen genutzt werden.

Am Nachmittag des 21.12. beenden wir die hochgradig erfolgreichen wissenschaftlichen Arbeiten und brechen gen Norden auf, um nach etwa 4 Wochen wieder in der portugiesischen Metropole einzulaufen. Dort werden Container gepackt, ehe SONNE ohne das Gros des wissenschaftlichen Teams nach ca. 12 Jahren wieder Kurs auf Deutschland nimmt.

Herzliche Grüsse, eine gesegnetes Weihnachtsfest und einen guten Start ins Jahr 2004 wünscht Fahrtleiter Achim Kopf und das sich nun in alle Winde verstreuende GAP-Team

## 8.7. Press coverage

**PRESSESPIEGEL**

rcom bremen
research center ocean margins

Medium: Bremer Tageszeitungen
Rubrik: Lokales
Seite: 11
Datum: 16.12. 2003

Dienstag, 16. Dezember 2003 · Nr. 294

# Mini-Expedition für 16 unserer Leser

**Wer möchte auf dem Forschungsschiff „Sonne" von Bremerhaven nach Bremen mitfahren?**

(eho) Nach über zwölf Jahren kehrt das Forschungsschiff „Sonne" der Bremer Reederei „RF Forschungsschiffahrt" in die Heimat zurück. Während dieser Zeit hat die etwa 100 Meter lange „Sonne" mehr als 550000 Seemeilen hinter sich gebracht, vorwiegend im Pazifik und im Indischen Ozean. 16 Leserinnen und Leser unserer Zeitung haben jetzt die Chance, mit der „Sonne" die letzten Seemeilen von Bremerhaven nach Bremen zurückzulegen. Knapp sechs Stunden wird die Weser-Fahrt am Montag, 29. Dezember, dauern. Morgens geht es los, und gegen 16 Uhr macht das Schiff im Europhahafen fest.

Während der Mini-Expedition möchten Kapitän und Besatzung ihren Gästen die Tätigkeit an Bord erläutern. Die Kommandobrücke und das Arbeitsdeck werden bei Rundgängen ebenso gezeigt wie Labore, Maschinenraum und die Schiffsmesse. Außerdem ist ein populärwissenschaftliches Programm für die Besucher vorbereitet worden: Professor Gerold Wefer, Direktor des Bremer Forschungszentrums Ozeanränder, gibt einen Überblick über Aufgaben und Ziele der deutschen Meeresforschung. Danach berichten die Fahrtleiter der beiden letzten Expeditionen in Kurzvorträgen über ihre Arbeiten im Golf von Cádiz beziehungsweise im Golf von Mexiko. Es sind dies die Professoren Achim Kopf und Gerd Bohrmann vom Forschungszentrum. Zwischendurch bleibt Zeit für Gespräche. Mittags gibt es einen zünftigen Eintopf auf dem Achterdeck.

Für den morgendlichen Bustransport von Bremen nach Bremerhaven beziehungsweise für den Transfer nachmittags vom Europahafen zurück in die City wird gesorgt. Weitere Details erfahren unsere 16 Gewinner rechtzeitig. Ihren Blick hinter die Kulissen der „Sonne" können diese übrigens ganz exklusiv vor dem offiziellen Tag der offenen Tür werfen. Der findet am 30. Dezember von 10 bis 16 Uhr auf dem Schiff im Europahafen statt.

■ Wer am 29. Dezember mitfahren möchte, schreibt an die Bremer Tageszeitungen AG, Lokalredaktion, 28189 Bremen, Telefax 3398136, E-Mail lokales@btag.info. Stichwort: „Sonne". Einsendeschluss: 19. Dezember.

Die „Sonne" bietet 25 Wissenschaftlern eine hochmoderne Forschungsplattform.

**Blick hinter die Kulissen**

**PRESSESPIEGEL**

rcom bremen
research center ocean margins

Medium: Bremer Tageszeitungen
Rubrik: Lokales
Seite:
Datum: 28.12. 2003

# Ein Tag auf der „Sonne“

## Forschungsschiff öffnet seine Türen

(ka) Der Europahafen bekommt hohen Besuch: Nach mehr als 12 Jahren kehrt das Bremer Forschungsschiff „Sonne“ am kommenden Dienstag wieder an die Weser zurück. Alle Bremer haben dann Gelegenheit, sich bei einem Tag der offenen Tür an Bord umzusehen und sich über die Arbeit der „Sonne“ zu informieren.

Von zehn bis 16 Uhr berichten die Wissenschaftler des Forschungszentrums Ozeanränder auf dem Schiff über ihre Arbeit. Wer Interesse hat, kann sich unter dem Mikroskop winzige Meeresorganismen ansehen, sich über Klima und Strömungen informieren oder die Arbeit eines Unterwasser-Roboters kennen lernen. Außerdem ist an diesem Tag das nahe gelegene Kernlager des Ozean-Bohr-Programms geöffnet. Ein Shuttle-Bus bringt die Besucher von der „Sonne“ zum Bohrkernlager. Wer zum Schiff möchte, fährt über Hansator und Konsul-Smidt-Straße in den Hafen, Parkplätze sind dort vorhanden.

Das Forschungsschiff „Sonne“ wird normalerweise im pazifischen und indischen Ozean eingesetzt. Das Schiff ist knapp 100 Meter lang.

# Im Hafen die „Sonne" sehen

## „Tag der offenen Tür" an Bord des Bremer Forschungsschiffs / Heimkehr nach mehr als zwölf Jahren

**Von Thomas Kuzaj**

**BREMEN** • Nach mehr als zwölf Jahren kehrt das Forschungsschiff „Sonne" zum ersten Mal wieder nach Deutschland zurück – und besucht Bremen, seinen Heimathafen. Willkommen an Bord: Morgen, am 30. Dezember, gibt es einen „Tag der offenen Tür".

Die von der Bremer Reederei RF Forschungsschiffahrt betriebene „Sonne" legt im Europahafen an. In den vergangenen zwölf Jahren hat das knapp 100 Meter lange Schiff mehr als 550 000 Seemeilen zurückgelegt – alle im Dienste der Meeresforschung. 550 000 Seemeilen – eine Strecke, die beinahe der dreifachen Entfernung des Mondes von der Erde entspricht. Doch zurück aufs Wasser: Die „Sonne" wird im pazifischen und indischen Ozean eingesetzt.

An Bord, wen wundert's, gibt es allerlei zu sehen – das Schiff ist schließlich mit hochmoderner Technik ausgerüstet: Unterwasserroboter und Tauchboote, Sonden und Kamerasysteme. Morgen, am „Tag der offenen Tür", werden Schiffsführungen angeboten, und zwar in der Zeit zwischen 10 und 16 Uhr. „Kommandobrücke und Arbeitsdeck sind ebenso Stationen des Rundgangs wie Labore, Maschinenraum und Schiffsmesse", hieß es.

Zur Ergänzung gibt es noch ein populärwissenschaftliches Rahmenprogramm. Fachleute des Forschungszentrums Ozeanränder berichten über ihre soeben abgeschlossenen Arbeiten im Golf von Cadiz und im Golf von Mexiko. Obendrein können die Besucher per Mikroskop in die Welt winziger Meeresorganismen eintauchen und erfahren, was es mit Schlammvulkanen und den vielfach diskutierten Gashydraten am Ozeanboden auf sich hat. Es geht um Fragen wie diese: „Wie hängen Meeresströmungen und Klima voneinander ab?" Kinder können sich derweil in die Obhut von „Captain Säbelzahn" begeben.

Neben der „Sonne" kann morgen auch das Sedimentkernlager des internationalen Ozeanbohrprogramms besichtigt werden. Dort werden Bodenproben gelagert, aus denen Erkenntnisse für die Klima- und Umweltforschung gewonnen werden können. Die Bohrkerne erlauben sogar Antworten auf Fragen nach dem Aussterben der Dinosaurier.

Wie berichtet, war Anfang Dezember im Bremer Rathaus ein Vertrag mit einem Volumen von etwa 70 Millionen Euro unterzeichnet worden – ein Chartervertrag. Rolf-Dieter Heitz vom Forschungszentrum Jülich und Vertreter der RF Forschungsschiffahrt hatten ihn unterschrieben. Damit bleibt die „Sonne" für weitere sieben Jahre – bis 2010 also – im Einsatz. Die 70 Millionen Euro kommen vom Bundesforschungsministerium.

Die „Sonne" wurde 1969 auf der Rickmers-Werft in Bremerhaven als Fischtrawler gebaut. 1977 folgte der Umbau, im Frühjahr 1978 die erste Forschungsfahrt. Das 97,90 Meter lange Schiff bietet 25 Wissenschaftlern und 30 Mann Besatzung Platz. Die Crewmitglieder gelten als hochqualifiziert, sie kennen die speziellen Anforderungen der Forschungsschifffahrt. Zu den wichtigsten Nutzern des Schiffs zählt die Bremer Universität mit ihren entsprechenden Forschungsschwerpunkten.

• Wer morgen die „Sonne" im Europahafen sehen möchte, muss über Hansator und Konsul-Smidt-Straße fahren. Per Straßenbahn geht es mit der Linie 3 bis zur Haltestelle Hansator. Von dort sind noch zehn bis 15 Minuten zu laufen (Richtung: Frischezentrum). Der Weg zur „Sonne" soll ausgeschildert sein, hieß es.

**WWW.**
rcom-bremen.de/Sonne.html
ozeanraender.de

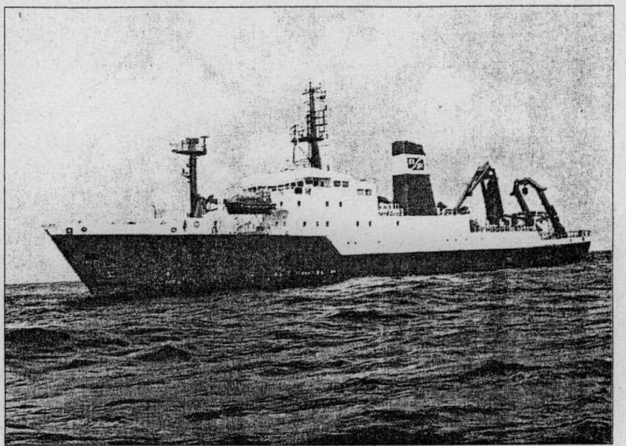

*Morgen, am 30. Dezember, im Europahafen zu besichtigen: Das Bremer Forschungsschiff „Sonne".*

WK 28.12.03

# „Sonne" kommt zum Heimatbesuch

## Forschungsschiff erstmals seit zwölf Jahren wieder in Bremen / Tag der offenen Tür

**Zu einem ganz seltenen Besuch in seiner Heimatstadt macht am Dienstag das Forschungsschiff „Sonne" im Bremer Europahafen fest. Gäste sind zur Besichtigung herzlich eingeladen.**

Nach mehr als zwölf Jahren und einer Fahrt über 550.000 Seemeilen kehrt das Bremer Forschungsschiff „Sonne" am kommenden Dienstag, 30. Dezember, erstmals wieder an die Weser zurück. Aus diesem Anlass findet am Schuppen 1 im Bremer Europahafen von 10 bis 16 Uhr ein Tag der offenen Tür statt, zu dem Besucher herzlich eingeladen sind. Auf dem Programm stehen Schiffsbesichtigungen, wissenschaftliche Ausstellungen sowie Gespräche mit Besatzung und Forschern. Für Kinder hat „Captain Säbelzahn" einiges vorbereitet. Er erzählt spannende Geschichten von Piraten und Seeräubern und lädt zu einer Kaperfahrt über die Weltmeere ein.

Zudem ist das nahe gelegene Kernlager des Ozeanbohr-Programms (Ocean Drilling Program) geöffnet. Dort werden Proben vom Meeresboden gelagert, die unter anderem das Aussterben der Dinosaurier dokumentieren. Von Bremen aus werden die Proben für spezielle Untersuchungen in die ganze Welt verschickt. Zwischen Schiff und Bohrkernlager wird ein kostenloser Shuttle-Verkehr eingerichtet.

Die „Sonne" ist insbesondere für geowissenschaftliche Meeresforschung ausgerüstet. Bevorzugtes Einsatzgebiet sind der pazifische und der indische Ozean. Das knapp 100 Meter lange Schiff bietet 25 Wissenschaftlerinnen und Wissenschaftlern eine hochmoderne Arbeitsplattform. Vom Arbeitsdeck können Unterwasserroboter, Tauchboote und verschiedene Sonden ausgesetzt werden. Biologen und Geologen nutzen modernste Kamerasysteme, um das Leben unter extremen Umweltbedingungen – zum Beispiel in der Umgebung aktiver Unterwasservulkane – zu erforschen.

■ Anfahrt zum Liegeplatz an Schuppen 1 über Hansator und Konsul-Smidt-Straße (Parkplätze in Schiffsnähe vorhanden). Oder mit der Straßenbahnlinie 3 bis Haltestelle Hansator. (eb)

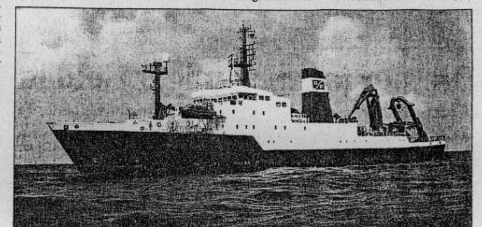

Das Forschungsschiff Sonne. Foto: pv

Delm. - Kreisbl. 30.12.03

# Im Europahafen geht die „Sonne“ auf

**MARITIM** Forschungsschiff nach zwölf Jahren wieder in Bremen

**BREMEN**/ME – Die Schlagzeilen über das Erdbeben im Iran sind erst wenige Tage alt. Solche Erdstöße sind dort keine Seltenheit, immer wieder bebt es aber auch in Italien und der Türkei. Doch wodurch entsteht ein Erdbeben? Mit dieser hochaktuellen Frage beschäftigt sich derzeit der Bremer Geo-Forscher Achim Kopf.

Kopf leitet ein internationales Wissenschaftlerteam, das an Bord des Forschungsschiffs „Sonne“ in den vergangenen Wochen im Golf von Cadiz (Spanien) den Beben auf der Spur war. „Unsere Vision ist es, zu einer Art Frühwarnsystem zu kommen“, erklärte der Geologe gestern auf der letzten Etappe der Expedition von Bremerhaven zum Heimathafen Bremen.

In der Hansestadt, genauer im Europahafen, hat die „Sonne“ gestern nach mehr als zwölf Jahren erstmals wieder festgemacht. In dieser Zeit hat das Schiff der Bremer Reederei RF mehr als 550 000 Seemeilen zurückgelegt und nach Angaben von Professor Gerold Wefer, Direktor des Forschungszentrums Ozeanränder, besonders auf dem Gebiet der Gashydratforschung weltweit große Aufmerksamkeit erregt.

Bevor die „Sonne“ Ende April 2004 nach Jakarta ausläuft, kommt sie zunächst noch in die Werft, wo das 25 Jahre alte Schiff mit technischen Neuerungen ausgerüstet wird.

Heute, Dienstag, gibt die knapp 30-köpfige Besatzung allen Interessierten von 10 bis 16 Uhr Einblicke in die speziellen Anforderungen des Bordbetriebs. Neuartige Unterwasser-Roboter veranschaulichen die wissenschaftliche Arbeit an Bord.

Per Mikroskop können die Besucher zudem in die Welt winziger Meeresorganismen eintauchen. „Captain Säbelzahn“ lädt Kinder zu einer spannenden Kaperfahrt über die Weltmeere ein.

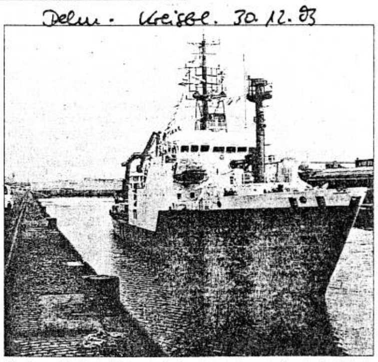

Die „Sonne“ läuft am Montagnachmittag in den Europahafen ein. Dort ist sie heute von 10 bis 16 Uhr zur Besichtigung freigegeben. BILD: LOEST

Universität Bremen

# Pressespiegel

Universität Bremen - Pressestelle - Pf 330 440 - D - 28334 Bremen

MARUM
Fachbereich 5
Herrn Albert Gerdes
- PR -
GEO2 5300

Uni - Botenpost

Nr. 51/52.2003 SK 02.01.04

Nordsee-Ztg 30.12.03

## „Open Ship" auf der „Sonne"

### Forschungsschiff nach zwölf Jahren wieder in Bremen – Heute Besichtigung

**Nach zwölf Jahren auf hoher See hat die „Sonne" jetzt den Heimathafen Bremen erstmals wieder angelaufen. Interessierte können sich das Schiff heute im Europahafen ansehen.**

Gestern waren die Festmacher mit dem Forschungsschiff „Sonne" beschäftigt – heute kann es im Europahafen besichtigt werden.

Insgesamt 550 000 Seemeilen hat das Forschungsschiff vorwiegend im Pazifik und Indischen Ozean zurückgelegt, um die Oberfläche des Meeresgrunds, Monsunzirkulationen, Gashydrate, Tiefwasserkorallenriffe und Ozeanränder zu entdecken und zu erforschen. „Es war schon bewegend, die Dame nach so langer Zeit auf der Außenweser begrüßen zu können", sagt Falk von Seck, Geschäftsführer der Reederei RF Forschungsschiffahrt GmbH. Er freut sich, gemeinsam mit der Besatzung und einigen Wissenschaftlern vom Sonderforschungsbereich Ozeanränder an der Universität Bremen heute beim so genannten Open Ship allen Neugierigen „in geballter Form Schiff und Ergebnisse vorstellen zu können". Dazu gehören Exponate in den Labors, anschauliche Poster zur Meeresforschung sowie der Blick durchs Mikroskop.

#### Koje mit Internetanschluss

Beim „Tag der offenen Tür" erhalten die Landratten einen kleinen Eindruck vom Leben auf dem gut 100 Meter langen Schiff. Den 30 Besatzungsmitgliedern und 25 Wissenschaftlern stehen neben Aufenthaltsräumen und Schlafkojen mit Internetanschluss insgesamt 21 Räume und 425 Quadratmeter zum Arbeiten zur Verfügung. Darunter sind beispielsweise Speziallabore für biologische, chemische und physikalische Analysen der Meeresgrundproben oder der Gashydrate, die angezündet wie „brennendes Eis" erscheinen, wie Professor Gerd Bohrmann erklärt, der von Oktober bis Mitte November im Golf von Mexiko gemeinsam mit amerikanischen und mexikanischen Kollegen die Gashydrate weiter erforscht hat. Seit 1996 werden diese Gemische aus Gas und Wasser auf dem Schiff untersucht. Die Zersetzung der stark Methan haltigen Gashydrate hat Rutschungen in den Ozeanen zur Folge.

In den vergangenen vier Wochen durchkreuzte das Schiff unter der Leitung von Professor Achim Kopf den Golf von Cadiz vor Spanien, um durch die Begutachtung dortiger Ozeanränder neue Erkenntnisse in der Erdbebenforschung gewinnen zu können. „1755 gab es bei Lissabon mit einer Magnitude 9 das schwerste Erdbeben auf europäischem Boden", erklärt Kopf, „es war spürbar bis zu den Kapverden." Jetzt haben die Forscher versucht, das damalige Beben zu orten, um aus Proben dann möglicherweise Frühwarnsysteme entwickeln zu können.

Das Forschungsschiff „Sonne" kann heute zwischen 10 und 16 Uhr im Europahafen, Konsul-Schmidt-Straße, besucht werden. Wer nicht mit dem eigenen Auto kommen mag, kann die Straßenbahnlinie 3 bis „Hansator" nehmen. Der Weg zum Schiff ist ausgeschildert, verspricht Falk von Seck. col

Herausgeber Uni-Pressestelle · Postfach 33 04 40 · 28334 Bremen · Telefon (0421) 218 - 27 51 · Fax (0421) 218 - 42 70 · eMail: presse@uni-bremen.de

# Großer Andrang auf der „Sonne“

## 2000 Gäste beim Tag der offenen Tür

Von unserem Redaktionsmitglied
Karen Adamski

Bremer und Wissenschaft – das passt offenbar bestens zusammen. Beim Tag der offenen Tür auf dem Forschungsschiff „Sonne“ im Europahafen herrschte gestern jedenfalls riesiger Andrang. Mehr als 2000 Leute kamen zwischen 10 und 16 Uhr an Bord. Die ersten Besucher warteten bereits um kurz nach neun am Anleger. „Wir sind sehr zufrieden“, bilanzierte Kirsten Achenbach vom DFG-Forschungszentrum Ozeanränder an der Bremer Uni.

Rund 15 Wissenschaftler und Studenten waren gestern auf dem Schiff, um den Besuchern ihre Arbeit zu erklären. Auch die 30-köpfige Besatzung war an Bord. Wer wollte, konnte an einer Führung über das Schiff teilnehmen, durch die Mikroskope blicken oder sich die Geräte zeigen lassen, mit denen die Forscher bei ihren Reisen Proben vom Meeresboden nehmen. „Die Stimmung an Bord war ganz toll“, freute sich Kirsten Achenbach über das Interesse.

Die „Sonne“ wird normalerweise im Auftrag des Bundesforschungsministeriums im Pazifischen und Indischen Ozean eingesetzt. Nach zwölf Jahren war sie jetzt zum ersten Mal wieder in heimatlichen Gewässern unterwegs. Bremen war allerdings nur eine kurze Zwischenstation. Bereits gestern Abend verließ die „Sonne“ den Europahafen wieder Richtung Bremerhaven, wo sie demnächst in die Werft einläuft. Erst im Juni wird sie wieder im Einsatz sein.


Hier geht's zur „Sonne“: Das Forschungsschiff stieß bei den Bremern auf großes Interesse. Mehr als 2000 Besucher kamen gestern zum Tag der offenen Tür und informierten sich über die Arbeit an Bord. Foto: Jochen Stoss

Datum: 30.12.2003

# Die „Sonne“ ist zurück in Bremen

## 16 Leser unserer Zeitung begleiteten das Forschungsschiff auf seinem Weg zum Europahafen

Von unserem Redaktionsmitglied
Karen Adamski

Zwölf Jahre lang war sie im internationalen Einsatz. Nun ist die „Sonne" wieder nach Deutschland zurückgekehrt – in den Bremer Europahafen, wo das Forschungsschiff heute besichtigt werden kann. Einige unserer Leser durften schon gestern einen Blick hinter die Kulissen werfen.

### Blick hinter die Kulissen

Hans Wilhelm Pelster hätte die Schiffsbrücke am liebsten gar nicht wieder verlassen. „Beeindruckend, die ganze Technik hier an Bord", staunte der 71-Jährige und ließ seinen Blick über Monitore und Instrumente schweifen. „Da merkt man gleich, dass man auf einem Forschungsschiff ist." Der gelernte Ingenieur war einer von 16 Lesern unserer Zeitung, die gestern die „Sonne" besichtigten. Von Bremerhaven nach Bremen begleiteten sie das Forschungsschiff – neben der „Meteor" und der „Polarstern" eines der drei großen deutschen Forschungsschiffe –, das nach zwölf Jahren nun zum ersten Mal wieder in deutschen Gewässern unterwegs ist.

War sehr beeindruckt: Hans Wilhelm Pelster.

Eingesetzt wird das rund 100 Meter lange Schiff vor allem im pazifischen und im indischen Ozean. An Bord arbeiten 30 Besatzungsmitglieder, außerdem bietet die „Sonne" Platz für 25 Wissenschaftler. Sie setzen von hier aus Unterwasser-Roboter, Tauchboote oder Sonden aus, mit denen der Meeresboden untersucht wird. Mit an Bord ist beispielsweise ein „TV-Greifer", der es ermöglicht, den Boden zunächst mit einer Kamera zu untersuchen, bevor dann – in vier bis sechs Kilometern Tiefe – Proben entnommen werden.

Würde hier gern arbeiten: Eva Wichert.

„Toll, was wir hier so alles zu sehen bekommen", fand auch Leserin Eva Wichert. Für die 50-Jährige medizinisch-technische Assistentin ist die „Sonne" so etwas wie ihr persönliches Traumschiff: „Ich wollte immer auf einem Forschungsschiff arbeiten. Aber mit der Familie lässt sich das schlecht unter einen Hut bringen." So nutzte sie gestern die Gelegenheit, um mit den Wissenschaftlern an Bord über deren Arbeit zu sprechen und Labore, Decks und Geräte zu besichtigen – und weiter von einer Forschungsreise zu träumen: „Ich hätte riesige Lust dazu. Am liebsten würde ich dann natürlich in den Süden fahren, aber ins Eis wäre auch in Ordnung."

Einer, der schon viele Tage seines Lebens auf der „Sonne" verbracht hat, ist Heinrich Villinger, Geologie-Professor an der Bremer Uni. Sechs Mal war er mit dem Schiff auf Forschungsreise, zuletzt ging es vor zwei Jahren nach Vancouver Island. „Ich hab die Enge hier nie als Problem empfunden", erzählte er, während die Besucher über schmale Flure, niedrige Decken und hohe Türschwellen staunten. „Wenn alle gut zu tun haben, dann geht man sich auch nicht gegenseitig auf die Nerven." Das Schwierigste bei einer solchen Fahrt sei vielmehr die optimale Koordination aller Beteiligten. „Jeder muss zu einem Recht kommen, so dass er am Ende mit optimalen Ergebnissen wieder von Bord gehen kann."

Bis der nächste Forscher mit seinen Ergebnissen von Bord geht, dauert es allerdings noch: Das Schiff bleibt bis zum Frühjahr in Bremen liegen. In dieser Zeit wird es gewartet und erneuert. Ende April läuft die „Sonne" dann wieder aus, um rund 40 Tage später in der Nähe von Jakarta das nächste Ziel zu erreichen.

Heinrich Villinger wird Ende des kommenden Jahres das nächste Mal mit der „Sonne" in See stechen. Dann fährt ein Team von Wissenschaftlern nach Südchile. „Ich freue mich schon", so der Geologie-Professor. „Ich bin gern auf der 'Sonne'. Dieses Schiff hat eine gute Arbeitsatmosphäre."

Pudelwohl fühlte sich auch Leser Heinz Everding. Kein Wunder, meinte der 64-Jährige: „Meine Vorfahren waren Walfänger in Grönland, und mein Vater hat sein Leben auf der Weser verbracht."

Mit dem Wasser vertraut: Heinz Everding.

Bei so viel familiärer Verbundenheit mit dem Wasser konnte ihn auch die Kälte an Deck nicht erschüttern. „Das ist wirklich eine interessante Sache hier", fand Everding. „Normalerweise hat man zu so etwas ja gar keinen Zugang." Klar, auch er könne sich gut vorstellen, an einer Forschungsfahrt teilzunehmen. „Bohrungen und Forschungen, das würde mich schon interessieren." Aber auch für einen geborenen Seebären gibt es Grenzen. „Nur in so ein Tauchboot", sagt Everding, „da würd ich mich nicht reinsetzen."

■ Die „Sonne" kann heute von 10 bis 16 Uhr beim Tag der offenen Tür im Europahafen besichtigt werden. Interessierte können mit Wissenschaftlern des Forschungszentrums Ozeanränder über die Arbeit an Bord sprechen und sich über Geräte und Forschungsergebnisse informieren. Außerdem wird heute das nahe gelegene Kernlager des Ozean-Bohr-Programms für Interessierte geöffnet. Besucher erreichen die „Sonne" über Hansator und Konsul-Smidt-Straße; Parkplätze sind ausreichend vorhanden. Vom Schiff aus führt ein Shuttle-Bus zum Kernlager.

Die „Sonne" im Rücken: Einige unserer Leser vor dem Forschungsschiff, das gestern von Bremerhaven nach Bremen fuhr und heute im Europahafen besichtigt werden kann. Fotos: Jochen Stoss

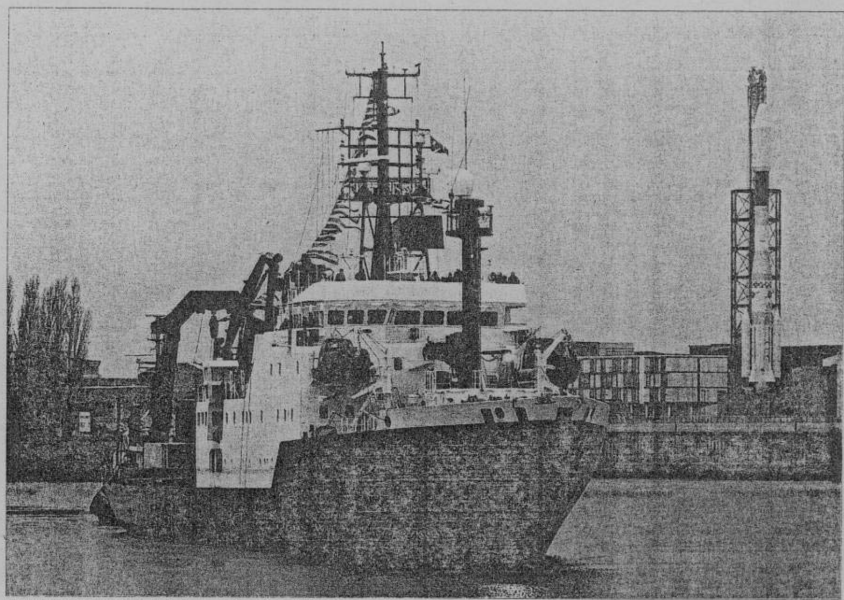

Am Montagnachmittag passierte die FS „Sonne" den Space Park – bei ihrer Abreise lag dort noch die Brache der AG Weser. Sie hat 550 000 Seemeilen zurückg FOTO: FRANK PUSCH

Die Welt 30.12.03

## Vom Pazifik die Weser hinauf: Die „Sonne" kehrt nach zwölf Jahren zurück

Die „Sonne" fährt nach zwölf Jahren wieder mit voller Fahrt die Weser hinauf. Am Montagnachmittag legte das Forschungsschiff das letzte Teilstück seiner Reise mit dem Weg von Bremerhaven nach Bremen zurück. Jetzt liegt es sicher vertäut im Europahafen und kann heute besichtigt werden.

In den vergangenen zwölf Jahren hat das hundert Meter lange und mit hoch moderner Technik ausgerüstete Schiff mehr als 550 000 Seemeilen im Dienst der Meeresforschung zurückgelegt, vorwiegend im Pazifik und im Indischen Ozean. Die 30-köpfige Besatzung und die Wissenschaftler freuen sich darauf, allen Besuchern Einblick in ihre Arbeit zu geben. *flo*

*Die Expeditionen im Netz:* www.rcom-bremen.de/Sonne.html

Die Welt 31.12.03

# Die FS „Sonne" bringt Licht ins Dunkel der Tiefsee

### Das Forschungsschiff ist Erdbeben und Klimawandel auf der Spur – Besichtigung beim „Open Ship" im Europahafen

VON CORINNA LAUBACH

Das Prinzip stammt aus der Raumfahrt. Das Gerät, das Christoph Waldmann und Eberhard Kopiske an Bord des Forschungsschiffes „Sonne" eingehend prüfen, ähnelt dem Mars-Erkunder „Beagle". Auf vier Rädern soll das sperrige Aluminium-Unterwasserfahrzeug „Move" mit Hilfe einer Kamera den Meeresboden erforschen. „Mittlerweile ist die Mars-Oberfläche besser erfasst, als der Meeresgrund", sagen die Geoforscher. Dies sollen Forschungsreisen in die Weltmeere jedoch ändern. Gemeinsam mit der „Polarstern" und der „Meteor" zählt die „Sonne" zum deutschen Dreigestirn der Meeresforschung.

Seit Montagabend liegt sie erstmals seit zwölf Jahren wieder in ihrem Heimathafen Bremen, am Dienstag lud sie Besucher zum „Open Ship" ein.

Mit neuen videogestützten Systemen werden Meeresareale kartiert. „Bislang haben wir Meeresforschung weitestgehend blind betrieben", sagt Achim Kopf vom Forschungszentrum Ozeanränder der Deutschen Forschungsgemeinschaft. In dem an der Universität Bremen angesiedeltem Forschungszentrum ist nicht nur „Move" entwickelt worden, sondern auch neue Tauchboote, die bis zu einer Tiefe von 1000 Metern Proben über Glasfaserleitungen entnehmen.

Zwölf Jahre war die FS „Sonne" ununterbrochen im Einsatz. „Es lohnte einfach nicht, das Schiff nach Deutschland zu holen, wenn wir hintereinander Programme im Pazifischen Ozean absolviert haben", sagt Gerold Wefer, Direktor des Forschungszentrums. Das 1978 auf der Bremerhavener Rickmers-Werft gebaute Forschungsschiff durchkreuzt vor allem den Pazifik und den Indischen Ozean. Auf den jeweiligen Törns „sind eine Vielzahl international beachteter Ergebnisse gesammelt worden", sagt Wefer. Dazu zählen die Entdeckungen neuer Tiefwasser-Korallenriffe, bislang ungekannter Bakterien im Sediment und das Auffinden einzigartiger Sedimentkerne vor Indien, die die Klimaforschung vorangebracht haben.

An Bord wird international geforscht: Neben den 30 Besatzungsmitgliedern, die ausnahmslos Deutsche sind, finden bis zu 25 Wissenschaftler Platz. Eng ist es auf dem Schiff, aber technisch hoch modern. Die Schlafkojen haben einen Internetanschluss. Es gibt Computerräume, ein Foto- und ein Seismik-Labor.

Die Bremer Reederei RF Forschungsschifffahrt hat für weitere sieben Jahre mit dem Bundesforschungsministerium einen Vertrag unterzeichnet. Allerdings: Statt bislang 340 Tage zahlt das Ministerium nur noch 250 Tage Forschungsarbeit auf der „Sonne". „Die restliche Zeit müssen wir jetzt versuchen, das Schiff kommerziell zu vermieten", sagt Reederei-Geschäftsführer Falk von Seck.

Bis April wird das knapp 100 Meter lange Schiff im Bremer Europahafen liegen. Dann sticht es mit Kurs Jakarta wieder in See. *ddp*

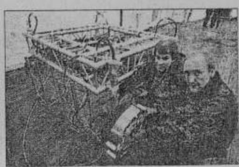

**Christoph Waldmann (r.) und Eberhard Kopiske zeigen an Deck der „Sonne" das Unterwasserfahrzeug „Move". Es kann mit Kameras oder Greifern bestückt den Meeresgrund erkunden**

Delm. Kreisbl. 18.12.03

# Forschungsschiff lädt zur Besichtigung ein

**SCHIFFFAHRT** Nach 550 000 Seemeilen kommt die „Sonne" in den Heimathafen

**BREMEN**/LO – Nach über einem Dutzend Jahren kehrt das in Bremen beheimatete Forschungsschiff „Sonne" wieder nach Deutschland zurück. Seit dem letzten Besuch hat das etwa 100 Meter lange Schiff mehr als 550 000 Seemeilen im Dienst der Meeresforschung zurück gelegt, vorwiegend im Pazifik und im Indischen Ozean.

Am Montag fährt die „Sonne" von Bremerhaven weseraufwärts nach Bremen. Dort macht sie im Europahafen fest. Das Forschungsschiff kann dann am 30. Dezember zwischen 10 bis 16 Uhr besichtigt werden. Die knapp 30-köpfige Besatzung steht bereit, um in Schiffsführungen und Gesprächen hautnah Einblicke in die speziellen Anforderungen des Bordbetriebes zu geben. Auch das benachbarte Bohrkernlager im Europahafen ist geöffnet.

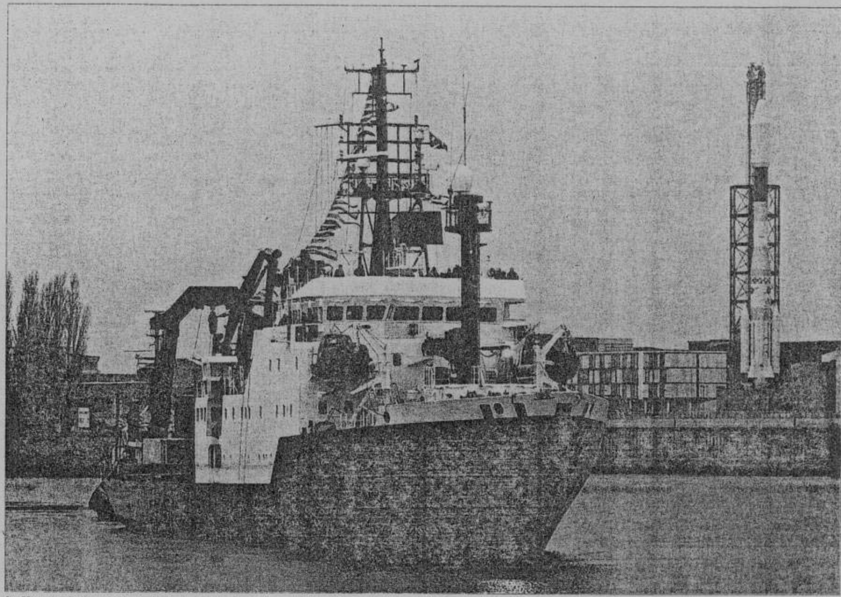

Am Montagnachmittag passierte die FS „Sonne" den Space Park – bei ihrer Abreise lag dort noch die Brache der AG Weser. Sie hat 550 000 Seemeilen zurückg FOTO: FRANK PUSCH

Die Welt 30.12.03

## Vom Pazifik die Weser hinauf: Die „Sonne" kehrt nach zwölf Jahren zurück

Die „Sonne" fährt nach zwölf Jahren wieder mit voller Fahrt die Weser hinauf: Am Montagnachmittag legte das Forschungsschiff das letzte Teilstück seiner Reise mit dem Weg von Bremerhaven nach Bremen zurück. Jetzt liegt es sicher vertäut im Europahafen und kann heute besichtigt werden.

In den vergangenen zwölf Jahren hat das hundert Meter lange und mit hoch moderner Technik ausgerüstete Schiff mehr als 550 000 Seemeilen im Dienst der Meeresforschung zurückgelegt, vorwiegend im Pazifik und im Indischen Ozean. Die 30-köpfige Besatzung und die Wissenschaftler freuen sich darauf, allen Besuchern Einblick in ihre Arbeit zu geben. *flo*

*Die Expeditionen im Netz:* www.rcom-bremen.de/Sonne.html

Die Welt 31.12.03

# Die FS „Sonne" bringt Licht ins Dunkel der Tiefsee

## Das Forschungsschiff ist Erdbeben und Klimawandel auf der Spur – Besichtigung beim „Open Ship" im Europahafen

VON CORINNA LAUBACH

Das Prinzip stammt aus der Raumfahrt. Das Gerät, das Christoph Waldmann und Eberhard Kopiske an Bord des Forschungsschiffes „Sonne" eingehend prüfen, ähnelt dem Mars-Erkunder „Beagle". Auf vier Rädern soll das sperrige Aluminium-Unterwasserfahrzeug „Move" mit Hilfe einer Kamera den Meeresboden erforschen. „Mittlerweile ist die Mars-Oberfläche besser erfasst, als der Meeresgrund", sagen die Geoforscher. Dies sollen Forschungsreisen in die Weltmeere jedoch ändern. Gemeinsam mit der „Polarstern" und der „Meteor" zählt die „Sonne" zum deutschen Dreigestirn der Meeresforschung.

Seit Montagabend liegt sie erstmals seit zwölf Jahren wieder in ihrem Heimathafen Bremen, am Dienstag lud sie Besucher zum „Open Ship" ein.

Mit neuen videogestützten Systemen werden Meeresareale kartiert. „Bislang haben wir Meeresforschung weitestgehend blind betrieben", sagt Achim Kopf vom Forschungszentrum Ozeanränder der Deutschen Forschungsgemeinschaft. In dem an der Universität Bremen angesiedeltem Forschungszentrum ist nicht nur „Move" entwickelt worden, sondern auch neue Tauchboote, die bis zu einer Tiefe von 1000 Metern Proben über Glasfaserleitungen entnehmen.

Zwölf Jahre war die FS „Sonne" ununterbrochen im Einsatz. „Es lohnte einfach nicht, das Schiff nach Deutschland zu holen, wenn wir hintereinander Programme im Pazifischen Ozean absolviert haben", sagt Gerold Wefer, Direktor des Forschungszentrums. Das 1978 auf der Bremerhavener Rickmers-Werft gebaute Forschungsschiff durchkreuzt vor allem den Pazifik und den Indischen Ozean. Auf den jeweiligen Törns „sind eine Vielzahl international beachteter Ergebnisse gesammelt worden", sagt Wefer. Dazu zählen die Entdeckungen neuer Tiefwasser-Korallenriffe, bislang ungekannter Bakterien im Sediment und das Auffinden einzigartiger Sedimentkerne vor Indien, die die Klimaforschung vorangebracht haben.

An Bord wird international geforscht: Neben den 30 Besatzungsmitgliedern, die ausnahmslos Deutsche sind, finden bis zu 25 Wissenschaftler Platz. Eng ist es auf dem Schiff, aber technisch hoch modern. Die Schlafkojen haben einen Internetanschluss. Es gibt Computerräume, ein Foto- und ein Seismik-Labor.

Die Bremer Reederei RF Forschungsschifffahrt hat für weitere sieben Jahre mit dem Bundesforschungsministerium einen Vertrag unterzeichnet. Allerdings: Statt bislang 340 Tage zahlt das Ministerium nur noch 250 Tage Forschungsarbeit auf der „Sonne". „Die restliche Zeit müssen wir jetzt versuchen, das Schiff kommerziell zu vermieten", sagt Reederei-Geschäftsführer Falk von Seck.

Bis April wird das knapp 100 Meter lange Schiff im Bremer Europahafen liegen. Dann sticht es mit Kurs Jakarta wieder in See. *ddp*

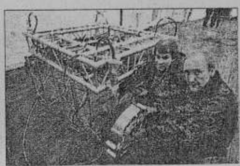

**Christoph Waldmann (r.) und Eberhard Kopiske zeigen an Deck der „Sonne" das Unterwasserfahrzeug „Move". Es kann mit Kameras oder Greifern bestückt den Meeresgrund erkunden**

Delm. Kreisbl. 18.12.03

# Forschungsschiff lädt zur Besichtigung ein

## SCHIFFFAHRT Nach 550 000 Seemeilen kommt die „Sonne" in den Heimathafen

**BREMEN**/LO – Nach über einem Dutzend Jahren kehrt das in Bremen beheimatete Forschungsschiff „Sonne" wieder nach Deutschland zurück. Seit dem letzten Besuch hat das etwa 100 Meter lange Schiff mehr als 550 000 Seemeilen im Dienst der Meeresforschung zurück gelegt, vorwiegend im Pazifik und im Indischen Ozean.

Am Montag fährt die „Sonne" von Bremerhaven weseraufwärts nach Bremen. Dort macht sie im Europahafen fest. Das Forschungsschiff kann dann am 30. Dezember zwischen 10 bis 16 Uhr besichtigt werden. Die knapp 30-köpfige Besatzung steht bereit, um in Schiffsführungen und Gesprächen hautnah Einblicke in die speziellen Anforderungen des Bordbetriebes zu geben. Auch das benachbarte Bohrkernlager im Europahafen ist geöffnet.

**9. Acknowledgements**

We thank Master Henning Papenhagen for his relaxed, superb manner steering SONNE through the North Atlantic waters, and later on into Bremen port. Thanks go also to the crew of SONNE for their friendly support and efficient technical assistance with the various devices used. Without them, neither the scientific success of the cruise nor the good humor during various parties during legs 2 and 3, and a fabulous Christmas Eve during leg 4.

Thanks go also to the German Ministry for Education and Research (BMBF) for providing the funds to make the *GAP* (Gibraltar Arc Processes) cruise happen (FKZ 03G0175A). Additional funding was provided by the German Science Foundation (to RCOM, Bremen), International University Bremen, and RWE Dea AG (Hamburg).

We want to thank our colleagues Eulalia Gracia, Karl Hinz and Nevio Zittelini for having provided (partly unpublished) material to help with *GAP* planning. Special thanks go to Albert Gerdes and Gerold Wefer for having ensured the outreach of the SO175 expedition to the public and press in Bremen, and beyond. Kathrin Sänger and Berndt Burckhardt are thanked for their expertise and enthusiasm when cutting and digitizing some cruise documentation for publication. Chantal Cowan and Barbara Donner are acknowledged for their help with getting the cruise report into shape.

Publications of this series:

**No. 1** **Wefer, G., E. Suess and cruise participants**
Bericht über die POLARSTERN-Fahrt ANT IV/2, Rio de Janeiro - Punta Arenas, 6.11. - 1.12.1985.
60 pages, Bremen, 1986.

**No. 2** **Hoffmann, G.**
Holozänstratigraphie und Küstenlinienverlagerung an der andalusischen Mittelmeerküste.
173 pages, Bremen, 1988. (out of print)

**No. 3** **Wefer, G. and cruise participants**
Bericht über die METEOR-Fahrt M 6/6, Libreville - Las Palmas, 18.2. - 23.3.1988.
97 pages, Bremen, 1988.

**No. 4** **Wefer, G., G.F. Lutze, T.J. Müller, O. Pfannkuche, W. Schenke, G. Siedler, W. Zenk**
Kurzbericht über die METEOR-Expedition No. 6, Hamburg - Hamburg, 28.10.1987 - 19.5.1988.
29 pages, Bremen, 1988. (out of print)

**No. 5** **Fischer, G.**
Stabile Kohlenstoff-Isotope in partikulärer organischer Substanz aus dem Südpolarmeer
(Atlantischer Sektor). 161 pages, Bremen, 1989.

**No. 6** **Berger, W.H. and G. Wefer**
Partikelfluß und Kohlenstoffkreislauf im Ozean.
Bericht und Kurzfassungen über den Workshop vom 3.-4. Juli 1989 in Bremen.
57 pages, Bremen, 1989.

**No. 7** **Wefer, G. and cruise participants**
Bericht über die METEOR - Fahrt M 9/4, Dakar - Santa Cruz, 19.2. - 16.3.1989.
103 pages, Bremen, 1989.

**No. 8** **Kölling, M.**
Modellierung geochemischer Prozesse im Sickerwasser und Grundwasser.
135 pages, Bremen, 1990.

**No. 9** **Heinze, P.-M.**
Das Auftriebsgeschehen vor Peru im Spätquartär. 204 pages, Bremen, 1990. (out of print)

**No. 10** **Willems, H., G. Wefer, M. Rinski, B. Donner, H.-J. Bellmann, L. Eißmann, A. Müller, B.W. Flemming, H.-C. Höfle, J. Merkt, H. Streif, G. Hertweck, H. Kuntze, J. Schwaar, W. Schäfer, M.-G. Schulz, F. Grube, B. Menke**
Beiträge zur Geologie und Paläontologie Norddeutschlands: Exkursionsführer.
202 pages, Bremen, 1990.

**No. 11** **Wefer, G. and cruise participants**
Bericht über die METEOR-Fahrt M 12/1, Kapstadt - Funchal, 13.3.1990 - 14.4.1990.
66 pages, Bremen, 1990.

**No. 12** **Dahmke, A., H.D. Schulz, A. Kölling, F. Kracht, A. Lücke**
Schwermetallspuren und geochemische Gleichgewichte zwischen Porenlösung und Sediment
im Wesermündungsgebiet. BMFT-Projekt MFU 0562, Abschlußbericht. 121 pages, Bremen, 1991.

**No. 13** **Rostek, F.**
Physikalische Strukturen von Tiefseesedimenten des Südatlantiks und ihre Erfassung in
Echolotregistrierungen. 209 pages, Bremen, 1991.

**No. 14** **Baumann, M.**
Die Ablagerung von Tschernobyl-Radiocäsium in der Norwegischen See und in der Nordsee.
133 pages, Bremen, 1991. (out of print)

**No. 15** **Kölling, A.**
Frühdiagenetische Prozesse und Stoff-Flüsse in marinen und ästuarinen Sedimenten.
140 pages, Bremen, 1991.

**No. 16** **SFB 261 (ed.)**
1. Kolloquium des Sonderforschungsbereichs 261 der Universität Bremen (14.Juni 1991):
Der Südatlantik im Spätquartär: Rekonstruktion von Stoffhaushalt und Stromsystemen.
Kurzfassungen der Vorträge und Poster. 66 pages, Bremen, 1991.

**No. 17** **Pätzold, J. and cruise participants**
Bericht und erste Ergebnisse über die METEOR-Fahrt M 15/2, Rio de Janeiro - Vitoria,
18.1. - 7.2.1991. 46 pages, Bremen, 1993.

**No. 18** **Wefer, G. and cruise participants**
Bericht und erste Ergebnisse über die METEOR-Fahrt M 16/1, Pointe Noire - Recife,
27.3. - 25.4.1991. 120 pages, Bremen, 1991.

**No. 19** **Schulz, H.D. and cruise participants**
Bericht und erste Ergebnisse über die METEOR-Fahrt M 16/2, Recife - Belem, 28.4. - 20.5.1991.
149 pages, Bremen, 1991.

**No. 20** **Berner, H.**
Mechanismen der Sedimentbildung in der Fram-Straße, im Arktischen Ozean und in der Norwegischen See. 167 pages, Bremen, 1991.

**No. 21** **Schneider, R.**
Spätquartäre Produktivitätsänderungen im östlichen Angola-Becken: Reaktion auf Variationen im Passat-Monsun-Windsystem und in der Advektion des Benguela-Küstenstroms.
198 pages, Bremen, 1991. (out of print)

**No. 22** **Hebbeln, D.**
Spätquartäre Stratigraphie und Paläozeanographie in der Fram-Straße. 174 pages, Bremen, 1991.

**No. 23** **Lücke, A.**
Umsetzungsprozesse organischer Substanz während der Frühdiagenese in ästuarinen Sedimenten.
137 pages, Bremen, 1991.

**No. 24** **Wefer, G. and cruise participants**
Bericht und erste Ergebnisse der METEOR-Fahrt M 20/1, Bremen - Abidjan, 18.11.- 22.12.1991.
74 pages, Bremen, 1992.

**No. 25** **Schulz, H.D. and cruise participants**
Bericht und erste Ergebnisse der METEOR-Fahrt M 20/2, Abidjan - Dakar, 27.12.1991 - 3.2.1992.
173 pages, Bremen, 1992.

**No. 26** **Gingele, F.**
Zur klimaabhängigen Bildung biogener und terrigener Sedimente und ihrer Veränderung durch die Frühdiagenese im zentralen und östlichen Südatlantik. 202 pages, Bremen, 1992.

**No. 27** **Bickert, T.**
Rekonstruktion der spätquartären Bodenwasserzirkulation im östlichen Südatlantik über stabile Isotope benthischer Foraminiferen. 205 pages, Bremen, 1992. (out of print)

**No. 28** **Schmidt, H.**
Der Benguela-Strom im Bereich des Walfisch-Rückens im Spätquartär. 172 pages, Bremen, 1992.

**No. 29** **Meinecke, G.**
Spätquartäre Oberflächenwassertemperaturen im östlichen äquatorialen Atlantik.
181 pages, Bremen, 1992.

**No. 30** **Bathmann, U., U. Bleil, A. Dahmke, P. Müller, A. Nehrkorn, E.-M. Nöthig, M. Olesch, J. Pätzold, H.D. Schulz, V. Smetacek, V. Spieß, G. Wefer, H. Willems**
Bericht des Graduierten Kollegs. Stoff-Flüsse in marinen Geosystemen.
Berichtszeitraum Oktober 1990 - Dezember 1992. 396 pages, Bremen, 1992.

**No. 31** **Damm, E.**
Frühdiagenetische Verteilung von Schwermetallen in Schlicksedimenten der westlichen Ostsee.
115 pages, Bremen, 1992.

**No. 32** **Antia, E.E.**
Sedimentology, Morphodynamics and Facies Association of a mesotidal Barrier Island Shoreface (Spiekeroog, Southern North Sea). 370 pages, Bremen, 1993.

**No. 33** **Duinker, J. and G. Wefer (ed.)**
Bericht über den 1. JGOFS-Workshop. 1./2. Dezember 1992 in Bremen. 83 pages, Bremen, 1993.

**No. 34** **Kasten, S.**
Die Verteilung von Schwermetallen in den Sedimenten eines stadtbremischen Hafenbeckens.
103 pages, Bremen, 1993.

**No. 35** **Spieß, V.**
Digitale Sedimentographie. Neue Wege zu einer hochauflösenden Akustostratigraphie.
199 pages, Bremen, 1993.

**No. 36** **Schinzel, U.**
Laborversuche zu frühdiagenetischen Reaktionen von Eisen (III) - Oxidhydraten in marinen Sedimenten.189 pages, Bremen, 1993.

**No. 37** **Sieger, R.**
CoTAM - ein Modell zur Modellierung des Schwermetalltransports in Grundwasserleitern.
56 pages, Bremen, 1993. (out of print)

**No. 38** **Willems, H. (ed.)**
Geoscientific Investigations in the Tethyan Himalayas. 183 pages, Bremen, 1993.

**No. 39** **Hamer, K.**
Entwicklung von Laborversuchen als Grundlage für die Modellierung des Transportverhaltens von Arsenat, Blei, Cadmium und Kupfer in wassergesättigten Säulen. 147 pages, Bremen, 1993.

**No. 40** **Sieger, R.**
Modellierung des Stofftransports in porösen Medien unter Ankopplung kinetisch gesteuerter Sorptions- und Redoxprozesse sowie thermischer Gleichgewichte. 158 pages, Bremen, 1993.

**No. 41** **Thießen, W.**
Magnetische Eigenschaften von Sedimenten des östlichen Südatlantiks und ihre paläozeanographische Relevanz. 170 pages, Bremen, 1993.

**No. 42** **Spieß, V. and cruise participants**
Report and preliminary results of METEOR-Cruise M 23/1, Kapstadt - Rio de Janeiro, 4.-25.2.1993. 139 pages, Bremen, 1994.

**No. 43** **Bleil, U. and cruise participants**
Report and preliminary results of METEOR-Cruise M 23/2, Rio de Janeiro - Recife, 27.2.-19.3.1993 133 pages, Bremen, 1994.

**No. 44** **Wefer, G. and cruise participants**
Report and preliminary results of METEOR-Cruise M 23/3, Recife - Las Palmas, 21.3. - 12.4.1993 71 pages, Bremen, 1994.

**No. 45** **Giese, M. and G. Wefer (ed.)**
Bericht über den 2. JGOFS-Workshop. 18../19. November 1993 in Bremen.
93 pages, Bremen, 1994.

**No. 46** **Balzer, W. and cruise participants**
Report and preliminary results of METEOR-Cruise M 22/1, Hamburg - Recife, 22.9. - 21.10.1992. 24 pages, Bremen, 1994.

**No. 47** **Stax, R.**
Zyklische Sedimentation von organischem Kohlenstoff in der Japan See: Anzeiger für Änderungen von Paläoozeanographie und Paläoklima im Spätkänozoikum.
150 pages, Bremen, 1994.

**No. 48** **Skowronek, F.**
Frühdiagenetische Stoff-Flüsse gelöster Schwermetalle an der Oberfläche von Sedimenten des Weser Ästuares. 107 pages, Bremen, 1994.

**No. 49** **Dersch-Hansmann, M.**
Zur Klimaentwicklung in Ostasien während der letzten 5 Millionen Jahre:
Terrigener Sedimenteintrag in die Japan See (ODP Ausfahrt 128). 149 pages, Bremen, 1994.

**No. 50** **Zabel, M.**
Frühdiagenetische Stoff-Flüsse in Oberflächen-Sedimenten des äquatorialen und östlichen Südatlantik. 129 pages, Bremen, 1994.

**No. 51** **Bleil, U. and cruise participants**
Report and preliminary results of SONNE-Cruise SO 86, Buenos Aires - Capetown, 22.4. - 31.5.93 116 pages, Bremen, 1994.

**No. 52** **Symposium: The South Atlantic: Present and Past Circulation.**
Bremen, Germany, 15 - 19 August 1994. Abstracts. 167 pages, Bremen, 1994.

**No. 53** **Kretzmann, U.B.**
$^{57}$Fe-Mössbauer-Spektroskopie an Sedimenten - Möglichkeiten und Grenzen.
183 pages, Bremen, 1994.

**No. 54** **Bachmann, M.**
Die Karbonatrampe von Organyà im oberen Oberapt und unteren Unteralb (NE-Spanien, Prov. Lerida): Fazies, Zyklo- und Sequenzstratigraphie. 147 pages, Bremen, 1994. (out of print)

**No. 55** **Kemle-von Mücke, S.**
Oberflächenwasserstruktur und -zirkulation des Südostatlantiks im Spätquartär.
151 pages, Bremen, 1994.

**No. 56** **Petermann, H.**
Magnetotaktische Bakterien und ihre Magnetosome in Oberflächensedimenten des Südatlantiks.
134 pages, Bremen, 1994.

**No. 57** **Mulitza, S.**
Spätquartäre Variationen der oberflächennahen Hydrographie im westlichen äquatorialen Atlantik.
97 pages, Bremen, 1994.

**No. 58** **Segl, M. and cruise participants**
Report and preliminary results of METEOR-Cruise M 29/1, Buenos-Aires - Montevideo, 17.6. - 13.7.1994
94 pages, Bremen, 1994.

**No. 59** **Bleil, U. and cruise participants**
Report and preliminary results of METEOR-Cruise M 29/2, Montevideo - Rio de Janiero 15.7. - 8.8.1994. 153 pages, Bremen, 1994.

**No. 60** **Henrich, R. and cruise participants**
Report and preliminary results of METEOR-Cruise M 29/3, Rio de Janeiro - Las Palmas 11.8. - 5.9.1994. Bremen, 1994. (out of print)

**No. 61** **Sagemann, J.**
Saisonale Variationen von Porenwasserprofilen, Nährstoff-Flüssen und Reaktionen in intertidalen Sedimenten des Weser-Ästuars. 110 pages, Bremen, 1994. (out of print)

**No. 62** **Giese, M. and G. Wefer**
Bericht über den 3. JGOFS-Workshop. 5./6. Dezember 1994 in Bremen.
84 pages, Bremen, 1995.

**No. 63** **Mann, U.**
Genese kretazischer Schwarzschiefer in Kolumbien: Globale vs. regionale/lokale Prozesse.
153 pages, Bremen, 1995. (out of print)

**No. 64** **Willems, H., Wan X., Yin J., Dongdui L., Liu G., S. Dürr, K.-U. Gräfe**
The Mesozoic development of the N-Indian passive margin and of the Xigaze Forearc Basin in southern Tibet, China. – Excursion Guide to IGCP 362 Working-Group Meeting "Integrated Stratigraphy". 113 pages, Bremen, 1995. (out of print)

**No. 65** **Hünken, U.**
Liefergebiets - Charakterisierung proterozoischer Goldseifen in Ghana anhand von Fluideinschluß - Untersuchungen. 270 pages, Bremen, 1995.

**No. 66** **Nyandwi, N.**
The Nature of the Sediment Distribution Patterns in ther Spiekeroog Backbarrier Area, the East Frisian Islands. 162 pages, Bremen, 1995.

**No. 67** **Isenbeck-Schröter, M.**
Transportverhalten von Schwermetallkationen und Oxoanionen in wassergesättigten Sanden.
- Laborversuche in Säulen und ihre Modellierung -. 182 pages, Bremen, 1995.

**No. 68** **Hebbeln, D. and cruise participants**
Report and preliminary results of SONNE-Cruise SO 102, Valparaiso - Valparaiso, 95.
134 pages, Bremen, 1995.

**No. 69** **Willems, H. (Sprecher), U.Bathmann, U. Bleil, T. v. Dobeneck, K. Herterich, B.B. Jorgensen, E.-M. Nöthig, M. Olesch, J. Pätzold, H.D. Schulz, V. Smetacek, V. Speiß. G. Wefer**
Bericht des Graduierten-Kollegs Stoff-Flüsse in marine Geosystemen.
Berichtszeitraum Januar 1993 - Dezember 1995.
45 & 468 pages, Bremen, 1995.

**No. 70** **Giese, M. and G. Wefer**
Bericht über den 4. JGOFS-Workshop. 20./21. November 1995 in Bremen. 60 pages, Bremen, 1996. (out of print)

**No. 71** **Meggers, H.**
Pliozän-quartäre Karbonatsedimentation und Paläozeanographie des Nordatlantiks und des Europäischen Nordmeeres - Hinweise aus planktischen Foraminiferengemeinschaften.
143 pages, Bremen, 1996. (out of print)

**No. 72** **Teske, A.**
Phylogenetische und ökologische Untersuchungen an Bakterien des oxidativen und reduktiven marinen Schwefelkreislaufs mittels ribosomaler RNA. 220 pages, Bremen, 1996. (out of print)

**No. 73** **Andersen, N.**
Biogeochemische Charakterisierung von Sinkstoffen und Sedimenten aus ostatlantischen Produktions-Systemen mit Hilfe von Biomarkern. 215 pages, Bremen, 1996.

**No. 74** **Treppke, U.**
Saisonalität im Diatomeen- und Silikoflagellatenfluß im östlichen tropischen und subtropischen Atlantik. 200 pages, Bremen, 1996.

**No. 75** **Schüring, J.**
Die Verwendung von Steinkohlebergematerialien im Deponiebau im Hinblick auf die Pyritverwitterung und die Eignung als geochemische Barriere. 110 pages, Bremen, 1996.

**No. 76** **Pätzold, J. and cruise participants**
Report and preliminary results of VICTOR HENSEN cruise JOPS II, Leg 6, Fortaleza - Recife, 10.3. - 26.3. 1995 and Leg 8, Vítoria - Vítoria, 10.4. - 23.4.1995.
87 pages, Bremen, 1996.

**No. 77** **Bleil, U. and cruise participants**
Report and preliminary results of METEOR-Cruise M 34/1, Cape Town - Walvis Bay, 3.-26.1.1996.
129 pages, Bremen, 1996.

**No. 78** **Schulz, H.D. and cruise participants**
Report and preliminary results of METEOR-Cruise M 34/2, Walvis Bay - Walvis Bay, 29.1.-18.2.96
133 pages, Bremen, 1996.

**No. 79** **Wefer, G. and cruise participants**
Report and preliminary results of METEOR-Cruise M 34/3, Walvis Bay - Recife, 21.2.-17.3.1996.
168 pages, Bremen, 1996.

**No. 80** **Fischer, G. and cruise participants**
Report and preliminary results of METEOR-Cruise M 34/4, Recife - Bridgetown, 19.3.-15.4.1996.
105 pages, Bremen, 1996.

**No. 81** **Kulbrok, F.**
Biostratigraphie, Fazies und Sequenzstratigraphie einer Karbonatrampe in den Schichten der Oberkreide und des Alttertiärs Nordost-Ägyptens (Eastern Desert, N'Golf von Suez, Sinai).
153 pages, Bremen, 1996.

**No. 82** **Kasten, S.**
Early Diagenetic Metal Enrichments in Marine Sediments as Documents of Nonsteady-State Depositional Conditions. Bremen, 1996.

**No. 83** **Holmes, M.E.**
Reconstruction of Surface Ocean Nitrate Utilization in the Southeast Atlantic Ocean Based on Stable Nitrogen Isotopes. 113 pages, Bremen, 1996.

**No. 84** **Rühlemann, C.**
Akkumulation von Carbonat und organischem Kohlenstoff im tropischen Atlantik: Spätquartäre Produktivitäts-Variationen und ihre Steuerungsmechanismen.
139 pages, Bremen, 1996.

**No. 85** **Ratmeyer, V.**
Untersuchungen zum Eintrag und Transport lithogener und organischer partikulärer Substanz im östlichen subtropischen Nordatlantik. 154 pages, Bremen, 1996.

**No. 86** **Cepek, M.**
Zeitliche und räumliche Variationen von Coccolithophoriden-Gemeinschaften im subtropischen Ost-Atlantik: Untersuchungen an Plankton, Sinkstoffen und Sedimenten.
156 pages, Bremen, 1996.

**No. 87** **Otto, S.**
Die Bedeutung von gelöstem organischen Kohlenstoff (DOC) für den Kohlenstofffluß im Ozean.
150 pages, Bremen, 1996.

**No. 88** **Hensen, C.**
Frühdiagenetische Prozesse und Quantifizierung benthischer Stoff-Flüsse in Oberflächensedimenten des Südatlantiks.
132 pages, Bremen, 1996.

**No. 89** **Giese, M. and G. Wefer**
Bericht über den 5. JGOFS-Workshop. 27./28. November 1996 in Bremen. 73 pages, Bremen, 1997.

**No. 90** **Wefer, G. and cruise participants**
Report and preliminary results of METEOR-Cruise M 37/1, Lisbon - Las Palmas, 4.-23.12.1996.
79 pages, Bremen, 1997.

**No. 91** **Isenbeck-Schröter, M., E. Bedbur, M. Kofod, B. König, T. Schramm & G. Mattheß**
Occurrence of Pesticide Residues in Water - Assessment of the Current Situation in Selected EU Countries. 65 pages, Bremen 1997.

**No. 92** **Kühn, M.**
Geochemische Folgereaktionen bei der hydrogeothermalen Energiegewinnung.
129 pages, Bremen 1997.

**No. 93** **Determann, S. & K. Herterich**
JGOFS-A6 "Daten und Modelle": Sammlung JGOFS-relevanter Modelle in Deutschland.
26 pages, Bremen, 1997.

**No. 94** **Fischer, G. and cruise participants**
Report and preliminary results of METEOR-Cruise M 38/1, Las Palmas - Recife, 25.1.-1.3.1997, with Appendix: Core Descriptions from METEOR Cruise M 37/1. Bremen, 1997.

**No. 95** **Bleil, U. and cruise participants**
Report and preliminary results of METEOR-Cruise M 38/2, Recife - Las Palmas, 4.3.-14.4.1997.
126 pages, Bremen, 1997.

**No. 96** **Neuer, S. and cruise participants**
Report and preliminary results of VICTOR HENSEN-Cruise 96/1. Bremen, 1997.

**No. 97** **Villinger, H. and cruise participants**
Fahrtbericht SO 111, 20.8. - 16.9.1996. 115 pages, Bremen, 1997.

**No. 98** **Lüning, S.**
Late Cretaceous - Early Tertiary sequence stratigraphy, paleoecology and geodynamics of Eastern Sinai, Egypt. 218 pages, Bremen, 1997.

**No. 99** **Haese, R.R.**
Beschreibung und Quantifizierung frühdiagenetischer Reaktionen des Eisens in Sedimenten des Südatlantiks. 118 pages, Bremen, 1997.

**No. 100** **Lührte, R. von**
Verwertung von Bremer Baggergut als Material zur Oberflächenabdichtung von Deponien - Geochemisches Langzeitverhalten und Schwermetall-Mobilität (Cd, Cu, Ni, Pb, Zn). Bremen, 1997.

**No. 101** **Ebert, M.**
Der Einfluß des Redoxmilieus auf die Mobilität von Chrom im durchströmten Aquifer. 135 pages, Bremen, 1997.

**No. 102** **Krögel, F.**
Einfluß von Viskosität und Dichte des Seewassers auf Transport und Ablagerung von Wattsedimenten (Langeooger Rückseitenwatt, südliche Nordsee). 168 pages, Bremen, 1997.

**No. 103** **Kerntopf, B.**
Dinoflagellate Distribution Patterns and Preservation in the Equatorial Atlantic and Offshore North-West Africa. 137 pages, Bremen, 1997.

**No. 104** **Breitzke, M.**
Elastische Wellenausbreitung in marinen Sedimenten - Neue Entwicklungen der Ultraschall Sedimentphysik und Sedimentechographie. 298 pages, Bremen, 1997.

**No. 105** **Marchant, M.**
Rezente und spätquartäre Sedimentation planktischer Foraminiferen im Peru-Chile Strom. 115 pages, Bremen, 1997.

**No. 106** **Habicht, K.S.**
Sulfur isotope fractionation in marine sediments and bacterial cultures. 125 pages, Bremen, 1997.

**No. 107** **Hamer, K., R.v. Lührte, G. Becker, T. Felis, S. Keffel, B. Strotmann, C. Waschkowitz, M. Kölling, M. Isenbeck-Schröter, H.D. Schulz**
Endbericht zum Forschungsvorhaben 060 des Landes Bremen: Baggergut der Hafengruppe Bremen-Stadt: Modelluntersuchungen zur Schwermetallmobilität und Möglichkeiten der Verwertung von Hafenschlick aus Bremischen Häfen. 98 pages, Bremen, 1997.

**No. 108** **Greeff, O.W.**
Entwicklung und Erprobung eines benthischen Landersystemes zur *in situ*-Bestimmung von Sulfatreduktionsraten mariner Sedimente. 121 pages, Bremen, 1997.

**No. 109** **Pätzold, M. und G. Wefer**
Bericht über den 6. JGOFS-Workshop am 4./5.12.1997 in Bremen. Im Anhang: Publikationen zum deutschen Beitrag zur Joint Global Ocean Flux Study (JGOFS), Stand 1/1998. 122 pages, Bremen, 1998.

**No. 110** **Landenberger, H.**
CoTReM, ein Multi-Komponenten Transport- und Reaktions-Modell. 142 pages, Bremen, 1998.

**No. 111** **Villinger, H. und Fahrtteilnehmer**
Fahrtbericht SO 124, 4.10. - 16.10.199. 90 pages, Bremen, 1997.

**No. 112** **Gietl, R.**
Biostratigraphie und Sedimentationsmuster einer nordostägyptischen Karbonatrampe unter Berücksichtigung der Alveolinen-Faunen. 142 pages, Bremen, 1998.

**No. 113** **Ziebis, W.**
The Impact of the Thalassinidean Shrimp *Callianassa truncata* on the Geochemistry of permeable, coastal Sediments. 158 pages, Bremen 1998.

**No. 114** **Schulz, H.D. and cruise participants**
Report and preliminary results of METEOR-Cruise M 41/1, Málaga - Libreville, 13.2.-15.3.1998. Bremen, 1998.

**No. 115** **Völker, D.J.**
Untersuchungen an strömungsbeeinflußten Sedimentationsmustern im Südozean. Interpretation sedimentechographischer Daten und numerische Modellierung. 152 pages, Bremen, 1998.

**No. 116** **Schlünz, B.**
Riverine Organic Carbon Input into the Ocean in Relation to Late Quaternary Climate Change. 136 pages, Bremen, 1998.

**No. 117** **Kuhnert, H.**
Aufzeichnug des Klimas vor Westaustralien in stabilen Isotopen in Korallenskeletten. 109 pages, Bremen, 1998.

**No. 118** **Kirst, G.**
Rekonstruktion von Oberflächenwassertemperaturen im östlichen Südatlantik anhand von Alkenonen. 130 pages, Bremen, 1998.

**No. 119** **Dürkoop, A.**
Der Brasil-Strom im Spätquartär: Rekonstruktion der oberflächennahen Hydrographie während der letzten 400 000 Jahre. 121 pages, Bremen, 1998.

**No. 120** **Lamy, F.**
Spätquartäre Variationen des terrigenen Sedimenteintrags entlang des chilenischen Konti-nentalhangs als Abbild von Klimavariabilität im Milanković- und Sub-Milanković-Zeitbereich. 141 pages, Bremen, 1998.

**No. 121** **Neuer, S. and cruise participants**
Report and preliminary results of POSEIDON-Cruise Pos 237/2, Vigo – Las Palmas, 18.3.-31.3.1998. 39 pages, Bremen, 1998

**No. 122** **Romero, O.E.**
Marine planktonic diatoms from the tropical and equatorial Atlantic: temporal flux patterns and the sediment record. 205 pages, Bremen, 1998.

**No. 123** **Spiess, V. und Fahrtteilnehmer**
Report and preliminary results of RV SONNE Cruise 125, Cochin – Chittagong, 17.10.-17.11.1997. 128 pages, Bremen, 1998.

**No. 124** **Arz, H.W.**
Dokumentation von kurzfristigen Klimaschwankungen des Spätquartärs in Sedimenten des westlichen äquatorialen Atlantiks. 96 pages, Bremen, 1998.

**No. 125** **Wolff, T.**
Mixed layer characteristics in the equatorial Atlantic during the late Quaternary as deduced from planktonic foraminifera. 132 pages, Bremen, 1998.

**No. 126** **Dittert, N.**
Late Quaternary Planktic Foraminifera Assemblages in the South Atlantic Ocean: Quantitative Determination and Preservational Aspects. 165 pages, Bremen, 1998.

**No. 127** **Höll, C.**
Kalkige und organisch-wandige Dinoflagellaten-Zysten in Spätquartären Sedimenten des tropischen Atlantiks und ihre palökologische Auswertbarkeit. 121 pages, Bremen, 1998.

**No. 128** **Hencke, J.**
Redoxreaktionen im Grundwasser: Etablierung und Verlagerung von Reaktionsfronten und ihre Bedeutung für die Spurenelement-Mobilität. 122 pages, Bremen 1998.

**No. 129** **Pätzold, J. and cruise participants**
Report and preliminary results of METEOR-Cruise M 41/3, Vítoria, Brasil – Salvador de Bahia, Brasil, 18.4. - 15.5.1998. Bremen, 1999.

**No. 130** **Fischer, G. and cruise participants**
Report and preliminary results of METEOR-Cruise M 41/4, Salvador de Bahia, Brasil – Las Palmas, Spain, 18.5. – 13.6.1998. Bremen, 1999.

**No. 131** **Schlünz, B. und G. Wefer**
Bericht über den 7. JGOFS-Workshop am 3. und 4.12.1998 in Bremen. Im Anhang: Publikationen zum deutschen Beitrag zur Joint Global Ocean Flux Study (JGOFS), Stand 1/ 1999. 100 pages, Bremen, 1999.

**No. 132** **Wefer, G. and cruise participants**
Report and preliminary results of METEOR-Cruise M 42/4, Las Palmas - Las Palmas - Viena do Castelo; 26.09.1998 - 26.10.1998. 104 pages, Bremen, 1999.

**No. 133** **Felis, T.**
Climate and ocean variability reconstructed from stable isotope records of modern subtropical corals (Northern Red Sea). 111 pages, Bremen, 1999.

**No. 134** **Draschba , S.**
North Atlantic climate variability recorded in reef corals from Bermuda. 108 pages, Bremen, 1999.

**No. 135** **Schmieder, F.**
Magnetic Cyclostratigraphy of South Atlantic Sediments. 82 pages, Bremen, 1999.

**No. 136** **Rieß, W.**
In situ measurements of respiration and mineralisation processes – Interaction between fauna and geochemical fluxes at active interfaces. 68 pages, Bremen, 1999.

**No. 137** **Devey, C.W. and cruise participants**
Report and shipboard results from METEOR-cruise M 41/2, Libreville – Vitoria, 18.3. – 15.4.98. 59 pages, Bremen, 1999.

**No. 138** **Wenzhöfer, F.**
Biogeochemical processes at the sediment water interface and quantification of metabolically driven calcite dissolution in deep sea sediments. 103 pages, Bremen, 1999.

**No. 139** **Klump, J.**
Biogenic barite as a proxy of paleoproductivity variations in the Southern Peru-Chile Current. 107 pages, Bremen, 1999.

**No. 140** **Huber, R.**
Carbonate sedimentation in the northern Northatlantic since the late pliocene. 103 pages, Bremen, 1999.

**No. 141** **Schulz, H.**
Nitrate-storing sulfur bacteria in sediments of coastal upwelling. 94 pages, Bremen, 1999.

**No. 142** **Mai, S.**
Die Sedimentverteilung im Wattenmeer: ein Simulationsmodell. 114 pages, Bremen, 1999.

**No. 143** **Neuer, S. and cruise participants**
Report and preliminary results of Poseidon Cruise 248, Las Palmas - Las Palmas, 15.2.-26.2.1999. 45 pages, Bremen, 1999.

**No. 144** **Weber, A.**
Schwefelkreislauf in marinen Sedimenten und Messung von *in situ* Sulfatreduktionsraten. 122 pages, Bremen, 1999.

**No. 145** **Hadeler, A.**
Sorptionsreaktionen im Grundwasser: Unterschiedliche Aspekte bei der Modellierung des Transportverhaltens von Zink. 122 pages, 1999.

**No. 146** **Dierßen, H.**
Zum Kreislauf ausgewählter Spurenmetalle im Südatlantik: Vertikaltransport und Wechselwirkung zwischen Partikeln und Lösung. 167 pages, Bremen, 1999.

**No. 147** **Zühlsdorff, L.**
High resolution multi-frequency seismic surveys at the Eastern Juan de Fuca Ridge Flank and the Cascadia Margin – Evidence for thermally and tectonically driven fluid upflow in marine sediments. 118 pages, Bremen 1999.

**No. 148** **Kinkel, H.**
Living and late Quaternary Coccolithophores in the equatorial Atlantic Ocean: response of distribution and productivity patterns to changing surface water circulation. 183 pages, Bremen, 2000.

**No. 149** **Pätzold, J. and cruise participants**
Report and preliminary results of METEOR Cruise M 44/3, Aqaba (Jordan) - Safaga (Egypt) – Dubá (Saudi Arabia) – Suez (Egypt) - Haifa (Israel), 12.3.-26.3.-2.4.-4.4.1999. 135 pages, Bremen, 2000.

**No. 150** **Schlünz, B. and G. Wefer**
Bericht über den 8. JGOFS-Workshop am 2. und 3.12.1999 in Bremen. Im Anhang: Publikationen zum deutschen Beitrag zur Joint Global Ocean Flux Study (JGOFS), Stand 1/ 2000. 95 pages, Bremen, 2000.

**No. 151** **Schnack, K.**
Biostratigraphie und fazielle Entwicklung in der Oberkreide und im Alttertiär im Bereich der Kharga Schwelle, Westliche Wüste, SW-Ägypten. 142 pages, Bremen, 2000.

**No. 152** **Karwath, B.**
Ecological studies on living and fossil calcareous dinoflagellates of the equatorial and tropical Atlantic Ocean. 175 pages, Bremen, 2000.

**No. 153** **Moustafa, Y.**
Paleoclimatic reconstructions of the Northern Red Sea during the Holocene inferred from stable isotope records of modern and fossil corals and molluscs. 102 pages, Bremen, 2000.

**No. 154** **Villinger, H. and cruise participants**
Report and preliminary results of SONNE-cruise 145-1 Balboa – Talcahuana, 21.12.1999 – 28.01.2000. 147 pages, Bremen, 2000.

**No. 155** **Rusch, A.**
Dynamik der Feinfraktion im Oberflächenhorizont permeabler Schelfsedimente. 102 pages, Bremen, 2000.

**No. 156** **Moos, C.**
Reconstruction of upwelling intensity and paleo-nutrient gradients in the northwest Arabian Sea derived from stable carbon and oxygen isotopes of planktic foraminifera. 103 pages, Bremen, 2000.

**No. 157** **Xu, W.**
Mass physical sediment properties and trends in a Wadden Sea tidal basin. 127 pages, Bremen, 2000.

**No. 158** **Meinecke, G. and cruise participants**
Report and preliminary results of METEOR Cruise M 45/1, Malaga (Spain) - Lissabon (Portugal), 19.05. - 08.06.1999. 39 pages, Bremen, 2000.

**No. 159** **Vink, A.**
Reconstruction of recent and late Quaternary surface water masses of the western subtropical Atlantic Ocean based on calcareous and organic-walled dinoflagellate cysts. 160 pages, Bremen, 2000.

**No. 160** **Willems, H. (Sprecher), U. Bleil, R. Henrich, K. Herterich, B.B. Jørgensen, H.-J. Kuß, M. Olesch, H.D. Schulz,V. Spieß, G. Wefer**
Abschlußbericht des Graduierten-Kollegs Stoff-Flüsse in marine Geosystemen. Zusammenfassung und Berichtszeitraum Januar 1996 - Dezember 2000. 340 pages, Bremen, 2000.

**No. 161** **Sprengel, C.**
Untersuchungen zur Sedimentation und Ökologie von Coccolithophoriden im Bereich der Kanarischen Inseln: Saisonale Flussmuster und Karbonatexport. 165 pages, Bremen, 2000.

**No. 162** **Donner, B. and G. Wefer**
Bericht über den JGOFS-Workshop am 18.-21.9.2000 in Bremen:
Biogeochemical Cycles: German Contributions to the International Joint Global Ocean Flux Study.
87 pages, Bremen, 2000.

**No. 163** **Neuer, S. and cruise participants**
Report and preliminary results of Meteor Cruise M 45/5, Bremen – Las Palmas, October 1 – November 3, 1999. 93 pages, Bremen, 2000.

**No. 164** **Devey, C. and cruise participants**
Report and preliminary results of Sonne Cruise SO 145/2, Talcahuano (Chile) - Arica (Chile), February 4 – February 29, 2000. 63 pages, Bremen, 2000.

**No. 165** **Freudenthal, T.**
Reconstruction of productivity gradients in the Canary Islands region off Morocco by means of sinking particles and sediments. 147 pages, Bremen, 2000.

**No. 166** **Adler, M.**
Modeling of one-dimensional transport in porous media with respect to simultaneous geochemical reactions in CoTReM. 147 pages, Bremen, 2000.

**No. 167** **Santamarina Cuneo, P.**
Fluxes of suspended particulate matter through a tidal inlet of the East Frisian Wadden Sea (southern North Sea). 91 pages, Bremen, 2000.

**No. 168** **Benthien, A.**
Effects of $CO_2$ and nutrient concentration on the stable carbon isotope composition of C37:2 alkenones in sediments of the South Atlantic Ocean. 104 pages, Bremen, 2001.

**No. 169** **Lavik, G.**
Nitrogen isotopes of sinking matter and sediments in the South Atlantic. 140 pages, Bremen, 2001.

**No. 170** **Budziak, D.**
Late Quaternary monsoonal climate and related variations in paleoproductivity and alkenone-derived sea-surface temperatures in the western Arabian Sea. 114 pages, Bremen, 2001.

**No. 171** **Gerhardt, S.**
Late Quaternary water mass variability derived from the pteropod preservation state in sediments of the western South Atlantic Ocean and the Caribbean Sea. 109 pages, Bremen, 2001.

**No. 172** **Bleil, U. and cruise participants**
Report and preliminary results of Meteor Cruise M 46/3, Montevideo (Uruguay) – Mar del Plata (Argentina), January 4 – February 7, 2000. Bremen, 2001.

**No. 173** **Wefer, G. and cruise participants**
Report and preliminary results of Meteor Cruise M 46/4, Mar del Plata (Argentina) – Salvador da Bahia (Brazil), February 10 – March 13, 2000. With partial results of METEOR cruise M 46/2. 136 pages, Bremen, 2001.

**No. 174** **Schulz, H.D. and cruise participants**
Report and preliminary results of Meteor Cruise M 46/2, Recife (Brazil) – Montevideo (Uruguay), December 2 – December 29, 1999. 107 pages, Bremen, 2001.

**No. 175** **Schmidt, A.**
Magnetic mineral fluxes in the Quaternary South Atlantic: Implications for the paleoenvironment.
97 pages, Bremen, 2001.

**No. 176** **Bruhns, P.**
Crystal chemical characterization of heavy metal incorporation in brick burning processes.
93 pages, Bremen, 2001.

**No. 177** **Karius, V.**
Baggergut der Hafengruppe Bremen-Stadt in der Ziegelherstellung. 131 pages, Bremen, 2001.

**No. 178** **Adegbie, A. T.**
Reconstruction of paleoenvironmental conditions in Equatorial Atlantic and the Gulf of Guinea Basins for the last 245,000 years. 113 pages, Bremen, 2001.

**No. 179** **Spieß, V. and cruise participants**
Report and preliminary results of R/V Sonne Cruise SO 149, Victoria - Victoria, 16.8. - 16.9.2000.
100 pages, Bremen, 2001.

**No. 180** **Kim, J.-H.**
Reconstruction of past sea-surface temperatures in the eastern South Atlantic and the eastern South Pacific across Termination I based on the Alkenone Method. 114 pages, Bremen, 2001.

**No. 181** **von Lom-Keil, H.**
Sedimentary waves on the Namibian continental margin and in the Argentine Basin – Bottom flow reconstructions based on high resolution echosounder data. 126 pages, Bremen, 2001.

**No. 182** **Hebbeln, D. and cruise participants**
PUCK: Report and preliminary results of R/V Sonne Cruise SO 156, Valparaiso (Chile) - Talcahuano (Chile), March 29 - May 14, 2001. 195 pages, Bremen, 2001.

**No. 183** **Wendler, J.**
Reconstruction of astronomically-forced cyclic and abrupt paleoecological changes in the Upper Cretaceous Boreal Realm based on calcareous dinoflagellate cysts. 149 pages, Bremen, 2001.

**No. 184** **Volbers, A.**
Planktic foraminifera as paleoceanographic indicators: production, preservation, and reconstruction of upwelling intensity. Implications from late Quaternary South Atlantic sediments. 122 pages, Bremen, 2001.

**No. 185** **Bleil, U. and cruise participants**
Report and preliminary results of R/V METEOR Cruise M 49/3, Montevideo (Uruguay) - Salvador (Brasil), March 9 - April 1, 2001. 99 pages, Bremen, 2001.

**No. 186** **Scheibner, C.**
Architecture of a carbonate platform-to-basin transition on a structural high (Campanian-early Eocene, Eastern Desert, Egypt) – classical and modelling approaches combined. 173 pages, Bremen, 2001.

**No. 187** **Schneider, S.**
Quartäre Schwankungen in Strömungsintensität und Produktivität als Abbild der Wassermassen-Variabilität im äquatorialen Atlantik (ODP Sites 959 und 663): Ergebnisse aus Siltkorn-Analysen. 134 pages, Bremen, 2001.

**No. 188** **Uliana, E.**
Late Quaternary biogenic opal sedimentation in diatom assemblages in Kongo Fan sediments. 96 pages, Bremen, 2002.

**No. 189** **Esper, O.**
Reconstruction of Recent and Late Quaternary oceanographic conditions in the eastern South Atlantic Ocean based on calcareous- and organic-walled dinoflagellate cysts. 130 pages, Bremen, 2001.

**No. 190** **Wendler, I.**
Production and preservation of calcareous dinoflagellate cysts in the modern Arabian Sea. 117 pages, Bremen, 2002.

**No. 191** **Bauer, J.**
Late Cenomanian – Santonian carbonate platform evolution of Sinai (Egypt): stratigraphy, facies, and sequence architecture. 178 pages, Bremen, 2002.

**No. 192** **Hildebrand-Habel, T.**
Die Entwicklung kalkiger Dinoflagellaten im Südatlantik seit der höheren Oberkreide. 152 pages, Bremen, 2002.

**No. 193** **Hecht, H.**
Sauerstoff-Optopoden zur Quantifizierung von Pyritverwitterungsprozessen im Labor- und Langzeit-in-situ-Einsatz. Entwicklung - Anwendung – Modellierung. 130 pages, Bremen, 2002.

**No. 194** **Fischer, G. and cruise participants**
Report and Preliminary Results of RV METEOR-Cruise M49/4, Salvador da Bahia – Halifax, 4.4.-5.5.2001. 84 pages, Bremen, 2002.

**No. 195** **Gröger, M.**
Deep-water circulation in the western equatorial Atlantic: inferences from carbonate preservation studies and silt grain-size analysis. 95 pages, Bremen, 2002.

**No. 196** **Meinecke,G. and cruise participants**
Report of RV POSEIDON Cruise POS 271, Las Palmas - Las Palmas, 19.3.-29.3.2001. 19 pages, Bremen, 2002.

**No. 197** **Meggers, H. and cruise participants**
Report of RV POSEIDON Cruise POS 272, Las Palmas - Las Palmas, 1.4.-14.4.2001. 19 pages, Bremen, 2002.

**No. 198** **Gräfe, K.-U.**
Stratigraphische Korrelation und Steuerungsfaktoren Sedimentärer Zyklen in ausgewählten Borealen und Tethyalen Becken des Cenoman/Turon (Oberkreide) Europas und Nordwestafrikas. 197 pages, Bremen, 2002.

**No. 199** **Jahn, B.**
Mid to Late Pleistocene Variations of Marine Productivity in and Terrigenous Input to the Southeast Atlantic. 97 pages, Bremen, 2002.

**No. 200** **Al-Rousan, S.**
Ocean and climate history recorded in stable isotopes of coral and foraminifers from the northern Gulf of Aqaba. 116 pages, Bremen, 2002.

**No. 201** **Azouzi, B.**
Regionalisierung hydraulischer und hydrogeochemischer Daten mit geostatistischen Methoden. 108 pages, Bremen, 2002.

**No. 202** **Spieß, V. and cruise participants**
Report and preliminary results of METEOR Cruise M 47/3, Libreville (Gabun) - Walvis Bay (Namibia), 01.06 - 03.07.2000. 70 pages, Bremen 2002.

**No. 203** **Spieß, V. and cruise participants**
Report and preliminary results of METEOR Cruise M 49/2, Montevideo (Uruguay) - Montevideo, 13.02 - 07.03.2001. 84 pages, Bremen 2002.

**No. 204** **Mollenhauer, G.**
Organic carbon accumulation in the South Atlantic Ocean: Sedimentary processes and glacial/interglacial Budgets. 139 pages, Bremen 2002.

**No. 205** **Spieß, V. and cruise participants**
Report and preliminary results of METEOR Cruise M49/1, Cape Town (South Africa) - Montevideo (Uruguay), 04.01.2000 - 10.02.2000. 57 pages, Bremen, 2003.

**No. 206** **Meier, K.J.S.**
Calcareous dinoflagellates from the Mediterranean Sea: taxonomy, ecology and palaeoenvironmental application. 126 pages, Bremen, 2003.

**No. 207** **Rakic, S.**
Untersuchungen zur Polymorphie und Kristallchemie von Silikaten der Zusammensetzung $Me_2Si_2O_5$ (Me:Na, K). 139 pages, Bremen, 2003.

**No. 208** **Pfeifer, K.**
Auswirkungen frühdiagenetischer Prozesse auf Calcit- und Barytgehalte in marinen Oberflächen-sedimenten. 110 pages, Bremen, 2003.

**No. 209** **Heuer, V.**
Spurenelemente in Sedimenten des Südatlantik. Primärer Eintrag und frühdiagenetische Überprägung. 136 pages, Bremen, 2003.

**No. 210** **Streng, M.**
Phylogenetic Aspects and Taxonomy of Calcareous Dinoflagellates. 157 pages, Bremen 2003.

**No. 211** **Boeckel, B.**
Present and past coccolith assemblages in the South Atlantic: implications for species ecology, carbonate contribution and palaeoceanographic applicability. 157 pages, Bremen, 2003.

**No. 212** **Precht, E.**
Advective interfacial exchange in permeable sediments driven by surface gravity waves and its ecological consequences. 131 pages, Bremen, 2003.

**No. 213** **Frenz, M.**
Grain-size composition of Quaternary South Atlantic sediments and its paleoceanographic significance. 123 pages, Bremen, 2003.

**No. 214** **Meggers, H. and cruise participants**
Report and preliminary results of METEOR Cruise M 53/1, Limassol - Las Palmas – Mindelo, 30.03.2002 - 03.05.2002. 81 pages, Bremen, 2003.

**No. 215** **Schulz, H.D. and cruise participants**
Report and preliminary results of METEOR Cruise M 58/1, Dakar – Las Palmas, 15.04..2003 - 12.05.2003. Bremen, 2003.

**No. 216** **Schneider, R. and cruise participants**
Report and preliminary results of METEOR Cruise M 57/1, Cape Town – Walvis Bay, 20.01. – 08.02.2003. 123 pages, Bremen, 2003.

**No. 217** **Kallmeyer, J.**
Sulfate reduction in the deep Biosphere. 157 pages, Bremen, 2003.

**No. 218** **Røy, H.**
Dynamic Structure and Function of the Diffusive Boundary Layer at the Seafloor. 149 pages, Bremen, 2003.

**No. 219** **Pätzold, J., C. Hübscher and cruise participants**
Report and preliminary results of METEOR Cruise M 52/2&3, Istanbul – Limassol – Limassol, 04.02. – 27.03.2002. Bremen, 2003.

**No. 220** **Zabel, M. and cruise participants**
Report and preliminary results of METEOR Cruise M 57/2, Walvis Bay – Walvis Bay, 11.02. – 12.03.2003. 136 pages, Bremen 2003.

**No. 221** **Salem, M.**
Geophysical investigations of submarine prolongations of alluvial fans on the western side of the Gulf of Aqaba-Red Sea. 100 pages, Bremen, 2003.

**No. 222** **Tilch, E.**
Oszillation von Wattflächen und deren fossiles Erhaltungspotential (Spiekerooger Rückseitenwatt, südliche Nordsee). 137 pages, Bremen, 2003.

**No. 223** **Frisch, U. and F. Kockel**
Der Bremen-Knoten im Strukturnetz Nordwest-Deutschlands. Stratigraphie, Paläogeographie, Strukturgeologie. 379 pages, Bremen, 2004.

**No. 224** **Kolonic, S.**
Mechanisms and biogeochemical implications of Cenomanian/Turonian black shale formation in North Africa: An integrated geochemical, millennial-scale study from the Tarfaya-LaAyoune Basin in SW Morocco. 174 pages, Bremen, 2004.

**No. 225** **Panteleit, B.**
Geochemische Prozesse in der Salz- Süßwasser Übergangszone. 106 pages, Bremen, 2004.

**No. 226** **Seiter, K.**
Regionalisierung und Quantifizierung benthischer Mineralisationsprozesse. 135 pages, Bremen, 2004.

**No. 227** **Bleil, U. and cruise participants**
Report and preliminary results of METEOR Cruise M 58/2, Las Palmas – Las Palmas (Canary Islands, Spain), 15.05. – 08.06.2003. 123 pages, Bremen, 2004.

**No. 228** **Kopf, A. and cruise participants**
Report and preliminary results of SONNE Cruise SO175, Miami - Bremerhaven, 12.11 - 30.12.2003. 218 pages, Bremen, 2004.